Functional Electrical Impedance Tomography of Adult and Neonatal Brain Function

Dr Alexander Thomas Tidswell

University College London

PhD Thesis

ProQuest LLC
789 East Eisenhower Parkway
P.O. Box 1346
Ann Arbor, MI 48106-1346

Abstract

Electrical Impedance Tomography (EIT) is a fast, portable imaging technique that produces tomographic images of the internal impedance of an object from surface electrode measurements. This thesis reports the first use of EIT to image evoked brain activity in adults and neonates and determines whether accurate EIT images could be obtained from the adult and neonatal brain. In addition, a realistic head-tank phantom was developed to test the performance of EIT with known impedance changes placed within a real human skull.

Two EIT systems were used. Images were obtained using 31 or 21 Ag/AgCl EEG scalp electrodes in adults and neonates, respectively, with either 256 or 187 individual impedance measurements from different electrode combinations: 2 applied a safe, alternating current and 2 measured the resultant scalp voltage. Imaging was performed using a block design with 6-15 stimulation periods of between 10-75s during either: 1) Visual, 2) Somatosensory or 3) Motor stimuli.

Impedance changes were detected in 38/39 adults and 9/9 neonates within 0.6-5.8s after stimulus onset, and returned to baseline 7.6-36s after stimulus cessation. Reconstructed images were noisy: ~20-70% images showed correct localisation to the expected area of cortex stimulated by the visual, motor or somatosensory paradigms. As EIT images from the head-tank localised changes within 10% of the impedance perturbation, this indicated that poor localisation in humans was not due to the head-shape or the skull, but may be related to unknown physiological factors. An improved EIT reconstruction algorithm, using a computerised finite-element model of the head, showed improved localisation for the adult images.

This is the first demonstration that EIT can detect and image impedance changes in the head, probably due to increased regional cerebral blood volume in the activated cortex. Improvements may enable more accurate neuroimaging of the adult and neonatal brain for use in clinical practice.

Acknowledgements

The work presented in this thesis would not have been possible without the work of my principle supervisor, Dr David Holder, who has worked towards the goal of neuroimaging with EIT and built up the team who have made this research possible. I would also like to thank Professor John Wyatt, for his supervision of and encouragement during the neonatal work.

The 3D reconstruction algorithm, based on a homogenous sphere model of the head and used in EIT image reconstruction in Chapters 2, 3 and 4, was developed by my colleague, Dr Adam Gibson.

The UCLH 1b EIT system, was developed in the UCLH Medical Physics Department by Mike Conway and Geoff Cuisack, with the final troubleshooting and software development completed by Dr Rebecca Yerworth.

Neuroimaging in the UCLH Neonatal Unit was made possible by Professor John Wyatt, and guidance on the neonatal project from Dr Judith Meek.

The reconstruction algorithm, based on a finite element model of the human head, was developed by my colleagues Dr Andrew Bagshaw, Dr Richard Bayford and Dr Andrew Tizzard.

Finally, but by no means least, my thanks to my family, Nikki Shack, Joe Tidswell and Zack Tidswell, for their support during this work, and in the case of Zack, his involvement in the neonatal experiments.

Table of contents

Index of figures

Index of tables

List of abbreviations

ADC	Apparent Diffusion Coefficient (of water)
BEM	Boundary Element Method
CSF	Cerebro-Spinal Fluid
CT	Computerised X-ray Tomography
deoxy-Hb	deoxygenated Haemoglobin
d.f.	degrees of freedom
DWI	Diffusion Weighted Imaging
EEG	Electroencephalography
EIT	Electrical Impedance Tomography
FEM	Finite Element Method
fMRI	functional Magnetic Resonance Imaging
FWHM	Full Width at half Maximum
HIE	Hypoxic-Ischaemic Encephalopathy
I-DEAS	Integrated Design Analysis Software
IVH	Intra-Ventricular Haemorrhage
MEG	Magneto-encephalography
MRI	Magnetic Resonance Imaging
MRS	Magnetic Resonance Spectroscopy
NIRS	Near Infra-Red Spectroscopy
oxy-Hb	oxygenated Haemoglobin
PET	Positron Emission Tomography
rCBF	regional Cerebral Blood Flow
rCBV	regional Cerebral Blood Volume
SD	Standard Deviation
SE	Standard Error
TOAST	Time Resolved Optical Absorption and Scattering Tomography

Chapter 1: Introduction

1.1 Purpose of research

The purpose of the work in this thesis was to develop an existing, portable imaging technique, Electrical Impedance Tomography (EIT), to a new application: the acquisition of functional information from the adult and neonatal brain. There are already existing techniques that provide functional information about the brain, particularly functional Magnetic Resonance Imaging (fMRI) and Positron Emission Tomography (PET), however these require large, expensive scanners which require the subject to be moved to the scanner and as such are not suitable for recording at the bedside in critically ill subjects who may be the recipients of intensive care. The specific advantages of EIT are that it is portable, fast - in that it can acquire several images a second, and is relatively inexpensive. If neuroimaging with EIT is successful then it could be used in several clinical areas in which other methods of imaging brain activity are unsuited, such as monitoring brain activity in adults and infants on intensive care, and the imaging of epilepsy on telemetry units, where prolonged periods of monitoring are required in order to record seizure activity (Holder and Gardner-Medwin 1988; Holder *et al.* 1994). In addition, EIT may be suited to provide images of brain impedance changes brought about by cell swelling in cerebral energy failure, in such pathological conditions as stroke, ischaemia, hypoxia or hypoglycaemia.

This thesis covers my work in the Department of Clinical Neurophysiology at the University College London Hospital, where EIT of the brain has been pioneered. The first demonstration that EIT could be used, non-invasively, to measure changes of brain impedance with scalp electrodes, was performed by my supervisor, Dr David Holder, in rats (Holder 1992). This led to work which demonstrated that EIT could image brain impedance in the exposed cortex of anaesthetised rabbits (Boone *et al.* 1994; Holder *et al.* 1996; Rao *et al.* 1997) during spreading depression, somatosensory and visual stimulation and in epilepsy. This pioneering research formed the precursor to the work in this thesis, in which I have imaged the first sensory evoked impedance changes in the adult and neonatal head and also developed realistic head phantoms to demonstrate the feasibility of imaging impedance changes within the head. The work in this thesis is presented in 5 main sections:

Chapter 1: an introduction and overview of EIT, bioimpedance of the brain, the underlying neurophysiology of brain impedance changes and an introduction to other functional neuroimaging techniques in both adults and neonates.

Chapter 2: The work in which the first impedance changes associated with sensory evoked activity in the human adult were detected and imaged with EIT.

Chapter 3: The work in which a realistic head shaped tank phantom, which contained a real human skull, was constructed in order to test the accuracy of EIT in the localisation of impedance changes within the skull.

Chapter 4: In which the first EIT images of sensory evoked changes in healthy neonates were obtained.

Chapter 5: Details a discussion of the work in the thesis and my conclusions, and introduces some of the work in progress and future work required for EIT of the head.

1.2 Introduction to EIT

1.2.1 Historical perspective

The first impedance tomography system was described in a paper by Benebid et al. in 1978, in which a brain impedance scanner was proposed which could be used to detect brain tumours (Benabid *et al.* 1978). This proposal arose from their measurements of brain impedance with a stereotactic device at neurosurgery, which demonstrated that the impedance of tumour tissue was lower, by a factor of 0.5-0.7, than the impedance of the normal surrounding brain. They proposed that the impedance contrast between the tumour and healthy tissue could be detected by an appropriate impedance scanner. Their proposal was backed up by details of a prototype impedance scanner which had two parallel arrays of electrodes immersed in a saline filled tank and they demonstrated that an impedance change, inserted between the electrode arrays, could be detected by measurements made through the electrode arrays. The paper then proposed how a brain impedance scanner might work: this had a similar set of electrodes in a saline filled tank, from which images of the head could be obtained when the head was inserted in the saline. Although this was impractical, it demonstrated the principles of the first impedance brain scanner.

The first clinical impedance tomography system, then called applied potential tomography (APT), was developed by researchers in the Department of Medical Physics in Sheffield (Barber and Brown 1984; Brown *et al.* 1985; Brown and Seagar 1987). The Sheffield Mark 1 EIT system made multiple impedance measurements of an object by a ring of 16 electrodes placed around the surface of the object (Figure 1.1). Each impedance measurement was made from a combination of 4 electrodes selected from the 16 surface electrodes by a multiplexer: 2 were used to apply an alternating current, which produced a voltage field on the surface of the object, which was

measured by different pairs of adjacent electrodes. From the 16 electrodes, 104 different impedance measurements were made of the object, with the constraint that the pair of electrodes selected for current injection were adjacent on the boundary, referred to as *'adjacent-drive'*. As these boundary impedance measurements are related to the internal impedance of the object, then impedance images could be reconstructed from the boundary measurements by means of a simple filtered back-projection algorithm.

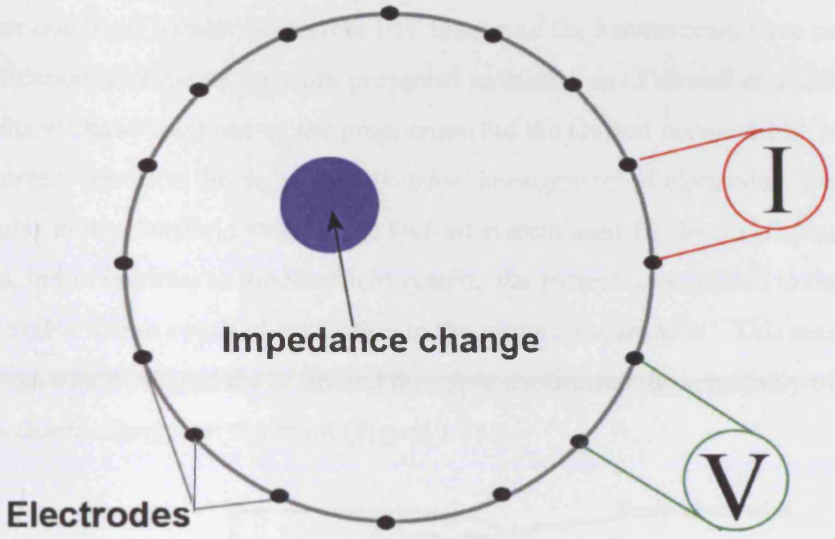

Figure 1.1 Impedance measurements in adjacent drive by the Sheffield Mark 1 system
16 electrodes are placed on the object's surface: 2 are selected to apply a current, **I**, and 2 selected to measure the resultant voltage, **V**. These current injection and voltage measurement pairs are switched, by means of a multiplexer, through 104 different combinations of electrodes. Information from these 104 impedance measurements are used to reconstruct an EIT image of the internal impedance of the object by the use of a reconstruction algorithm. An impedance change (blue circle) would cause a related change in the surface voltage, as the applied current remains constant.

One of the first EIT images published was of an arm, immersed in a tank of saline (Barber and Brown 1984). As EIT was developed, images of gastric emptying (Mangall *et al.* 1987) the cardiac cycle (Eyuboglu *et al.* 1987) and the lung ventilation cycle in the thorax (Harris *et al.* 1987; Metherall *et al.* 1996) were obtained and published. The Sheffield EIT system had the advantage that 10 images could be obtained a second, the system was portable and the system was relatively inexpensive compared to ultrasound, CT and MRI scanners. However, since the EIT images

obtained were of low resolution compared to other clinical techniques such as cardiac ultrasound and X-ray contrast studies of the gut, EIT did not gain widespread clinical acceptance.

Around the same time, a group in Oxford proposed that EIT could be used to image the neonatal brain (Tarassenko *et al.* 1985). They developed a clinical EIT system and obtained preliminary EIT images in a total of 2 neonates (Tarassenko 1985; Murphy *et al.* 1987), in which there was a correlation between the features in the EIT images and abnormalities in the cerebral ultrasound. However, as no further neonatal studies have been published, the data were not sufficient to demonstrate the reproducibility of the findings, either within the same neonates or in a larger cohort of babies. No further EIT images of the human brain have since been published, until publication of some of the work presented in this thesis (Tidswell *et al.* 2001). To obtain these results we have used one of the propositions of the Oxford neonatal EIT research, which is the use of current injection through a *'polar-drive'* arrangement of electrodes (Tarassenko *et al.* 1985). Similar to the Sheffield system, the Oxford system used 16 electrodes placed in a ring around the head, but in contrast to the Sheffield system, the current was applied to the head by pairs of electrodes which opposed each other in the ring in *'polar-drive'*. This maximised the amount of current which entered the brain and therefore maximised the sensitivity of the EIT system to impedance changes in the brain (Figure 1.2).

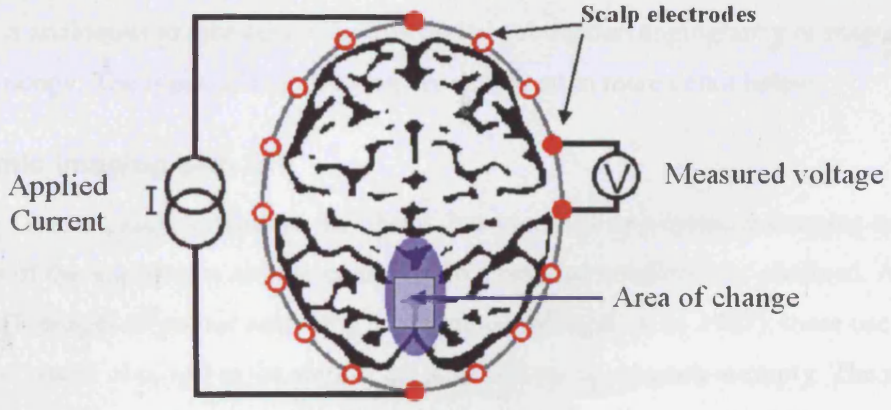

Figure 1.2 Polar drive method of current application
For head imaging, an increased current will enter the skull if the current is applied in polar drive. For each impedance measurement, 4 electrodes are used: 2 apply a constant current in *polar drive* with the electrodes diametrically opposed across the head, and two adjacent voltage measurement electrodes record the resultant scalp voltage.

Experimentally, the polar-drive method maximises current injection within the human skull compared to the adjacent drive method. This was demonstrated in a saline filled tank which

contained a human skull (Rush and Driscoll 1968), in which current was injected by electrodes on the outside of the skull and measurements of current density recorded within the skull. Approximately a fivefold increase in current density in the centre of the skull was achieved with a polar drive electrode arrangement compared to adjacent electrodes 5 cm apart. As the sensitivity of the boundary measurements is related to the current density at the point of the impedance change, increased current density within the brain would produce similar increases in the sensitivity of the EIT system. This was confirmed using a finite element method (FEM) simulation of the adult head in 2-dimensions, in which the sensitivity of boundary impedance measurements to changes of impedance in the centre of the head were up to 210 times greater when current was applied by polar-drive instead of using adjacent pairs of electrodes (Bayford *et al.* 1996).

1.2.2 Types of EIT imaging

There are several ways in which EIT imaging has been used, and these have parallels to other medical imaging technologies. EIT is most commonly used to provide dynamic images of impedance change, compared to a reference baseline, similar to the dynamic changes of blood flow detected in the brain by fMRI. EIT can also be used to image absolute impedance in the body, similar to images provided by X-ray radiographs and computerised tomography (CT) or EIT can be used to detect spectroscopic differences in impedance at two different measurement frequencies, which is analogous to techniques such as digital subtraction angiography or magnetic resonance spectroscopy. The types of EIT imaging are described in more detail below.

Dynamic imaging with EIT

Most EIT work, and the work in this thesis, has used EIT as a dynamic imaging method, in which images of the impedance *change* compared to a baseline condition are obtained. An example is how EIT images of gastric emptying are obtained (Mangall *et al.* 1987): these use a reference baseline image obtained at the start of the study when the stomach is empty. The stomach is then filled by the subject drinking a conductive saline solution. Subsequent EIT images are reconstructed with reference to the baseline image and demonstrate the impedance change as the stomach fills and then empties the conductive solution. A second example is of cardiac imaging (Metherall *et al.* 1996): images are gated to the electrocardiogram (ECG) to demonstrate the change in impedance during the cardiac cycle compared to a reference baseline image when the heart is emptied of blood in diastole. The final example is of lung ventilation (Harris *et al.* 1987), in which a reference image is obtained when the lungs are partially emptied of air at the end of

expiration and EIT images of the changes during normal ventilation are reconstructed with reference to the baseline image.

The main reason for imaging dynamic impedance changes is to eliminate or reduce reconstruction errors that occur due to differences between the mathematical reconstruction model of the object and the actual object imaged. The commonest errors that exist between the model and the object imaged are the impedance of the electrode skin interface, the difference in shape between the object and the reconstruction model, and errors in electrode position (Barber and Brown 1988). To reduce these errors, impedance changes are reconstructed with reference to a baseline condition; if the electrode placement errors in the baseline images and the impedance change images are the same, then these errors cancel if only *impedance change* is imaged (Barber and Brown 1988). Although the dynamic imaging approach minimises reconstruction errors, it limits the application of EIT to experiments in which an impedance change occurs over a short experimental timecourse, otherwise the phenomenon of electrode impedance drift introduces artefacts in the data which cannot be predicted from the baseline condition. Over short periods of a few minutes, this drift is either negligible or is approximately linear and can be corrected; however longer intervals produce larger, non-linear changes which cannot be corrected and therefore result in reconstruction errors.

As dynamic imaging cannot be used to image objects present at the start of imaging and therefore in the baseline images, dynamic EIT cannot be used to obtain images of tumours or cysts. This contrasts with images obtained with CT, which can obtain static images of contrasting tissues such as brain tumours.

Static imaging with EIT

To obtain static images of impedance contrasts, then errors between the reconstruction model and the object imaged have to be minimised. There has been limited work in which static images of tank phantoms and of the breast have been obtained with multi-frequency EIT, with some images of breast cysts and tumours produced (Kerner *et al.* 2001; Kerner *et al.* 2002), although this has not been shown to work in more extensive clinical studies. In order to do this, the exact position of the electrodes are measured experimentally and incorporated in the reconstruction model, as well as estimates of electrode impedance. In these studies the breast is inserted into an array of electrodes which are manipulated into a ring in contact with the breast. As the manipulator which moves the electrodes into position also provides information about the position of the electrodes, then the electrode positions are accurately recorded. This approach is suited to the breast as it can be deformed around a fixed array of electrodes, and therefore a similar electrode and breast model used in the reconstruction algorithm. However, this approach is less suited for non-deformable

parts of the body such as the head and chest, in which it is difficult to apply electrodes in a symmetrical ring, and in addition it is difficult to record the three-dimensional position of the electrodes with such accuracy.

Multi-frequency EIT imaging

Dynamic EIT images usually use one measurement frequency, usually between 10-50kHz, to make impedance measurements. An alternative approach is to compare the difference between impedance images measured at different measurement frequencies, so called multi-frequency EIT or contrast EIT (Griffiths and Ahmed 1987). This technique exploits the different impedance characteristics of tissues at different measurement frequencies and therefore an impedance contrast at different frequencies (Gabriel *et al.* 1996). An example of such a contrast would be the difference between cerebro-spinal fluid (CSF) and the grey matter of the brain. As the CSF is an acellular, ionic solution, it can be considered a pure resistance, so that its impedance is identical and equal to the resistance for all frequencies of applied current. However, the grey matter, which has a cellular structure, has a higher impedance at low frequencies than at high frequencies (Ranck 1963). This difference arises due to the high capacitance of the cell membrane. The impedance, **Z**, of a capacitor, **C**, is given by the equation

$$Z = (j\omega C)^{-1}$$

when a current is applied at a frequency, ω. The complex number, **j**, indicates that the impedance of a capacitor will cause the phase of the voltage across the capacitor to lag behind the phase of the applied current by 90°. At low frequency currents, the impedance is high, and at high frequency currents the impedance is low. This frequency difference can theoretically be exploited to provide a contrast in the impedance images obtained at different frequencies, and provide a means of identifying different tissues in a multifrequency EIT image. Some EIT work has now taken advantage of the different frequency responses of tissues to perform difference imaging between different frequencies (Kerner *et al.* 2001; Kerner *et al.* 2002). This technique, if successful in brain impedance imaging, has the potential to image longstanding changes in the brain, such as tumours, cysts and stroke.

1.2.3 How EIT works

There are two main steps in the acquisition of EIT images. The first step is the method by which the actual impedance measurements are made from the body, using specialised EIT hardware. Once

the measurements are made, then the second step is the reconstruction of this data into the EIT images. These steps will now be considered in more detail.

1.2.3.2 Impedance measurements

The majority of EIT systems and those used in the work for this thesis, have a similar method of measuring the trans-impedance of an object, through electrodes placed around the object's surface. Each impedance measurement is made from a combination of four electrodes: two electrodes are used to apply a medically safe, alternating current to the object (maximum current of 5mA at 50kHz and above, decreasing to1mA at 10kHz - see Appendix 2 for more details). This produces a voltage field on the surface of the object, which is sampled between different pairs of voltage measurement electrodes. The boundary impedance is calculated from the known voltage and applied current. For the Sheffield mark 1 system 16 electrodes are used on the object's surface from which 104 independent combinations of adjacent current and adjacent voltage pair impedance measurements can be made. The different combinations of electrodes used for these measurements are selected by the use of a multiplexer (Figure 1.1).

As the different boundary impedance measurements made from the object are related to the internal impedance of the object, then EIT images can be reconstructed from these measurements by the use of a reconstruction algorithm calculated from a mathematical model of the object.

The EIT equipment used to measure the impedance at the electrode needs to take into account the phase lag of the voltage measured to the applied current. The impedance of the object at that electrode combination is given by Ohm's Law:

$$|\mathbf{Z}| = \mathbf{V} / \mathbf{I}$$

where **I** is the magnitude of the applied current, $|\mathbf{Z}|$ is the magnitude of the object's impedance and **V** the magnitude of the measured voltage. For a constant current, used by the Sheffield and UCLH EIT systems, an impedance change is directly proportional to the measured voltage change.

The impedance of biological tissue has both a capacitative component, e.g. due to cell membranes, and a resistive component, e.g. due to current passing through fluid such as the CSF and extracellular space. The impedance, **Z**, is a combination of the reactance, **X**, and the resistance of the tissue, **R**, such that:

$$|\mathbf{Z}| = (\mathbf{R}^2 + \mathbf{X}^2)^{1/2}$$

In direct biological impedance measurements the reactive component of impedance is generally small, approximately 1-5% of the resistive component (Ranck 1963), except for the case of

unabraded skin in which the reactance can be equal to the resistance (Yamamoto and Yamamoto 1976). However, when the transimpedance of the head is measured, this incorporates the impedance from all the tissues, including skin.

The resistance of the head is determined by its dimensions and the resistivity of its component tissues. The resistivity is a property of the tissues, from which the resistance can be calculated for a sample of that tissue, given the dimensions of the tissue: as the area is increased, the resistance is decreased in proportion to the area; as the length is increased, resistance is increased in proportion to the length. The resistance, R, is related to the resistivity by the equation:

$$\mathbf{R = \rho \times Length/Area}$$

Where ρ is the resistivity of the material with units Ω.cm or Ω.m.

Tissue resistivity is determined by the number of free charge carriers available to conduct the applied current. These are the positively and negatively charged ions and molecules present throughout the body. The ability to carry a current depends on the mobility of the ions or molecules: e.g. mobile ions in a solution can carry more current than charged molecules attached to cell membranes. Mobility of the charge carriers is increased with small size, such as Cl^-, Na^+, Ca^{2+} and K^+ ions compared to larger ionic molecules such as proteins; and ion mobility increases with temperature which will decrease impedance as temperature rises (Van-Harreveld and Ochs 1956). Ion mobility may be reduced by components in the tissue such as the presence of larger molecules and cells. The presence of cells in a conducting fluid, such as in blood or extra-cellular fluid, which increase resistivity is known as the 'tortuousity effect': where the current has to travel around the cells in its path. In blood the resistivity is increased with increased number of red cells within it (Geddes and Baker 1967) and the extracellular fluid (ECF) space of the brain has a higher resistivity than an equivalent solution without cells present due to the presence of the neuronal and glial cells. Finally, the resistivity is affected by the ability of current to enter that tissue: if it is surrounded by a high resistivity lipid membrane, such as neurones, then little transverse current will pass into it; if the membrane is permeable to ions, as the glial cell membrane is to K^+ (Lux *et al.* 1986), the tissue will have a lower resistivity (Ranck 1963).

These factors are important when considering the impedance changes of brain during neuronal activation: a current which enters the brain will be conducted through the neuronal, glial, blood and ECF compartments. Changes in the relative size of these compartments, secondary to neuronal activity and blood volume changes, will affect current flow and therefore brain impedance. It is this impedance change we propose to measure with EIT.

1.2.3.3 Image reconstruction

Although the aim of this thesis was to develop the clinical technique of EIT towards neuroimaging, a knowledge of the method by which EIT images were reconstructed was required, in order to understand the presence of image artefacts and factors which may affect image localisation. What follows is a brief overview of image reconstruction, with particular attention to the techniques used to reconstruct the images of the human head and the head-shaped tank phantoms. The majority of the work performed in the development of the 3-D reconstruction algorithm used to produce the majority of the images in this thesis, is credited to Dr Adam Gibson (Gibson 2000).

EIT images, reconstructed from the boundary impedance measurements, represent a spatially smoothed and low resolution image of the impedance changes within the object, which in this thesis is the human head or head-shaped tank phantoms. In these images, the pixels are inversely related to the conductivity changes, $\Delta\sigma$. These conductivity changes are related to voltage changes measured at the scalp, $\Delta\mathbf{V}$, when a current is applied to the head. This relationship is expressed in matrix form by equation (1):

$$\mathbf{(1)} \qquad \Delta\mathbf{V} = \mathbf{A}\,\Delta\sigma$$

where $\mathbf{A}$ is known as the sensitivity matrix. The problem is to solve the equation to find $\Delta\sigma$, given the changes in the measured boundary voltages, $\Delta\mathbf{V}$.

There are two steps to this problem: 1) The forward solution, which creates a simplified mathematical model or computer simulation of the head, in order to calculate the sensitivity matrix, $\mathbf{A}$, and 2) The inverse solution, which inverts the sensitivity matrix. Once the inverted sensitivity matrix, $\mathbf{A}^{-1}$ is calculated, equation (1) can be rewritten as equation (2):

$$\mathbf{(2)} \qquad \Delta\sigma = \mathbf{A}^{-1}\,\Delta\mathbf{V}$$

from which the image of impedance change in the head can be calculated for any set of measured voltage changes. The conductivity changes, $\Delta\sigma$, at each pixel are inversely related to the resistivity changes in the image.

The Forward problem

One of the main methods used to solve the forward problem uses a simplified computer model of the object and the electrode positions on its boundary. For each impedance measurement made on the object, a sensitivity coefficient is calculated for each pixel in the EIT image, which determines

the size of the voltage change which would be measured at that electrode combination for a change in conductivity at that pixel (Geselowitz 1971).

One way to solve the forward problem is to use an analytical technique, in which a simplified geometric representation of the object is used. In this thesis, the forward model which represents the head is a sphere of uniform conductivity (Gibson 2000). The advantage of this technique is that it is relatively straightforward to implement in a computer program, for simple geometric models of the object. Even information about different tissue layers can be incorporated in the model to improve its accuracy (Liston *et al.* 2002). However, the disadvantage of the analytical technique is that it cannot be used to implement complex geometric shapes, such as the shape of the head, holes in the head - such as eye sockets, nor can it incorporate information about tissue anisotropy: the different electrical properties that a tissue has to a current applied in different directions.

For more complex and more realistic information to be incorporated into the forward model, computer simulations of the object need to be used. Examples of these are finite element method (FEM), or the computationally less demanding boundary element method (BEM). The advantage of such models is that they can be constructed from real images of the head, obtained by either MRI or CT (Bayford *et al.* 2001), to incorporate realistic shape information. In addition they can also include information about the tissue layers in the head, such as the scalp, the skull, the CSF and the brain. Once this information is incorporated, each tissue component can be given a resistivity value, obtained from impedance measurements of that tissue published in the literature. The FEM can be used to calculate the field produced throughout the model upon current injection, and from this a sensitivity matrix can be generated which relates the sensitivity of each voltage measurement to a conductivity change at each location in the model. These locations are analogous to the pixel positions in the final EIT image slices. Once the sensitivity matrix is calculated for all the boundary impedance measurements, it can then be inverted to obtain the EIT images from the scalp voltage changes. The disadvantage of the FEM solution is that it is difficult to implement for a complex head-shape. Initial attempts (Gibson 2000) used a FEM with elements of different geometric shapes that produced large errors in the forward solution. Subsequent work has used a variety of software packages to create a finer FEM model, with more elements, in order to reduce these errors. This has required the use of a variety of commercially available software packages, and software developed within UCL in order to create and solve the FEM, respectively. The failure to develop a realistic FEM forward model, is the primary reason why the EIT images in this thesis

are produced using the more simplified analytical solution which uses a spherical model of the head (Tidswell *et al.* 2001).

The inverse problem

The inverse problem is the method by which the sensitivity matrix **A**, is inverted to $\mathbf{A}^{-1}$ in order to be used in equation (2) and reconstruct images of conductivity change from the changes in the boundary voltage measurements.

There are many techniques by which the sensitivity matrix can be inverted (Bertero and Boccacci 1998; Gibson 2000). One of the solutions which is most widely used in EIT, and which is used in the images in this thesis, is to invert the matrix using truncated singular value decomposition (SVD) (Breckon 1990). In singular value decomposition (SVD), the sensitivity matrix is decomposed into a series of orthogonal matrices, each associated with a weighting factor – a singular value (Breckon 1990; Golub and Loan 1996; Gibson 2000). Each of these orthogonal matrices represents a basis image, which are summated to provide the final image. However, as errors in the sensitivity matrix are emphasised by the inversion process and can severely distort the final images, these errors are suppressed by truncating the inversion process at a point before the errors are introduced into the images. This truncation therefore minimises image noise. This threshold depends on the level of noise in the impedance data, the size of the errors in the sensitivity matrix and the numerical rank of the sensitivity matrix, determined by the number of independent impedance measurements (Breckon 1990; Gibson 2000). For example, the adult human EIT data in this thesis consisted of 258 separate impedance measurements from the head for each image. Of these the number of independent measurements was determined by SVD and 255 appeared independent (Gibson 2000). However, a truncation threshold of 62 singular values was chosen, as this was appropriate for the level of noise present in the impedance data.

Theoretical advantages of EIT compared with EEG

Although both EIT and EEG make measurements of boundary voltages, EIT has an advantage over EEG in that the inverse problem, which for EIT consists of finding the internal impedance of an object and for EEG the internal voltage sources of the head, is theoretically unique for EIT, whereas in EEG many possible solutions exist for the inverse problem. This theoretical uniqueness of a solution for EIT is because EIT has an additional level of information in that information about the current sources that generate the boundary voltage is known. This situation is analagous to that of CT scanning, in which information about the inside of an object is calculated from passing X-rays through the object and making measurements of the attenuation caused by that object; the

advantage that CT has over EIT is that the X-rays pass in approximately straight lines through the object under test so the solution of the inverse is comparitively simple compared to that of EIT, in which current passes in all directions through the head. In EIT the indirect passage of the applied current contributes to the ill-posedness of the EIT inverse solution, as assumptions about current paths have to be made by the use of a Forward-model, which is a simplified model of the conductivity of the object under test. It follows from this that the more accurate the Forward model, the better the inverse solution for EIT.

The existence of a theoretically unique solution for EIT does not mean that the inverse problem of finding the internal impedance of the object is well defined. An additional problem, and one of the main sources of the ill-defined nature of the solution, is the non-linearity problem in that the relationship between a change in the surface voltage is not linearly related to the change in the impedance in the head – an example that illustrates this point is that a similarly sized impedance change close to the surface of the object is expected to produce a much larger surface voltage change than the same sized impedance change in the centre of the object; this problem is partly overcome by the use of a Forward-model (in the experiments for this thesis this is a Forward model for the head), but as this Forward-model is a simplified model, errors between the model and the head will produce errors in the solution and therefore contribute to the ill-posed nature of the EIT inverse problem. The second problem that contributes to the ill-posed nature of the EIT solution is that not all the scalp voltage change data can be recorded – this is because boundary impedance changes may be small, so if measurements are noisy, then small boundary impedance changes will be undetected – this is often a problem ignored by EIT groups who provide theoretical inverse solutions to EIT using computer simulations, and much more of a problem when EIT is applied to measure noisy biological signals. In addition as the number of boundary measurements on the head are limited – up to 256 surface measurements were used to image the adult head in Chapter 2 – then this contributes to inaccuracies in the measurements of the boundary voltage changes; the electrode numbers are limited for two main reasons: 1) The initial EIT equipment was slow, necessitating a small number of measurements, and 2) Larger numbers of electrodes introduce a problem of reduced inter-electrode voltage differences in the measurement of the boundary voltage, which although would theoretically introduce higher spatial sampling of the scalp potentials actually results in decreased signal to noise.

All these problems also have an impact on the theoretical resolution of EIT, if the number of measurements are small – even if making the false assumption that the information each electrode records is independent – then the amount of independent information within an image

will also be small. In practice, the amount of information in the EIT images is truncated well below the number of measurements made, reducing independent information in the image further. If a rough assumption that the forward model used to produce the head images in Chapter 2 truncates information at 62 singular values this would roughly equate to a voxel cube representative of the head of 4x4x4 voxels, and if each voxel was truly independent then I estimate that a theoretical maximum number of 8 objects could be resolved independently giving an approximate full-width at half-maximum of 25% of the diameter of the head (aproximately 5cm, depending on the size of the head).

In summary, although EIT has theoretical advantages over EEG in that there is a theoretically unique solution for an image, the main practical problems encountered by EIT of the head is the non-linearity of impedance responses, the theoretical resolution limits of EIT, so that if there are many impedance changes in the head then these will not be independently resolved in the final EIT images, and there is also the problem of using an accurate forward model in the EIT image reconstruction which may limit the accuracy of impedance change localisation and resolution still further than that estimated from a theoretical consideration of the maximum number of independent changes that EIT can resolve.

1.2.4 The development of EIT towards neuroimaging

Impedance techniques have been in use for over 40 years, to measure impedance changes in the animal brain. These studies were the start of the research which has progressed to the development of EIT for imaging the animal and human brain.

In the early 1960's, several researchers demonstrated, using intra-cortical electrodes, that impedance changes occurred in the animal brain during a variety of normal or abnormal neurological states. One of the first demonstrations that brain impedance changed during normal brain activity was in a study performed on the exposed cortex of cats (Adey *et al.* 1962), in which reproducible impedance decreases of 1-3 % were detected during the presentation of visual stimuli, the exposure of the cat to milk or in the case of an experimental female cat, the presentation of a male. A similar study also detected impedance changes in a series of similar experiments, however the main difference was that the impedance variation with pulsatile blood flow was measured in the head (Birzis and Tachibana 1962; Birzis and Tachibana 1964; Birzis and Carregal 1965). These experiments demonstrated that the size of the impedance variation was due to the size of blood flow in the brain, then the experiments went on to demonstrate that impedance amplitude, and therefore blood flow, increased during stimuli such as smells, petting, pain and noise. The latency

of these changes were 2-6 seconds, and returned to baseline after 10-40 seconds. Changes of absolute impedance were also reported in rabbits (Aladjolova 1964), with impedance changes produced by electrical stimulation of the motor cortex, which produced impedance increases if the stimulation produced motor movements in the animal, or impedance decreases if the electrical stimuli did not produce movements.

The initial proposal that imaging these changes could be performed with an impedance tomography system (Benabid *et al.* 1978), was not followed up with a practical EIT device. The first neuroimaging in human neonates by EIT was proposed and performed by a group in Oxford, however their attempts failed as they had attempted to image long term impedance changes in the neonatal head due to intra-ventricular haemorrhage (Tarassenko 1985; Tarassenko *et al.* 1985; Murphy *et al.* 1987). Their EIT images, of intra-ventricular haemorrhage in two infants, were unconvincing, which was probably due to the long term monitoring of the babies which produced large and unpredictable electrode impedance drifts which introduced artefacts in their images; after these pilot studies, their neonatal EIT research stopped.

After that time, there was been little interest in imaging the head, until EIT was again proposed for the purpose of functional neuroimaging. This proposal was from my supervisor, Dr David Holder at University College London, who backed up the proposal with pilot animal studies which were to be a precursor to the human EIT research in this thesis. He demonstrated, for the first time, that impedance changes in the rat brain could be measured using scalp electrodes (Holder 1992). In this experiment, simultaneous cerebral impedance measurements were recorded from the scalp and the brain of anaesthetised rats, during the induction of cerebral ischaemia. Impedance increased at the scalp by 10% of the impedance increase recorded by intra-cortical electrodes. The scalp changes were demonstrated to have originated from the brain, as they were abolished by the insertion of an electrically insulating polythene sheet between the scalp and brain.

Although this study measured single channel impedance, from 4 electrodes, this work paved the way for subsequent EIT studies of the animal brain. At that time, the only available EIT system was the Sheffield system, which was limited in the application of current via an adjacent drive method (Figure 1.1). This system was unlikely to be able to image impedance changes in the brain from scalp electrodes, as most of the applied current would be shunted through the scalp. In order to demonstrate that brain impedance changes could be imaged, the effect of the skull was excluded by using a ring of electrodes placed on the exposed cortex of anaesthetised rabbits. In these studies, the first EIT images of brain activity were obtained, during visual (Figure 1.3) and somatosensory stimulation (Holder *et al.* 1996) and during epilepsy (Rao *et al.* 1997). The images

demonstrated impedance changes localised to either the contralateral somatosensory cortex during forepaw stimulation, the visual cortex during visual stimulation or the focus of seizure activity during epilepsy. The impedance changes varied between a 2-5 % decrease during somatosensory or visual stimulation and a 10 % increase during epilepsy. In similar studies, EIT was also successful at imaging spreading depression (Boone *et al.* 1994), which produced much larger impedance increases of up to 100%. The mechanisms behind these changes are thought to arise from a combination of cell swelling and blood volume changes which occurred in the area of the brain which was neuronally active during somatosensory or visual stimulation or during the induced epilepsy.

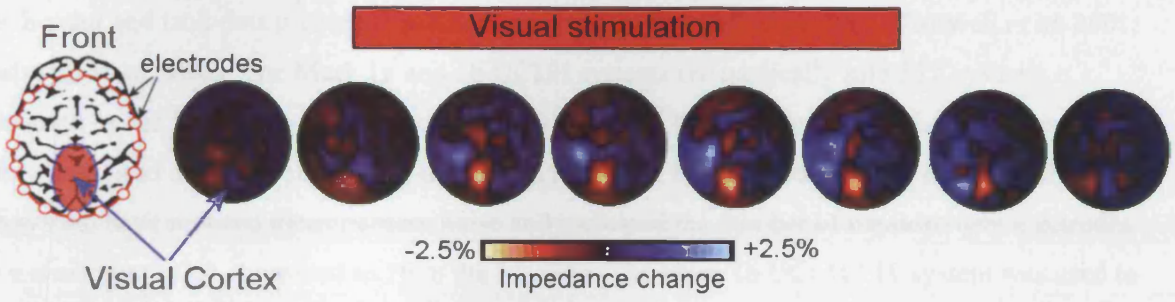

Figure 1.3 EIT images of rabbit cortex during visual stimulation
Images were obtained from the exposed rabbit cortex, using a ring of 16 electrodes placed on the brain. Each image represents 30s of time. The stimulus used was a stroboscopic light with a flash frequency of 8Hz, and the duration of stimulation indicated at the top. The orientation of the images is described by the diagram on the left of the picture, with the area of the visual cortex indicated.

The images demonstrate that an impedance decrease occurs over the area of the visual cortex, during the period of visual stimulation, and the changes return to baseline 30s after the cessation of visual stimulation. These are the first EIT images of functional cortical activity ever obtained (Holder *et al.* 1996). Note: The impedance scale in these images is reversed compared to the human images in this thesis.

The evidence that functional activity changed brain impedance by 2-5%, and combined with evidence from rats that the skull attenuated impedance changes by a factor of 10, was used to predict that scalp impedance changes of 0.2-0.5% may be detected during functional activity in humans. As such changes were within the sensitivity of an EIT system, then these pioneering studies paved the way for human functional imaging studies.

The limiting factor to human research was the constraint of adjacent drive present in the only commercially available EIT system designed and built in Sheffield (Brown and Seagar 1987).

As demonstrated in the work by Rush and Driscoll (Rush and Driscoll 1968), adjacent drive would decrease the sensitivity of EIT by a factor of 10 for changes in the centre of the head, compared to polar drive. As this would reduce the scalp impedance changes to below the level of the equipment noise, then in order to pursue the goal of adult functional EIT, new EIT systems were developed.

In total, three EIT systems have been built specifically for neuroimaging: 1) The EIT system based on a Hewlett Packard (HP) impedance analyser (Bayford *et al.* 1996), 2) The Mark 1a UCLH EIT system and 3) The Mark 1b UCLH EIT system (with a fourth, multi-frequency EIT system in development at the time of writing). Although these shall be discussed in more detail in the appropriate chapters, the HP based EIT system was primarily designed for tank imaging, it was slow in that it acquired an image every 25s, and accurate, but was only intended for human imaging under medical supervision and within the confines of the research laboratory. It was used to acquire the human and tank data presented in Chapters 2 and 3 (Tidswell *et al.* 2001; Tidswell *et al.* 2001; Tidswell *et al.* 2001). The Mark 1a and 1b UCLH systems are medically safe EIT systems, designed by the Department of Medical Physics at UCLH (University College London Hospital). They both used the same underlying technology, however improvements to the design of the Mark 1b system have reduced measurement noise and increased the number of measurement electrodes to a maximum of 64 compared to 16 in the Mark 1a. The Mark 1b UCLH EIT system was used to acquire the neonatal data, presented in chapter 4 (Tidswell *et al.* 2001; Tidswell *et al.* 2002).

1.3 Mechanism of Cerebral Impedance Changes

1.3.1 Introduction

There are several physiological mechanisms that may be responsible for the impedance changes demonstrated in rabbits during physiologically stimulated brain activity, epilepsy and spreading depression. These changes are a combination of changes in blood volume, and of changes in cell size (cell swelling) and cortical temperature during the various experiments. The increased impedance measured in rats during cerebral ischaemia (Holder 1992) and in rabbits during spreading depression (Boone *et al.* 1994) are a result of cell swelling. To understand how these physiological and pathological changes cause impedance change, some background information is required on how current travels through the brain, and the physiological responses that occur in the brain during neural activity, spreading depression and ischaemia.

1.3.2 How current travels in the brain

When an alternating current is applied to the head, the current is transferred between the electrodes by movements of free ions. This current will tend to take the path of least electrical resistance. When the current enters the scalp tissue, it will encounter a large resistance from the presence of the skull and so the majority of the current will pass through the scalp. This has been demonstrated experimentally inside a saline filled tank, which contained a real human skull, and in which the current was applied at electrodes in the 'scalp layer', outside the skull and current density measured within the skull (Rush and Driscoll 1968). This work demonstrated that approximately half the current applied in *polar-drive* from scalp electrodes, entered the cranial cavity. Similar results have been obtained in live, anaesthetised rabbits, in which scalp electrodes apply a current to the rabbit's head inside an MRI scanner; the MRI detects the magnetic component of the electrical current in two orthogonal directions, from which the current density can be calculated in each part of the head (Joy *et al.* 1999). This work demonstrated that 15% of the applied current entered the brain. Some of the difference between the rabbit and human skull experiments probably arise from different sizes and shapes, and the method of detecting current in a live animal, compared to a saline filled sank. However, if these results apply to EIT in the human head, then these studies provide limits on the size of attenuation of impedance changes due to the skull of a factor of between 2 to 7.

Once inside the skull, the CSF will provide a shunt path to the current due to its lower resistivity compared to brain, which are, respectively, 65 Ω.cm and 390 Ω.cm (Ranck 1963; Geddes and Baker 1967; Lattikka *et al.* 2001). However as the CSF has a low volume compared to the brain, a significant proportion of current will be conducted through the brain.

Once the current is in the brain, the current will be distributed through several anatomical compartments: the neuronal and glial cells, the extracellular space and the blood volume. Estimates of the size of these spaces in humans are unknown, although the cerebral blood volume (CBV) fraction has been non-invasively measured with PET in normal volunteers. The CBV varies between 1.9 to 3.5 ml/100g, or 2-3.5% of the brain volume (Derdeyn *et al.* 2002). In rabbits, the blood volume has been demonstrated to contribute to 10% of the impedance of the brain (Van-Harreveld and Ochs 1956), by an experiment in which blood was drained from the rabbit and replaced with a more conductive solution of 0.9% saline. Estimates of the extracellular space (ECS) in humans has to be derived from animal studies, in which invasive tests can be performed. Such measurements of the ECS, measured by die dilution techniques in rats, demonstrates that it comprises 12-18% of the brain volume. The resistivity of the ECS can be estimated from measurements of the ion concentration of the ECS in the exposed cat sensorimotor cortex (Dietzel

et al. 1982), which contains 146 mmol Na^+, 149 mmol Cl^- and 3 mmol K^+ ions. These results imply that the resistivity of the ECS is similar to 0.9% saline (140mmol NaCl) which has a resistivity of 51 Ω.cm at body temperature (Geddes and Baker 1967). The final two compartments, the neurones and glial cells, comprise the remaining 80% of the volume of the brain.

The relative size and contribution to the resistivity of the brain of these cells has been calculated on measurements of the impedance of rabbit cortex (Ranck 1963). In which the estimated volumes of the neuronal and glial cells were calculated to be 40% each of the cortex volume. In the same analysis, in which the resistivity of rabbit cortex was measured at 240 Ω.cm at 50 kHz (Ranck 1963), Ranck calculated that the path of a low frequency current in the brain would be predominantly through the large volume low resistivity glial cells, as well as the lower resistivity extracellular fluid space and blood volume. This is because although the blood and ECS have a lower resistivity than glial cells, they have less conductive volume, and therefore bulk current flow would be through the glial cells. The reason that glial cells conduct current is that they are permeable to potassium and chloride ions (Lux *et al.* 1986), unlike the neuronal cells which have a highly insulating membrane which is only permeable to ions during depolarisation with the action potential or during cell energy failure. This explains why in healthy brain, there is only a small amount of current that will conduct through the intra-cellular space of the neuronal cells due to their high membrane resistance. Some conduction does occur through neuronal cells, due to those nerves which are aligned with the direction of current flow; in this scenario the surface area of the cell membranes "seen" by the current is very large, and despite a high resistivity, the resistance to current is low.

Changes in impedance would therefore be expected from changes in blood volume, neuronal cell size and the size, and concentration of ions within the extracellular space. Such changes may arise directly from the neuronal activity, for example during sensory stimulation or during epilepsy, or the impedance changes may arise from the vascular changes of blood flow and blood volume that are a secondary consequence of neural activity. The physiology of these changes will be briefly considered.

1.3.3 Physiological Mechanism of Impedance Changes

1.3.3.1 Action potentials

The neurones of the brain transmit information to other parts of the brain or the body via action potentials propagated down the nerve axons. Action potentials are electrical signals which travel in an all or none fashion down the length of a nerve axon and are produced by the depolarisation of

the nerve from its resting membrane potential. So, when the visual cortex is stimulated, such as with a flashing checkerboard pattern, photons activate the rods and cones of the retina which transmit information to the visual cortex in the form of action potentials via the optic nerve, which result in large groups of stimulated neurones in the visual cortex which in turn transmit signals in the form of action potentials to other areas of the brain. In the visual cortex, billions of neurones are stimulated simultaneously, resulting in a large volume of activation over a strip of cortex several centimetres long and it is this group effect of neuronal activity and its effect on the blood vessels in the area that we wish to measure with EIT.

At the neuronal level and at rest, an inactive nerve has a resting potential across its membrane: this is due to a net positivity of ions on the outside of the cell compared to within maintained by an outward potassium (K^+) current which takes place because the neuronal membrane is permeable to K^+ ions and the concentration of potassium within the cell is twenty times that outside the cell. The potassium ions within the cell diffuse down the concentration gradient and charge the outer cell membrane positive with respect to the inside. As this positive charge builds up, it opposes further outward potassium current until an electrical gradient is reached which counterbalances the potassium concentration gradient. This electrical gradient is the resting potential (Hodgkin 1967).

The outward potassium current is partially counteracted by a small inward sodium ion current: the neuronal membrane contains voltage sensitive sodium channels which are closed at the membranes' resting potential and opened at a lower membrane potential, produced by nerve depolarisation. However at rest some of the sodium channels open randomly and allow sodium to enter the neurone down the electrical and sodium concentration gradient. The effect of this is small and the outward potassium current dominates. The sodium and potassium concentration gradients, across the neuronal membrane, are maintained by an ion pump, the Na^+/K^+ ATPase. This pumps 3 Na^+ ions out of the cell in exchange for 2 K^+ ions back into the cell. The net outward current of positive ions out also contributes to the resting potential. Because the Na^+/K^+ ATPase acts against both a concentration and an electrical gradient, energy is required for the pump mechanism; this energy is produced by the metabolism of high energy phosphate bonds from the molecule adenosine triphosphate (ATP). The ATP is broken down into 2 smaller molecules ADP (adenosine diphosphate) and inorganic phosphate and these smaller energy metabolites have a greater osmotic effect than the single molecule of ATP: therefore during high energy turnover, i.e. during periods of neuronal activity, the osmolarity inside the neurone is increased which results in a net influx of water (Lux *et al.* 1986), resulting in neuronal cell swelling.

When a nerve is depolarised, by afferent stimulation from other nerves or stimulation of a sensory receptor, the voltage sensitive sodium channels are opened and sodium ions enter the neurone down an electrical and concentration gradient. This inward sodium current depolarises the nerve membrane at and adjacent to that area, more sodium channels are opened and the process repeats itself further and further down the nerve: this propagation of depolarisation is the action potential. The action potential is transient and unidirectional because the sodium channels are only opened for a short period of time before they become temporarily refractory to further opening; this prevents back-propagation of the action potential up to its origin. After the sodium channels are closed the nerve resting potential is restored by the outward potassium current; once this repolarisation takes place and the sodium channels no longer refractory, the nerve is ready for the transmission of the next action potential. To restore the ionic concentration gradients after the action potential, the Na+/K+ ATPase activity increases which results in increased energy metabolism and increased intraneuronal osmolarity.

When whole groups of neurones are activated in a particular cortical area, the changes in ionic concentration, the increased osmolarity of the neurones and the need for increased oxygen and glucose has an impact on the cortical environment at a macro- and microscopic level. These changes affect the size of the cell volume, the size of the ECF and the blood supply to that cortical area which can be measured by a variety of methods. These methods are discussed in the following sections.

1.3.3.2 Ionic changes and cell swelling during neuronal activity

The simplified explanation of the action potential, illustrates the mechanism by which changes of intra- and extracellular ion concentration and cell swelling may occur as a result of neuronal activity. These changes have been measured experimentally.

In the exposed cortex of cats, epileptiform activity (Dietzel *et al.* 1982) increased the concentration of extracellular ions and decreased extracellular fluid volume. The reduction of extracellular fluid volume by 30 % was calculated to be due to two major mechanisms: 1) Neuronal cell swelling: due to increased intraneuronal osmolarity from the breakdown of ATP into smaller molecules by increased ATPase activity, which acts to draw in water from the extra-cellular space. Neuronal cell swelling accounts for approximately 8 % of the ECF volume reduction, 2) Glial cell swelling: the extracellular potassium ion concentration increased from 3 to 12 mmol as a result of enhanced neuronal activity and as glial cells are freely permeable to potassium, K^+ ions diffuse down a concentration gradient into the glial cells and are released into the extra-cellular fluid space in areas of low neuronal activity and low potassium concentration. This sets up a current along the

glial cells, transmitted in the extracellular fluid by a chloride ion current to the area of potassium release and a sodium ion current to the area of glial potassium entry. Because the sodium ions only partially replace the potassium and chloride ions which leave the extracellular space within the neuronally active area, there is a reduction in osmolarity and a subsequent diffusion of water into the higher osmolarity glial cells (Lux *et al.* 1986): the glial cells swell and the size of the extracellular space decreases. Cell swelling has also been detected with optical imaging techniques in the isolated cortex of the rat during electrical stimulation (Lipton 1972; Andrew and MacVicar 1994).

In summary these changes: 1) Increase cell swelling at the site of increased neuronal activity and reduce extra-cellular fluid volume and 2) Decrease cell size and increase extra-cellular fluid volume in surrounding areas of lower neuronal activity. The net effect of a 30% decrease of ECF volume and a 10 % increase in osmolarity will be to increase impedance at the neuronally active area (Figure 1.4). A smaller impedance decrease is expected in the surrounding less active area where potassium and water are redistributed into the extracellular space.

As this work has been performed in animals under extremes of neuronal activity, e.g. epilepsy or electrical stimulation of cortical slices, the cell swelling measured is not necessarily applicable to physiological ranges of neuronal activity such as those produced by evoked responses. However it is conceivable that repetitive neuronal stimulation from evoked responses would result in similar ionic and cell swelling changes of epilepsy, but to a lesser degree.

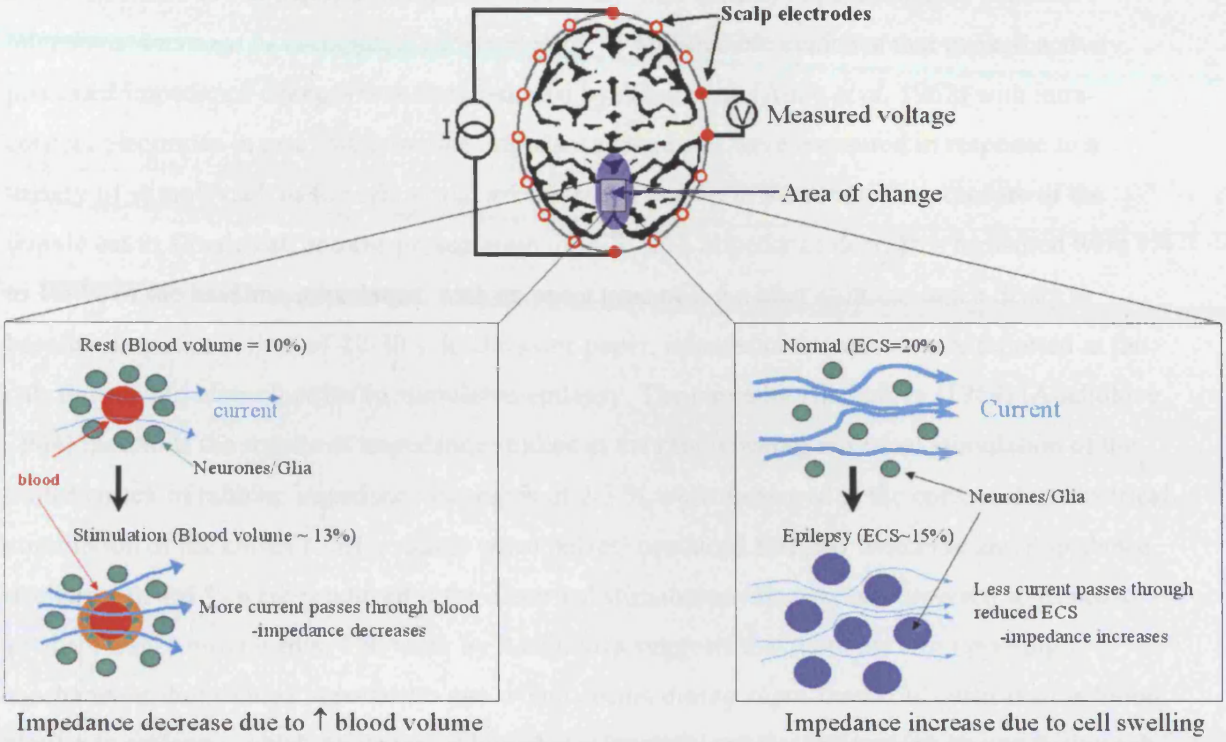

Figure 1.4 Mechanisms of impedance change within the brain
Left figure: **Impedance decrease due to increased blood volume.** This diagram represents the neuronal cells in green, with a blood vessel in the centre of the cells. During physiological activity, a signal is sent to the blood vessels which increases blood flow and blood volume to that cortical area (Malonek *et al.* 1997). As blood has a lower resistivity than the surrounding brain (150 Ω.cm and 350 Ω.cm, respectively), the increase in the lower resistivity volume of blood will allow more current to flow through that area of tissue and decrease the bulk impedance of that volume of cortex.
Right figure: Impedance increase due to cell swelling. In this figure, the cells are represented in green (top), and expand during cell swelling (blue - bottom). During normal function, the size of the conductive extra-cellular space (ECS) is 20% of the brain volume. During epilepsy, moderate cell swelling occurs as water and ions enter the glial cells and the neurones (Lux *et al.* 1986), and the volume of the low resistivity ECS is reduced. This will increases the bulk impedance of that area of cortex. Larger changes of cell swelling are seen during ischaemia and spreading depression, which cause much larger increases in brain impedance (Holder 1992; Boone *et al.* 1994).

1.3.3.3 Evidence for impedance changes during neuronal activity

Early evidence for impedance changes during physiological evoked responses is mentioned, but without much detail, in three papers. Van-Harreveld and Schade (1962) measured impedance increases of 3-10% in the rabbit brain with intra-cortical electrodes during stimulated seizures. Work of impedance recordings in the visual cortex of cats and rabbits during visual stimulation was

also mentioned in that paper in which they state that *'...in none of the experiments could an impedance increase be recognised with certainty.'* Reproducible evidence that evoked activity produced impedance changes was demonstrated by Adey et al. (Adey *et al.* 1962) with intra-cortical electrodes in cats: reproducible impedance decreases were measured in response to a variety of stimuli such as the cats visual attention to a person in the room, the exposure of the female cat to a male cat, and the presentation of milk. The impedance decreases measured were 1.4 to 1.8 % of the baseline impedance, with an onset time of 2-5 s after stimulus and a decay to baseline impedance time of 20-30 s. In the same paper, impedance increases were reported in the cats during and after electrically stimulated epilepsy. The paper by Aladjalova (1964) (Aladjolova 1964) mentions the results of impedance studies in the rabbit during electrical stimulation of the motor cortex of rabbits: impedance increases of 2-3 % were measured in the cortex when electrical stimulation of the cortex (50Hz, square wave pulses) produced forepaw twitching and impedance decreases of 1.5 % were produced if the electrical stimulation intensity was lowered so as not to produce motor movements. The work by Aladjalova suggests that there are two opposing mechanisms that change impedance: one which occurs during supra-threshold cortical stimulation, similar to epilepsy, which produces an impedance increase and the other which occurs during sub-threshold stimulation, which may be similar to physiological levels of neuronal activity, which produces an impedance decrease. These findings, although not presented in detail in his paper, seem to agree from the EIT studies of epilepsy and evoked responses in rabbits (Holder *et al.* 1996; Rao *et al.* 1997).

The imaging of impedance changes during evoked response and epilepsy in rabbits was first performed by Holder et al. (Holder *et al.* 1996; Rao *et al.* 1997). Impedance decreases of 2-5 % were imaged during evoked responses and impedance increases of 12 % during epilepsy. Simultaneous measurements of blood flow were measured with laser doppler flowmetry during epilepsy only and demonstrated significant increases of regional cerebral blood flow during epilepsy. The finding of an impedance increase during epilepsy contradicts the expected impedance change from the blood flow and predicted blood volume increase, as this would act to decrease cortical impedance due to an increase of the volume of low resistivity blood in relation to the high resistivity cortex. The likely explanation for this is that epilepsy also produces focal cell swelling, a finding in cortical slice preparations during electrical stimulation (Lipton 1972; Andrew and MacVicar 1994; Holthoff and White 1996). This would indicate that in the rabbit EIT studies, the area of epilepsy had a greater impedance increase produced by cell swelling than the impedance decrease produced by increased blood volume, and therefore an impedance increase was imaged.

The size of the impedance change reported in the rabbit EIT experiments was measured from the EIT images; as the size of an image change is not necessarily proportional to the actual impedance change, these values are estimates.

1.3.3.4 Haemodynamic changes with functional brain activity

Other studies have also demonstrated that cortical activity is associated with an increased cerebral blood flow and cerebral blood volume, the basis of which underlies human functional brain mapping with Positron Emission Tomography (PET) and functional Magnetic Resonance Imaging (fMRI) in humans.

Both changes of cerebral blood flow and volume have been identified in cat visual cortex during visual stimulation (Malonek *et al.* 1997). This study made invasive measurements of blood flow using laser Doppler flowmetry, and blood volume by optical spectroscopy. The optical spectroscopy technique measured changes in the reflectance of light at two different wavelengths, 605nm and 570nm, which are differentially sensitive to changes in deoxy-Haemoglobin and oxygenated Haemoglobin, respectively. During visual stimulation changes to reflected light at 570nm occurred almost immediately after stimulus onset and preceded the change in laser Doppler flow by 2 seconds; both changes peaked at 5-6 seconds after stimulus onset and decayed to baseline within 6s of stimulus cessation. The study indicates that blood volume increases prior to changes in blood flow, which is probably as a result of venous pooling in advance of arterial dilation. Other studies have also measured blood volume changes; in rats contrast MRI was used to give high resolution maps of changes of cerebral blood volume during forepaw and hindpaw stimulation (Palmer *et al.* 1999): a 5 minute stimulus increased blood volume in 5 rats which commenced 3-6 s after the onset of stimulation and returned to baseline 13-51 s after stimulus cessation. The findings from these animal studies indicate that blood volume increases occur as a consequence of neural activity, and also indicate the extent of the variation of the blood volume response.

In humans, similar changes of regional cerebral blood flow during visual stimulation are found with PET (Fox *et al.* 1986; Zeki *et al.* 1991; Zeki *et al.* 1993) and functional MRI studies (Belliveau *et al.* 1991; Kwong *et al.* 1992). The time course of the blood flow response from fMRI studies (Kim *et al.* 1993; Karni *et al.* 1995; Tootell *et al.* 1995) is similar to that measured in animals: blood flow increases 1-2 s after stimulus presentation, rises to a peak at 5-7 s and then decays to baseline blood flow within 6-10 s of stimulus cessation. These findings are reproducible across a variety of different cognitive, motor, and sensory paradigms. In addition, parallel increases in cerebral blood volume have been shown to occur with increased blood flow occur, as demonstrated with Near Infra-Red Spectroscopy (NIRS) studies in adults (Villringer *et al.* 1993;

Meek *et al.* 1995) and in infants (Meek *et al.* 1998; Sakatani *et al.* 1999; Bartocci *et al.* 2000; Benaron *et al.* 2000; Bartocci *et al.* 2001; Hintz *et al.* 2001; Isobe *et al.* 2001; Zaramella *et al.* 2001). Because of the lower resistivity of blood compared to brain, then these studies indicate that a rise in local cortical blood volume will decrease cortical impedance during functional activity.

The size of the impedance change which may be expected due to changes of blood volume can be estimated from a study in which the overall contribution of cerebral blood to brain resistivity was measured in rabbits (Van-Harreveld and Ochs 1956). In this study, the impedance of exposed rabbit cortex was measured while the resistivity of the blood, initially at 133 Ω.cm, was decreased by dilution with Ringer's solution, which has a resistivity of 59 Ω.cm. As the resistivity of blood is mainly determined by the ion containing plasma, an increase of plasma to red cell mass by this dilutional method decreased resistivity. The contribution of blood to the resistivity of the brain was measured by this method and was calculated at 9-13%, and gave similar results to the measurement of brain impedance when the brain was drained of blood in the same study. If the cerebral blood volume in humans contributes 10% of the brain resistivity, then an increase in blood volume of around 30 % would produce an approximate 3 % impedance decrease (Figure 1.4), although this figure is a likely overestimate as cerebral blood volume may not show a linear increase with blood flow.

1.3.3.5 Other possible contributions to cerebral impedance change

There are two additional factors which may influence the impedance of brain but for which there is little experimental information. During increased neuronal and therefore metabolic activity an increased generation of heat may occur which would increase brain temperature. Decreased brain temperature increases brain impedance by approximately 2-3 % per degree Celsius change (Van-Harreveld and Ochs 1956; Li *et al.* 1968). Small increases of temperature by up to 0.4 °C were measured by Rao et al. (Rao 2000) during epilepsy, which would account for only 1-1.5 % of the 10 % impedance change measured. The temperature change may have been the result of the experimental preparation as the exposed cortex was at a lower temperature than the body temperature of the rabbit (by 2 °C); therefore the temperature increase could have been due to the effect of increased blood flow at body temperature to the epileptic cortex. As the exposed cortex was subject to atmospheric cooling during the study, the measured temperature changes during seizures are not likely to occur in the brain in the intact animal, due to the maintenance of the cortical temperature closer to the body temperature. However, such temperature changes have been detected non-invasively, with combined MRI and fMRI, in humans during prolonged visual stimulation (Yablonskiy *et al.* 2000). The study studied the MRI signal frequency in voxels within

the visual cortex, and in control voxels outside it, while a prolonged, 4 minute visual stimulus was given to the subjects. The study measured changes in the frequency of the MRI signal in the visual cortex voxels, which corresponded to a BOLD increase, and no change in MRI frequency in control voxels. As the frequency of the MRI signal is temperature dependent, the change in MRI frequency in voxels in the visual cortex represented changes in cortical temperature; these MRI frequency, and therefore temperature changes could either increase or decrease, occurred after approximately 1 minute of stimulation, and were not present in all subjects. The cortical temperature could change by up to 1°C during functional activity, with an average 0.2°C decrease in temperature after 1-2 minutes of visual stimulation. Such cortical temperature changes could produced changes in impedance, which could be detected by EIT, however these changes would occur over minutes, rather than changes over seconds expected by blood volume change.

The second factor that may affect impedance is a change in the cerebro-spinal fluid (CSF) thickness which overlies the activated cortex: an expansion of local cerebral blood volume would shift small amounts of CSF to areas of lower volume. The effect of seizures on CSF pressure has been investigated in two human studies (Minns and Brown 1978; Gabor *et al.* 1984). Changes of CSF pressure, monitored by indwelling intracranial pressure sensors, were measured during seizures in 7 subjects. The cause of the pressure change is likely to be due to an increase in cerebral blood volume due to increased cerebral blood flow which occur during seizures (Vollmer-Haase *et al.* 1998); the brain volume will attempt to increase into the CSF with a resultant pressure rise. A smaller change in cerebral blood volume would be expected from local cerebral blood volume change in neuronally active cortex during functional stimulation, which is likely to shunt CSF away from the cortex with increased volume. If this occurs locally during functional stimulation, the overall effect would be a decreased cortical impedance, due to a larger volume of blood, which would be offset by a local increase in impedance in the thinned layer of CSF over the activated cortex; as this would produce opposing impedance changes in the same area, then the overall effect on impedance measured from the scalp by EIT is difficult to predict, and may depend on how superficial or deep the stimulated area of cortex is to the superficial layer of CSF.

1.3.3.6 Summary

The evidence discussed so far suggests that there are two major physiological changes which will produce brain impedance changes, these are: 1) Changes of blood volume during functional brain activity, and 2) Cell swelling measured during epilepsy, ischaemia and spreading depression.

When applied to the results of the rabbit EIT experiments both these mechanisms seem to have a role (Holder *et al.* 1996; Rao *et al.* 1997), during functional activity an increase in regional blood volume during sensory stimulation accounts for impedance decrease imaged. However, in seizures where cerebral blood flow was known to increase, yet an impedance increase was measured, the implication is that the impedance increase due to cell swelling is greater than the impedance decrease produced by the increase in regional cerebral blood volume.

In the light of available evidence, from preliminary studies of impedance changes in the animal brain, to the demonstration that blood flow and blood volume changes occur during sensory stimulation in adults, it appears likely that significant impedance changes will occur in the human brain during functional activity, and that these changes are of a magnitude that could be detected with EIT from measurements made from scalp electrodes. It also seems likely that during physiological levels of activity, impedance decreases should be imaged in areas of cortex expected to undergo increased neural activity during functional stimulation. However, before progressing, an overview of current human functional imaging methods will be briefly discussed.

1.4 Overview of Adult Functional Neuroimaging

1.4.1 Other methods of human functional imaging

The evidence, in humans, that cortical blood flow (CBF) and cortical blood volume (CBV) changes occur during stimulation is provided by the adult neuroimaging literature, particularly in studies which have used PET and fMRI. Information provided by these studies, imply that impedance changes should occur in the adult cortex during sensory stimulation.

The physiological changes that PET and fMRI measure are similar, in that the signal they measure arise from changes in cerebral blood flow, produced as a secondary consequence of increased neuronal activity (Logothetis *et al.* 2001). The techniques used in PET and fMRI to study such haemodynamic changes differ. The similarity between these two methods arise from the sensory or cognitive paradigms used to produce changes in blood flow. The basic principle is similar to that used by difference imaging with EIT, discussed in Chapter 1, by which images are constructed of blood flow *change* in comparison to a baseline condition.

Positron Emission Tomography

Images obtained with PET, depend upon the uptake of tissues of an injected positron emitting tracer such as ^{15}O-labelled water. The PET scanner detects gamma rays produced when a positron,

emitted by the tracer, collides with an electron and both are annihilated. As the gamma rays travel in opposing directions from the point of annihilation, if the two gamma rays are detected simultaneously by the array of detectors surrounding the head, then the PET scanner can calculate the line along which the annihilation event took place. PET scanners which can detect the time difference between the time of arrival of the two photons can also determine where along that line the annihilation event took place. As many annihilation events are recorded, a 3D image of the source of activity can be reconstructed. Increased areas of activity in an image, represent areas of increased uptake of the tracer, which is proportional to the blood flow to that area of tissue. Therefore, areas of tissue which increase blood flow during a particular task, or stimulus, will have increased signal when compared to the resting baseline PET image.

During a cognitive or sensory stimulation experiment, different areas of brain will be subject to increases or decreases in regional cerebral blood flow (rCBF), which can be detected by this method. One example is the increased blood flow in the visual cortex which occurs during visual stimulation (Fox *et al.* 1986; Zeki *et al.* 1991; Mentis *et al.* 1996; Mentis *et al.* 1998). The purpose of the experimental design is to develop stimuli which will differentially activate different areas of the brain, and the changes detected by the PET study will allow the study to draw conclusions about the functioning of the brain under these different experimental conditions.

In the visual cortex, for example, simple flash stimuli of increasing frequencies have been demonstrated to produce a proportional increase in the change in rCBF in the primary visual cortex (Mentis *et al.* 1996). The use of annular checkerboard patterns in different areas of the visual field have allowed mapping of the retinotopic map of the primary visual cortex (Fox *et al.* 1986), and the use of colour and movement stimuli have allowed experimenters to delineate the colour and movement areas of the visual cortex (Zeki *et al.* 1991) and have even produced activation of the movement area of the visual cortex with illusory visual motion stimuli (Zeki *et al.* 1993). Such studies not only confirm invasive experimental evidence obtained from animal experiments, and neuro-pathological studies in humans (Zeki 1990) but also allow experimenters to determine the haemodynamic changes that occur during the progression of neurological disease, such as Alzheimer's Dementia (Mentis *et al.* 1996; Mentis *et al.* 1998), or to detect changes of cerebral blood flow that occur during sleep (Braun *et al.* 1997; Maquet *et al.* 1997). The use of PET has therefore increased our understanding of the function of the brain, at least from a neuro-haemodynamic model of human brain function.

The advantage of PET is its flexibility as it can also be used to provide information about other physiological parameters of the brain, by the measurement of blood volume (Derdeyn *et al.*

2002) and the cerebral metabolic rates of glucose and oxygen (Chugani *et al.* 1987; Altman *et al.* 1993; Kinnala *et al.* 1996). However the disadvantages of PET are that the images have a relatively long acquisition time of up to 2 minutes (Mentis *et al.* 1998), and that PET involves the use of a dose of radiation in the radiolabelled tracer. The first places time constraints on the experimental paradigm used in the study and the second limits the number of scans that a subject can have within a session and within a year, due to cumulative doses of radiation. The other limitation of PET is its availability, as the positron emitting tracers have a short half-life and need to be produced in specialist centres with access to a linear accelerator; these requirements limit the use of PET to geographical regions near such accelerators.

Although PET is still widely used for functional imaging, advances in the field of fMRI over the last decade have resulted in widespread research in functional neuroimaging, mainly because of the more widespread availability of MRI scanners.

Functional Magnetic Resonance Imaging (fMRI)

Since the early 1990's, the development and use of fMRI in human functional imaging studies has been rapid. Functional MRI has several advantages, due to a much faster image acquisition time of a few seconds (Kwong *et al.* 1992) compared to minutes required for PET scans, the high resolution of the images which allow detailed (and media friendly) maps of rCBF changes to be imaged, the widespread availability of MRI and the absence of irradiation for the subjects studied. Research with fMRI also benefits from freely available image analysis software, such as the Statistical Parametric Mapping programs produced by the Functional Imaging Laboratory in London (www.fil.ion.ucl.ac.uk (Frackowiak *et al.* 1997)).

The physiological mechanisms responsible for changes in the signal detected with fMRI differ to that of PET. Functional MRI detects changes in the blood oxygen level dependent (BOLD) signal in the brain. This signal is dependent on the concentration of oxygenated haemoglobin (oxy-Hb) in the tissues, so as regional cerebral blood increases the supply of oxy-Hb is increased and an increase in the BOLD signal is detected, which in turn implies an increase of local neural activity. The difference between the BOLD signal and PET, is that the BOLD signal can be attenuated by increases in the concentration of deoxygenated haemoglobin (deoxy-Hb), which will be produced by increased oxygen extraction and metabolism of the neuronally active cortex. In comparison, the PET signal is only dependent on blood flow.

Theoretically rCBF may increase with an increase in the concentration of deoxy-Hb and a BOLD decrease occur. This has been demonstrated to occur in the visual cortex, during visual stimulation, in adults sedated with phenobarbitone (Martin *et al.* 2000). It is not possible to

determine whether the BOLD decrease is the result of decreased rCBF or an increased rate of metabolism of oxygen in the cortex in relation to the oxygen supply. In neonates, BOLD decreases are usually detected during stimulation, despite the absence of sedation. This reversal of the BOLD signal, in unsedated neonates, seems to occur despite an increase in blood flow to the activated cortex. This is illustrated by a comparison of two studies which measured the signal changes in the auditory cortex of unsedated neonates subjected to auditory stimulation; one in which the haemodynamic changes were measured with near infra-red spectroscopy (Zaramella *et al.* 2001) and the other which used fMRI (Anderson *et al.* 2001). The near infra-red study demonstrated that although blood flow and blood volume increased, the concentration of oxy-Hb and deoxy-Hb (measured with respect to the volume of cortex under the detectors) both increased in two thirds of the infants. This increase in the level of deoxy-Hb, would attenuate any BOLD signal increase produced by the rise in oxy-Hb. This was the finding of the second, fMRI study, in which BOLD decreases were imaged in the auditory cortex of two-thirds of the infants. These findings indicate that the cerebral metabolic rate of oxygen exceeds the increase of oxygen supply to the brain, despite an increase in rCBF.

In contrast, in adults, NIRS demonstrates increased blood volume, increased oxy-Hb and decreased deoxy-Hb concentrations over the visual cortex during visual stimulation (Meek *et al.* 1995). This would be expected to increase the BOLD signal in the adult visual cortex during stimulation, borne out in several fMRI studies of vision (Ogawa *et al.* 1993; Schneider *et al.* 1993; DeYoe *et al.* 1994) and also the finding of the adult auditory cortex, used as a control group for the neonatal fMRI study of auditory activation (Anderson *et al.* 2001).

This presents a problem for fMRI in that areas of brain which have a higher metabolic demand for oxygen than their supply may cause a negation or even a decrease of the BOLD signal, which has implications for studies which only report BOLD increases, as areas of brain which are active are ignored by the statistical analysis. One way around this is to compare the results obtained with both BOLD fMRI and PET in the same subjects with similar paradigms (Kinahan and Noll 1999). An alternative is to compare the relation of the BOLD signal and the cerebral metabolic rate of oxygen with graded stimuli, this has been performed for the visual cortex, in which the ratio of oxygen supply to metabolism is 2:1 (Hoge *et al.* 1999; Hoge *et al.* 1999; Hoge and Pike 2001). It may be reasonable to assume a metabolic parity between the visual cortex and other areas of the brain, however, as yet, studies have not yet tested this hypothesis, and in the human neonate this metabolic ratio does not appear to be appropriate, as the BOLD decreases are probably a result of oxygen metabolism exceeding supply. Despite this caution, BOLD-fMRI has had many uses in

identifying areas of brain activated by a wide variety of cognitive or sensory paradigms, and more practical uses of fMRI have been found in applications such as imaging inter-ictal epileptiform activity (Lemieux *et al.* 2001; Lemieux *et al.* 2001) or identifying important areas of the brain prior to resective neurosurgery (Bookheimer 1996).

Design of experimental paradigms

Probably the most important aspect of functional neuroimaging studies is the design of the experiment. The paradigms used for the EIT studies of adult brain function (Chapter 2) and neonatal brain function (Chapter 4) are very simplistic in comparison to current methodologies in use in functional imaging studies. In the EIT studies of this chapter, a block design experiment was used (Figure 1.5), which consisted of a 150s baseline, in which there was no stimulation, followed by a 75s stimulation period with either a visual or sensory stimulus or an active hand movement, followed by a final baseline of 150s. This experimental design allowed sufficient EIT images to be obtained during baseline and stimulation periods to be certain that if there was a change, then there would be enough data to allow a statistical analysis of the impedance change.

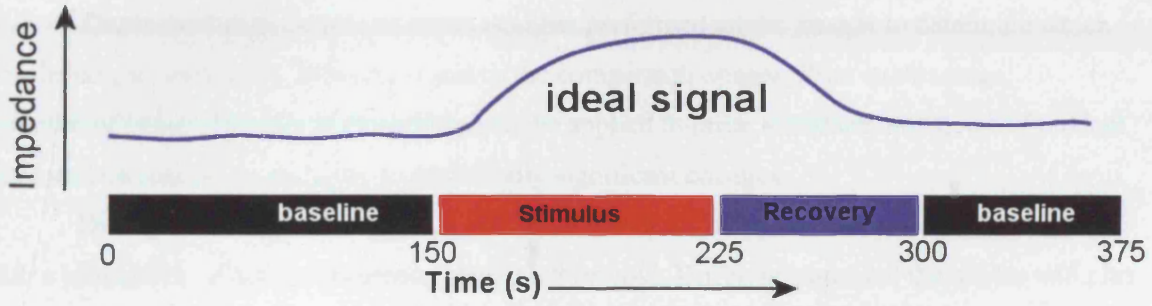

Figure 1.5 Illustration of experimental design, using a block paradigm for the EIT studies
An idealised EIT signal (top, blue line) is shown, with the experimental design illustrated below. EIT images were obtained continuously for 150s (baseline, at rest), followed by a 75s stimulation period, then the stimulus was switched off and a further set of baseline images obtained during recovery (in which the impedance change would return to the baseline resting level) and a further set of baseline EIT images used for the linear correction of baseline impedance drift.

The design used in these EIT studies, is very similar to those fMRI studies in which a block design paradigm is used (Frackowiak *et al.* 1997). An alternative method, used for fMRI, is called the event design, in which images are obtained of the BOLD signal produced by a very brief stimulus. The advantage with an event related design, is that many more events or stimuli can be used and alternated during the experiment. As the image acquisition time for the EIT studies presented in Chapter 2 was 25s, then this event related design was unsuited to the EIT studies.

Often in fMRI studies, the baseline/resting images are obtained while the subject performs a minor attention task, such as fixating on a cross hair on a screen prior to the onset of a visual stimulus (Gjedde and Marrett 2001), or a more complex task as a result of a cognitive subtraction paradigm. These 'active' baseline conditions are designed to maintain the subject's attention during the course of the study, which may produce confounding cerebral blood flow changes.

Statistical image analysis and thresholding

At this point, it is worth briefly reviewing some of the current statistical approaches used to analyse images of brain activity. The approaches used in analysis of PET and fMRI images have two main stages. The first stage warps the images onto a standard brain template, which enables the images to be averaged between subjects. Otherwise an activation in the somatosensory cortex of one subject may not be aligned with other subjects and therefore a group average of the images would not demonstrate a significant activation. This stage of image processing is not suited to EIT at the moment, as the difference images obtained by EIT do not contain structural information to allow image co-registration between subjects.

The second stage is the statistical analysis performed on the images to determine which voxels have a statistically different signal to the comparison images. Prior to this stage, a means of image filtering or smoothing may be applied in order to reduce the effects of random noise and increase the sensitivity to statistically significant changes.

During the statistical analysis, a statistical threshold is applied to show only those voxels with a probability of activation greater than the threshold. Different statistical thresholds will alter the way in which an image appears, as higher and higher thresholds will demonstrate a smaller number of activated voxels. In performing the statistical analysis with SPM (Frackowiak *et al.* 1997), each pixel in an image series is examined to see how it fits to a generic haemodynamic response function (a mathematical model of the BOLD response over time for a brief stimulus, fitted or convolved to the duration of the stimulus). This is applied using the General Linear Statistical Model. Voxels with a good fit to the haemodynamic response function have a higher probability of 'activation'. Those voxels which do not fit the function, either due to a small or non-existent signal change or, conceivably, a stimulus related signal change that does not fit the function, will score a low probability. The probability is given as a t-value (Student's t-test), or is normalised to a Z-value.

The next step is to correct for the multiple statistical comparisons made by performing such t-tests on each voxel in an image which may contain up to 30,000 voxels (for an image of 64 pixels square, with 16 slices). One method of doing this is to use the Bonferroni correction, which

corrects the level of significance used in a statistical analysis to compensate for multiple tests. An example to illustrate this method is if multiple tests are performed with a confidence level of 0.95, on random data. Twenty such analyses will be likely to throw up one or two 'significant' results, which arise by chance. The way around this is to reduce the p value, **alpha**, used to reject the null hypothesis of no difference for each of the **k** statistical comparisons. The overall confidence level of 0.95 is used in the following equation to calculate **alpha**:

$$\textbf{overall confidence level}=(1-\textbf{alpha})^{\textbf{k}}$$

So for a confidence level of 0.95, and 20 comparisons, the p-value used to accept or reject the null hypothesis for each test, will be reduced from 0.05 to 0.0026. Only tests which give a probability value of less than alpha will be used to reject the null hypothesis.

In practice, the Bonferroni correction is suited towards multiple statistical comparisons on independent data sets. However, in the case of image analysis, an activation at each voxel is not independent. For example, during simple visual stimulation, a cluster of voxels activated in the primary visual cortex are related events and not independent of each other. The probability that a large number of adjacent voxels show a signal increase, would have a vanishingly small probability that they were activated by chance. Therefore clusters of voxels increase the probability of a real activation in that region and some form of statistical correction is made for voxels activated in clusters, reducing the alpha level at which the null hypothesis is rejected. This prevents studies falsely accepting the null hypothesis that there is no change.

The final interpretation of the fMRI and PET images therefore depend on the significance level at which the images are thresholded. This is usually at a corrected threshold of $p<0.05$, but some studies use much higher levels of thresholding, perhaps to demonstrate only limited areas of activation. In addition, when interpreting the results of fMRI research, it is also important to consider what correlations were examined in the data analysis and whether the data were examined for both signal increases and signal decreases. The tendency to look for signal increases may be due to the relatively easy explanation that these arise form areas of increased neural activity from which inferences about different cortical regions and their relation to the task may ensue. BOLD decreases, which are more difficult to explain, have been found in two studies during motor activity (Ogawa *et al.* 1993; Nirkko *et al.* 2001), but not in similar motor fMRI studies in which only positive correlations between the BOLD signal and the graded motor task seemed to have been examined (Boecker *et al.* 1994; Oostende *et al.* 1997; Ye *et al.* 1997). When negative correlations between the signal and the stimulus are examined, surprising results are reported. Examples of this are two PET studies which used a graded, frequency variant visual stimulus (Mentis *et al.* 1997;

Mentis *et al.* 1998) in which a positive correlation between flash frequency and rCBF increase was seen in primary visual and visual association cortices - this is as expected. However the unexpected finding of a negative correlation between flash frequency and rCBF in the frontal cortex was more difficult to explain as there seems little logic as to why visual stimulation should decrease blood flow in the frontal cortex. Similar findings of decreased BOLD signal during motor activity have been demonstrated with unthresholded fMRI images (Nirkko *et al.* 2001). These studies serve to illustrate how the analysis of the data may affect the conclusions of functional imaging studies. The phenomena of BOLD signal decreases and blood flow decreases indicate that the brain is more complex than the *neural activation=blood flow increase* model implies.

The final caution of interpretation is whether the studies have examined the entire brain, or looked at a specific region of interest in the analysis. Examining a region of interest has the advantage that the number of voxels in the region is smaller, and therefore the correction for multiple comparisons is smaller, so that smaller signals will not be thresholded out by an analysis of the entire brain. This is perfectly justified if the study aims to demonstrate changes within a particular area of cortex, expected to be activated by the stimulus. An example of such a study is the use of a region of interest around the visual cortex when examining for retinotopic mapping by fMRI (Hoge *et al.* 1999).

The work in this thesis does not use the statistical image packages mentioned above, although some of the techniques such as statistical thresholding are used. This is because the impedance response to stimulation was unknown and therefore the haemodynamic response function used for fMRI would not be appropriate. There are also differences between the images obtained with fMRI and PET, in comparison to EIT: the signal at a voxel in a PET of fMRI image is relatively independent of signals in other voxels of the image (prior to spatial smoothing). In contrast the signal in one voxel of an EIT image is shared by all the other voxels but with different sensitivities, this arises from the sensitivity matrix in which a boundary voltage change produces a change of different size in all the voxels of the EIT image. Therefore a statistical analysis which assumes a relative independence of signal between voxels would be inappropriate to use on EIT.

1.5 Functional brain imaging in the neonate

1.5.1 Overview

So far, I have concentrated on reviewing techniques which have been used to investigate the neuro-haemodynamic changes during functional activity. Although these techniques will be useful to test

EIT as an imaging system to known stimuli, one of the aims of EIT research is to provide a neuroimaging tool that is useful in the clinical setting.

One of these settings would be in Neonatal Intensive Care, where sick infants on life support are at risk of different mechanisms of brain injury and it is important to understand what happens to their brain function, in order to improve standards of neonatal care and their neurological outcome. This review revises some of the brain injuries that neonates are susceptible to, the current methods of providing functional neuroimaging information about these infants, and the possible applications of EIT in the Neonatal Intensive Care setting.

Neonatal Intensive Care is designed to provide life support and treatment to infants with life threatening conditions. This treatment differs between infants born prematurely, from 23 weeks gestation, than those born at term, as premature infants require life support for undeveloped systems; examples are ventilation, cardiac support, and nutritional support. At term, from 36 weeks gestation, infants are mature enough to survive ex-utero, but they may develop life threatening problems which require specific treatments, such as antibiotics for neonatal sepsis, phototherapy or blood transfusions for neonatal jaundice, glucose infusions for neonatal hypoglycaemia, respiratory support for sepsis or meconium aspiration, or life support and anticonvulsant therapy after birth asphyxia.

These conditions subject the premature and full term neonatal brain to a variety of stresses that affect the growth, development and function of the brain. One of the goals of neonatal research is to provide information about the brain in order to optimise treatment for these infants. Neuroimaging techniques, such as ultrasound, allow clinicians to monitor the structure of the neonatal brain. One of its uses is to monitor the development of intra-ventricular haemorrhage (IVH) or periventricular leucomalacia (PVL) which can affect up to 20% of premature infants (Volpe 1995). Such information may influence decisions about whether to withdraw intensive care, or inform clinicians of the likelihood of physical or learning disabilities. In addition, if clinical factors which lead to brain damage can be identified, then steps can be made to improve the care of the premature infant and improve the outcome of future neonatal care.

Common clinical methods used to image the neonatal brain are: cranial ultrasound, structural T1 or T2 weighted Magnetic Resonance Imaging (MRI) and Computerised Tomography (CT). However, as the purpose of this chapter is to develop a neuroimaging technique that provides functional information, then these structural imaging techniques will not be discussed further.

Functional imaging techniques have been used to provide information about how the neonatal brain works in normal and pathological conditions. Most of these techniques, such as

functional Magnetic Resonance Imaging (fMRI), Positron Emission Tomography (PET) and Near Infra-Red Spectroscopy (NIRS), have been used as research tools to demonstrate that changes in cerebral blood flow (CBF) or cerebral blood volume (CBV) occur under conditions such as sensory stimulation, seizures, post-asphyxia and during drug intervention. In addition, the use of Magnetic Resonance Spectroscopy (MRS) and Diffusion Weighted Imaging (DWI) has been used to provide information about ischaemic brain lesions in neonates. However the most widely used clinical technique to provide functional brain information is Electroencephalography (EEG), used primarily for the detection of neonatal seizures. These techniques will now be discussed more fully.

1.5.2 Electroencephalography (EEG)

Although EEG is not usually regarded as an imaging technique, it uses scalp electrodes to provide a topographical map of cortical electrical activity. EEG is portable, so can be used at the cotside during intensive care.

EEG has two main clinical uses: 1) To diagnose abnormalities of brain activity, such as seizures, and 2) To report on abnormalities of background activity which can arise from a variety of disorders

Use of EEG in seizures

Many studies have investigated the role of EEG in the diagnosis of seizures, which occurs in up to 5% of infants in neonatal intensive care (Sheth 1999). As seizure activity can occur anywhere in the cortex, the tendency for neonatal seizures to remain focal (Bye and Flanagan 1995) means that clinical seizure activity is only apparent if the motor cortex is affected. In one neonatal EEG study 85% of electrical seizures did not produce clinical activity (Bye and Flanagan 1995). Therefore EEG can be clinically important in the detection of seizures without clinical activity and enable appropriate anti-convulsant treatment to be given.

However, EEG is only sensitive to small areas of cortex below the scalp electrodes, as demonstrated by improved seizure detection in a study which compared simultaneous 12 and 4 electrode EEG (Bye and Flanagan 1995), in which 2/30 infants had seizures missed by the limited 4-electrode EEG. The physical reason for this is that the sensitivity of a scalp electrode to a voltage source is inversely proportional to the distance separating the two. In practice, this means that seizures in deeper brain structures and cortex a long way from the scalp electrodes may not be detected by the EEG. Seizure detection can be improved by using more scalp electrodes, but this does not alter the sensitivity to electrical seizure activity in deeper brain structures. The reduced sensitivity to deep seizures is probably the reason for the phenomenon of electro-clinical

dissociation in which obvious clinical seizure activity occurs, without EEG evidence of seizure activity.

The finding that impedance changes occur during seizure activity (Van-Harreveld and Schade 1962; Rao *et al.* 1997) indicates that EIT could be used to detect seizure activity in the newborn. EIT would have the advantage that it was sensitive to changes deep in the brain – not just to surface changes, and therefore improve seizure detection.

1.5.3 Neonatal functional imaging with fMRI, PET and NIRS

1.5.3.1 fMRI in neonates

In contrast to many thousands of fMRI studies performed in adults, there are only a handful of fMRI studies in neonates and children. This probably reflects the difficulty of keeping infants still inside a scanner unless sedated or asleep, which therefore limits the complexity of the stimulus paradigms that can be used, such as flash visual stimulation (Yamada *et al.* 1997; Martin *et al.* 1999; Morita *et al.* 2000) or auditory stimulation (Anderson *et al.* 2001). Results are usually obtained in 70-80% of infants with sedation, and the study of auditory stimulation in 70% of unsedated infants (Anderson *et al.* 2001). Similar findings have been found in both unsedated and sedated infants, which differ to the BOLD findings of adults.

Whereas in adults, the BOLD-fMRI response increases in response to stimuli, due to increased regional cerebral blood flow (rCBF) delivering an increased oxygen in excess of local oxygen metabolism (Hoge *et al.* 1999), in neonates the BOLD response is often reversed and a BOLD decrease is measured to visual (Yamada *et al.* 1997; Martin *et al.* 1999; Morita *et al.* 2000) or auditory (Anderson *et al.* 2001) stimulation. This implies that the concentration of deoxy-haemoglobin in the active cortex is increased during increased neural activity due to either: 1) Reduced regional cerebral blood flow (rCBF), 2) Increased oxygen extraction by the cortex over and above the increase in oxygen supply by increased arterial blood flow or 3) A haemodilution effect, due to an increase in deoxygenated blood volume by volume expansion of the venous bed.

Support for a reduction in rCBF during stimulation has been found in some sedated infants during visual stimuli in which both the BOLD response was measured and found to decrease which corresponded to a decrease of rCBF measured by the FAIR technique (Martin *et al.* 2000). However these infants were sedated and as sedation has been shown in monkeys to reduce the BOLD response (Logothetis *et al.* 1999), then this finding may be related to sedation rather than the underlying neonatal cerebral physiology. Stronger evidence from PET and near infra-red spectroscopy (NIRS) suggests that the neonatal brain produces an increase in rCBF to stimulation,

but there is an increase of oxygen extraction by the brain which exceeds oxygen delivery; this increases the concentration of deoxyhaemoglobin and accounts for negative BOLD response. Support for this hypothesis will now be considered.

1.5.3.2 PET in neonates

PET studies have been useful in providing information about neonatal cerebral blood flow (CBF), the cerebral metabolic rates of glucose (CMR-glucose) and the cerebral metabolic rate of oxygen ($CMRO_2$). Similar CBF information has been obtained by $Xenon^{133}$ clearance studies (Colditz *et al.* 1988; Baenziger *et al.* 1999) in normal infants, the results of which will be included in this section. The CBF values measured with PET in infants normal at follow-up and Xenon clearance studies in normal infants agree, with a value of 10-20ml/100g/min. In contrast, CBF in adults is up to 3 times greater at 40-50ml/100g/min (Friston *et al.* 1990; Ramsay *et al.* 1993; Arndt *et al.* 1996), yet the CMR glucose is only slightly greater in adults at 25-33 micromol/100g/min (Chugani *et al.* 1987) than in term neonates at 15-25 micromol/100g/min (Chugani *et al.* 1987; Kinnala *et al.* 1996). These differences suggest that a similar proportional increase in the metabolic rate of glucose between neonates and adults requires a much greater proportional increase in rCBF. If the increase in rCBF is proportional to resting levels then in neonates the situation may arise in which the brain depletes oxygen more than the increased supply, resulting in increased deoxy-haemoglobin concentrations and producing a decreased BOLD signal.

1.5.3.3 Near-Infra Red Spectroscopy in Neonates

Further support for the hypothesis of increased oxygen extraction in the neonatal brain accounting for increased deoxy-haemoglobin concentrations in active cortex has been provided by Near Infra-Red Spectroscopy (NIRS), which has become an increasingly popular method of detecting blood flow and volume changes in the neonatal brain. NIRS can be used to detect changes in oxy-haemoglobin (HbO_2) and deoxy-haemoglobin (deoxy-Hb) during an activation task compared to a null baseline condition. These measurements then are combined to measure the total change in haemoglobin, which represents the change in regional cerebral blood volume (rCBV). Initial neonatal work with NIRS has used single channel measurements, in which a light emitter and detector are placed over a particular region of the brain (Meek *et al.* 1998; Zaramella *et al.* 2001). Although such studies do not provide images of brain activity, topographical images of motor evoked blood flow changes have been achieved with multi-optode NIRS systems (Isobe *et al.* 2001).

The results of single and multiple channel NIRS neonatal studies are similar. In general, during sensory stimulation in the neonate, an increase in HbO_2, deoxy-Hb and therefore cerebral

blood volume all occur in the visual cortex during visual stimulation (Meek *et al.* 1998), the motor cortex during passive motor movements of the arms or legs (Benaron *et al.* 2000; Hintz *et al.* 2001; Isobe *et al.* 2001), over the temporal cortex during auditory stimulation (Zaramella *et al.* 2001) and over the frontal cortex during the presentation of different smells (Bartocci *et al.* 2000).

The results of NIRS studies supply evidence as to the cause of the negative BOLD-fMRI response in infants. In studies performed without sedation an increase in the concentration of deoxy-Hb occurs in 90% of infants during visual stimulation (Meek *et al.* 1998) and two-thirds of infants during auditory stimulation (Zaramella *et al.* 2001). A similar proportion of unsedated infants demonstrate a negative BOLD-fMRI response during auditory stimulation (Anderson *et al.* 2001). The results of such studies indicate that blood flow and blood volume increase during stimulation, but it is the increased concentration of deoxy-Hb which is the cause of the negative BOLD response.

It is interesting (but not necessarily relevant to this thesis) to consider why increased cerebral oxygen extraction occurs in infants. There are likely to be several reasons that the neonatal brain has to be more efficient at extracting oxygen from its blood supply: 1) To compensate for the proportionally smaller resting rCBF to CMR-Glucose in neonates compared to adults, 2) In order to acquire oxygen from fetal haemoglobin which has a higher affinity for oxygen than adult haemoglobin, 3) To compensate for the lower arterial oxygen tension of fetal blood in-utero 4) A greater neuronal energy requirement in the developing brain, probably due to the increased Na/K-ATPase energy requirements needed to stabilise the nerve membrane potential across a greater number of inter-neuronal connections and synapses in the developing brain (Chugani *et al.* 1987; Chugani 1998).

1.5.3.4 Conclusions from neonatal functional imaging studies

The conclusions drawn from these functional studies is that the neonatal brain has a similar cortical haemodynamic response to adults in response to sensory stimulation, but differs in the rate of the metabolic extraction of oxygen and that this is likely to account for the reversed BOLD response seen in infants. The importance of these studies, with regards to EIT, is that they provide evidence for both an increase in rCBF and cerebral blood volume in the neonatal brain in response to stimulation, which is predicted to decrease cortical impedance because blood has a lower impedance than the surrounding cortex. This therefore supports the attempt to use EIT to measure such cerebral impedance changes in neonates and the results of which will be discussed in Chapter 4.

1.5.4 Magnetic Resonance Spectroscopy and Diffusion Weighted Imaging of neonatal cerebral ischaemia

In contrast to blood flow studies, further information about brain metabolism can be obtained with magnetic resonance spectroscopy (MRS). Studies using this technique have been particularly suited to the acquisition of information about cortical metabolism after perinatal asphyxia. The main reason for discussing these techniques is that they provide evidence for energy failure and cell swelling that, in animal models, produced very large impedance changes of up to 100 % (Holder 1992) which could be detected by, and would be an important clinical application of, EIT.

To understand the significance of the results of such studies, a brief (and simplified) overview of normal and ischaemic cerebral metabolism is presented. Normal cerebral metabolism derives energy from the oxidative metabolism of glucose; this provides ATP, from the precursors ADP and inorganic phosphate (Pi). Although ATP is required by many cells and for many different metabolic reactions, one of the main uses of ATP is to supply energy to the sodium/potassium-ATPase ion pump which maintains a concentration gradient of sodium and potassium across the nerve membrane and thereby maintains the resting potential of the nerve membrane. The main supply of ATP is derived from the oxidative metabolism of glucose via the citric acid cycle, in which 36 molecules of ATP are synthesised for each molecule of glucose.

During asphyxia, oxygen deprivation slows and eventually stops oxidative metabolism, this switches on the anaerobic metabolism of glucose to lactate, which returns 2 ATP molecules for each glucose molecule. If the oxygen supply is not restored, eventually anaerobic metabolism fails and supplies of ATP are rapidly depleted. Other stores of energy, such as phosphocreatine molecules, can be utilised, briefly, to produce ATP and creatine but once these are consumed the sodium/potassium-ATPase will fail, and the neuronal membranes depolarise with the entry of sodium in to the nerve cells. During this stage of energy failure, intracellular osmolarity is increased, which results in cell swelling as a result of water influx into the cells from the extra-cellular space.

Therefore, energy failure produces a rapid reduction in high energy molecules, such as ATP and phosphocreatine, and an accumulation of energy metabolites such as inorganic phosphate (Pi) and ADP. In addition molecules, such as lactate, which are normally in low concentration during normal oxidative metabolism are increased due to the anaerobic metabolism. Many of these molecules can be detected with MRS and can indicate the level of energy failure as a result of hypoxia-ischaemia.

Examples of such studies are those that measure the concentration changes of metabolites in asphyxiated newborn infant compared to normal controls. Such changes are increased lactate/NAA (N-acetylaspartate) ratio (Penrice *et al.* 1996; Miller *et al.* 2002), a simultaneous increase of the lactate/creatine ratio and an increase in myo-inositol/Creatine ratio (Robertson *et al.* 2001). Similar findings have also been demonstrated in piglet models of asphyxia (Thorenson *et al.* 1995; Amess *et al.* 1997). These studies have also demonstrated that the magnitude of these adverse changes can be ameliorated with the introduction of brain cooling after the hypoxic-ischaemic insult.

Some MRS studies have also used diffusion weighted imaging (DWI) which detects the ability of water to diffuse in the brain and which is reduced during cell swelling as a result of ischaemia. Water in the extracellular space has a high degree of diffusibility (apparent diffusion coefficient = ADC), whereas if the water is bound within a cell membrane, the ADC is reduced; DWI provides an image of the ADC changes in the brain. These DWI images are an indirect measure of cerebral energy failure, and are associated with MRS findings of energy failure in piglets (Thronton *et al.* 1997). In addition, DWI studies in human neonates have demonstrated that changes occur earlier than changes on traditional MRI structural imaging using T1 and T2 parameters (Bydder *et al.* 2001; Soul *et al.* 2001), although infants have not been studied immediately after asphyxia. As the changes in DWI reflect a decrease in the volume of the extracellular space, this would increase brain impedance due to the loss of the conductive, and therefore low impedance, extracellular path. This is in agreement with fetal sheep models of asphyxia, in which cerebral impedance was recorded, this demonstrated that impedance changes occur early during the initial asphyxial insult and 12-24 hours later during secondary energy failure (Williams *et al.* 1991; Tan *et al.* 1993; Tan *et al.* 1996; Gunn *et al.* 1997). Similar findings, but with DWI changes instead of impedance measurements are reported in rats (Li *et al.* 2000).

The demonstration that the initial energy failure is associated with cell swelling and impedance changes indicates that impedance tomography has the potential to image these changes. As such, EIT may provide a suitable, cot-side method of determining brain damage to aid the clinician in the selection of infants for brain cooling, in order to reduce brain damage and improve neurological outcome.

1.6 Summary

This chapter has provided an overview of the history and development of neuroimaging with EIT, and outlined the experimental and physiological evidence by which EIT should be able to detect

impedance changes from both the adult and the neonatal head. In addition, current methods of establishing functional information about the adult and neonatal brain have been reviewed, which support the hypothesis that impedance changes occur in the human brain during a variety of physiological and pathological conditions.

1.7 Objectives of Research

The primary objective of this research was to determine whether scalp impedance measurements can detect the expected changes of cerebral impedance during brain activity. If these changes can be detected, then the secondary objective is to determine whether the EIT images, reconstructed from these changes, localise changes to the expected areas of cortex stimulated.

The next chapter details the first EIT studies of adult functional brain activity, and determines whether the predicted brain impedance changes during sensory stimulation can be detected and imaged with EIT.

1.8 Statement of own work

Chapter 2: EIT of the adult human head

The HP impedance analyser based EIT system used to detect the functional impedance changes in adults was developed by the UCL EIT research group (Dr David Holder, Dr Richard Bayford), however I optimised the data acquisition protocol to increase the speed of data acquisition to enable the acquisition of data from the human head. The experimental protocols, recruitment of subjects, and acquisition of data in adults was my own work. I developed the programmes for the analysis of the raw impedance data and the reconstruction and analysis of the EIT images. The 3-dimensional reconstruction algorithm, based on a homogenous spherical model of the human head, and the optimised impedance measurement protocols were developed by Dr Adam Gibson (Gibson 2000).

Chapter 3: Imaging in a Head Shaped Tank

This work used the same HP impedance analyser based EIT system as Chapter 2 and similar data analysis and reconstruction methods. I developed and built the head shaped tank with help from Dr David Holder. The data acquisition and analysis was my own work. The results of my work in this chapter were used by Dr Adam Gibson to make corrections to errors in the reconstruction algorithm.

Chapter 4: Functional EIT in Neonates

This work used the newly developed UCH 1b EIT system, which was based on a modified design of the Sheffield EIT system in collaboration with the Sheffield EIT group headed by Professor Brian Brown. Mike Conway, based at the Department of Medical Physics UCL, was instrumental in the design, build and medical safety testing of the UCH 1b system. Acquisition software, written in HP Vee, was written by myself, Dr Rebecca Yerworth and Dr Tony Fitzgerald, all based in the UCH EIT research group. I was instrumental in the safety testing of the system in adults, prior to its use in neonates. I developed the stimulus acquisition software (HP Vee and Visual Basic) and the stimulation equipment for use in the neonatal experiments. The design of the experimental protocols, consent documents, data analysis software and the acquisition of the neonatal data was my own work.

Chapter 5: Improved Adult Reconstruction Algorithm

The finite element model used to produce the reconstruction algorithm in this chapter was developed by Dr Andrew Bagshaw, with contributions from Dr Adam Gibson, Dr Richard Bayford and Andrew Tizzard. The human data reconstructed by this algorithm was the same data used in Chapter 2. The reconstruction, analysis, presentation and interpretation of the image data in this Chapter was my own work.

Chapter 2: EIT of the adult human head

2.1 Introduction

2.1.1 Overview and purpose

This chapter describes the methods used to acquire, analyse and image the first impedance changes detected from human adults during functional brain activity. Previous EIT work, performed on the exposed cortex of rabbits (Holder *et al.* 1996), indicated that such changes occur during sensory stimulation. In addition, the results of fMRI (Mora *et al.* 1989; Kwong *et al.* 1992; Schneider *et al.* 1993), PET (Mazziotta and Phelps 1984; Perlman *et al.* 1985; Fox *et al.* 1986) and NIRS (Villringer *et al.* 1993; Meek *et al.* 1995) studies in the adult human indicate that an impedance change should occur due to blood flow and blood volume changes during neural activity (Logothetis *et al.* 2001). The evidence for this is discussed in more detail in Chapter 1. However, prior to these studies, it was not known whether these changes could be detected from the brain, when there is likely to be an attenuation of the impedance signal by the presence of the highly resistive skull (Gibson *et al.* 1999; Tidswell *et al.* 2001).

The primary purpose of the work in this chapter was to determine whether impedance changes, expected during functional stimulation as a result of blood flow and blood volume change, can be detected by scalp electrodes despite the expected signal attenuation from the skull. The secondary purpose was to determine whether such changes could be reconstructed into images, and if so, if the changes were in the expected location of the cortex stimulated by the sensory and motor paradigms used in these studies.

2.2 Methods

2.2.1 Overview

Impedance was recorded, in 39 adult volunteers, by a series of 4 terminal impedance measurement selected from 31 silver/silver chloride EEG scalp electrodes in each subject (Figure 2.6). The measurements were made with an Hewlett-Packard 4284A impedance analyser connected to the electrodes via a multiplexer (Figure 2.8). One data set comprised recordings from 258 electrode combinations and was recorded every 25s for just over 6 minutes (375 seconds), a total of 15 frames of data. This was repeated at least 6 times for each subject. Visual, motor, or somatosensory activation of the brain was achieved by either: 1) The observation of a 0.6° checkerboard oscillating at 8 Hz, 2) Sequential apposition of the thumb with the fingers or 3) Stimulation of the median nerve at the wrist at 3 Hz, respectively. Stimulation was performed for a period of 75s in the middle of a 6 minute imaging experiment. The 3D images were produced from the data by a reconstruction algorithm based on the inversion, by singular value decomposition of a sensitivity matrix produced for a homogeneous sphere model of the human head. The work in this Chapter has been published in the journal Neuroimage (Tidswell *et al.* 2001).

A second study was performed to identify the contribution of scalp impedance changes during motor evoked responses. Impedance changes were first identified at an electrode combination during a standard EIT experiment, and the scalp impedance measured at those electrode sites during a similar experiment of motor stimulation. Scalp impedance could have contributed to EIT signal if there had been stimulus related sweating, muscle activity or scalp blood flow changes. Scalp blood flow has previously been demonstrated to change during visual evoked responses (Villringer *et al.* 1993), in which changes were detected by laser Doppler flowometry during presentation of either a 10 Hz flashing light or a picture stimulus. If such changes produced blood volume changes, then the scalp impedance would be expected to change. It was important to identify or exclude such changes as the underlying cause of the transcranial impedance changes detected during the functional EIT studies.

Figure 2.6 Subject during EIT experiment
31 silver/silver-chloride electrodes were attached to the scalp with electrode paste, and connected to the computer controlled multiplexer (left side of image). Velcro head straps were used to minimise electrode movement and artefact. EIT images were obtained during either visual, somatosensory or motor stimulation.

2.2.2 Equipment and Experimental Procedures

2.2.2.1 Subjects

Measurements were made in 39 healthy adults, mean age 42 years (range 16-64), who had no neurological problems and had given informed consent to the study. They were recruited by a poster campaign from the outpatient department of the Middlesex Hospital (part of UCLH). This study was approved by the UCLH local ethics committee. For the study, the subjects were seated in a reclined chair in a quiet and darkened room: 26 subjects took part in one experimental paradigm and 13 in two stimulation paradigms, a total of 52 recordings.

2.2.2.2 The HP EIT system

Each EIT image consisted of 258 measurements made at different combinations of 4 electrodes selected from the 31 scalp electrodes. Each 4 electrode measurement was made with a Hewlett Packard 4284A impedance analyser: two electrodes were used to apply an alternating current across the head in a polar drive arrangement (Figure 2.7) and two electrodes measured scalp voltage. As the Impedance analyser was not designed for 4 terminal impedance measurements, a modification to the Impedance Analyser had been made (Gersing 1991) and the outputs multiplexed through a computer controlled multiplexer. The controlling PC used the multiplexer to switch the HP system between different voltage measurement and current injection electrodes.

The 258 measurements that comprised each image, were acquired over 25s. The order and the position of the electrodes selected to make the measurements were read from a programmable electrode protocol file.

The HP 4284A impedance analyser measured the resistive component of impedance at an alternating current frequency of 50 kHz. The data acquisition speed was maximised by disabling the automatic level control (ALC), setting a short acquisition time and applying a constant voltage of 2.0 V across the current injection electrodes. The equipment ran off a mains isolator power supply device (RS safety isolating transformer 209-099, RS Limited). The multiplexer was supplied with a constant DC voltage of +/- 15V from an Isotech IPS2303D DC power supply. A foot switch was incorporated in the mains supply circuit to act as a safety cut-out.

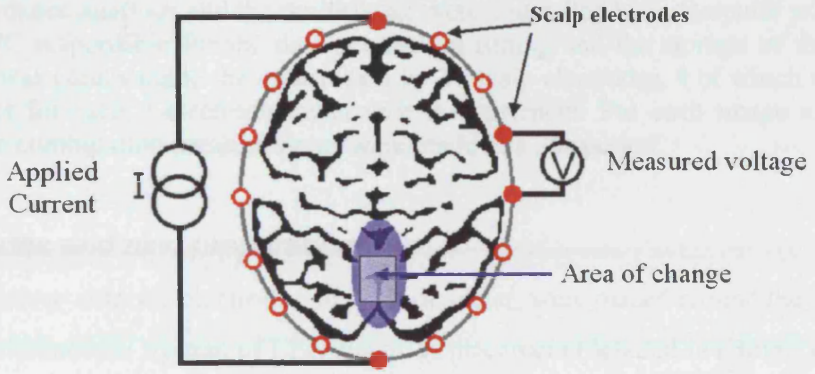

Figure 2.7 Measurement of transcranial impedance with 'Polar Drive'
A 4-electrode transcranial impedance measurement is made with 2 electrodes in opposition across the head used to apply a current in 'Polar Drive'. This current produces a scalp voltage, which is sampled by different pairs of voltage measurement electrodes. If an impedance change were to occur in an area of brain, possibly due to a change in blood volume or cell swelling, the path of the current through the brain changes which will change the measured scalp voltage. These changes can be detected by EIT and reconstructed into images that represent changes in the internal impedance of the head.

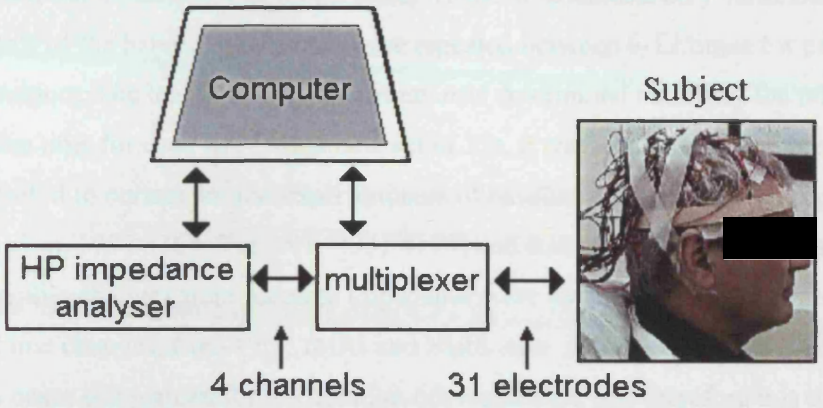

Figure 2.8 Diagram of the HP 4284A impedance analyser EIT system
Both the HP impedance analyser and the multiplexer were controlled by a computer program which ran on the host PC responsible for the data acquisition timing and the storage of the impedance data. The subject was connected to the multiplexer by 31 scalp electrodes, 4 of which were selected by the multiplexer for each 4-electrode impedance measurement. For each image a total of 258 different electrode combination measurements were made in a 25s period.

2.2.2.3 Electrodes and skin preparation

Thirty-one silver/silver-chloride electrodes, of 1 cm diameter, were placed around the scalp using a modified 10-20 International System of EEG electrode placement (detailed in (Binnie *et al.* 1982), see also Appendix 3). The electrodes were chlorided and sterilised in a solution of Sodium Dichloroisocyanurate made from Haztab granules (Guest Medical, Kent,UK). The electrode/skin impedance was reduced at each electrode site by rubbing it with an abrasive gel soaked cotton bud, prior to electrode placement. Then EEG electrodes were attached to the abraded skin with a conductive paste (Ten20 conductive EEG paste and Nuprep Abrasive Skin Prepping Gel both products of D.O.Weaver and Co. 565-C Nucla Way, Aurora, CO 80011, USA). Electrode impedance at the current drive electrodes was calculated from the current which was applied at a constant 2.0V. High electrode/skin impedance was defined as a transimpedance greater than 2 kΩ, and when it occurred the electrode was reapplied after repeated skin abrasion.

2.2.3 Evoked response experiment design

2.2.3.1 Data Acquisition

The stimulus was presented to the subjects by a block design experimental paradigm (Frackowiak *et al.* 1997). During a 6 minute experiment, 15 EIT image data sets were acquired continuously. The subject was either at rest in a darkened room during the baseline condition in the first and last 150s of the experiment (6 images each), and in the middle of these baseline conditions a 75s (3

image) stimulus condition took place: either visual or somatosensory stimulation or active motor movements of the hand. Experiments were repeated between 6-12 times for each type of stimulus in each subject. The length of the experiment was determined mainlyby the relatively slow acquisition time for each EIT image data set of 25s, it was felt that enough baseline measurements were required to correct for the small amounts of baseline drift recorded in previous preliminary data [Balchin, 1997 #364; Tidswell, 2001 #199] and that at least 3 stimulus data sets were acquired to be sure that changes from baseline impedance were real. The expected timecourse of the blood flow/volume changes, from PET, fMRI and NIRS data, was expected to take place within 5s of stimulus onset and plateau for the duration of stimulation, and therefore this duration of experiment was expected to be able to detect such changes. The aim of repeated experiments was to enable an increase of signal to noise through averaging across experiments. From the EIT work in rabbits [Holder, 1996 #3], we expected an approximate 0.05-0.2% signal change in the EIT raw data, and from early human studies the noise from the HP-EIT system was approximately 0.05-0.1%, therefore in the best case, with a signal of 0.2% and noise of 0.05% repetitions would only be required to demonstrate reproducibility of the signal (a minumum of 3 experiments), but if the worse case occurred with a signal of 0.05% and noise of 0.1% up to 16 repetitions of an experiment would be required. In the prelimary experiments (not shown here) it was found that the signal to noise was nearer to the best case so that it was not necessary to develop experiments with large numbers (16 or more) repetitions of the stimulus.

2.2.3.2 Visual evoked responses

Visual evoked responses (n=14 experiments) were performed in a darkened room. A black and white television screen was placed 66 cm in front of the subject at head height, subtending a visual angle of 28° horizontally and 23° vertically. The checkerboard stimulus was produced from a Medelec ST10 stimulator and had a check size of 0.7°, which reversed at maximum contrast and at 16 reversals/sec (8Hz). Activation of the chequerboard pattern was performed manually, by the experimenter, in response to a visual prompt from the EIT data acquisition program; this took place out of the subject's field of view. The stimulation period was timed to coincide with the start of the 7^{th} image acquisition. The subjects had their eyes open throughout the experiments.

2.2.3.3 Somatosensory evoked responses

Sensory, electrical stimulation of the median, radial and ulnar nerves at the wrist with a 3 Hz, 0.1ms square wave pulse at a threshold required to produce a thumb twitch was performed in 18 experiments (10 right, 8 left) Stimulation was produced by a Medelec ST10 stimulator (Oxford Instruments, UK), which applied current to the wrist through electrodes made from pipe cleaners (felt covered wire) soaked in a conductive gel (Nuprep Abrasive Skin Prepping Gel both products

of D.O.Weaver and Co. 565-C Nucla Way, Aurora, CO 80011, USA): the positive electrode (anode) was positioned at the flexor crease and the cathode 3 cm proximal to this. The stimulus current was determined by the production of a vigorous, non-painful twitch of the subject's thumb and fingers. The 3 Hz stimulus frequency was chosen, as an adult fMRI study indicated that the BOLD response in the somatosensory cortex was maximal at a stimulation frequency of between 2-4 Hz (Ibanez *et al.* 1995). Subjects had their eyes closed throughout the experiments; they were given a quiet verbal warning, "start", prior to stimulus onset to prevent them jumping. A 5 s latency was present between the data frames acquired before and after the start of and end of stimulation during which the stimulator was switched on or off, respectively.

2.2.3.4 Motor evoked responses

Motor stimulation was performed in 20 experiments (13 right hand, 7 left hand) by a self paced finger thumb apposition task (finger order 1-2-3-4-3-2-1) which was started and stopped by quiet verbal cues from myself, sitting beside the subject. The task was practised for one minute prior to data collection. The subjects were asked to perform the task as fast as possible without concern for errors. Subjects had their eyes closed throughout the experiments.

2.2.4 Data Analysis

2.2.4.1 Raw data analysis

The data was downloaded after the experiments to an Intel based PC running Matlab (MathWorks inc, USA) for offline analysis. The data was corrected for baseline drift by a least squares linear fit to the baseline (the first 6 and last 3 frames of data, which corresponded to times 0-150s, and 300-375s), for each electrode combination in each experiment from each subject. The baseline drift corrected impedance data was then expressed as a percentage change from the mean baseline; this was calculated by first calculating the mean impedance for the each electrode combination from the first 6 and last 3 frames of data, subtracting this from the drift corrected data, then dividing by the mean baseline impedance and multiplying by 100; as a result all impedance data is expressed as a percentage change from the mean baseline impedance, relative to a zero baseline. Experiments in which the subject moved, talked, or did not complete the task (e.g. fell asleep during motor activity) were recorded at the time of the experiment in the experiment notes, and excluded from the analysis. Significant impedance changes were defined as those electrode combinations where the impedance during stimulation was more than 2 standard errors of the mean (2SEM) from the baseline in two or more consecutive stimulus frames. Peak impedance changes were recorded for each subject from the electrode combination with the most significant change, i.e. the highest signal to noise.

2.2.4.2 Noise Correction:

Prior to image reconstruction, the raw data was displayed and corrected for levels of noise which exceeded specific, predetermined, exclusion criteria:

1) Noise spikes of greater than 2 % of baseline which returned to within 1 % of the baseline in the successive data frame.

2) Discontinuities of greater than 2 % of the baseline which did not return to within 1 % of the baseline and which did not occur within the stimulation period.

3) Non-linear baseline drift which was defined as a drift which exceeded 1 % of the baseline in the first 6 or last 4 baseline frames after baseline correction.

4) Baseline noise, defined as the standard deviation of the baseline data for each experiment in each electrode measurement, greater than 1 %.

The noise correction procedure was performed for each experiment in each subject and at each electrode combination in each experiment. If the impedance measurements at an electrode combination met the criteria for exclusion, then the voltage at that electrode combination was set to a zero value. This method was verified in a simulated noise correction of data collected from a head-shaped tank phantom, detailed in Chapter 3. The finding from that work was that images of a small 12% impedance change, produced by a sponge, imaged in the head-tank was not affected by the exclusion of up to 40% of electrode measurements, although the size of the impedance change within the image was reduced. More stringent limits were placed on the human data, so that experiments were rejected from image analysis if more than 25% (65 out of 258) of the impedance measurements were excluded from the raw data.

Images were reconstructed by the SVD_62 reconstruction algorithm, which had a sensitivity matrix based on a forward model of an analytical solution of a homogenous sphere model of the head. The sensitivity matrix was inverted by Singular Value Decomposition (SVD) with a truncation of 62 singular values. The truncation level of the SVD algorithm was determined by calibration on some of the human data, as detailed in Section 2.2.4.4.

2.2.4.3 Image Analysis:

Images were reconstructed, using the SVD_62 algorithm (see Section 2.2.4.4) each experiment from the noise-corrected data; the images were averaged for each type of stimulus in each subject and visually assessed for a significant impedance change in or outside the expected location of the stimulated cortex. In one subject all the experimental data was excluded on the basis of the noise criteria as the subject fidgeted throughout the experiments. Images were therefore reconstructed for 51/52 experiments.

A significant impedance change in the images was defined as a change which occurred during the stimulus period, had a FWHM of 25 % or more and a peak change which was more than 2SEM from baseline. The appropriate localisation of a significant impedance change was defined for each modality from the knowledge of the anatomy of the evoked cortical area and imaging studies of the same stimulus from PET and fMRI and the location of the change within the image.

A significant impedance change which met the above criteria was then assessed to determine whether it was in the appropriate cortical area: defined from knowledge of the anatomical position of the evoked cortex, from fMRI and PET data, and its approximate location in the image:

1) For visual images: the posterior quadrant of the lower 4 slices.

2) For motor and somatosensory images: the lateral quadrant of the lower 4 slices contralateral to the stimulated hand.

2.2.4.4 Optimisation of the reconstruction algorithm

The truncation threshold of the reconstruction algorithm depends on the amount of noise or error present in the images. For human data the noise in the reconstructed image includes: instrumental noise, physiological noise and reconstruction errors which arise due to differences between the forward model (a sphere) and the object imaged (the head). Instrumental noise can be assessed by the use of the system in tank phantoms, physiological noise is assumed to be the additional noise present in human imaging in comparison to tank studies, however the noise due to reconstruction errors is difficult to quantify and therefore prevents setting a predetermined truncation threshold.

In order to solve this problem, the optimal truncation threshold was determined empirically. This method truncated the algorithm at different levels, and used each truncation level to reconstruct the EIT data from the human visual or right motor evoked response experiments during the peak impedance change during stimulation. The images were visually inspected by three independent observers who determined: 1) A range of acceptable inversions based on the criteria listed below and 2) The optimal singular value image.

Acceptable inversions of the images were determined by the following: 1) The presence of an impedance change greater than 25 % of the diameter of the image, the maximum resolution obtained from tank studies (Chapter 3), 2) The absence of features less than 25 % of the image diameter; defined to be noise artefacts and 3) The absence of electrode artefacts determined by 5 adjacent electrodes with alternating positive and negative impedance changes of less than 25 % of the image diameter.

In eight experiments, no inversions were deemed acceptable so could not be used to obtain the final singular value. The ranges of acceptable singular values and the optimal singular values

for the remaining 26 experiments were similar between the three observers. The optimal singular values for the 26 experiments were averaged to give a truncation value of 62. The SVD_62 algorithm was then was subsequently to reconstruct all the human images. Only the images reconstructed by this algorithm, and the Transpose algorithm are presented and analysed in this work. Calibration of the algorithms were performed by imaging objects within a skull inside a head-shaped tank, as described in Chapter 3.

2.2.5 Scalp impedance experiments

To examine the possibility that the impedance changes had arisen from changes in the scalp tissues, further experiments were performed in 5 additional subjects. Impedance data were obtained, as described above for the imaging experiments, during a right hand motor paradigm. The data were immediately analysed and an electrode combination selected that demonstrated a significant impedance change (a significant impedance changes was defined as an impedance during stimulation which was more than 2 SEM from the baseline in two or more consecutive stimulus frames, Section 2.2.4.1). At each of the four EEG electrode positions used to make this measurement a specially designed set of scalp impedance electrodes were placed and scalp impedance recorded during repetition of the motor task. The details of the design and calibration of the scalp impedance electrodes are to be found in Appendix 4.

The scalp impedance electrodes consisted of a small array of four electrodes: 2 outer current injection electrodes separated by 15 mm, designed to apply current to the scalp, and 2 inner voltage electrodes to record scalp impedance. The design of the electrode array was based on a study which demonstrated that current injection electrode separations of less than 2 cm minimise current entry into the intracranial cavity, due to the shunting effect of the scalp (Rush and Driscoll 1968). This study used a skull in a saline tank, applied a current through two electrodes outside the skull and measured current density within the skull. As the separation of the current injection electrodes decreased to below 5 cm , the majority of the current was shunted through the saline 'scalp' layer and the current density within the skull decreased dramatically with smaller electrode separations. Therefore, in this study, I employed a current injection electrode spacing of 15 mm, on the principle that most of the current applied would be conducted through the scalp, so that the impedance measurements made would sensitive to changes of scalp impedance only.

2.3 Results

2.3.1 Raw data

2.3.1.1 Number and size of impedance changes

Significant impedance changes, defined as those electrode combinations where the impedance during stimulation was more than 2 standard errors of the mean (2SEM) from the baseline in two or more consecutive stimulus frames, were observed in 51/52 experiments. Both impedance increases and impedance decreases were seen (Figure 2.9, Figure 2.10, Figure 2.11 and Figure 2.12).

The mean percentage of electrode measurements in which a significant impedance change was detected were 25% for visual (range 7-51%, n=14), 26% for motor (range 3-55%, n=20), and 12% for somatosensory stimulation (range 0-31%, n=18).

For each subject a peak impedance increase and decrease during stimulation was measured. For this a computer programme was used to sort the impedance changes for each paradigm in each subject by the size of the signal to noise ratio during stimulation; the peak impedance increase and decrease were then selected which had the largest signal to noise. These peak impedance increases and decreases were averaged for each stimulation paradigm and expressed as percentage impedance change from baseline. The peak impedance increases for visual, motor, and somatosensory paradigms, respectively, were 0.62 ± 0.19 % (mean ± SEM), 0.63 ± 0.14 % and 0.19 ± 0.02 % , whilst average peak decreases were -0.46 ± 0.07 %, -0.44 ± 0.20 % and -0.22 ± 0.03 %. Both the number of somatosensory changes and the size of the peak somatosensory changes were significantly smaller than the visual and motor changes ($p<0.01$, t-test). There was no significant difference between the size of the peak changes and the number of changes in the visual and motor responses (Table 2.1).

Table 2.1 Summary of raw data changes. (all results Mean ± SEM)

Stimulus (no of experiments)	Number of electrodes with an impedance change (% of measurements)	Peak impedance increase	Peak impedance decrease
Visual (n=14)	64 ± 9 (25 ± 3%)	0.62% ± 0.19	-0.46% ± 0.07
Motor (n=20)	68 ± 9 (26 ± 3%)	0.63% ± 0.14	-0.44% ± 0.20
Somatosensory (n=18)	30 ± 6 (12 ± 2%)	0.19 ± 0.02	-0.22 ± 0.03

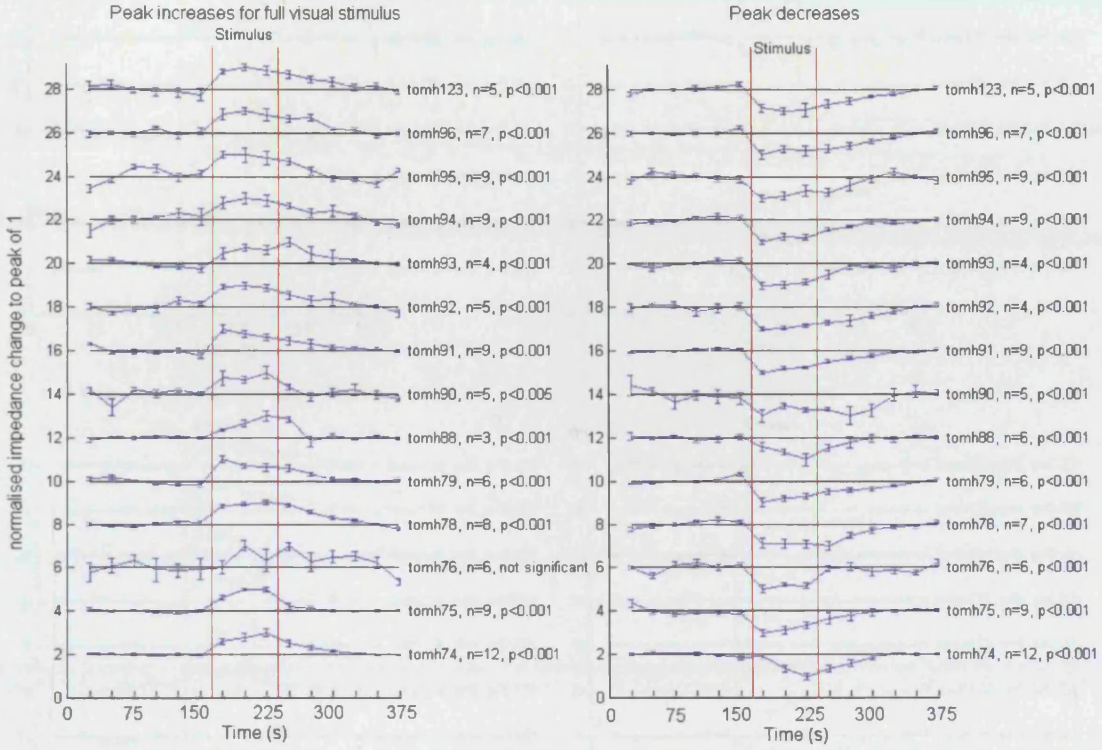

Figure 2.9 Visual evoked responses: raw data changes
Timecourse of the peak impedance increases (left) and decreases (right) in each of the 14 subjects during visual evoked responses. Time on the x-axis in seconds. Each timeseries, stacked on the y-axis, represents the impedance variation at that electrode combination from the mean baseline impedance for that electrode combination with the Standard Error represented on the error bars; both the mean and standard error bars are adjusted by the same factor that scales each measurement to have a peak impedance change of 1, represented by the units on the y-axis (the increments in the y-axis units are arbitrary and have no meaning other than to indicate the relative variation of the impedance changes and their errors relative to the normalised peak impedance change). The number of experiments averaged is indicated next to the subject label to the right of the graphs.

Significant impedance changes, with the same timecourse as the stimulus period are seen in all the experiments. The p-value represents the t-test probability that either 1) Impedance at 175 and 200s or 2) Impedance at 200 and 225s are both significantly different from the baseline impedance.

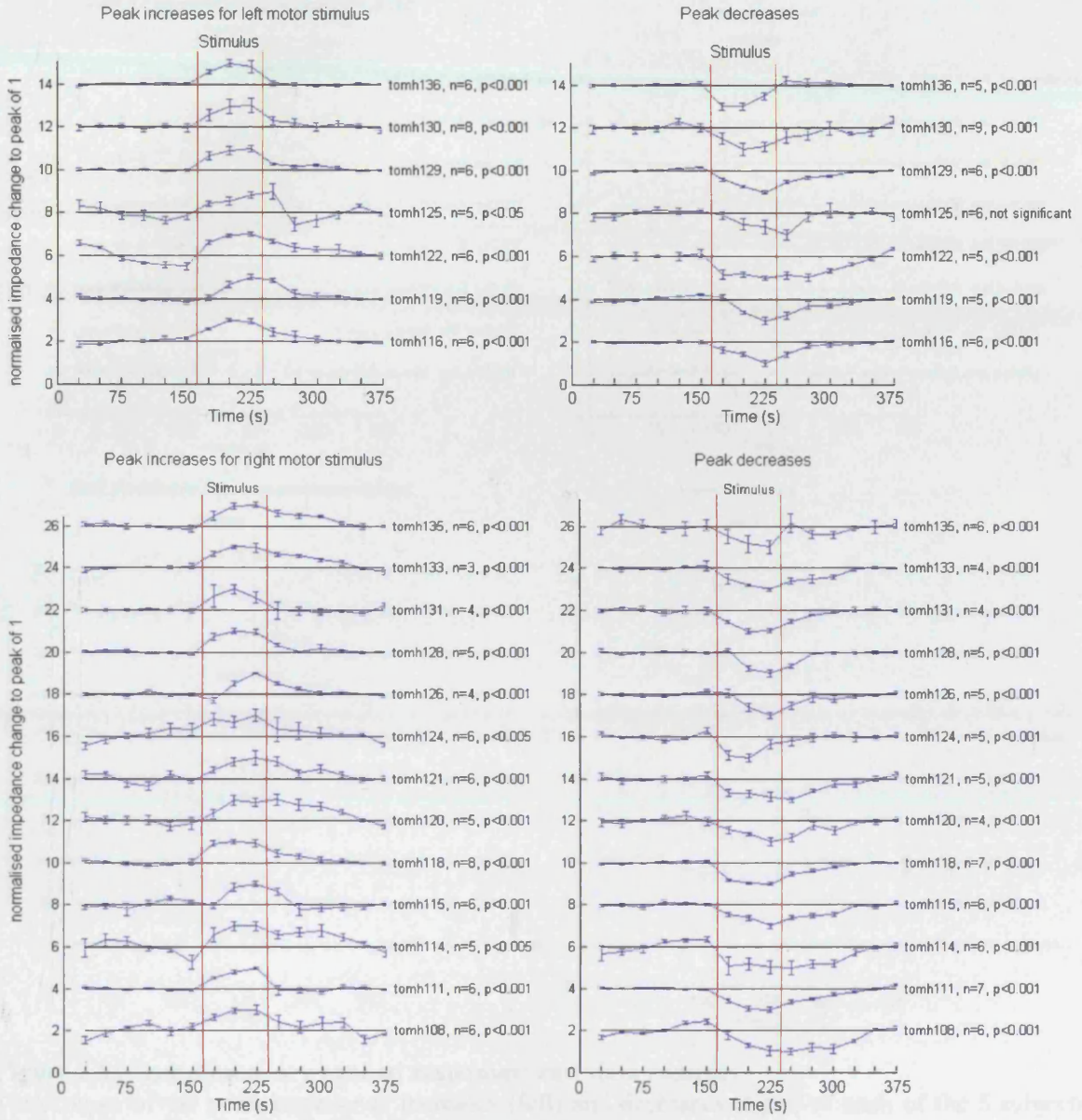

Figure 2.10 Motor evoked responses: raw data changes

Timecourse of the peak impedance increases (left) and decreases (right) of each of the 7 subjects during left motor (top) and 13 subjects from the right motor (bottom) experiments. Time on the x-axis in seconds. The y-axis represents the mean±SE impedance change normalised by the maximum impedance change in each data series. The number of experiments averaged is indicated next to the subject label to the right of the graphs.

Significant impedance changes, with the same time course as the stimulus period are seen in all the experiments. In one left motor experiment, tomh125, the impedance decrease did not achieve significance, even though the impedance changed during the stimulation period The p-value represents the t-test probability that either 1) Impedance at 175 and 200s or 2) Impedance at 200 and 225s are both significantly different from the baseline impedance.

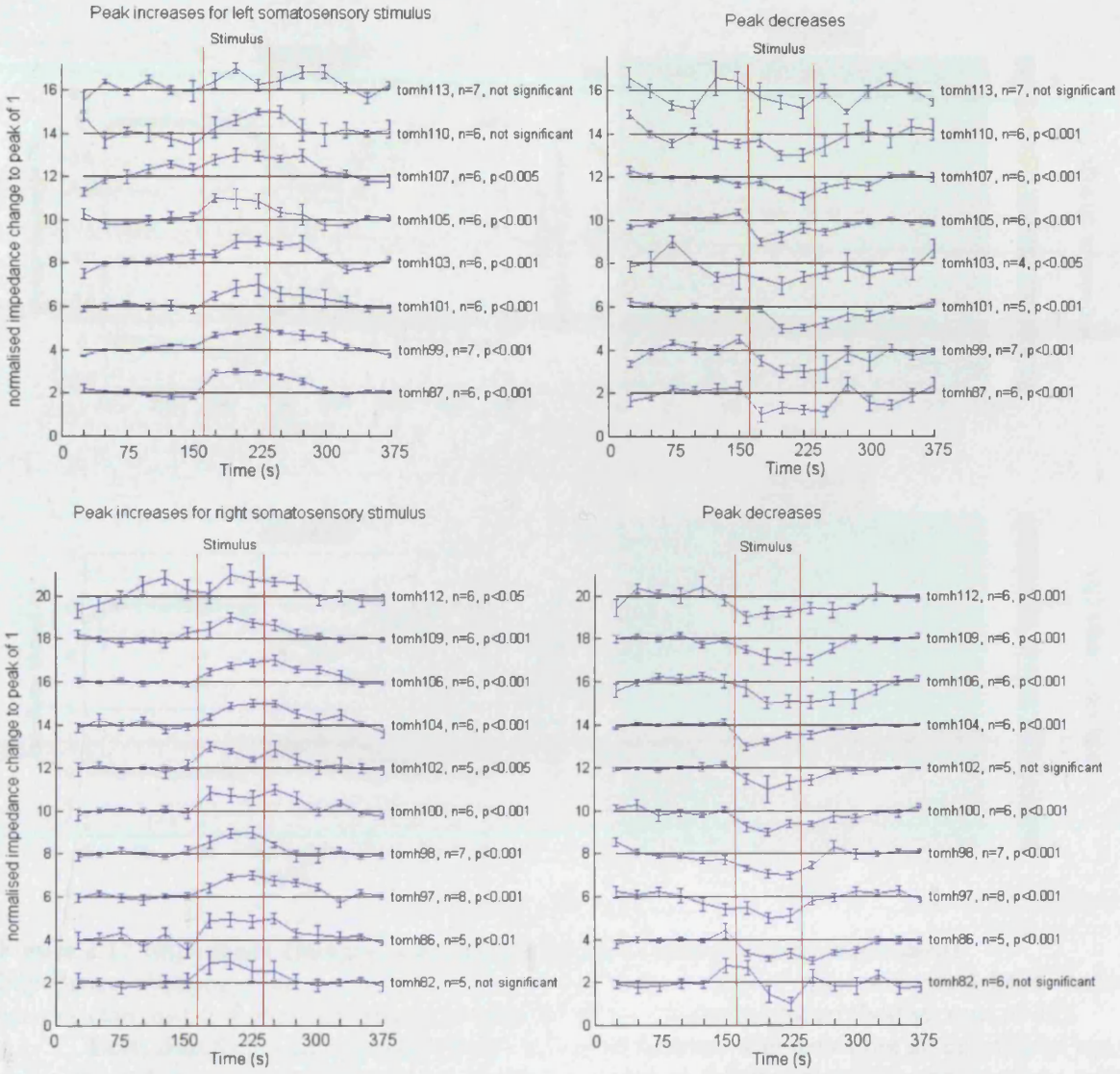

Figure 2.11 Somatosensory evoked responses: raw data changes
Timecourse of the peak impedance increases (left) and decreases (right) of each of the 8 subjects during left somatosensory (top) and 10 subjects during right somatosensory (bottom) stimulation. Time on the x-axis in seconds. The y-axis represents the mean±SE impedance change normalised by the maximum impedance change in each data series. The number of experiments averaged is indicated next to the subject label to the right of the graphs.

Significant impedance changes, with the same timecourse as the stimulus period are seen in 7/8 of the left somatosensory experiments and 9/10 of the right somatosensory stimulation experiments. The p-value represents the t-test probability that either 1) Impedance at 175 and 200s or 2) Impedance at 200 and 225s are both significantly different from the baseline impedance.

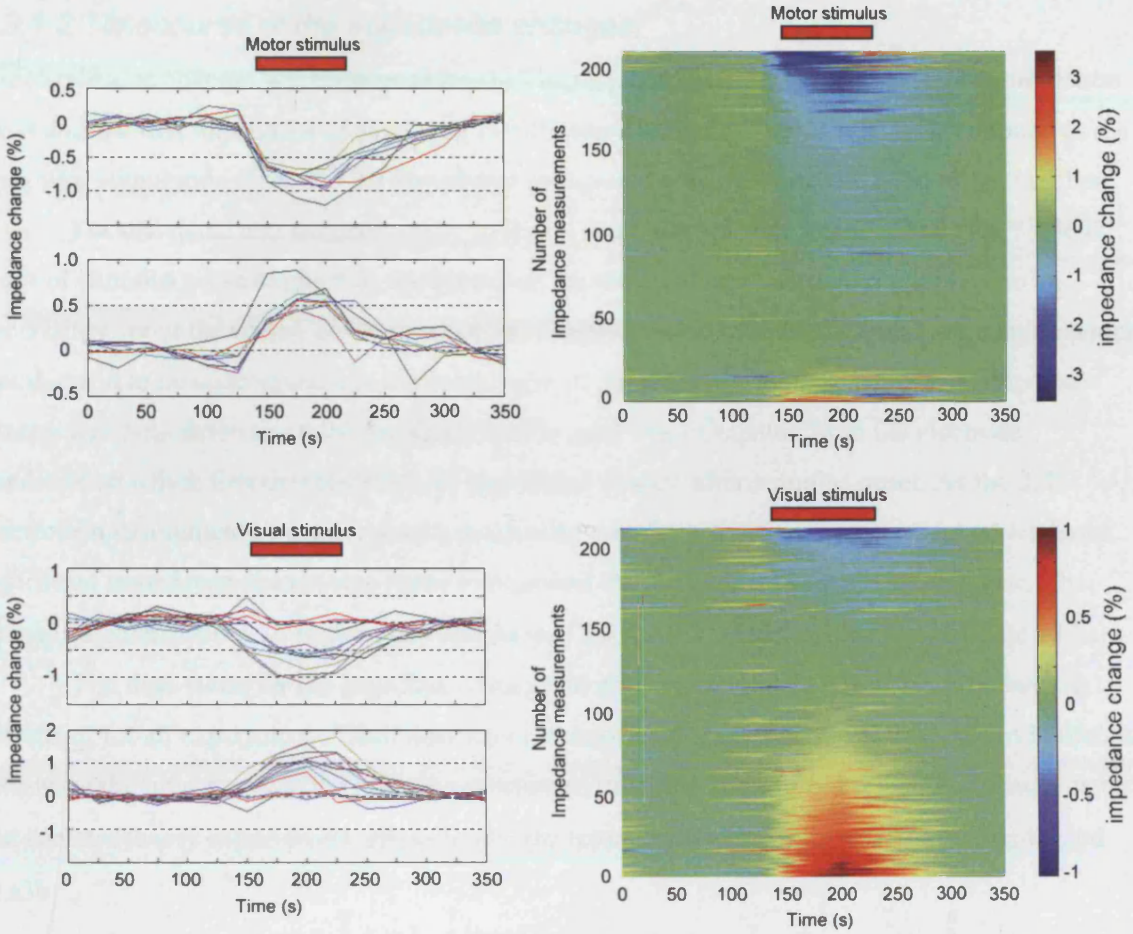

Figure 2.12 Impedance changes in a motor (top) and visual (bottom) experiment
Impedance changes, prior to image reconstruction from a subject who performed hand motor activity (top row, n=8 experiments) and a subject during visual stimulation (bottom row, n=12).

Left: data from single, selected electrode combinations, with data from all experiment runs superimposed. Reproducible impedance changes are seen at selected electrode combinations with the same timecourse as the stimulation paradigms. The y-axis indicates the percentage change from baseline impedance. Impedance measurements were made every 25 s; the lines between these measurements are drawn for clarity. Both impedance increases and decreases were observed.

Right: surface plot of data for the same subjects. The 8-12 runs for each electrode combination were averaged together. For clarity, the resulting 258 impedance data sets were sorted due to the size of the impedance change during stimulation and stacked on the vertical axis. Measurements with baseline noise greater than the impedance changes, are excluded from these plots so the changes are not obscured. Stimulus related impedance increases and decreases are seen in approximately 30 % of electrode measurements in these subjects.

2.3.1.2 Timecourse of the impedance changes:

The impedance changes were analysed for: 1) The response latency, the time between stimulation onset and the first impedance change, and 2) The return to baseline time, which was defined as the time after stimulation cessation for impedance changes to return to within 2 SEM of the baseline.

For the visual and somatosensory studies a short, but variable latency (less than 3s) in the onset of stimulus presentation was introduced as the stimulus was switched on; this led to an uncertainty about the timing of the onset of the stimuli in relation to the EIT data acquisition which was deemed to be unacceptable in the calculation of an accurate response latency. A response latency was only determined for the motor studies, and was calculated from the electrode combination which first demonstrated an impedance change after stimulus onset. As the 258 electrode measurements were acquired sequentially over 25 s, the first measurement which had a significant impedance change was taken to represent the delay of the impedance response. The latency calculated from 20 motor experiments was 5.8 ± 0.9 s (Mean ± SEM, range 0.5 to 14.7s).

The time taken for the impedance change to return to within 2SEM of the baseline was calculated for all experiments. Each impedance change in an experiment was analysed in Matlab to determine the time at which the impedance returned to within 2SEM of baseline. For visual, motor and somatosensory experiments, respectively, the return to baseline time was 36±4s, 36±4s, and 21±3s.

Table 2.2 Timecourse of the impedance responses (Mean±SE)

Stimulus	Response latency (range)	Return to baseline time (range)
Visual, n = 14	n/a	36 ± 4 s (15-57)
Motor, n = 20	5.8 ± 0.9 s (0.5-14.7)	36 ± 4 s (6-95)
Somatosensory, n = 18	n/a	21 ± 3 s (4-51)

2.3.1.3 Signal and Noise

For each stimulus modality, the signal and noise were calculated. The average signal for each subject was calculated by averaging the impedance data acquired during stimulation for all the experiments at each electrode combination; then the magnitude of the impedance change was averaged for the 258 electrode measurements in that subject. Noise in each subject was calculated from the standard deviation of the baseline data for each experiment, averaged for all experiments and all electrode combinations.

There was a significantly lower signal in the somatosensory experiments (0.09 ± 0.01 %, Mean ± SEM) compared to both the visual (0.23 ± 0.02 %) and motor (0.22 ± 0.03 %) experiments ($P<0.001$, 2-tailed t-test, d.f.=30 and 36 for visual and motor comparisons respectively, Bonferroni corrected), no significant signal difference existed between the visual and motor groups.

The noise was similar for all experiments: 0.17 ± 0.01 %, 0.14 ± 0.01 % and 0.13 ± 0.01 % for visual, motor and somatosensory groups respectively. A statistical difference between the noise of the visual and somatosensory experiments only was found ($p<0.05$, 2-tailed t-test, d.f.=30, Bonferroni corrected for multiple comparisons). As the visual experiments were performed in the first volunteers for the EIT studies, a few months prior to the somatosensory experiments, then my improved electrode placement technique in the somatosensory experiments may have helped to reduce measurement noise.

Table 2.3 Signal and noise characteristics of evoked responses. (Mean±SE)

Stimulus	Signal (%)	Noise (%)	Signal: Noise
Visual, n = 14	0.23 ± 0.02	0.17 ± 0.01	1.3 ± 0.1
Motor, n = 20	0.22 ± 0.03	0.14 ± 0.01	1.5 ± 0.2
Somatosensory, n = 18	0.09 ± 0.01	0.13 ± 0.01	0.70 ± 0.04

2.3.1.4 Local impedance during motor evoked responses

Scalp impedance did not change from baseline noise during motor activity (0.04 ± 0.01 % vs. 0.08 ± 0.02 %, p=0.36, t-test), whereas the impedance change measured during image acquisition was significantly greater than baseline noise (0.42 ± 0.04 % vs. 0.12 ± 0.02 %, p<0.00005, t-test, Figure 2.13).

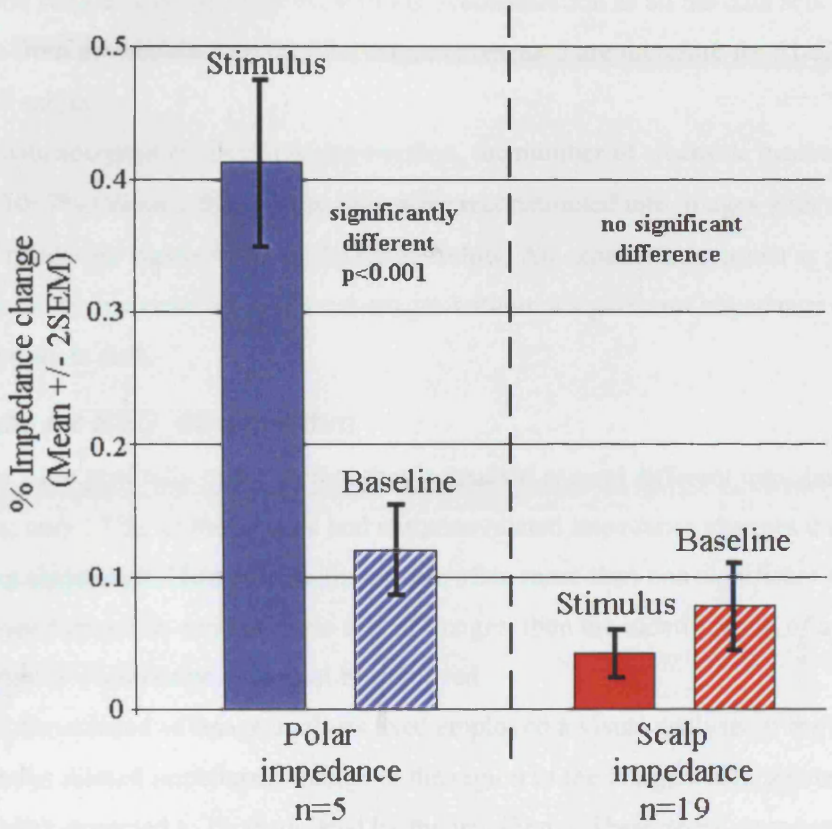

Figure 2.13 Transcranial and scalp impedance changes during motor stimulation
Transcranial impedance (left) and scalp impedance at the same 4 electrode sites (right, Mean±SE) are compared during motor stimulation (solid colour) to the baseline noise (hatched) in 5 subjects. Scalp impedance did not change from baseline noise (0.04 ± 0.04 % vs. 0.08 ± 0.07 %, p=0.36, t-test, d.f.=36). Polar impedance measurements, during identical motor activity, were significantly different from baseline noise (0.42 ± 0.09 % vs. 0.12 ± 0.04 %, p<0.00005, t-test, d.f.=8). There were a total of 20 scalp impedance measurements in the 5 subjects, but one was excluded from analysis due to movement artefact, the results are displayed for the remaining 19 measurements.

2.3.2 Image data

2.3.2.1 Noise correction of data prior to reconstruction

A total 342 data sets were collected from the 52 experiments in the 39 subjects. Of these, 44 data sets were excluded due to noise in more than 25 % electrodes, so 298 were reconstructed into images. Only one subject was excluded from image reconstruction as all the data sets were affected by excess noise from movement artefact. The images presented are therefore for 51/52 experiments performed in 38 subjects.

Of the data accepted for image reconstruction, the number of electrode measurements excluded were 10±7% (mean ± SD). These data were reconstructed into images with the SVD_62 algorithm. The results are summarised in the tables below. An experiment number is given for each significant increase or decrease and for those images without a significant impedance change in or outside the appropriate area.

2.3.2.2 Results for SVD_62 algorithm

The EIT images were generally noisy, in that they contained several different impedance changes of different size; only 37/51 of the images had stimulus related impedance changes that met the criteria for being significant. However, as there were often more than one significant stimulus related impedance changes in each of these sets of images, then the identification of a single impedance change in each image could not be achieved.

Instead, the method of image analysis used employed a visual analysis of the images for a significant stimulus related impedance change in the region of the image which approximated the region of the cortex expected to be stimulated by the paradigms. These areas were broad, partly due to the low resolution of the EIT algorithm, and corresponded to the contralateral quadrant of the image to the hand stimulated or moved, or the posterior quadrant for visual stimulation.

In these areas, significant impedance changes were found for 9/13 visual experiments of which 4 were impedance decreases, 8/20 for the motor experiments, of which 4 were decreases and 2/18 for the somatosensory experiments, of which one was an impedance decrease (Table 2.4).

The total number of images that had significant changes in the approximate location to the area expected to have a change was 19/51 (9 with impedance decreases). Of the remaining sets of images, 18/51 had significant image changes, but none were in the expected quadrant of the images, and the remaining 14/51 experiments demonstrated no significant stimulus related impedance change.

As each image had approximately 2 significant impedance changes, then the probability that one of these changes would appear in the correct quadrant was approximately 0.5. It is therefore possible that the correct localisation of a significant impedance change arose by chance.

Table 2.4 Correct localisation of impedance changes in SVD_62 images

Evoked Response	Increases > 25% image diameter in right area	Decreases > 25% image diameter in right area	No change > 25% of image diameter	Total number in correct location
	Experiment numbers with that change			Number out of the total experiments for that stimulus
Visual	78,91,92,96	74,75,76,88,123	none	9/13
Right motor	114,128,135	120,124,133	111	6/13
Left motor	136	119	125,130	2/7
Right somatosensory	none	98	100,102,104,106,109, 112	1/10
Left somatosensory	87	none	101,103,105,110,113	1/8

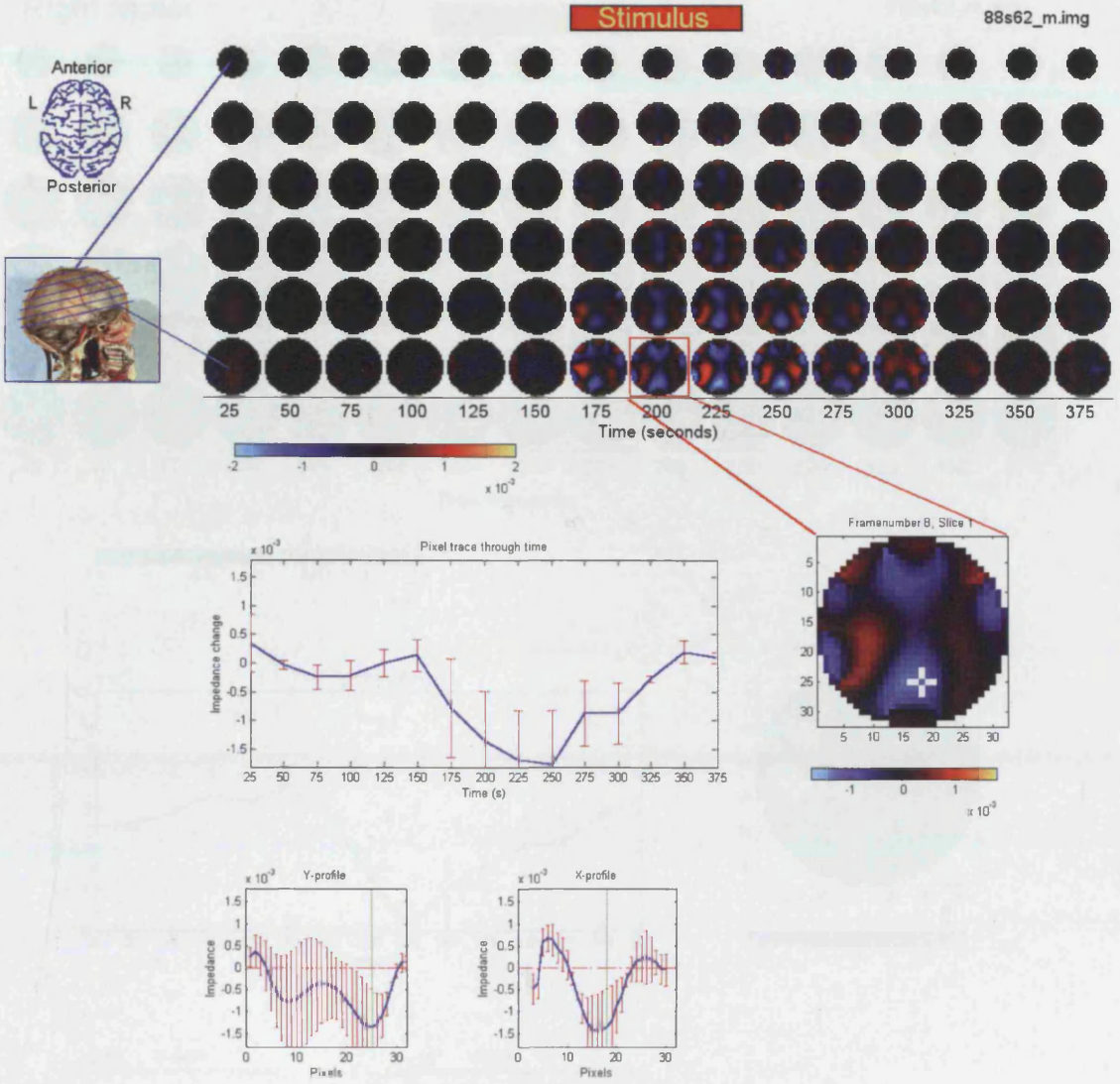

Figure 2.14 EIT of visual activity in one subject

Top: Time series of EIT images during visual stimulation in one subject. Each column represents an image acquired every 25s in the dark, with a checkerboard visual stimulus, flashing at 8Hz presented between 175-250 seconds. Images are viewed as if looking down on the head from above, and the slice levels are indicated by the head model on the left.

A significant impedance decrease, in which the mean change is more than 2SE from baseline, with a similar timecourse to the stimulus, is seen over the area of the visual cortex posteriorly. There are also other impedance changes present in the images; a decrease at the front and an increase to the left of the image.

Middle: Enlargement of the impedance decrease (right), with a cross hair indicating the position of the pixel for which the mean±2SE impedance timecourse is plotted on the left graph, and the position of the profiles of the image shown below..

Bottom: Image profiles, which demonstrate the size of the impedance decrease.

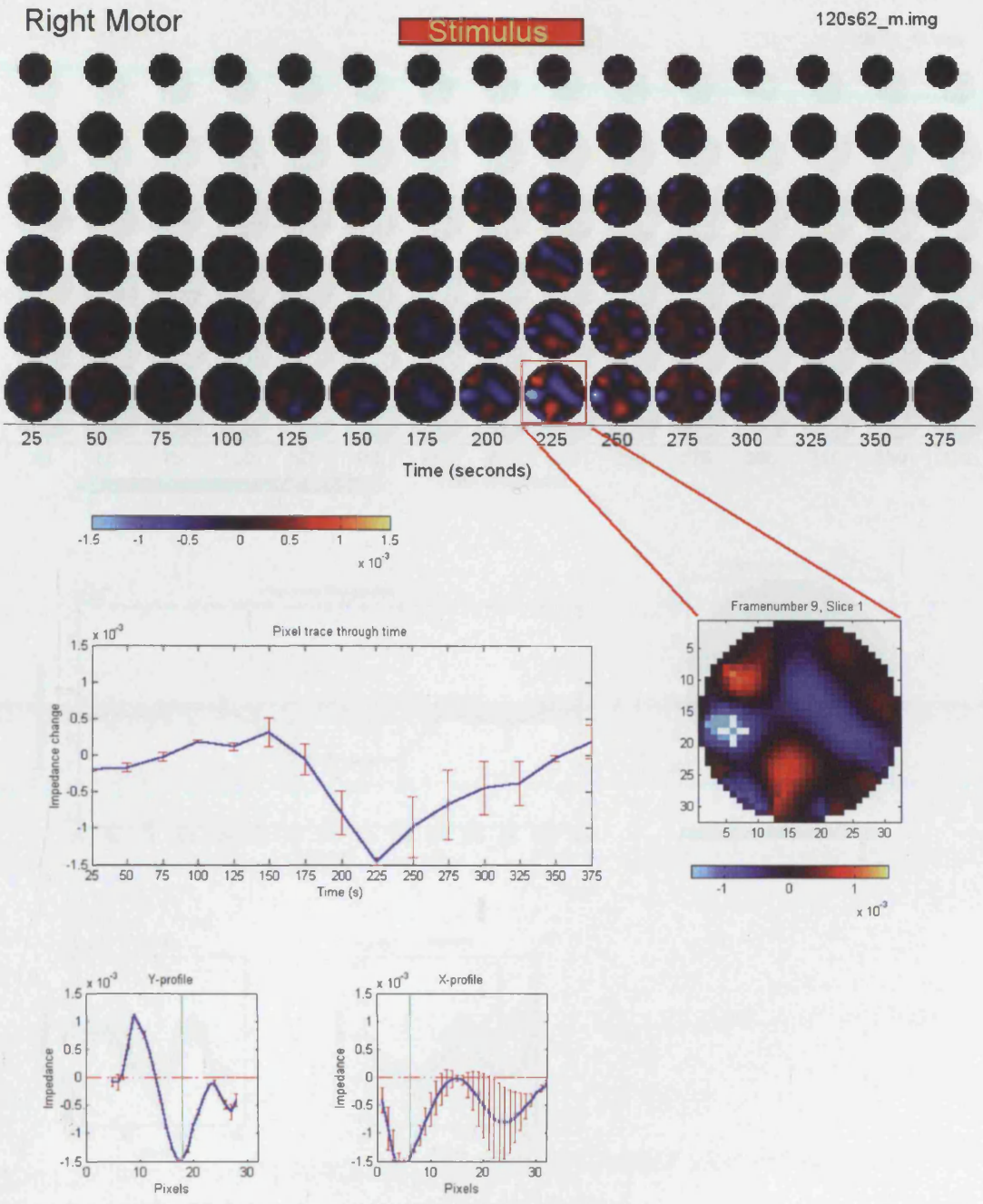

Figure 2.15 EIT of right hand motor activity in one subject
Top: Time series of EIT images during right hand motor stimulation in one subject. A significant impedance decrease on the left is seen, which is appropriate to the side of the contralateral motor cortex, but is probably too low to reflect the real position of the hand represented in the motor cortex. Although the decrease outlined is the largest impedance change in the image, there are additional impedance decreases (red) and impedance increases (blue) in areas away from the side of the left motor cortex.

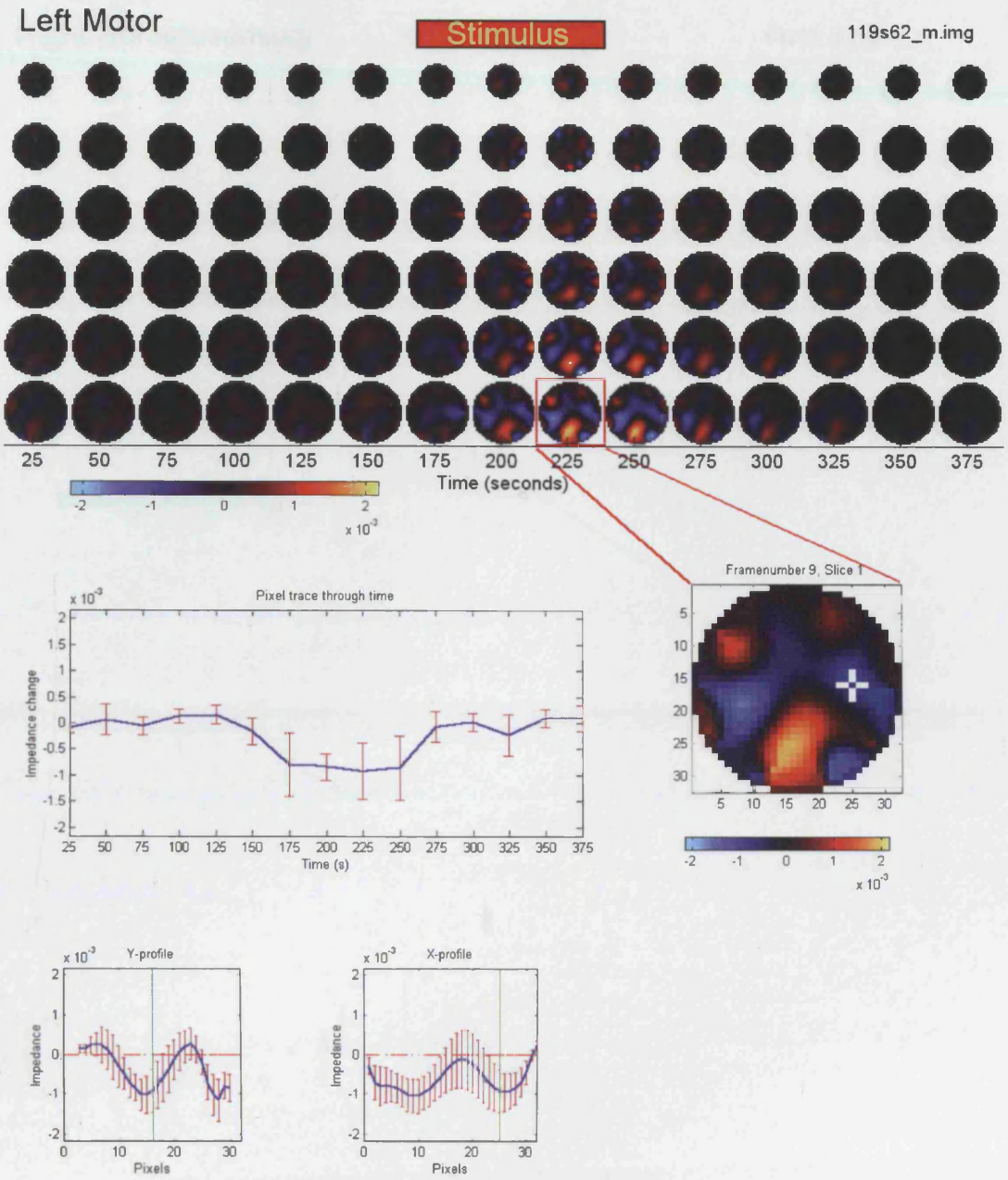

Figure 2.16 EIT of left hand motor activity in one subject
Top: Time series of EIT images during left hand motor stimulation in one subject. A significant impedance decrease is seen contralaterally to the moving hand. However, the images are noisy, with a larger impedance change on the left and an impedance decrease posteriorly which are not expected from movement of the left hand.

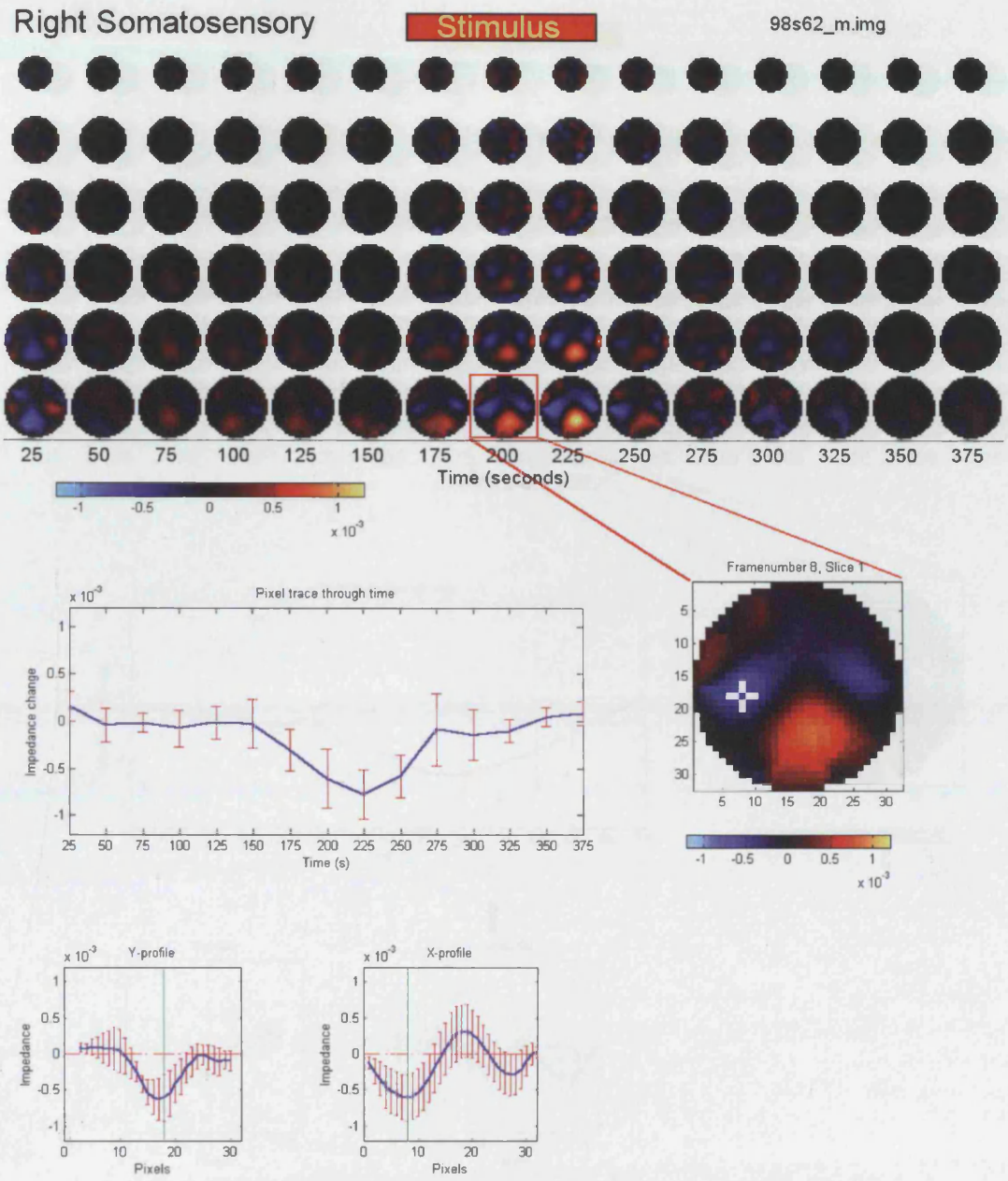

Figure 2.17 EIT of right hand somatosensory stimulation activity
Top: EIT images of right hand somatosensory stimulation, with a 3Hz electrical pulse delivered to the right wrist. Images are an average of 6 experiments. A significant impedance decrease is seen contralaterally to the stimulated hand on the left of the images, although this is low for the region of the somatosensory cortex that corresponds to the hand. In addition, a larger impedance increase is seen posteriorly and a small impedance decrease seen over the right side of the images. The images are therefore noisy, despite thresholding.

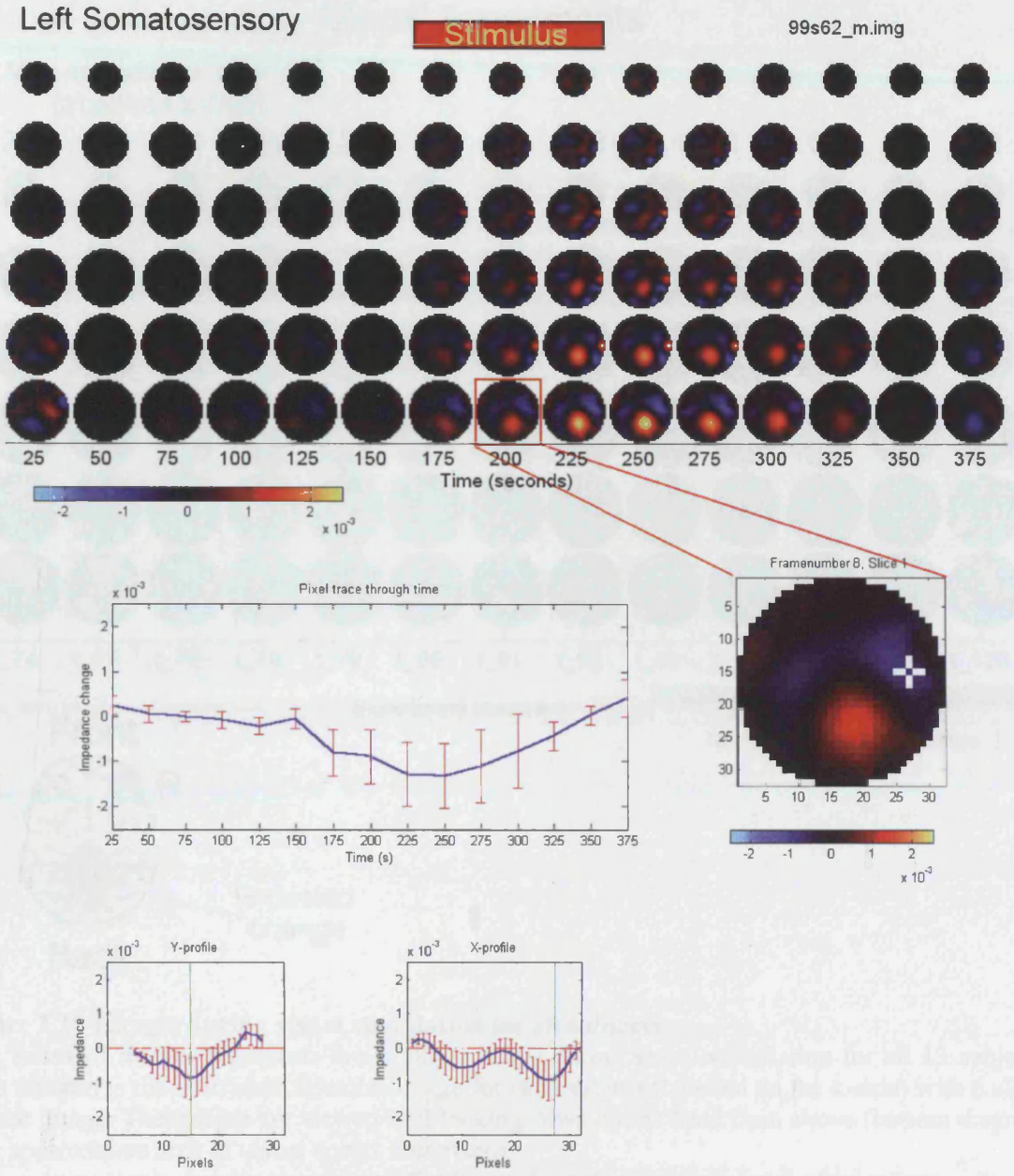

Figure 2.18 EIT of left hand somatosensory stimulation activity
Top: Mean impedance changes from 6 experiments are shown. A significant impedance decrease on the right side is seen, which is contralateral to the hand stimulated but low in comparison to the area of the right somatosensory cortex. A large impedance increase is also present during stimulation over the area of the visual cortex, which is not expected to be produced during somatosensory stimulation.

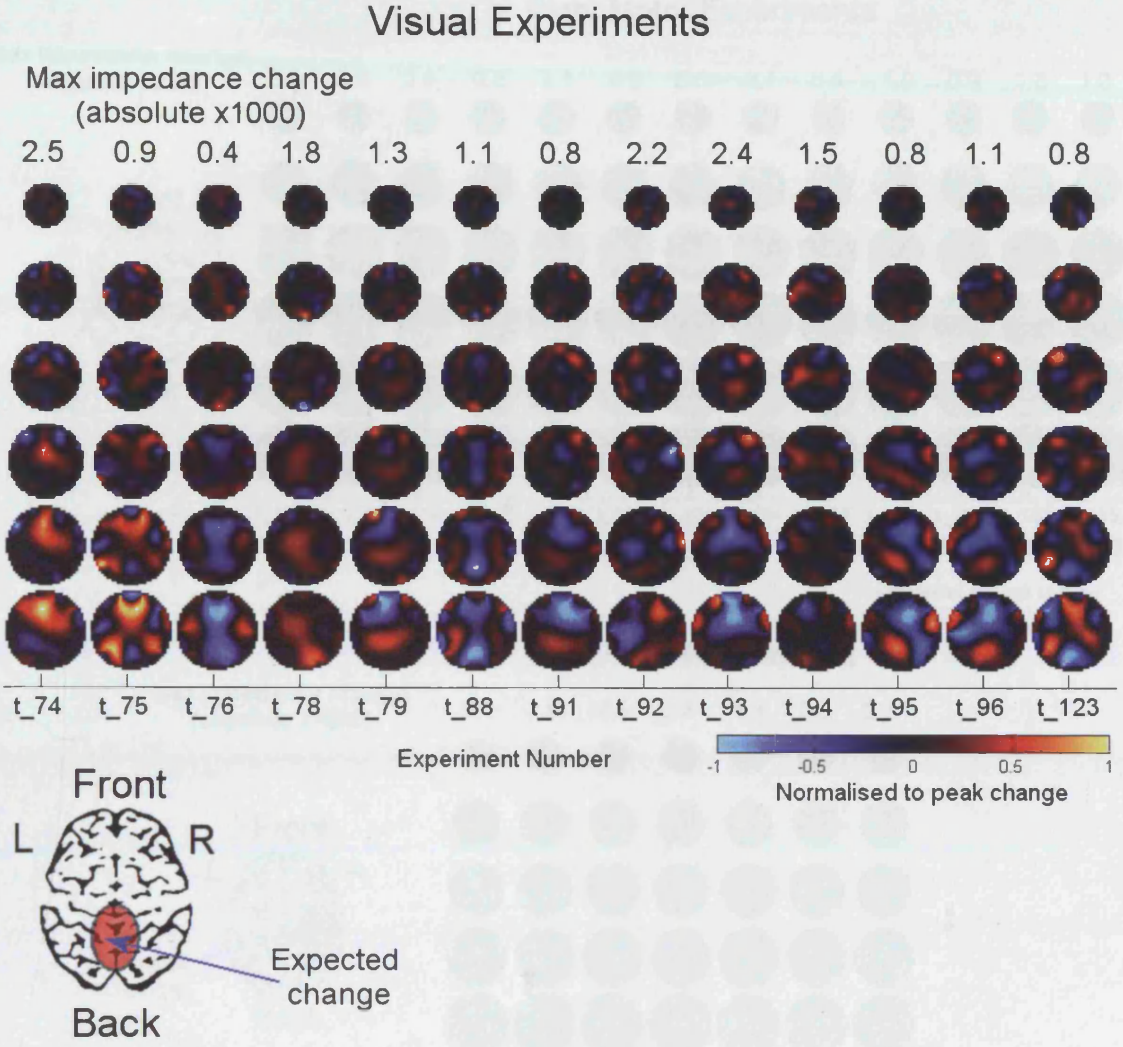

Figure 2.19 Images during visual stimulation for all subjects
This series of images represents the stimulus image during visual stimulation for all 13 subjects. Each column is the individual stimulus image for each subject (labelled on the x-axis) with 6 slices in each image. The images are viewed as if looking down on the head from above (bottom diagram, with approximate area of visual cortex illustrated).

Impedance changes are seen in all subjects during stimulation, but the images are noisy, as impedance changes appear during stimulation throughout the images, even when there is a significant impedance change appear in the posterior quadrant in the approximate region of the visual cortex. For clarity, the images are normalised to the maximum absolute impedance change (in each subject), the value of which is given at the top of each image.

Impedance decreases over the approximate region of the visual cortex are seen in subjects 74,75,76,88 and 123, and an impedance increase in subjects 78,91,92 and 96. Only impedance decreases are expected to be imaged in the visual cortex, due to the expected blood volume increase produced by increased neural activity.

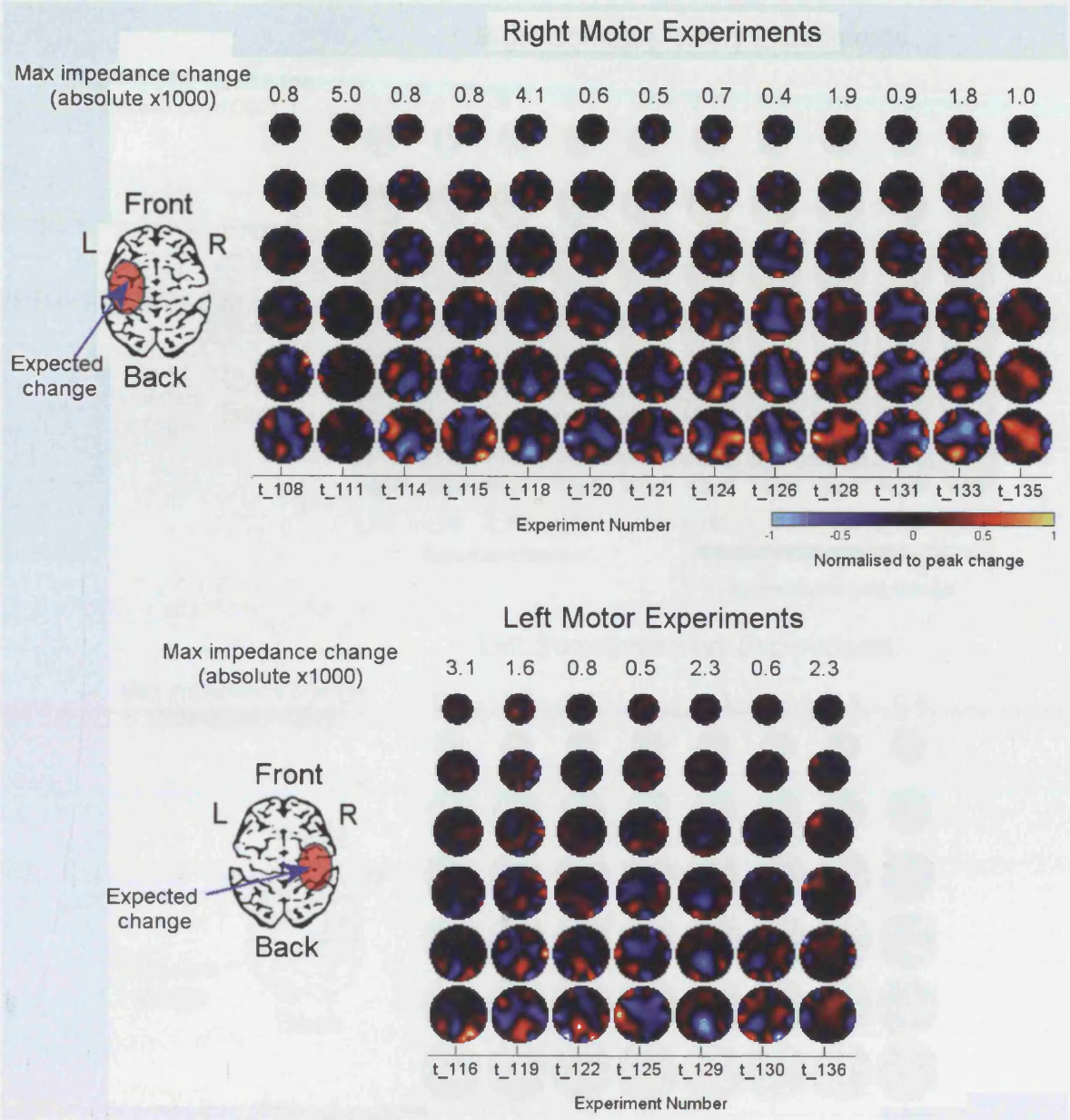

Figure 2.20 Images during motor stimulation for all subjects
This series of images represents the stimulus image during right hand motor stimulation (top) in 13 subjects and left hand motor stimulation (bottom) in 7 subjects. The orientation of the images and the approximate area of the contralateral motor cortex is indicated in the diagrams on the left of each set of images. For clarity, the images are normalised to the maximum absolute impedance change (in each subject), the value of which is given at the top of each image.

Again, these EIT images are noisy. The image analysis criteria allowed identification of significant contralateral impedance increases to the moving hand in subjects 114,128,135 for right and subject 136 for left motor movement respectively. Correctly localised impedance decreases are seen in subjects 120,124 and 133 for right and subject 119 for left motor movement, respectively. The amount of noise in the images would make it difficult to identify a single impedance change, if the viewer was not informed of the hand stimulated.

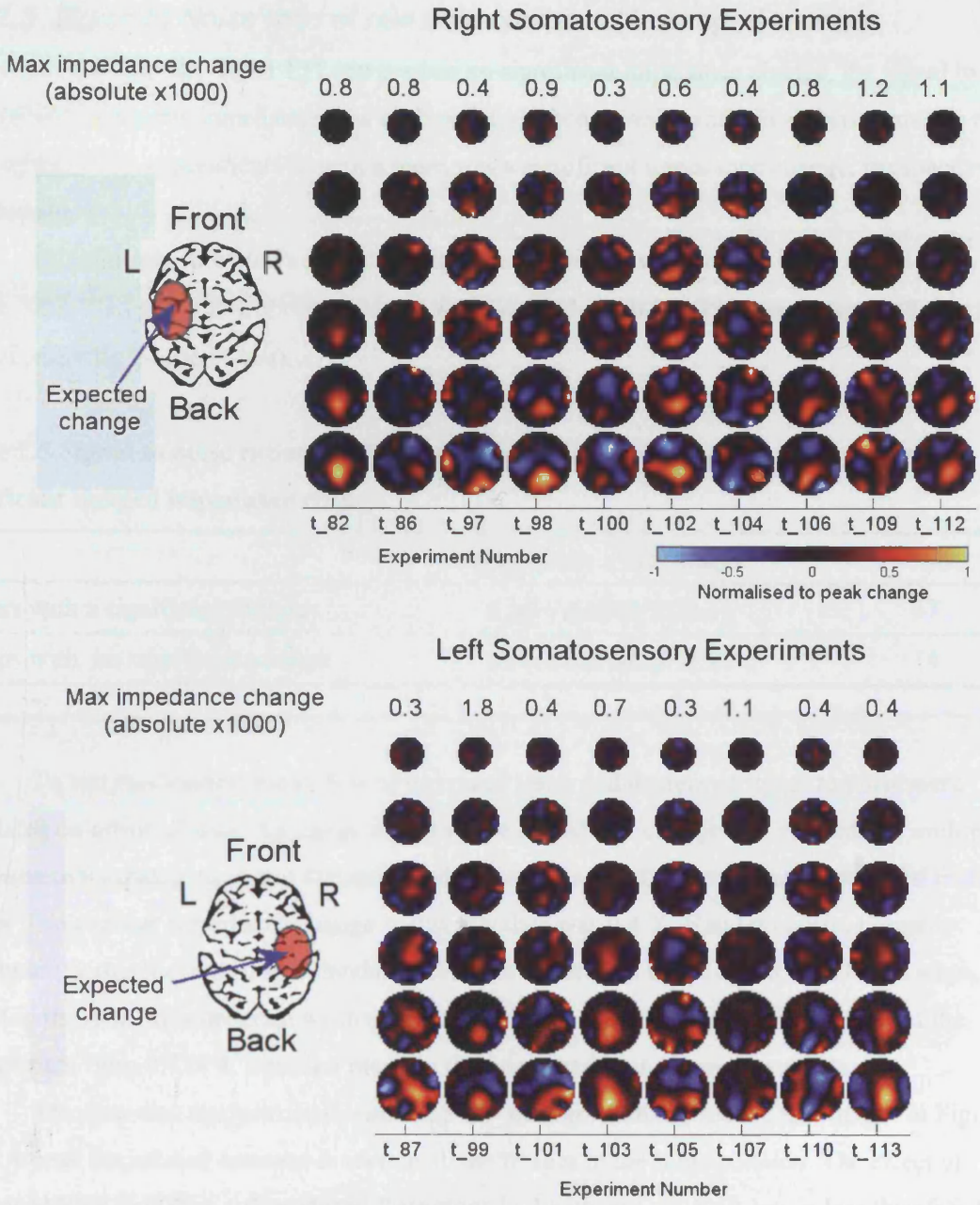

Figure 2.21 Images during somatosensory stimulation for all subjects
Stimulus image during right hand somatosensory stimulation (top) in 10 subjects and left hand somatosensory stimulation (bottom) in 8 subjects. The orientation of the images and the approximate area of the contralateral somatosensory cortex is indicated in the diagrams on the left of each set of images. For clarity, the images are normalised to the maximum absolute impedance change (in each subject), the value of which is given at the top of each image.

Stimulus related impedance changes are seen in all subjects, but due to the amount of image noise, changes are difficult to localise to any particular area. Examination of the contralateral image quadrant to the hand stimulated identified significant impedance increases in only subject 87 for left motor stimulation. A correctly localised impedance decrease is seen for subject 98 for right hand stimulation only.

2.3.2.3 *Signal to Noise ratio of raw data compared to imaged changes*

To try and find out why 14/51 EIT images had no significant impedance change, the signal to noise ratio (SNR) in the raw impedance data of those experiments was quantified and compared to the SNR of the 37/51 experiments in which there was a significant impedance change, irrespective of localisation.

Experiments in which a significant impedance change was imaged had a significantly higher SNR than subjects without a change, of 1.34±0.63 and 0.76±0.36, respectively (Table 2.5, $p<0.01$, d.f.=50, 2-tailed t-test).

Table 2.5 Signal to noise ratios (SNR) in the raw data for subjects with and without a significant imaged impedance change.

	SNR mean ± SD (range)	Number
Images with a significant change	1.34 ± 0.63 (0.52-3.4)	37
Images with no significant change	0.76 ± 0.36 (0.37-1.9)	14

To test this further, the effects of increased noise and decreased signal to noise were simulated on artificial data. An image with a single impedance change was created and multiplied by a sensitivity matrix to obtain the simulated voltage changes that would have produced that image. The average impedance change in this raw data was 0.4 %. Random noise, normally distributed with a mean of 0 and standard deviation of between 0.1 % to 1.0 % in 0.1 % steps, was added to the data, by a program written in Matlab. This varied the signal to noise ratio of the voltage data from 0.4 to 4, a similar range to that measured in the human raw data.

The data was reconstructed with the SVD_62 algorithm to produce the images in Figure 2.22. A peak impedance increase is seen in all the images in the same position. The effect of decreased SNR less than 1.0 produced distortions in the images. At SNR levels less than 0.5, the images appear to have 2 impedance increases in opposite sides of the images, whereas there was only one impedance change in the artificial data.

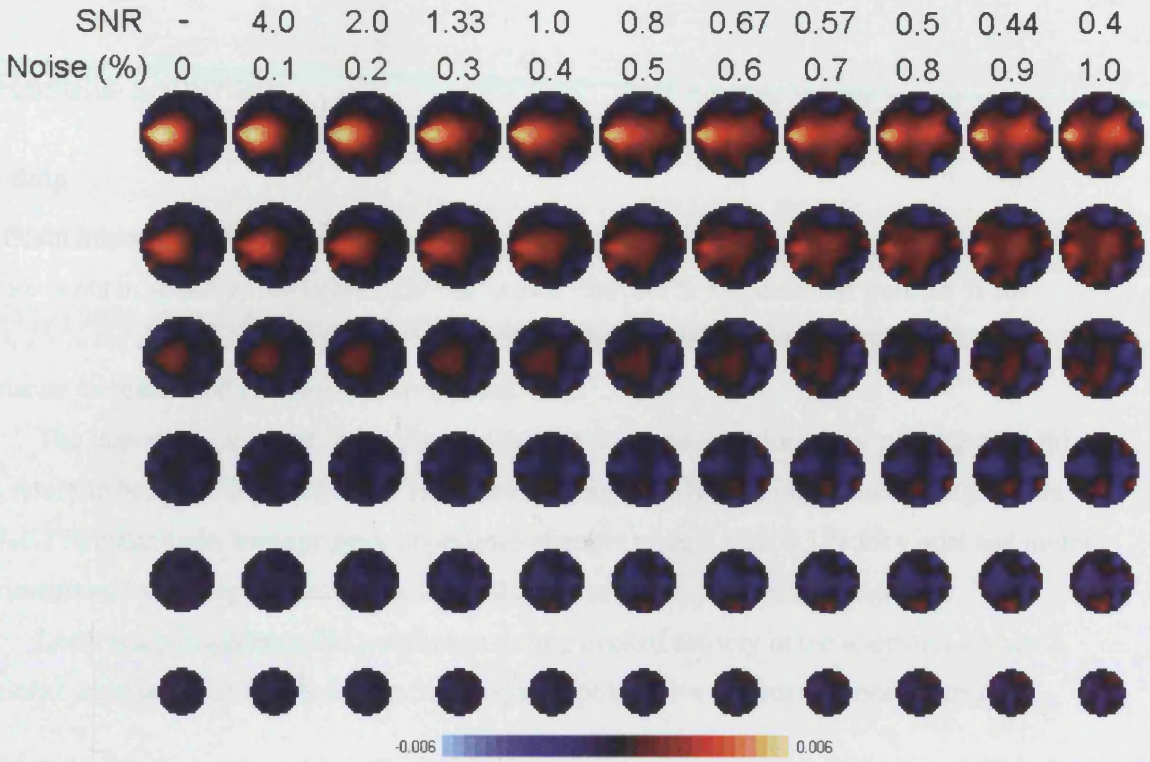

Figure 2.22 Effect of random noise, added to artificial EIT data, on image quality
Artificial impedance data was created with an average impedance change of 0.4 %. Random noise, was added to the data, between 0.1 % to 1.0 % of the baseline impedance, and the images reconstructed. Each column represents an image reconstructed from data with decreasing SNR from 4 (second on left) to 0.4 (far right). These SNRs represent a similar range to those measured in the human raw data.

A peak impedance increase is seen in the expected location in the left quadrant of all the images. The effect of decreased SNR progressively distorts the images. At SNR levels less than 0.5, the images appear to have 2 impedance increases in opposite sides of the images. This indicates that an improvement in the SNR of the raw impedance data should improve image quality.

2.3.3 Results summary

Raw data

Significant impedance changes were measured in all subjects. The proportion of scalp impedance measurements in which an impedance change greater than 0.1% was detected were 25 % for visual, 25 % for motor and 10 % for somatosensory experiments. Both stimulus related impedance increases and decreases were detected.

The impedance response had a latency time of 5 s (measured for motor paradigms only) and a return to baseline time of 33-50 s (in all paradigms). The largest impedance changes were of 0.5-1.3 % magnitude, average peak impedance changes were 0.5 %, 0.5 % for visual and motor experiments and were significantly smaller, at 0.2 %, for the somatosensory responses.

Local scalp impedance did not change during evoked activity in the scalp areas where a significant impedance change had been detected with polar drive impedance measurements.

Image data

Although significant impedance changes were detected in 37/51 images during the period of stimulation, image quality was poor due to the presence of multiple significant impedance changes and image noise. No significant impedance changes were detected in 14/51 experiments, and there was a correlation between the absence of an imaged change and low signal to noise in the raw scalp impedance data.

Localisation of significant impedance changes to the contralateral quadrant of the hand moved or stimulated, or the posterior quadrant during visual stimulation, was seen in 18/51 subjects, of which only 9 were impedance decreases. However, these images are noisy, so the impedance changes which correctly localised may have arisen by chance, rather than due to the ability of the EIT system to identify changes in the cortex stimulated.

The discussion that follows will consider the evidence that supports cerebral impedance changes as a cause of the raw impedance changes. Possible explanations for the failure to consistently localise significant impedance changes to the expected area of cortex stimulated and for the presence of EIT image noise will also be discussed.

2.4 Discussion

2.4.1 Raw data changes

2.4.1.1 Experimental support for cerebral impedance change

This is the first experimental evidence that reproducible impedance changes can be measured from the human head during sensory stimulation and motor activity. Similar changes have previously been recorded from the exposed cortex of rabbits (Holder *et al.* 1996; Rao *et al.* 1997; Rao 2000). The impedance changes recorded in this study had a similar timecourse to the stimulus, and were present in 51/52 of the experiments performed in 39 adult volunteers. It is likely that these changes arose from within the skull, and therefore from the brain, as scalp impedance was demonstrated to not change during motor activity.

The most likely physiological mechanism of the human impedance changes, is of a change of cerebral blood volume during brain activity. The evidence for this from a variety of animal and human studies will now be discussed, in addition to a consideration of other physiological mechanisms that may contribute to cerebral impedance change.

2.4.1.2 Likely physiological mechanisms of cerebral impedance change

Cerebral blood flow/volume changes

One of the most likely mechanisms that explains the presence of adult EIT changes in the raw data, is the existence of blood volume changes in the human brain during stimulation. This mechanism is supported experimentally in rabbit EIT work which has demonstrated the existence of co-localised increases of CBF, measured with laser Doppler flowimetry ,and decreases of impedance, imaged with EIT, in the visual cortex and somatosensory cortex of rabbits during visual and sensory stimulation, respectively (Holder *et al.* 1996; Rao 2000). The presence of both these changes indicates that the mechanism of the impedance change is an increase of cortical blood volume (CBV) in the stimulated cortex, which lowers local impedance due to the lower resistivity of blood compared to the surrounding cortex. Similar impedance decreases have been measured with intracortical electrodes in the cat during a variety of stimuli, such as presentation of food or milk, looking at an observer, or the presentation of a male cat to a female (Adey *et al.* 1962); these impedance decreases are similar to those measured in the rabbit studies of Holder et al. (Holder *et al.* 1996; Rao 2000) and therefore these changes are likely to share the same underlying physiological mechanism of an increase in CBV during presentation of stimuli.

Evidence to support a blood volume change in parallel to blood flow change, has been demonstrated in cats (Harel *et al.* 2002), in which both BOLD-fMRI (to measure blood flow) and MRI contrast (to measure blood volume) images were made serially during visual stimulation. Increased BOLD signal, due to increased flow, was identified in the primary visual cortex, which correlated with increased CBV in the same area. In this study a surrounding decrease of BOLD signal was detected in the visual association cortex, which correlated with decreased CBV. The results of this study indicate that the blood volume changes parallel changes in blood flow, and also that blood volume can increase and decrease in different areas of cortex.

In human adults, visual stimulation also produces parallel increases of blood flow and volume occur in the visual cortex, as measured with single channel Near Infra Red Spectroscopy (Kato *et al.* 1993; Villringer *et al.* 1993; Meek *et al.* 1995). Although NIRS does not provide images of increased rCBF, these have been provided by PET during a variety of visual stimuli (Fox *et al.* 1986; Mentis *et al.* 1996) and by fMRI (Ogawa *et al.* 1993; Schneider *et al.* 1993; Hoge *et al.* 1999). Extrapolating the results from these modalities implies that cortical increases in cerebral blood volume occur over a wide area of the visual cortex, dependent on the stimulus used, and that these should correlate with impedance change.

Similar findings are found with electrical somatosensory stimulation of the wrist, where increased blood flow has been demonstrated in the contralateral somatosensory cortex with PET (Ibanez *et al.* 1995) and with fMRI (Iramina *et al.* 1999; Holloway 2000), and similarly with motor activity, in which increased blood flow occurs in contralateral motor cortex, again demonstrated by PET (Sadato *et al.* 1996; Weiller *et al.* 1996; Catalan *et al.* 1998) and fMRI (Kim *et al.* 1993; Ye *et al.* 1997; Kinahan and Noll 1999).

All these studies have used similar visual, motor or sensory stimulation paradigms to those used in this adult EIT study. Therefore the areas of cortex shown to undergo an increased blood flow in response to stimulation are likely to undergo increased blood volume in the adult EIT studies, from which I would predict a decrease of cortical impedance with a similar timecourse between the impedance changes and blood flow changes measured with fMRI and NIRS.

In this EIT study the timecourse of the impedance changes to change from rest during motor activity was 5.8 ± 0.9 s (Mean ± SEM) and the time taken to return to baseline impedance was similar for all stimuli: visual, motor and somatosensory responses took 36 ± 4 s, 36 ± 4 s and 21 ± 3 s after stimulus cessation to return to baseline respectively. fMRI studies of similar motor stimuli (Kim *et al.* 1993; Boecker *et al.* 1994) demonstrate variable timings of the BOLD signal changes, with a rise time of 2-5 s, a peak at between 5-10 s and a return to baseline within 15-40 s

of stimulus cessation, which are similar to, but slightly faster than the EIT changes. The similarity between the BOLD and EIT timecourses strongly support the hypothesis that blood flow/volume change underlies the impedance change measured in adults. The faster timecourse of fMRI may reflect either that fMRI is sensitive to smaller changes that occur earlier during stimulation, or that the blood volume change detected by EIT lags behind the change in blood flow detected by fMRI.

In summary, both human and animal evidence strongly supports a mechanism of blood volume change as the cause of impedance change measured in the raw EIT data. It is also possible that other physiological mechanisms may have contributed to the impedance change, such as cell swelling, temperature or changes in the thickness of CSF, which are now considered.

Cell Swelling

In Chapter 1, the mechanism of cell swelling during seizure activity was discussed. Briefly, the cell swelling that occurs during seizures reduces the size of the extra-cellular fluid (ECF) space by up to 30% (Lux *et al.* 1986). As the ECF space is predicted to conduct a large proportion of the intra-cranial current applied by the EIT system (Ranck 1963; Ranck 1963; Lipton 1972; Andrew and MacVicar 1994; Holthoff and White 1996; Rector *et al.* 1997; Muller and Somjen 1999); then a reduction of ECF volume would increase impedance; such impedance changes have been measured with EIT in rabbits during epilepsy (Rao *et al.* 1997) and with direct cortical impedance measurements (Van-Harreveld and Schade 1962). As the mechanism of cell swelling is due to increased neural activity during epilepsy, then it is possible that the increased neural activity during physiological levels of stimulation, i.e. produced by evoked responses, then cell swelling may contribute to the impedance changes measured in this Chapter. However there is little support for the evidence of cell swelling in humans in vivo.

Initial support for cell swelling in humans during functional activity was provided by studies that measured the reflectance of light from the human cortex exposed at neurosurgery. These intrinsic optical imaging studies showed changes during somatosensory stimulation (Cannestra *et al.* 2001; Sato *et al.* 2002) and voluntary motor movements (Haglund *et al.* 1992); in general these responses were fast, peaking within 2 seconds of stimulus onset, with onset faster than the corresponding fMRI-BOLD signal measured the same subjects (Cannestra *et al.* 2001). These changes were thought to be due to a number of possible physiological changes which included changes in the concentration of de-oxygenated and oxygenated haemoglobin, changes in cerebral blood volume (Grinvald *et al.* 1986; Grinvald *et al.* 1991), and a possible contribution from changes of cell size (cell swelling) or cell conformation - evidence for which has been

provided from intrinsic optical studies of avascular animal brain preparations (Cohen *et al.* 1972; Lipton 1972; Andrew and MacVicar 1994). Until recently, the relative contribution of these physiological mechanisms to the intrinsic optical signals have not been measured. Fortunately, a recent study has addressed this issue (Sato *et al.* 2002). In this study the intrinsic optical absorption spectra of the exposed rat cortex in-vivo was made during somatosensory stimulation. The absorption spectra were compared to those obtained from a biological phantom that constituted rat blood and intralipid; the purpose of the phantom was to simulate the properties of the brain without the contribution of neural tissue and exclude any possible contribution to the optical signals of cell swelling and cell conformation changes. The concentrations of oxygenated and deoxygenated haemoglobin in the phantom were varied to simulate changes in haemoglobin of the rat brain during stimulation. The absorption spectra obtained from both the biological tissue phantom and the rat brain were nearly identical, and from these results the study concluded that any contribution of cell swelling/neuronal cell conformation changes to the intrinsic optical signals were negligible. It now seems clear from this rat study, that the changes in the intrinsic optical signals measured in the human cortex during somatosensory and motor stimulation are mainly due to changes in cerebral blood volume and concentrations of deoxy and oxygenated haemoglobin, with no significant contribution to these signals from cell swelling.

In conclusion, there is no evidence from optical studies of animal or human cortex that cell swelling occurs in vivo. However, there is also insufficient evidence to conclude that cell swelling does not occur in the brain during physiological levels of neuronal activity as studies have not been performed that examine cell swelling specifically. The main evidence that cell swelling does not have a significant contribution to impedance changes during functional activity is provided by EIT of the exposed rabbit cortex during evoked responses (Holder *et al.* 1996); as the changes imaged were impedance decreases, then the predominant effect of cerebral impedance change during functional stimulation is due to increased blood flow/blood volume in the area of active cortex.

Temperature Changes

Increases in temperature produce decreased impedance, due to the increased mobility of charge carrying ions. The amount by which impedance changes has been demonstrated in the rabbit cortex, where impedance decreases by 2 % for every 1 °C rise in temperature (Van-Harreveld and Ochs 1956). It is feasible that increased metabolic activity in the brain would produce an increase in temperature and give rise to an impedance change.

Temperature changes have been demonstrated in the human cortex during prolonged visual stimulation, using an fMRI technique (Yablonskiy *et al.* 2000). In this study, drifts of the frequency of the BOLD signal were calculated to occur due to changes of cortical temperature, from which changes in cortical temperature by up to 1°C were calculated. Both temperature increases and decreases were measured, increases due to increased metabolic activity, or decreases due to a cooling effect from increased cerebral blood flow. These changes occurred over a long timecourse with an onset after stimulation of up to 60 seconds. It is therefore unlikely that these contributed to the impedance signal, as the timecourse of the EIT changes were over a much shorter period of time.

Other possible contributions to impedance change

An additional mechanism by which impedance may change is due to a change of the thickness of the cerebro-spinal fluid (CSF) layer overlying the active cortex as a result of increased cerebral blood volume. This has been suggested by a theoretical study of NIRS (Firbank *et al.* 1998). If increased cerebral blood volume in the cortex results in an increase of local cortical volume, then this would shift the cortical surface towards the CSF layer and an equivalent volume of CSF would be moved away from the area of the active cortex. As CSF has a lower resistivity than blood, 80 Ω.cm and 150 Ω.cm, respectively, then a change in cerebral blood volume displacing an identical volume of CSF would result in an overall impedance increase. This may be more of a problem in the region of the somatosensory and motor cortex, that lie on the outer surface of the parietal cortex, adjacent to the CSF layer. This may be less of a problem in visual cortex, which lies within the calcarine fissure in which the layer of CSF over the visual cortex may be smaller.

If CSF changes do occur, then this could have a significant effect on mislocalisation of impedance changes within the EIT images. However, if CSF volume changes do exist, then it is likely that these would have been detected from the measurements of scalp impedance. These measurements were likely to be sensitive to impedance changes deep to the electrodes by approximately 7mm, which would have included the CSF. As no changes were measured with direct measurements of local scalp impedance change, then it is unlikely that significant impedance changes occurred in the CSF layer.

2.4.1.3 Conclusion

The raw impedance changes measured during stimulation almost certainly arise from the brain, with the most likely cause of the impedance change to be due to a change in cerebral blood volume at the site of the neurally active cortex. Changes of cerebral blood flow and blood volume have been demonstrated extensively in humans with PET, fMRI and NIRS, and these changes

have a similar timecourse to the evoked impedance response. From the evidence considered above there is little support that significant impedance changes occur due to cell swelling or due to changes in cortical temperature. Although a theoretical complication may arise due to changes in CSF volume, the absence of impedance changes from direct measurements of the scalp are against significant impedance changes due to changes of CSF volume.

2.4.2 Mechanism of bi-directional impedance changes

In the raw data both impedance increases and decreases were measured for most of the subjects. This initially seems counter-intuitive if the brain impedance change is in one direction only. However, even if there is a single, well localised and unidirectional impedance change within the head, then both impedance increases and decreases can be detected on the scalp surface. This is illustrated in the following diagram (Figure 2.23). There is direct evidence that single, uni-directional impedance changes can produce bi-directional changes in the raw impedance data from studies in tank phantoms (Tidswell *et al.* 2001) (see Chapter 3). These studies used a tank phantom to simulate the human head, and both impedance increases and decreases were measured when a uni-directional impedance change (an impedance increase) was introduced into the tank

Bi-directional impedance changes may also occur physiologically, due to the presence of multiple and bi-directional impedance changes within the head. These may result from changes of blood volume that occur away from the stimulated cortex and are opposite in magnitude. Evidence for this can be derived from human PET studies of visual function, in which blood flow increases in the visual cortex during stimulation and blood flow decreases, of smaller magnitude but larger volume, occur in frontal cortex (Mentis *et al.* 1996; Mentis *et al.* 1997; Mentis *et al.* 1998).

In conclusion, the presence of both impedance increases and decreases in the raw data can be brought about either by single, uni-directional and well localised impedance changes, or multi-focal, bi-directional impedance changes in the human brain during stimulation. The presence of both types of change in the raw data does not help to distinguish between these two possibilities.

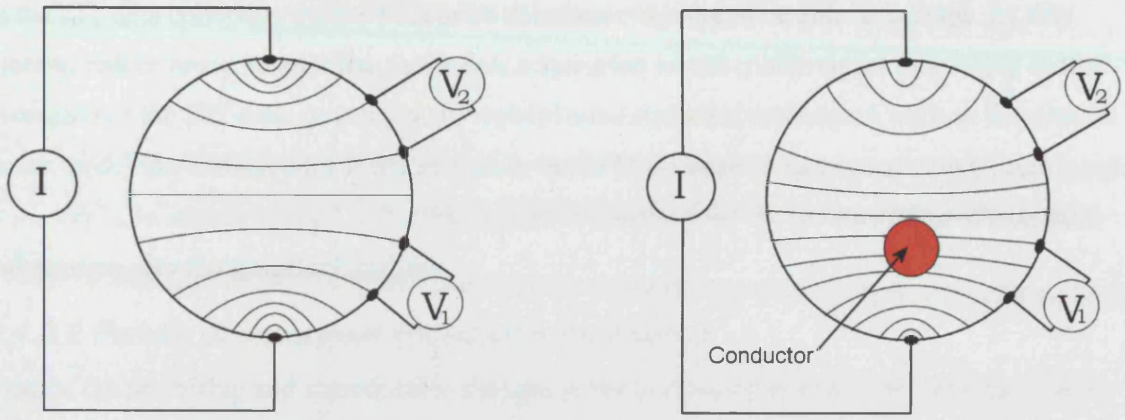

Figure 2.23 Bi-directional surface impedance changes from a single impedance change
This diagram illustrates how both an impedance increase and decrease can be detected on the surface of an object, despite only an impedance decrease within the object. Both diagrams represent an impedance object; the left represents an object without impedance change, the right diagram represents the object with an impedance decrease (conductor, red) within it.
Left diagram: an applied current spreads uniformly throughout the object, resulting in symmetric isopotential lines. Both measurement electrodes, **V1** and **V2** record a similar potential difference.
Right diagram: an impedance decrease (a conductor) is introduced at the bottom of the object. The current will not be unevenly distributed through the object as more will be conducted through the lower half in which there is increased conductivity (due to the presence of the conductor). This has an effect on the surface isopotentials, which are closer together in the lower of the object compared to the top. The voltage electrodes, **V1** and **V2** now record different potential differences which are larger in **V1** and smaller in **V2** than in the left diagram. As impedance is proportional to voltage, an impedance increase is recorded at **V1** and an impedance decrease at **V2**.

2.4.3 EIT image changes

2.4.3.1 Absence of imaged impedance changes

There was an absence of impedance changes in 14/51 experiments. This was associated with low signal to noise in the raw impedance data. The majority of images without a change arose in the somatosensory experiment group, of which 11/18 had no change. In this group the peak impedance changes were statistically smaller than the motor and visual evoked responses (0.2 % vs. 0.4-0.6 % respectively) and occurred in a smaller number of measurements (12 % vs. 25-26 % respectively).

These findings indicate that there are limits of the sensitivity of the EIT images to changes in the raw data and indicates that signal to noise may need to be improved to increase the number of images with a significant impedance change. This could be achieved by improvements

to the EIT data collection system to acquire data faster in order to be able to average the data more to reduce noise. In addition, faster data acquisition would enable signal processing or time-averaging of the EIT data, or using more sophisticated statistical techniques, such as the general linear model implemented for fMRI images in the SPM package (Friston *et al.* 1990; Frackowiak *et al.* 1997), to improve signal extraction and noise reduction by the incorporation of temporal information into the statistical analysis.

2.4.3.2 Failure of consistent impedance localisation

Despite the promising and reproducible changes in the raw impedance data, the images of those experiments with significant impedance changes were disappointing. The images demonstrated stimulus related, and significant impedance changes in 37/51 experiments, however the images were noisy, demonstrating multiple impedance changes, of which only 18/51 were localised near to the expected area of cortex stimulated. Due to the presence of the multiple impedance changes and the broadly defined area of a correctly localised change into a quadrant of the image, then the 18/51 experiments with an impedance change in the 'correct location' could have arisen by chance. In addition there was a lack of consistency in the direction of the impedance change; of those changes in approximately the correct position 9/18 were increases and 10/18 decreases. This lack of consistency between similar experimental paradigms casts uncertainty as to the cause of the impedance changes, and to the ability of EIT to image physiological changes in the brain during stimulation.

The EIT results are not consistent with the hypothesis that a simple sensory stimulus produces neural activation in a focal cortical area that results in a single impedance change. Images expected from this hypothesis should demonstrate a clear, localised impedance change. As this is not the case, then there is either an inability of the EIT system to image changes accurately within the head, or there is an oversimplification in the above hypothesis. These can be discussed separately under Physiological Factors and EIT Factors

Localisation failure due to possible Physiological factors

The majority of evidence, so far discussed, supports the hypothesis of a single large blood flow change in the activated cortex, that will increase blood volume and change impedance. However evidence for multiple, multi-focal blood flow changes exists which may contribute to impedance changes in the images, and the evidence for this will be considered,

The strongest evidence for a single large impedance change occurring in visual and somatosensory cortex during respective stimulation has been demonstrated by EIT in rabbits (Rao 2000). There is evidence from plenty of functional imaging studies in humans that demonstrate

visual checkerboard, similar to the stimulus used in this study, produce localised blood flow increases in the visual cortex detected with PET (Mazziotta and Phelps 1984; Fox *et al.* 1986) and fMRI (Schneider *et al.* 1993; DeYoe *et al.* 1994; Hoge *et al.* 1999; Hoge *et al.* 1999; Hoge and Pike 2001). Cerebral blood volume has been demonstrated to increase in the human visual cortex during patterned flash stimulation, as detected by MRI of an injected gadolinium contrast agent (Belliveau *et al.* 1991). Similar, well localised, blood flow responses have been demonstrated in the sensory or motor cortex, with PET (Mazziotta and Phelps 1984; Fox *et al.* 1986; Mentis *et al.* 1997; Catalan *et al.* 1998), and fMRI (Kim *et al.* 1993; Ogawa *et al.* 1993). However, one of the main problems with these studies, is that regions of interest have often been used to analyse the data, either to increase statistical thresholds in a region of interest (Hoge *et al.* 1999; Hoge *et al.* 1999; Hoge and Pike 2001) or due to the limitations of early neuroimaging with fMRI, used surface coils to increase signal to noise in the cortical region of interest (Belliveau *et al.* 1991; Kwong *et al.* 1992; Ogawa *et al.* 1993; Schneider *et al.* 1993). The additional difficulty in assessing these early papers, is that it is often not clear whether the data are examined for positive and negative changes (Fox *et al.* 1986). This raises the possibility that significant blood flow responses outside the primary visual or somatosensory cortex stimulated have not been excluded, and even though such blood flow changes may be small compared to the area of interest, if they occur over a wider cortical area then significant impedance changes outside the activated sensory cortex may occur. Such changes could account for the presence of multiple impedance changes in the EIT images.

There is some evidence that blood flow changes occur outside the area of interest, with fMRI studies having demonstrated that changes of blood flow occur outside the primary stimulated area. For example, in a simple unilateral hand motor task, although the largest blood flow changes occur in the contralateral primary motor cortex, ipsilateral blood flow changes, of up to 10% of the changes in contralateral cortex, may also occur (Kim *et al.* 1993; Boecker *et al.* 1994; Sadato *et al.* 1996). Blood flow changes have also been demonstrated to occur outside the area of the motor cortex, in the areas of the frontal and parietal cortex (Oostende *et al.* 1997). These are again smaller than the changes in contralateral motor cortex, but occur over a wider area, which, for EIT, may result in a similarly sized impedance change.

Decreased cerebral blood flow and volume outside the area of cortex stimulated have been demonstrated in some human studies, both with optical, fMRI and PET functional imaging techniques. Haglund et al. (1992) optically imaged the human motor cortex during neurosurgery in 5 subjects (Haglund *et al.* 1992), and found that tongue movement increased blood flow and volume in contralateral primary motor cortex with decreased flow and volume in surrounding

cortical areas. Blood flow decreases measured with fMRI during hand motor activity have been reported by Ogawa et al. (Ogawa *et al.* 1993): these decreases were observed simultaneous with increased blood flow in contralateral motor cortex during finger thumb apposition with the decreased blood flow imaged in adjacent cortical areas. During painful stimuli, one PET study demonstrated that a 25 % decreases of global cerebral blood flow occurred (Coghill *et al.* 1998). In addition, PET studies have demonstrated that blood flow decreases in the parietal and frontal cortex of 14% during visual stimulation (Mentis *et al.* 1996; Mentis *et al.* 1997; Mentis *et al.* 1998) compared to a 30 % blood flow increase in primary visual cortex, and that these decreases are correlated with the flash frequency of the visual stimulus. As the regions of decreased cerebral blood flow in this particular study occurred over a much larger volume than the increases in the visual cortex, then they would be expected to produce a similarly sized impedance change if reproduced in the adult EIT subjects.

In summary, although the majority of functional imaging literature reports increased blood flow, some of which may reflect a reporting or statistical thresholding bias, there is also evidence that even simplistic visual or motor stimuli do not lead to single areas of blood flow change. As some evidence indicates that smaller changes may occur over larger cortical areas, then both sets of changes would be expected to change impedance. If the changes are far enough apart, then the EIT images should be able to resolve the two changes, however if the changes are closely spaced, and of opposite sign (e.g. due to a blood volume increase and surrounding blood volume decrease), then due to the low spatial resolution of EIT the combined impedance would be imaged with partial cancellation of the changes leading to mislocalisation in the images.

However, even considering the likelihood of multiple, multi-focal cortical impedance changes, it is reasonable to assume that the largest impedance change should be in the area of the cortex with the largest change in blood flow and volume. The functional imaging studies which demonstrated blood flow change outside the area of activated cortex, also indicated that the largest blood flow changes occurred in the expected area of cortex stimulated by their experimental paradigms. The inference from this is that the EIT images should still be able to localise and impedance change in the appropriate area. As this is not the case, then other likely causes of mislocalisation should be considered such as errors in the EIT system or in the EIT reconstruction algorithm.

Localisation failure due to EIT System

Errors in the EIT system may account for the noise in the EIT images and the failure of consistent image localisation. These errors can be subdivided into errors produced by the EIT measurement system or errors produced by the reconstruction process.

1. EIT hardware - potential errors

Errors from the EIT equipment will mainly be due to either equipment noise or measurement errors due to factors such as stray capacitance. These will be discussed individually.

Most of the measurement noise in the subjects varied between 0.1-0.2%. Some of the variation in the EIT signal is likely to be physiological, as small variations in blood flow occur during the cardiac cycle and during respiration. The rest of the variation in EIT signal is likely to be due to electronic noise from the EIT system. A reduction of equipment noise would enable smaller changes in scalp impedance to be detected, and result in less noise being reconstructed in the images. However, the current levels of noise of the EIT hardware did not prevent significant impedance changes from being detected in the images of 37/51 experiment, so it is unlikely that noise alone contributed to the inability of the EIT system to correctly localise the impedance changes in the EIT images.

In contrast to this, stray capacitance may influence the size of the impedance changes measured. This would result in clear impedance changes in the raw data, but influence the reconstruction of these changes in the EIT images. The effect of stray capacitance acts as a current shunt between sets of current injection and voltage measurement electrodes, and is most likely to occur along the length of the electrode leads to the subject. As the EIT reconstruction algorithm assumes that the current delivered by the EIT system is the same current applied at the head, then a reduction of the applied head current would lead to a reduction in the voltage changes measured. Because stray capacitance would vary between different leads, and between subjects, then the size of the error is unpredictable, with unpredictable consequences on the quality and localisation of the images. Such errors could lead to a failure of the EIT system to localise impedance changes to the area of origin.

2. EIT Reconstruction - potential errors

The reconstruction algorithm, used to reconstruct the raw EIT data, is based on a simplified model of the head. As this model is a sphere of uniform conductivity, then differences between the properties of the head and the model are likely to lead to reconstruction errors. In turn these

reconstruction errors may account for the failure to localise an impedance change to the area of origin (Barber and Brown 1988).

There are several differences between the spherical head model and the head; these are: 1) The head shape, 2) The presence of the skull, 3) The presence of other tissue layers of different resistivity in the head, such as the low resistivity cerebro-spinal fluid (CSF), 4) Tissue resistivity anisotropy, by which the resistivity of tissue differs with respect to it's orientation and 5) The presence of electrode position errors on the human scalp compared to the idealised scalp electrode positions on the spherical reconstruction model.

1) Effect of head shape: The presence of the irregular head shape not only leads to errors of electrode positioning (discussed below), but is likely to affect the way in which current traverses the head. One example is that a longitudinally applied current will pass through a smaller cross-sectional area of the head than a transversely applied current, and therefore encounter a higher total resistivity with the effect of shunting a greater proportion of current through the relatively low resistivity scalp. As the spherical head model assumes a uniform resistivity, then such differences may give rise to errors in the reconstructed images.

2) Reconstruction errors arising from the skull: As discussed in the introduction (section 1.3.2), the skull has a high resistivity and acts to shunt current around the scalp (Rush and Driscoll 1968). This will have two effects, the first is to attenuate the size of the impedance change measured and the second is to introduce a localisation error of the impedance change (Gibson *et al.* 2000). The imaged change is moved towards the centre of the image in comparison to the real position (Avis *et al.* 1992) which can be compensated for by means of a radial correction (Ary *et al.* 1981).

3) Reconstruction errors arising from the CSF: The effect of the CSF is to act as a current shunt, as the current entering the cranial cavity encounters a low resistance CSF path. Evidence that this shunt effect occurs has been demonstrated in live rabbits (Joy *et al.* 1999). In this study, two sets of orthogonal MRI images were obtained of the magnetic field produced by a current applied to the rabbit's scalp. From these images, an image of current density within the head was calculated. They demonstrated that the current density arising from a longitudinally applied current (anterior-posterior direction) was concentrated along longitudinal CSF spaces. In contrast a current applied transversely across the rabbit's head was evenly distributed throughout the brain due to a smaller cross-sectional area of CSF in the direction of current. This study implies that an accurate reconstruction algorithm needs to account for the shunt effect of the CSF in order to map out the current distribution in the head, in order to produce an accurate sensitivity matrix. As the spherical model of the head in this EIT reconstruction algorithm does not account

for this, then localisation errors due to CSF shunting are likely to occur. Such errors may result in the failure to image impedance changes to the predicted areas of activated cortex.

4) Reconstruction errors arising from tissue anisotropy: The EIT reconstruction model does not account for the different resistivity of tissues in different directions. This mainly applies to the muscles in the scalp, and the white matter of the brain, both of which have fibres orientated in one direction, along which the resistivity is decreased. As with CSF, the different resistivities in different directions may increase current density in one direction compared to another and therefore introduce errors when compared with a model of uniform resistivity.

5) Reconstruction errors arising from errors of Scalp electrode placement: Despite using a standardised method of electrode placement, errors in positioning, due to the different shapes of the various subject's heads, or due to positioning error from the electrode placement itself, will result in changes of position away from the idealised electrode positions on the surface of the spherical model and result in errors in the image (Barber and Brown 1988). The way around this problem is to only reconstruct impedance changes, as the electrode placement errors are present in both the baseline and comparison images they are effectively cancelled out (Barber and Brown 1988), and this was the approach used in this chapter.

There are therefore many potential errors present in the current reconstruction method. Although a solution would be to create a more realistic head model for use in the forward model used to construct the sensitivity matrix of the reconstruction algorithm, such a model was unavailable during most of the work obtained in this thesis. Therefore work was performed to try to quantify some aspects of the possible sources of reconstruction errors discussed above. This work is presented in Chapter 3 and utilised a realistic head-shaped tank, containing a human skull, to assess image reconstruction of known impedance changes.

2.4.4 Conclusions

This is the first work to demonstrate that evoked impedance changes can be measured non-invasively in humans. These changes are most convincing in the raw data, as the changes follow the timecourse of the stimulus and are reproducible within and between subjects across three different sensory modalities. As scalp impedance does not change during the evoked activity, then the likely cause of the measured impedance changes are from increased blood volume in the area of neurally active cortex. However, although blood volume increases are expected to decrease impedance, when considered with possible changes in the thickness of the CSF layer an impedance increase is theoretically possible. The expected direction of the evoked impedance

change cannot therefore be determined from either this study or the available evidence from the neuroimaging literature.

The EIT images were less convincing and failed to demonstrate a consistent localisation of impedance change to the area expected to be stimulated by the sensory paradigms. Some of this failure was due to low signal to noise in the raw data. However, those images which demonstrated significant changes were noisy and still failed to localise a change. The possible reasons for this localisation failure have been discussed and may arise from physiological factors or errors from the EIT system and reconstruction algorithm.

The major question raised from this study is the cause of this localisation failure. The experiments in the next chapter try to exclude some of the EIT system and algorithm factors that could account for these errors, by means of a realistic head shaped phantom designed to test the accuracy of the EIT system.

Chapter 3: Imaging in a Head-Shaped Tank

3.1 Introduction

3.1.1 Overview

The previous chapter has demonstrated that reproducible impedance changes can be measured at the scalp during sensory stimulation. However, images of these changes were not reproducible between subjects and did not localise the impedance changes to the expected area of the cortex stimulated. This localisation failure could have arisen from a variety of factors which may be either physiological, due to the EIT hardware or due to EIT reconstruction errors. In particular, errors are likely to have arisen from the EIT reconstruction model, based on a simplified spherical model of the human head, when used to reconstruct data obtained from the human head. Differences between the head and the spherical model used in the reconstruction algorithm, such as the shape of the head, the presence of the skull, the presence of various tissue layers such as the skin, scalp and CSF, or the presence of tissue anisotropy, may lead to reconstruction errors.

3.1.2 Previous EIT tank studies

Previous tank studies performed at the UCLH EIT research group have initially tested the HP-EIT system in two dimensional (2D), cylindrical tanks (Boone *et al.* 1994), with a 2D electrode array present in a ring on the circumference of the tank and images were reconstructed using a 2D reconstruction algorithm. Images obtained from these studies showed impedance changes in the area of the tank that the impedance changes were placed and indicated that in 2D, the HP-EIT system could localise impedance changes correctly with minimal localisation errors. On the development of the 3D reconstruction algorithm, used on the adult EIT data in Chapter 2, it was necessary to produce 3D tank phantoms.

Previous 3D tank-phantoms in our laboratory have used hemispherical Perspex tanks with a hemispherical simulation of the skull made from plaster of Paris (Balchin 1997). Again images from these studies indicated that single impedance changes could be localised within the tanks to an accuracy of approximately 10% of the diameter of the tank. However, these are simplistic models which do not account for the irregular anatomy of the head and skull, nor the low resistive paths present in the skull, for example the eye sockets, cranial sutures and holes left by blood vessels (Law 1993). In addition, the use of a reconstruction algorithm based on a model of the head as a homogenous sphere is likely to have produced less reconstruction errors when applied to EIT

data obtained from a spherical tank model than to EIT data obtained from the human head (Gibson 2000).

3.1.3 The effect of the skull:

The main effect of the skull is due to its high resisitivity; this acts as a barrier to the applied scalp current, so that a large proportion of the current will flow through the scalp and a smaller proportion enter the skull; this will reduce the sensitivity of scalp impedance measurements to impedance changes within the brain. One previous study examined this by the use of a fetal skull inside a cylindrical tank phantom to demonstrate that the effect of the skull is to reduce the sensitivity of EIT to an impedance change within the skull to 44% (McArdle *et al.* 1988). However, no mention was made in this study of the effect of the skull on object localisation, which is more relevant to the problem of poor image quality in the adult human EIT studies of Chapter 2. In addition, the EIT system used in this study used adjacent electrodes to apply current to the tank which reduces the amount of applied current that enters the skull in comparison to current applied from electrodes which are placed on opposite sides of the skull in a polar-drive arrangement (Rush and Driscoll 1968).

With the adult skull, the proportion of current entering the skull cavity has been determined for a current applied by electrodes placed on opposite sides of the skull, with one on the occiput and one on the frontal region (Rush and Driscoll 1968), the equivalent to the 'polar drive' application of current in the adult EIT studies in Chapter 2. The proportion of current that enters the skull is 44% of the current applied by this method. The results of this study agree with theoretical EIT work, performed with a 2D finite element model (FEM) of the head, which demonstrated that the skull reduces the sensitivity of EIT to changes within the skull and that this sensitivity reduction is correlated with increased resistivity values of the skull (Bayford *et al.* 1996; Gibson *et al.* 2000). However, this study did not examine the proportion of current that enters the skull if applied at other points on the skull surface, which is exactly what the HP-EIT system does in obtaining impedance data in the adult human EIT studies. It is expected that the proportion of current that enters the skull will vary due to inhomogeneities within the skull, such as conductive gaps from sutures and eye sockets, and due to variability of the skull geometry in different directions of applied current; this probable variation will introduce a variability in the sensitivity of each EIT measurement to changes within the skull. As the homogenous spherical model of the head assumes that each measurement is equally sensitive to changes within the skull then this may be a source of reconstruction error when the reconstruction algorithm is used to reconstruct EIT data obtained from the human head. Therefore, this emphasises the need to use a real human skull in tank-studies which are designed to test the HP-EIT system and the 3D reconstruction algorithm.

3.1.4 Purpose of the study:

The purpose of the work in this Chapter was to test the 3D HP-EIT system and 3D reconstruction algorithms, used for the adult EIT studies in Chapter 2, in a realistically shaped head-tank phantom which modelled the scalp, the head shape, the electrode positions used in the adult EIT study and the presence of a real human skull. In addition the development of a head-tank enabled an assessment of the resolution of the EIT system/algorithm to known perturbations within the skull, and this model could be used to test the effects of noisy data on the quality of EIT images.

3.1.5 Experimental design

A realistic head shaped tank, with electrodes embedded on the surface of the 'scalp' surface of the tank, was constructed from a latex mould of a model of the human head constructed around a real human skull. Once complete, the human skull could either be placed or removed from the head-tank and the HP EIT system was used to acquire data from the tank during the insertion of impedance objects in specific locations. As the position of the impedance perturbations were known, the localisation error in the reconstructed images could be calculated from the difference between the expected position of the object in the image and the position of the object in the reconstructed images. These localisation errors were used to:

1) Test the positional accuracy of two reconstruction algorithms, the SVD_62 algorithm (used to construct the adult EIT data) and the Transpose algorithm, introduced in this chapter.

2) Assess errors introduced by the skull, by a comparison of errors between objects imaged in the tank, with or without the skull.

3) Assess errors introduced by the head shape, by comparing image errors in the head tank, without the skull, to images within a hemispherical tank, made of Perspex. The hemispherical tank was used as it resembled the spherical head model used in the production of the reconstruction algorithms.

These results were taken together and an assessment was made of:

1) The adequacy of the head tank as a model for the human head,

2) The likelihood that the head shape and/or skull were responsible for the localisation errors in the human EIT images.

3.2 Method

3.2.1 Construction of the head shaped tank

The head-shaped tank (Figure 3.24) was constructed from a latex mould of a clay head model. When cast, the rubber mould contained an empty head shape, with electrodes around its surface, in which a real human skull could be placed with a scalp gap between the skull and the electrodes. Once completed the mould, with the skull, was filled with saline, the EIT system connected to the tank electrodes and EIT data acquired of objects placed in the tank. The main steps in the production of the tank were:

1) Construction of the realistically shaped, clay head mould based around a real human skull

2) Placement of silver electrodes on the head mould, in the modified 10-20 positions used in the adult EIT studies. These electrodes were specifically designed to embed in the rubber head mould.

3) Construction of the rubber head mould, made from a rubber cast of the clay head mould.

Construction of the clay head mould

The steps taken in the manufacture of the tank are illustrated in Figure 3.24. A human skull, protected with foil, was built up into the head model with oil based clay to simulate the tissues of the scalp, head and neck (Figure 3.24, image 1). Scalp thickness was calculated from measurements of an MRI scan of a human head, which varied between 3-4 mm. The optimum clay thickness was determined by depth measurements made over a 1 cm spaced grid over the skull. This used a 3 mm metal probe inserted into the clay, which was either thickened or thinned to a 3-4 mm depth. The 'face' and 'neck' of the head model were modelled approximately and were not based on MRI measurements.

Construction of electrodes

1 cm diameter silver electrodes were cut from 0.05 cm thickness silver foil, with two strips of foil either side of the electrode face. The strips were bent backwards to act as anchors into the mould. Silicone coated wire was soldered onto the strips and the solder join coated with silicone to prevent contact with saline within the tank (Figure 3.24, image 2).

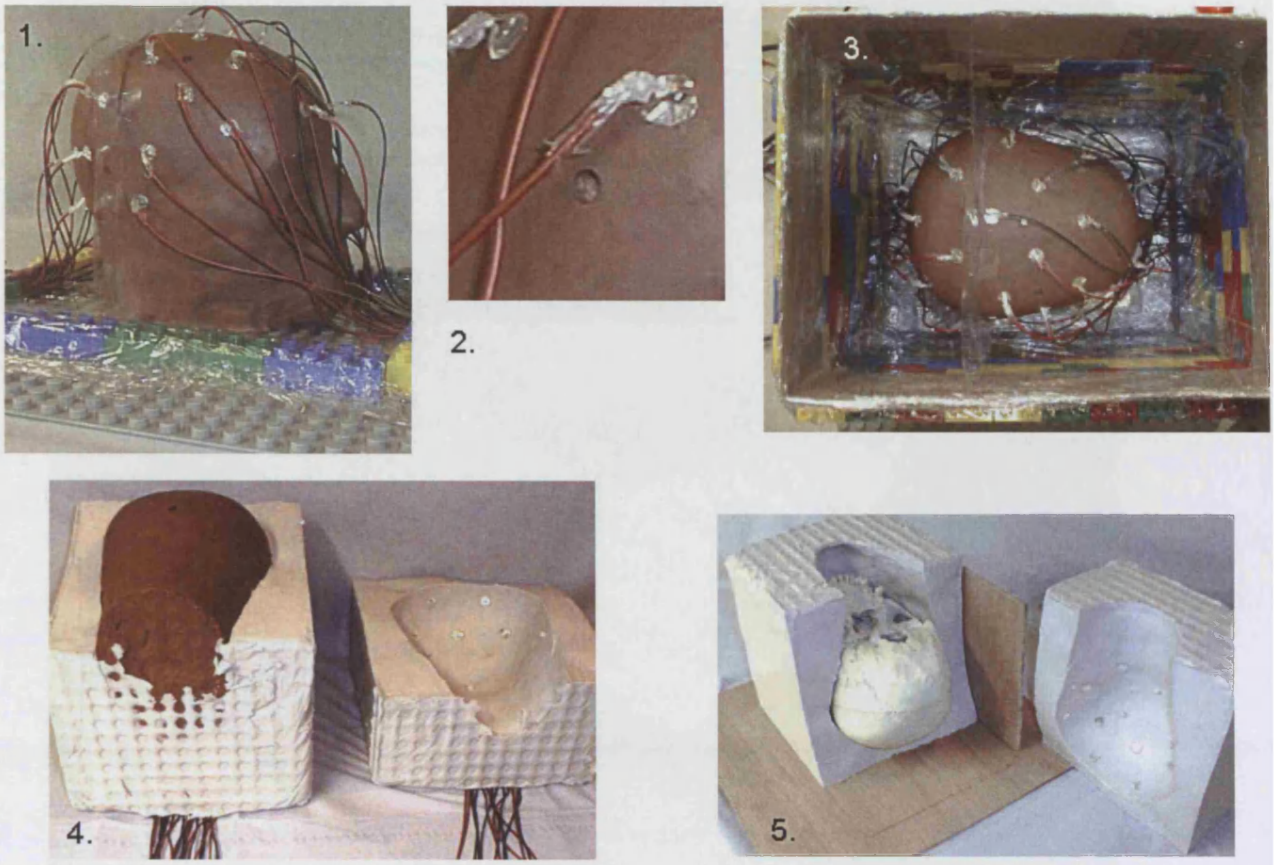

Figure 3.24 Manufacture of the head shaped tank
Image 1: Head shaped model, constructed with oil based clay built up around a real human skull, with the electrodes in place. The model stands on a Lego (www.lego.com) base. **Image 2.** A close up of the silver electrodes held in position with staples. In the centre of the picture is one of the holes in the clay head which will fill with rubber and act as a support for the skull in the silicone rubber tank. **Image 3.** The head shaped model is in position within the Lego box ready for the silicone rubber mould to be cast. **Image 4.** Removal of the head model from the silicone mould. The electrodes are now embedded within the mould and the mould ready for use as a tank phantom. **Image 5:** The skull is inserted in the head shaped tank. The two halves are sealed, with petroleum based jelly (Vaseline, www.vaseline.com), and the tank filled with 0.2% saline. The internal dimensions of the tank are 19.5 in the antero-postero midline plane and 14.6 cm in the coronal plane passing through the central axis of the foramen magnum.

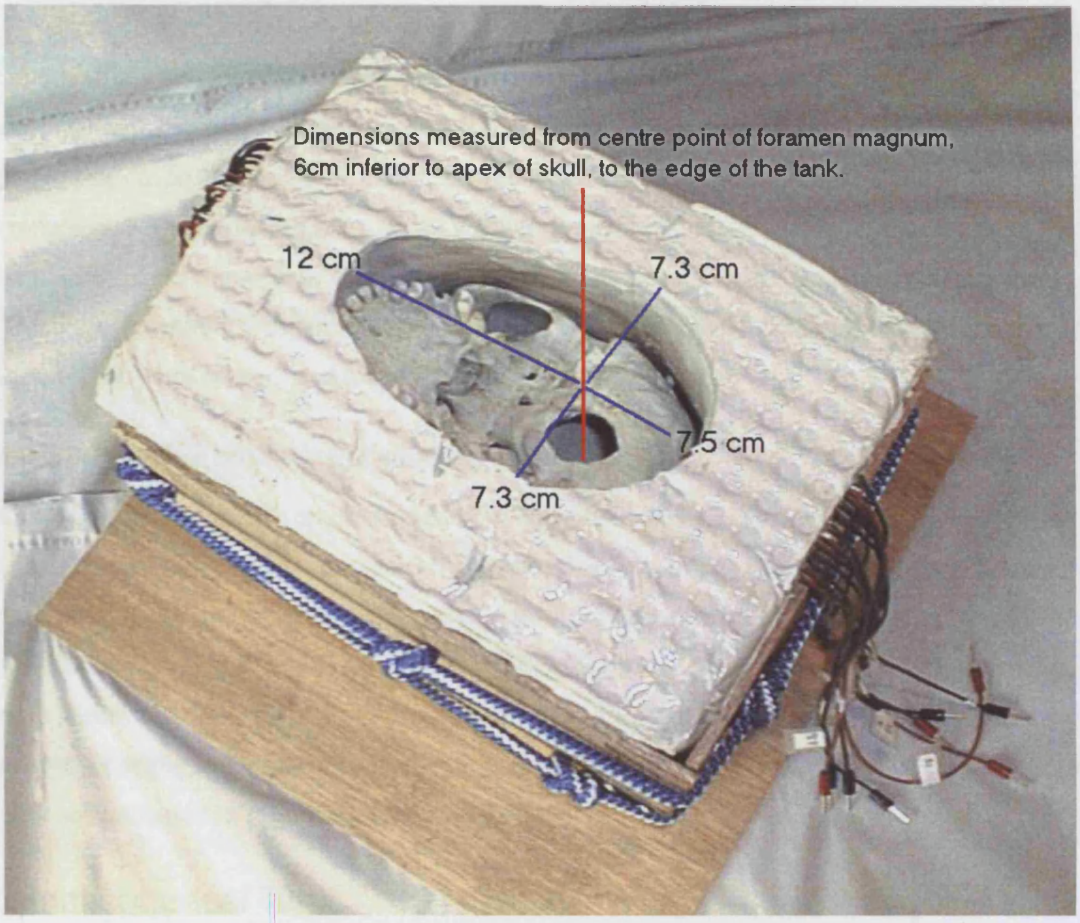

Figure 3.25 Completed head-shaped tank, with skull in-situ
The dimensions of the tank from the centre of the foramen magnum (the hole in the base of the skull) are shown. In an experiment, the tank was filled with 0.2% saline solution and EIT images acquired of either a sponge or a Perspex rod inserted through the foramen magnum and held in specific positions by a wooden support (not in the picture). The leads on the outside of the tank are used to connect the EIT machines to the electrodes within the tank.

Construction of the latex head-shaped tank

When completed the head model was placed on a Lego base (Lego Group, Denmark) and 31 of the silver 'scalp' electrodes positioned on the head model using the modified 10-20 EEG system of electrode placement, used in the human EIT studies. The electrodes were pinned to the scalp with half staples inserted into the clay (Figure 3.24, image 2) .Ten 8 mm diameter holes were bored into the clay scalp, which filled with liquid rubber during the cast and solidified to became skull supports: these were required to maintain the skull/scalp separation when the skull was placed in the tank during EIT studies.

The boundary of the mould was made with Lego Duplo bricks built up from the Lego base. The inside of the boundary was coated with Clingfilm to prevent leakage during pouring of the mould (Figure 3.24, image 3). The space within the mould was divided into two by a piece of acetate paper, cut to fit around the clay head and placed in the central coronal plane of the mould. The mould was filled with ten litres of RTV silicone rubber compound (Made from a mix of Tiranti T20 and T28 rubber compound mixed with T6 setting catalyst, Tiranti, Reading) and allowed to set. Once set, the mould was split and the head and staples removed. This left the electrodes in position on the inner 'scalp' surface of the tank (Figure 3.24, image 4).

Preparation of the tank for EIT studies

Prior to experiments, the silver electrodes were chlorided: the tank was filled with 0.2% sodium chloride solution and a current passed through the silver electrodes (the anodes) to a platinum electrode (the cathode) elsewhere in the tank. The chlorided electrodes were shorted for 24 hours to allow equilibration: the effect of this, with the chloriding, was a reduction in the resting potential between electrodes from 50-60 mV to less than 1 mV. EIT experiments were performed in the tank either with or without the presence of the human skull (Figure 3.24, image 5). The dimensions of the tank are indicated in Figure 3.25.

3.2.2 Hemispherical Tank

The hemispherical tank (Figure 3.26) was made from a 19 cm diameter Perspex bowl. 31 electrodes, made of chlorided silver balls 1 mm in diameter, were inserted on the inner surface of the bowl in positions based on a modified 10-20 system of electroencephalography (EEG) electrode placement. The same electrode positions were used in the adult human EIT imaging studies and on the head-shaped tank.

Figure 3.26 Hemispherical Tank
A hemispherical Perspex tank, with 31 silver ball electrodes located in the 10-20 positions used in the adult EIT study. The red plugs connect the EIT machine to the silver electrodes on the inner surface of the tank.

3.2.3 Equipment

3.2.3.1 The HP EIT system

All Impedance measurements were made with the modified Hewlett Packard 4284A impedance analyser, described in the methods section of Chapter2. The data collection was performed under the same measurement conditions and with identical electrode combinations as the adult EIT studies. Each image was acquired over 25 seconds and consisted of 258 different combinations of 4 electrode measurements taken from the 31 "scalp" electrodes.

During data acquisition in the tank a PC computer ran a programme which: 1) Selected an electrode protocol file, 2) Switched the multiplexer so the impedance could be measured between the different electrode combinations determined by the protocol file and 3) Stored the resistive component of impedance, measured at 50kHz, to disk for offline analysis (Figure 3.27). Impedance measurements of skull and sponge resistivity were made using the HP 4284A impedance analyser alone, with measurements recorded from the analyser's digital panel.

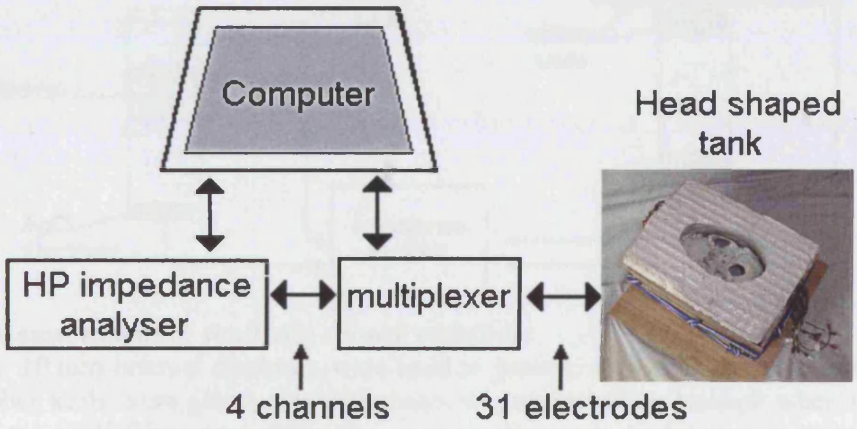

Figure 3.27 Representation of the EIT system.
The HP analyser and multiplexer were under computer control, which was also used to store the acquired EIT data. For each measurement, 4 tank electrodes were selected, under computer control, by the multiplexer. The impedance from these electrodes was recorded at 50 kHz by the HP 4284A impedance analyser and downloaded to the computer. The electrode combinations were switched between 258 different electrode combinations, in a 25 s period, for each image. The data was analysed offline, corrected for noise and reconstructed into impedance images.

3.2.3.2 Impedance probes for skull and sponge resistivity measurements

Measurements of skull and sponge resistivity were made with 2 point impedance measurements: each electrode used to inject current and measure voltage. The main problem with this technique is

that both the object impedance and the electrode impedance are measured. This required an experimental design which could cancel out the effect of the electrode impedance (Figure 3.28). Measurements were made with the electrodes with or without the object between them. Object resistance was calculated from the difference between these measurements.

The probe electrodes were manufactured from Perspex tubes with an internal diameter of 10 mm. Each probe had a chlorided silver electrode at one end. Some of the probes had rubber seals, attached with Araldite (Ciba Geigy, UK), at one end. The seals were made from the rubber bungs of 10 ml syringes with an 8 mm diameter hole cut through them by a cork borer. The uppermost probe was open at the top to allow it to be filled with saline. The saline filled probes were used to measure the saline soaked skull between the probes, or saline soaked sponges inside the probe.

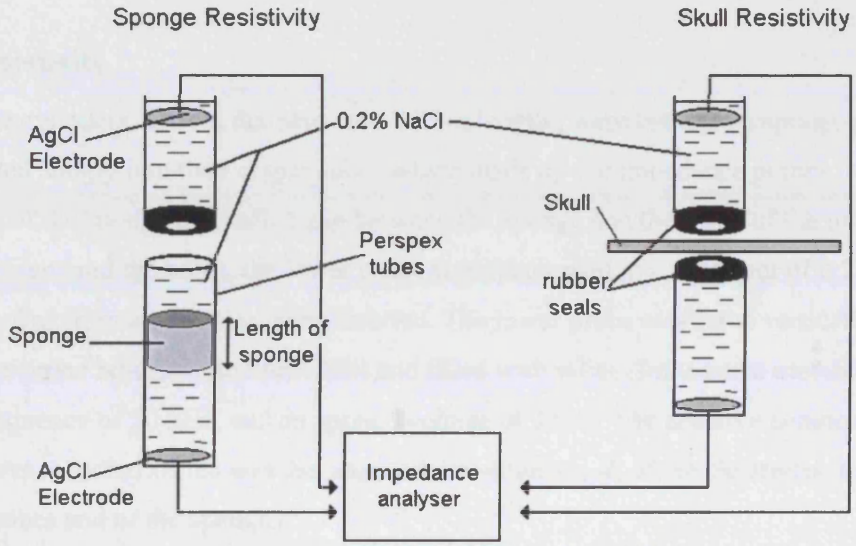

Figure 3.28 Measurement of skull and sponge resistivity
Perspex tubes, 10 mm internal diameter, were used as probes, each with an Ag/AgCl electrode at one end. Rubber seals were glued onto the probes to prevent saline leakage when in opposition either side of the skull. The upper probe was open to allow it to be filled with saline. Two point impedance measurements were made from the upper and lower electrodes.
Sponge resistivity: Between 0-3 sponges were inserted in the saline filled lower probe. The upper probe was sealed against the lower probe, filled with saline and the impedance measured.
Skull resistivity: The saline soaked skull was positioned above the lower saline filled probe. The upper probe was sealed against the upper surface of skull and filled with saline. Two electrode impedance measurements were made in different areas of skull. The electrode/probe impedance was measured without the skull and subtracted from measurements with the skull. Skull resistivity was calculated from this value and the thickness and area of the skull between the probes.

3.2.4 Experiment Protocols

3.2.4.1 Protocol for sponge resistivity experiment:

Two electrode measurements of resistance were made with the probes connected to the HP 4284A impedance analyser.

Saline resistivity and probe resistance

Saline and electrode resistance were calculated in one experiment. The upper probe remained constant; the lower probe used the same silver electrode attached to Perspex tube lengths of 5, 10 and 13 cm, filled with 0.2% saline at 26 C. A graph of measured resistance vs. total tube length was plotted and interpolated to a tube length of 0 cm. This value was the electrode resistance. From this and the internal dimensions of the probe, the resistivity of saline was calculated.

Sponge resistivity

Three sponge cylinders, 1.0 cm diameter and 2.8 cm length , were cut from a sponge pad. These cylinders fitted snugly into the Perspex tubes which made up the impedance probes, without compression of the sponge or a saline gap between the sponge and the walls of the tube. To ensure no air bubbles entered the tubes, the lower probe was submerged in a container of 0.2% saline and 0-3 sponges, free from air bubbles, were inserted. The lower probe was fixed vertically in a vice and the upper probe brought into opposition and filled with saline. Impedance measurements were made at a frequency of 50 kHz, and an applied voltage of 1.0 V. The resistive component of impedance was recorded which was the sum of the resistances, R, of the electrodes, the saline within the probes and of the sponges:

$$R_{measured} = R_{saline} + R_{electrodes} + R_{sponge}$$

The resistance of the length of saline in the tube and electrode resistance were subtracted from the measurements to calculate sponge resistance, and sponge dimensions were used to calculate resistivity.

Skull resistivity

Two saline filled probes either side of an unvarnished adult human skull (Figure 3.28) were used to measure skull resistivity. The skull had been cleaned with acetone to remove any grease on the skull which may have been present due to handling. The skull was soaked in 0.2% saline for 2 days prior to the experiment. The same saline concentration was used in the tank EIT studies. The aim of the experiment was to determine the skull resistivity under the experimental conditions in which it was to be used.

The lower measurement probe was fixed vertically in a vice and filled with the 0.2% saline (in which the skull had been soaked). The skull was manoeuvred over the probe, with the probe inserted through the foramen magnum, so that the internal surface of the skull was in contact with the lower probe. The upper probe was placed vertically above the lower probe on the external surface of the skull and filled with saline. Two electrode impedance measurements were quickly made with the HP 4284A impedance analyser, at a frequency of 50 kHz, a voltage of 1.0 V and the resistive component recorded. These measurements were the sum total of the resistances of the wires, the electrodes, the saline in the Perspex rods and of the skull between the probe tips:

$$R_{measured} = R_{skull} + R_{probes}$$

Resistance was recorded in 3 positions in each of the frontal, left parietal and right parietal areas. Nine measurements were made in total. Impedance measurements with a high capacitance were caused by air bubbles accumulating in the lower probe; so these results were repeated after refilling the lower the probe and the high capacitance measurements discarded. Probe resistance was recorded from 6 separate measurements of the probes in opposition without the skull between them. Skull resistance was therefore obtained by subtracting the probe resistance from resistance measurements made with the skull in place. Skull resistivity was calculated from the area of the probe contacts, 8 mm diameter, and the averaged skull thickness obtained from micrometer measurements in 15 areas of the skull. One criticism of this method is that the current flow is not purely cylindrical through the skull, however this simplification is likely to introduce only small errors into the calculation of skull resistivity.

3.2.4.2 Protocols for the tank EIT experiments

For the imaging studies the skull was placed in the tank, the tank sealed and filled with 0.2% sodium chloride solution to a marked level. The tank was left for 4 hours, to allow the skull to soak. A concentration of 0.2% saline was used because the resistivity of 212 Ω.cm is close to that of the scalp, 230 Ω.cm (Geddes and Baker 1967), and similar to that of rabbit cortex, 230 Ω.cm at 5 kHz (Ranck 1963), and human cortex of 194 to 501 Ω.cm (Lattikka *et al.* 2001) measured in vivo at 50 kHz.

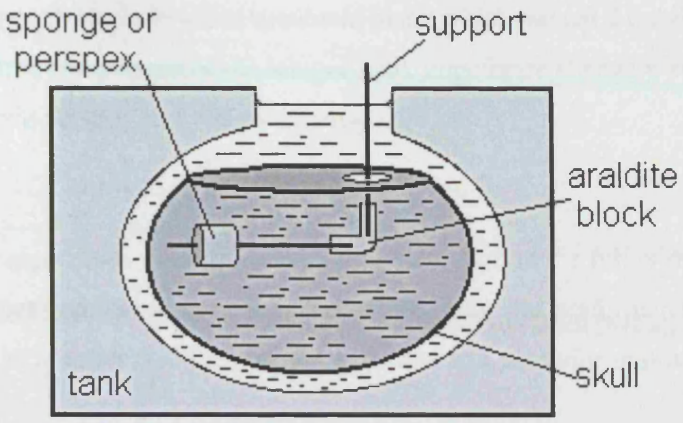

Figure 3.29 Insertion of an impedance change into the head-shaped tank
Diagrammatic representation the head-shaped tank containing a human skull. The tank was filled with 0.2% saline then an impedance object suspended in it on a wooden support inserted through the foramen magnum. The position of the impedance change, made by the sponge or Perspex rod, could be varied. The effect of the impedance of the wooden support, although small, was eliminated from the final images by reconstructing EIT images with the sponge/Perspex + support with reference to baseline images of the support only.

Impedance perturbations used in the experiments were either a Perspex cylinder of 20 mm diameter and 20 mm height, or a cylindrical sponge soaked in 0.2% saline of 25 mm diameter and 28 mm height. These were suspended by a support constructed from 2 wooden sticks, 1 mm diameter, fastened at right angles by a small Araldite mould (Figure 3.29). The impedance object suspended on the support were inserted through the foramen magnum and manoeuvred into the desired position. Because the support had a small, but measurable impedance, this was eliminated from the reconstructed images by a comparison of the EIT data acquired with the support and Perspex rod or sponge in the tank to the baseline EIT data obtained with the support in an identical position. The difference between these conditions, either the presence of the Perspex rod or the sponge, was reconstructed into EIT images.

The main aim of the tank imaging studies was to answer the questions of the localisation accuracy and the resolution of the EIT system with the different reconstruction algorithms and also determine the effect of the skull on the size and position of the imaged impedance change. Several experiments were performed to answer these questions, described below:

Localisation accuracy

The localisation accuracy was assessed by placing the Perspex cylinder in different positions inside the skull. The position of the Perspex rod was varied either: 1) Along the anterior-posterior in the

midline sagittal plane or 2) Right to left in a coronal plane which passed through the central axis of the foramen magnum. A comparison of the imaged peak impedance change was made to the expected position of the Perspex rod within the images.

Resolution

The resolution of the algorithms was assessed by the calculation of the full width at half maximum (FWHM) of the Perspex rod. An additional experimental study was performed to determine if two Perspex rods, one in an anterior midline position and other in a posterior midline position, could be distinguished.

Sensitivity

The sensitivity of the EIT system and the algorithms to small, physiologically sized impedance changes, was assessed using a cylindrical sponge placed in separate positions within the skull. These positions corresponded to the approximate locations of the right/left motor or somatosensory cortex and the visual cortex. The sponge was placed in either parietal right, parietal left, or posterior midline positions and also in superior and inferior positions along the axis from the centre of the foramen magnum to the skull apex.

Effect of the skull and the head shape

The purpose of this study was to assess the effect of the skull and the head shape on EIT images with small impedance changes. The test object used was a small cylindrical sponge with a resistivity contrast of 12%, similar to the impedance change found in rabbits during brain activity (Holder *et al.* 1996). The sponge was imaged in three positions in saline filled tanks under three different conditions: 1) A hemispherical tank was used to assess the localisation accuracy produced by the use of a homogenous sphere reconstruction algorithm on data acquired from a homogenous hemispherical tank. 2) The head-shaped tank, without the skull, was used to assess the localisation accuracy of the spherical algorithm on data acquired from a head-shaped phantom, and 3) The head-shaped tank with a real human skull present was used to assess the effect that the skull had on localisation accuracy.

All images were reconstructed with the homogeneous sphere SVD_62 algorithm (Appendix 1), as this was demonstrated to have better spatial resolution and localisation accuracy than the transverse algorithm.

Effect of noise correction on the EIT images

This experiment tested the effect that the noise correction procedure, used on the adult EIT data, had on image localisation. Impedance data of the sponge in 2 different positions in the skull were noise corrected. The noise correction procedure randomised the order of the 258 electrode measurements used by the EIT system to acquire images from the tank. The randomisation was generated in Matlab. Progressive levels of "noise correction" were performed by setting the impedance data to zero for 0, 20, 40, 60, 80 and 100 successive electrode combinations in the randomly generated series of electrode measurements.

The "noise corrected" impedance data was reconstructed with the Transpose and SVD_62 algorithms and the effect of progressive noise correction on the images assessed visually.

3.2.5 Raw data analysis:

3.2.5.1 Raw impedance tank data

The impedance data obtained from the tank studies was analysed and displayed in Matlab, using programmes written for the analysis of EIT data. The data was linearly corrected for baseline drift then displayed graphically for visual analysis and correction of noise artefacts. Noise which needed correction was defined from the following:

1) Noise spikes defined as changes of impedance >1% of baseline impedance which returned to the baseline impedance. These were probably due to electrical interference, seemed to vary with the time of the day and seemed to be produced by light switching. Despite extensive investigation no reliable cause for these spikes could be found.

2) Discontinuities of baseline, defined as impedance changes greater than the maximum expected impedance change (1% for Perspex cylinder, 0.2% for the sponge) between consecutive impedance data sets. These either occurred at the time of insertion or removal of the object from the tank and were due to accidental movement of the skull during the insertion or removal.

3) Noise, defined as the standard deviation of baseline impedance averaged across all the experiments after exclusion of 1 and 2 above, greater than twice the maximal expected signal, 2% for the Perspex cylinder and 0.4% for the Perspex rod. Elimination of electrodes on the basis of baseline noise was usually less than 1% of electrode combinations.

If the criteria for elimination were met, the data for that electrode combination in that experiment was set to a zero impedance change with respect to the baseline impedance. As these experiments were being used to calibrate the reconstruction algorithms, experiments with more than 15 (6%) of the 258 electrode combinations removed, were excluded from further analysis.

3.2.5.2 Sources of error

There were several sources of error which appeared in the raw data during the experiments. These were:

1) Noise spike activity which varied with time. No cause for the noise glitches were found, they were reduced by placing the equipment on a spike removal mains plug and were assumed to be electrical interference or noisy earth. These were corrected by a manual deglitching of the data.

2) Temperature change: During the experiments, the room temperature reached 33 °C which probably caused evaporation of the water from the tank and increased concentration of the saline in the top of the tank. As the temperature at the top of the tank was warmer than at the bottom, this may also have affected the impedance measurements when a change was introduced.

These two mechanisms resulted in impedance decreases produced when the sponge was inserted at the top of the tank, where the solution was warm and concentrated, and moved to within the skull where the solution was cool and less concentrated. Convection currents may also have occurred, but were not specifically investigated These effects were minimised by stirring the saline between experiments, squeezing the sponge in the saline below the surface of the tank, and reducing evaporation by covering the tank in Clingfilm. Results in which the sponge produced an impedance decrease were discarded and the experiment repeated after the tank had been stirred.

3) Movement artefact: some experiments demonstrated impedance changes larger than the signal of the sponge or the Perspex at the time of insertion or removal of the object. These artefacts were produced by movement of the skull in the tank during insertion or removal of the object. The timing of these artefacts were readily identified and experiments in which it occurred were repeated.

3.2.6 Image analysis

3.2.6.1 Image reconstruction

The noise corrected data was reconstructed into images using either the Transpose or SVD_62 algorithms used for the adult EIT data (chapter 2 and appendix 1). Difference images were reconstructed of the presence of the Perspex rod or Sponge.

3.3 Results

3.3.1 Tank properties

3.3.1.1 Sponge and saline resistivity

The resistivity of 0.2% saline, at 23 °C, was 212 ± 2.5 Ω.cm (mean ± SD). The average sponge resistivity, at the same temperature, from 12 measurements was 237 ± 5.2 Ω.cm (mean ± SD), an impedance increase of 12.1 ± 2.5% compared to 0.2% saline only.

3.3.1.2 Skull resistivity

The mean skull resistance was calculated from 9 different areas of skull and was 20.4 kΩ at a temperature of 26 °C. The average skull thickness from 15 similar areas of skull where resistivity was measured was 0.49 cm. The resistivity of the skull was calculated:

$$\textbf{Resistivity}_{\textbf{skull}} = \textbf{Resistance}_{\textbf{skull}} \times \textbf{area /skull thickness}$$

The area of the probe tips, between which skull resistance was measured, was 50.3 mm^2. The resistivity of the skull at 23 °C was 20.8 ± 6.4 kΩ.cm (mean ± SD). The resistivity ratio of skull to 0.2% saline resistivity was 98:1.

3.3.2 Tank: Raw impedance data

3.3.2.1 Signal and noise

The average signal was calculated for each experiment by an average of the data acquired during insertion of the impedance object for each electrode measurement. The absolute value of these averages was averaged across all electrode combinations to produce an average signal for the experiment. Noise was calculated for each experiment from the average of the standard deviation of the baseline data at each electrode combination for all electrode measurements.

Baseline noise was between 0.04-0.06% in all experiments. Signal for the sponge imaged in the tank without the skull was 0.25±0.01% with a signal to noise ratio (SNR) of 6.6±1.4; when imaged within the skull the signal was 0.05±0.01% and SNR 0.9±0.2. Signal for the Perspex rod imaged within the skull was 0.17±0.04% and the SNR 3.2±1.3 (Table 3.6).

Table 3.6 Summary of raw data changes

Impedance object (no of expts)	Skull Present	Signal (Mean±SD%)	Noise (Mean±SD%)	Signal to noise (Mean±SD%)
Perspex rod (n=7)	Yes	0.17 ± 0.04	0.06 ± 0.02	3.2 ± 1.3
Sponge (n=10)	Yes	0.05 ± 0.01	0.06 ± 0.01	0.9 ± 0.2
Sponge (n=3)	No	0.25 ± 0.01	0.04 ± 0.01	6.6 ± 1.4

3.3.2.2 Effect of the skull

The effect of the skull on the size of the impedance changes measured was determined by imaging a sponge in 3 different positions in the tank, with or without the presence of the skull. The effect of the skull attenuated the impedance signal produced by a sponge by an average factor of 5.

3.3.3 Head Tank: Image data

3.3.3.1 Image localisation of the Perspex rod inside the skull

The Perspex rod, imaged inside the skull, produced an impedance increase which was located appropriately in the images produced by both algorithms (Figure 3.30, Figure 3.32). Both algorithms localised the peak impedance change in the same place. The images differed quantitatively in the size of the imaged impedance change, which was largest for the Transpose algorithm with a FWHM of 55 ± 21% of the image diameter compared to 34 ± 15% of the image diameter for the SVD_62 algorithm. In addition the SVD_62 algorithm introduced negative impedance changes which were reconstruction artefacts. To indicate the scale of each pixel in terms of distance, as the anterior-posterior diameter of the head tank was 19.5 cm and lateral diameter 15 cm, each pixel represented 0.6 cm and 0.5 cm in the anterior-posterior and lateral diameters respectively, with a slice thickness of approximately 2.5 cm. The FWHMs expressed in terms of distance along the anterior-posterior direction of the tank were therefore 11 cm and 7 cm for the Transpose and SVD_62 algorithms, respectively.

There was a linear relationship between the localisation of the peak impedance change imaged within the skull and the object's predicted location in the images (Figure 3.31, Figure 3.33). For the right to left movement of the Perspex, the imaged change was shifted towards the centre by 4 pixels (12.5% of the image diameter) for an object near the edge. In the images of the rod in which movement was from front to back, objects at the front were accurately localised, but as the object moved backwards there was a distortion of the position of the imaged change which was biased towards the front of the tank: this bias was maximal for an object at the back of the head-

tank with a localisation error of 4 pixels (12.5% of the image diameter) or 5 pixels (15.6% of the image diameter) for the Transpose and SVD_62 algorithms respectively.

The error of the impedance localisation was quantified for the two algorithms in two ways: 1) A one–dimensional error was calculated in pixels along the axis of the movement of the rod and 2) A 2-dimensional (2D) error calculated in the image plane in which the object was expected to be localised. The slice information (z-dimension) was not included in the error calculation, as all, except one image, localised the change in the expected image plane. Errors are expressed as a percentage of the image diameter.

The errors are summarised in Table 3.7. The localisation errors in 2D were significantly smaller for the SVD_62 algorithm for the front-to-back movement of the rod 8.8±3.8% vs. 10.6±5.6% ($p<0.05$) and right-to-left movements of the rod, 6.9±3.1% vs. 9.7±3.4% ($p<0.001$). For the one dimensional (1D) errors the SVD_62 algorithm was only smaller than the Transpose for the front-to-back movement, -6.9±5% vs. -8.8±6.3% ($p<0.05$). No significant difference in error between the algorithms was detected along the axis of movement for the object moved from right to left in the tank.

Table 3.7 Localisation errors for the Perspex rod imaged inside the skull, reconstructed with the Transpose and SVD_62 algorithms

Position of Perspex Rod (No. of measurements)	Algorithm	Localisation error n the image slice (Mean±SD,% image diameter)	
		1D along movement axis	2D in image plane
Front to back (n=52)	Transpose	-8.8 ± 6.3%	10.6 ± 5.6%
	SVD_62	-6.9 ± 5% ($p<0.05$)	8.8 ± 3.8% ($p<0.05$)
Right to left (n=70)	Transpose	1.9 ± 7.5%	9.7 ± 3.4%
	SVD_62	2.8 ± 5.9 (not significant)	6.9 ± 3.1% ($p<0.001$)

The sizes of the peak impedance changes were different for the different algorithms, with a peak change of 0.94 for the Transpose algorithm and 2.1×10^{-3} for the SVD_62 algorithm. The difference in these values reflect the type of reconstruction used to produce the images and should be considered as arbitrary units which can only be used to compare different images reconstructed with the same algorithm.

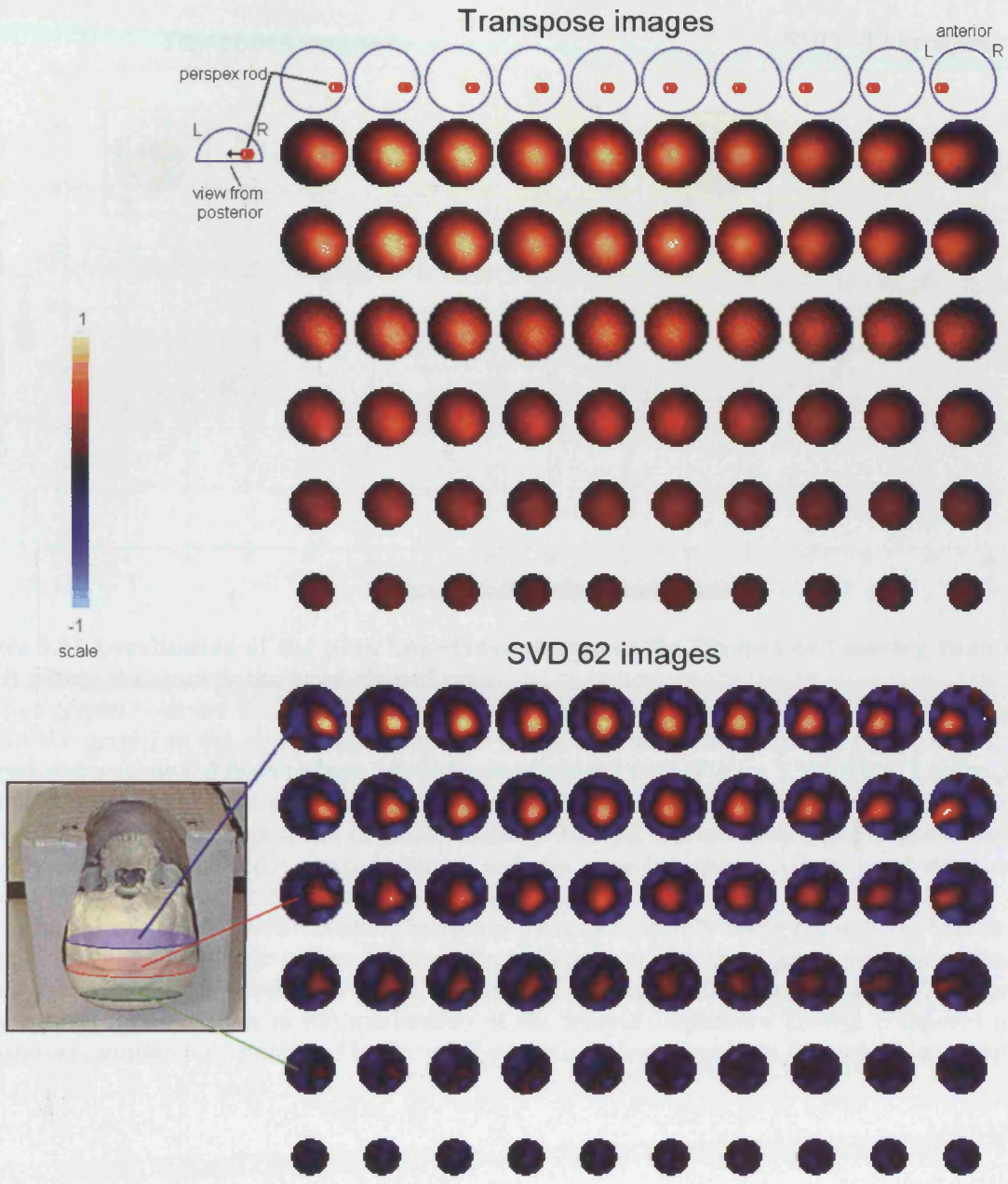

Figure 3.30 Perspex rod moving from right to left within the skull: Transpose and SVD_62 images.

Transpose images (top) and SVD_62 images (bottom) of the Perspex rod moved in 1cm increments from right to left. Each column represents one position of the rod. Each row represents a single slice through the tank, the level of which is indicated by the cutaway photo of the head-tank on the bottom left. The images are viewed as if looking down from the top of the head. The Perspex rod is imaged as an impedance increase in red/yellow. Good positional localisation of the Perspex rod is achieved with both algorithms, with improved localisation in the SVD_62 images.

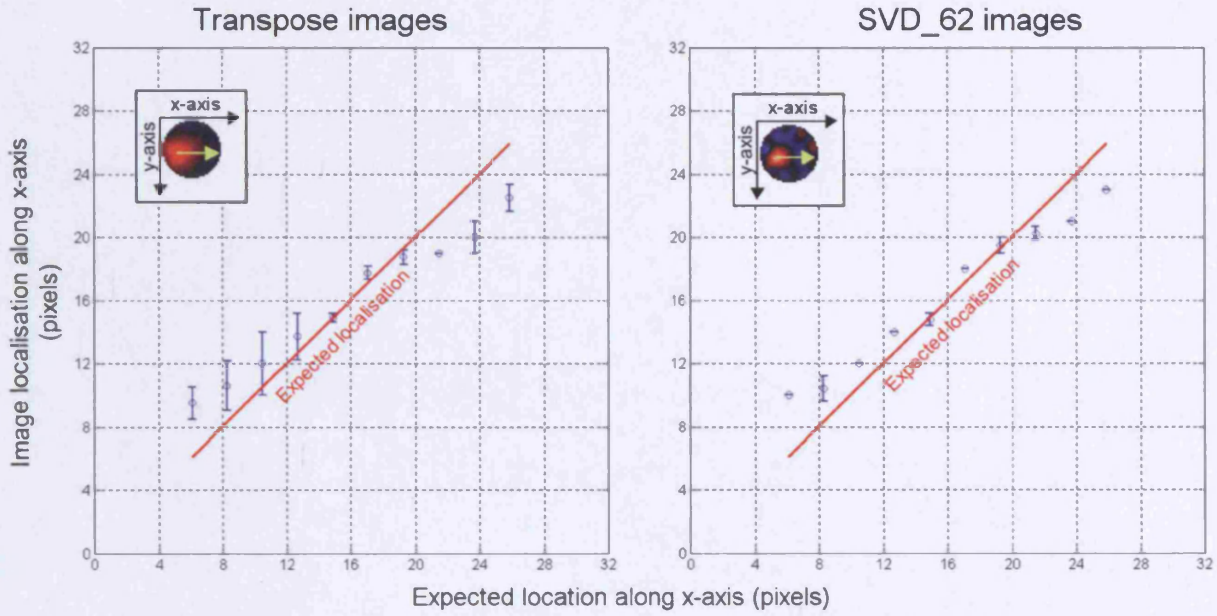

Figure 3.31 Localisation of the peak impedance change of the Perspex rod moving from right to left within the skull in the head-shaped tank.

The two graphs compare the localisation of the peak image change along the x-axis of the image (y-axis of the graph) to the object's expected true localisation in the tank (x-axis of the graph). The Perspex rod was moved from right to left in the head-shaped tank (Figure 3.30). Pixel 1 corresponds to the left of the image and pixel 32 to the right of the image. The mean and standard deviation are shown for each position (minimum of 4 experiments). The red line indicates a one to one correlation between the positions of the imaged change and the expected change. Each pixel represents a distance of 0.5 cm in the lateral diameter of the tank.

The results are similar between the two algorithms: an approximately linear relationship between the imaged and expected change is seen however the objects located at the edge of the tank are imaged towards the centre of the tank by 4 pixels or 12.5% of the image diameter. The SVD_62 algorithm demonstrates less variation in the localisation of the imaged impedance change compared to the Transpose algorithm, as determined by the smaller standard deviations seen for each object position.

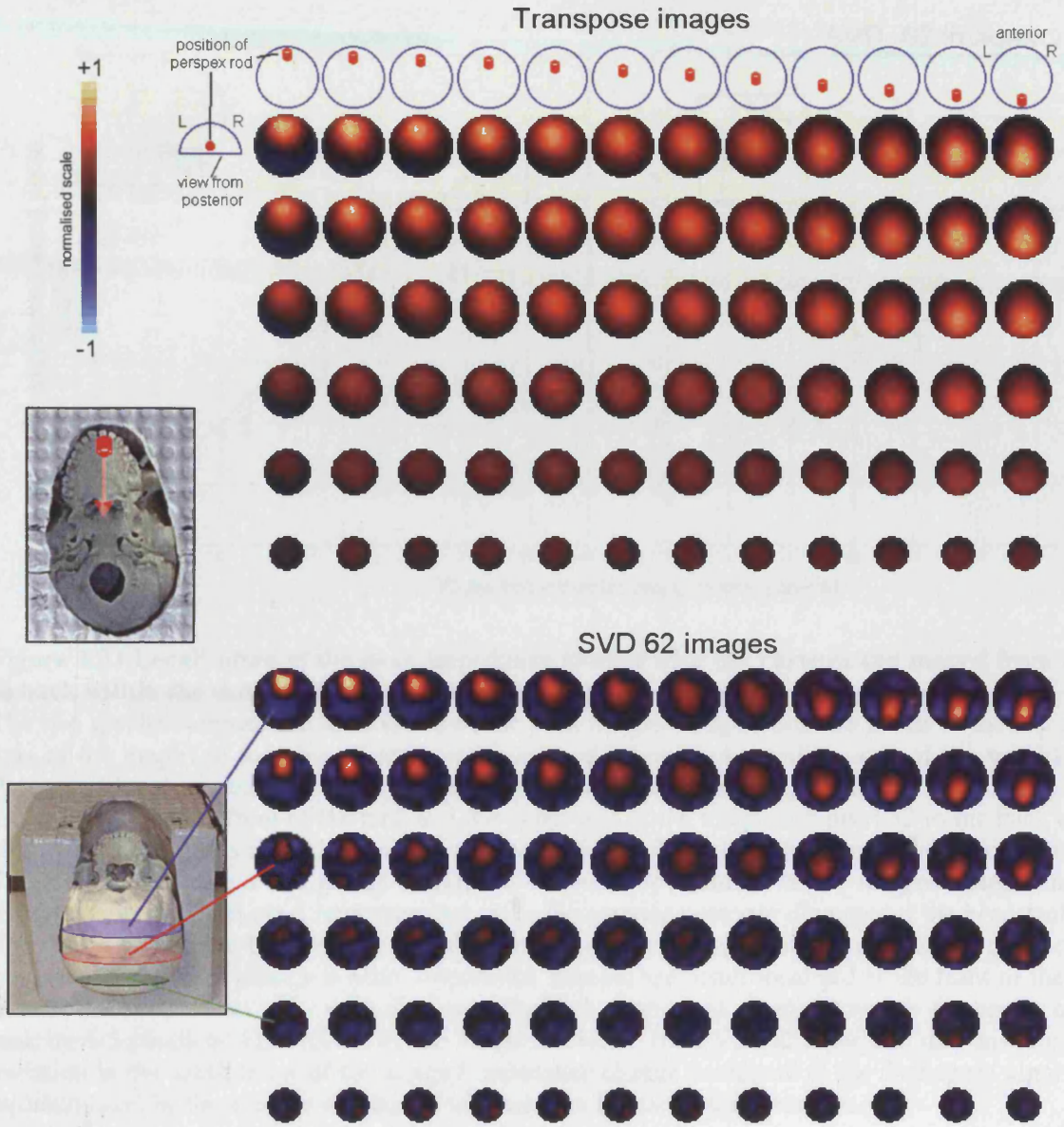

Figure 3.32 Perspex rod moving from front to back within the skull in the head tank Transpose and SVD_62 images

Transpose images (top) and SVD_62 images (bottom) of the Perspex rod moved in 1cm increments from front to the back of the tank (illustrated top). Each column represents one position of the rod. Each row represents a single slice through the tank, the level of which is indicated by the cutaway photo of the head-tank on the bottom left. The images are viewed as if looking down from the top of the head. The Perspex rod is imaged as an impedance increase in red/yellow. Good positional localisation of the Perspex rod is achieved with both algorithms, with clearer localisation in the SVD_62 images due to the decreased full width at half maximum of the impedance change in these images.

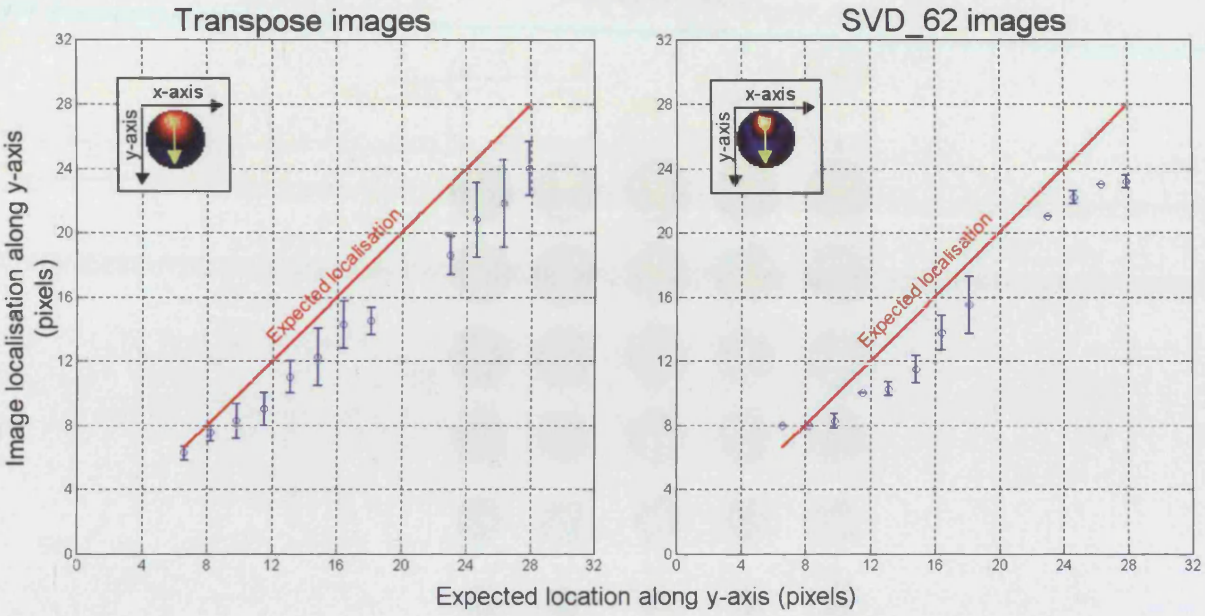

Figure 3.33 Localisation of the peak impedance change with the Perspex rod moved from front to back within the skull in the head-shaped tank.

The two graphs compare the localisation of the peak image change along the y-axis of the image (y-axis of the graph) to the object's expected true localisation in the tank (x-axis of the graph). The Perspex rod was moved from moved from front to back in the head-shaped tank ((Figure 3.32). Pixel 1 corresponds to the front of the tank and the upper part of the image and pixel 32 to the back of the tank. The mean and standard deviation are shown for each position (minimum of 4 experiments). The red line indicates a one to one correlation between the positions of the imaged change and the expected change. Each pixel represents 0.6 cm in the anterior-posterior diameter of the head-tank.

The results are similar between the two algorithms: an approximately linear relationship between the imaged and expected change is seen. Impedance changes are better localised at the front of the tank than at the back of the tank, with objects at the back of the tank imaged towards the centre of the tank by 4-5 pixels or 12.5-15.6% of the image diameter. The SVD_62 algorithm demonstrates less variation in the localisation of the imaged impedance change compared to the Transpose algorithm, as determined by the smaller standard deviations seen for each object position.

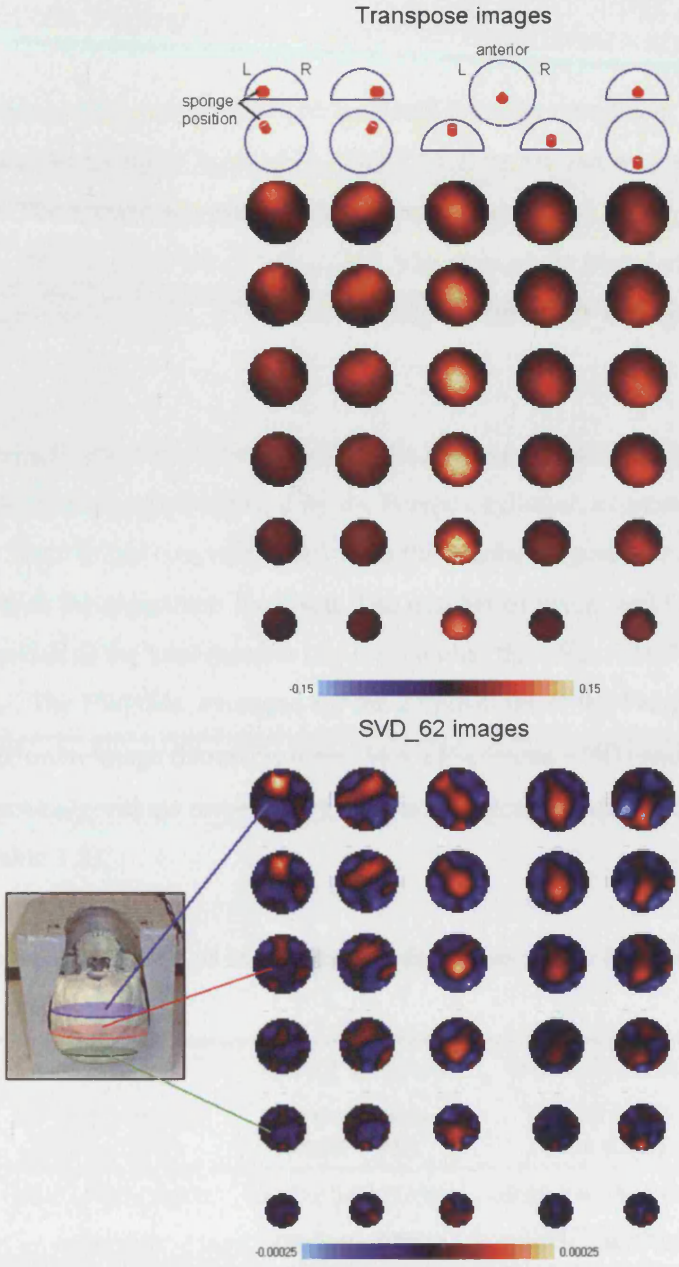

Figure 3.34 Images of the sponge within the skull in the head tank: Transpose and SVD_62 images

Transpose images (top) and SVD_62 images (bottom) are shown of the sponge in different positions in the head-tank (positions indicated above each image column). 30 images were averaged for each sponge position in order to increase signal to noise of the images. The 12% impedance increase produced by the sponge produces a smaller impedance change than that of the Perspex rod. The scales are different for the two algorithms; this is because each algorithm has an arbitrary scale. These images demonstrate that:

1) A small, 12% impedance change from a sponge can be imaged within the skull.

2) The sponge can be localised to the appropriate area.

3) When compared to the Perspex rod images, the impedance change from the sponge is ~1/7 that of the Perspex cylinder.

Sponge

The 5 different positions of the sponge could be localised in images produced with the Transpose and the SVD_62 algorithms (Figure 3.34): each algorithm demonstrates an impedance increase in the appropriate location. The sponge produced an impedance increase of 0.14 for the Transpose algorithm and 0.38×10^{-3} for the SVD_62 algorithm. The ratio of the impedance increase of the Perspex rod to sponge was 6.7:1 and 5.5:1 for the Transpose and SVD_62 algorithms respectively

Resolution

The resolution of a single object was determined by the average full width at half-maximum (FWHM) of the impedance change produced by the Perspex cylinder, expressed as a percentage of the image diameter. The FWHM was calculated from the number of pixels within the FWHM in the 2D image slice in which the object was localised. The number of pixels within this area was expressed as a proportion of the total number of pixels within that slice. The FWHM was the square root of this area ratio. The FWHMs, averaged for the 22 positions of the Perspex rod and expressed as percentage of maximum image diameter, were: 34 ± 15% (mean ± SD) and 55 ± 21% for the SVD_62 and Transpose algorithms respectively, with a significantly smaller FWHM for the SVD_62 images ($p<0.001$, Table 3.8).

Table 3.8 FWHM and magnitude of increases and decreases in the images of the Perspex within the skull in the head tank

Algorithm (no. of positions)	FWHM % image diameter (mean ± SD)	Sum of increases % no of pixels (mean ± SD)	Sum of decreases % no of pixels (mean ± SD)	Ratio of Increase: Decrease (pixel ratio)
SVD_62 (n=22)	32 ± 15 (P<0.001)	0.22 ± 0.02 (53%)	-0.08 ± 0.03 (47%)	2.7 (1.1:1)
Transpose (n=22)	55 ± 21	281 ± 48 (98%)	-0.5 ± 2.0 (2%)	540 (50:1)

A variation of the size of the FWHM was seen with a change in position; the FWHM was smallest when the object was close to the edge of the tank, and largest when the object was in the middle of the tank. This was true for both the Transpose and the SVD_62 algorithm. The change in the size of the FWHM with the object's position is demonstrated in Figure 3.35.

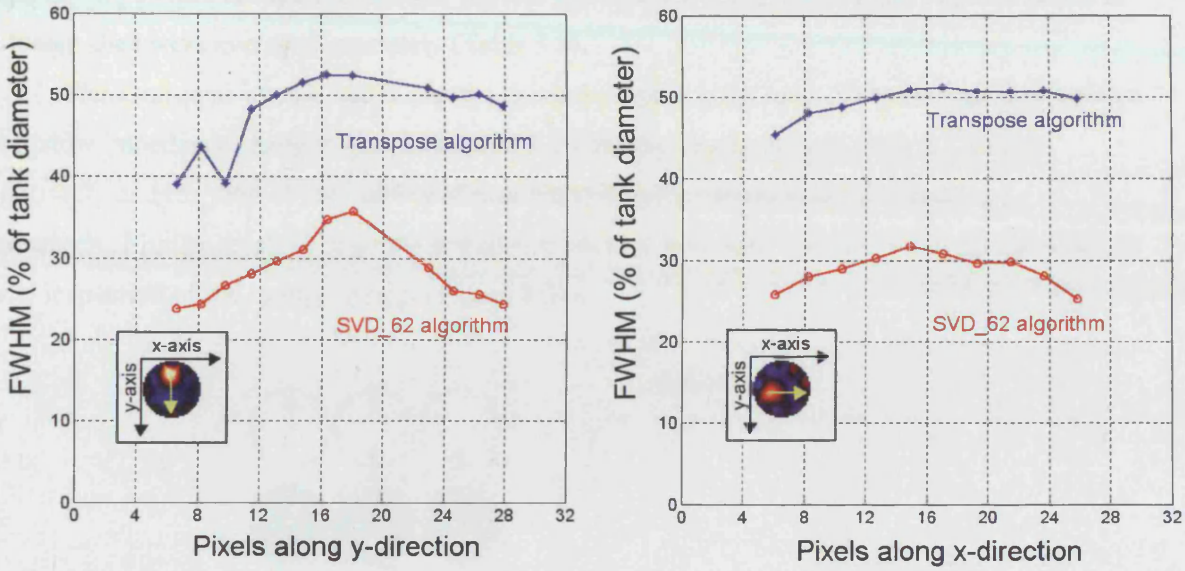

Figure 3.35 Change in full-width at half maximum (FWHM) with object position
The size of the FWHM, expressed as % diameter of the tank (y-axis), is plotted against the real position of the object, expressed as pixels in the image (x-axis). The results are shown for an object moving along the anterior-posterior diameter of the tank (left graph) and from right to left in the tank (right graph). This demonstrates that:
1) The FWHM for the SVD_62 algorithm is approximately half that of the equivalent images reconstructed by the Transpose algorithm, for all positions in the tank
2) That both algorithms produce images with smaller FWHMs at object positions close to the edge of the tank compared to the centre.

The experimentally derived FWHM of the Perspex rod leads to the expectation that EIT system could resolve two objects in the tank with the SVD_62 algorithm but not with the Transpose algorithm. This was confirmed experimentally by imaging two Perspex rods at opposing ends of the skull and reconstructing the data with the SVD_62 algorithm only (Figure 3.36). The rods were positioned anteriorly and posteriorly within the skull, the image profile in the anterior-posterior axis of the images demonstrates a double-hump from the two impedance objects, with the dip between the 2 impedance peaks of 80% of the smaller peak. Although the Perspex objects were the same size, the magnitude of the impedance change at the front of the tank was half that produced by the Perspex rod at the back of the tank.

Image artefacts

Impedance artefacts were defined as impedance changes of opposite sign to the actual impedance perturbation. Such artefacts were mainly present in the SVD_62 images and were minimal in the Transpose images. Quantitative assessment of the image artefact was performed for the slice in

which the impedance change was moved: the size and number of the positive and negative pixels in the image slice were averaged separately (Table 3.8).

The Transpose images had the least impedance artefact: the ratio of the average size positive to negative impedance changes were 540:1 and 2.7:1 for the Transpose and SVD_62 images, respectively and the ratio of the number of positive to negative pixels were 50:1 and 1.1:1, respectively. Similar levels of negative impedance artefact were seen with the SVD_62 algorithm on visual inspection of the sponge images (Figure 3.34).

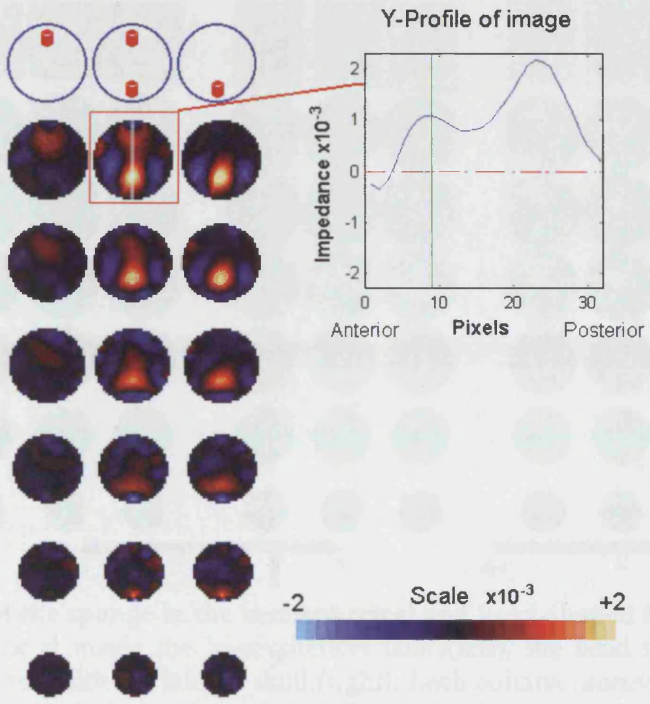

Figure 3.36 Resolution of two Perspex rods within the skull by the SVD_62 algorithm .
Three SVD_62 images were reconstructed from data taken with either one or two Perspex cylinders, 2cm diameter and length, suspended within the skull. Each column represents the images of different Perspex rod positions as indicated by the top row diagrams. The positions were either as anterior or as posterior as the skull dimensions would allow.

The images demonstrate a reduction in the magnitude of the impedance change when the Perspex rod is anterior in the skull. The two objects in the central image can be distinguished from each other in the image and in the profile of the image along the central longitudinal axis of the head-tank. The two peaks in the cross section correspond to the two Perspex rods, the dip in the centre of the profile is approximately 80% of the smaller impedance change at the front of the head-tank.

3.3.3.2 Comparison of image localisation of the sponge in different tank phantoms

Localisation errors

Images of the sponge in 3 different positions within the hemispherical tank and the head-tank with and without the skull were compared to assess the effect of localisation of head shape and the presence or absence of the skull (Figure 3.37).

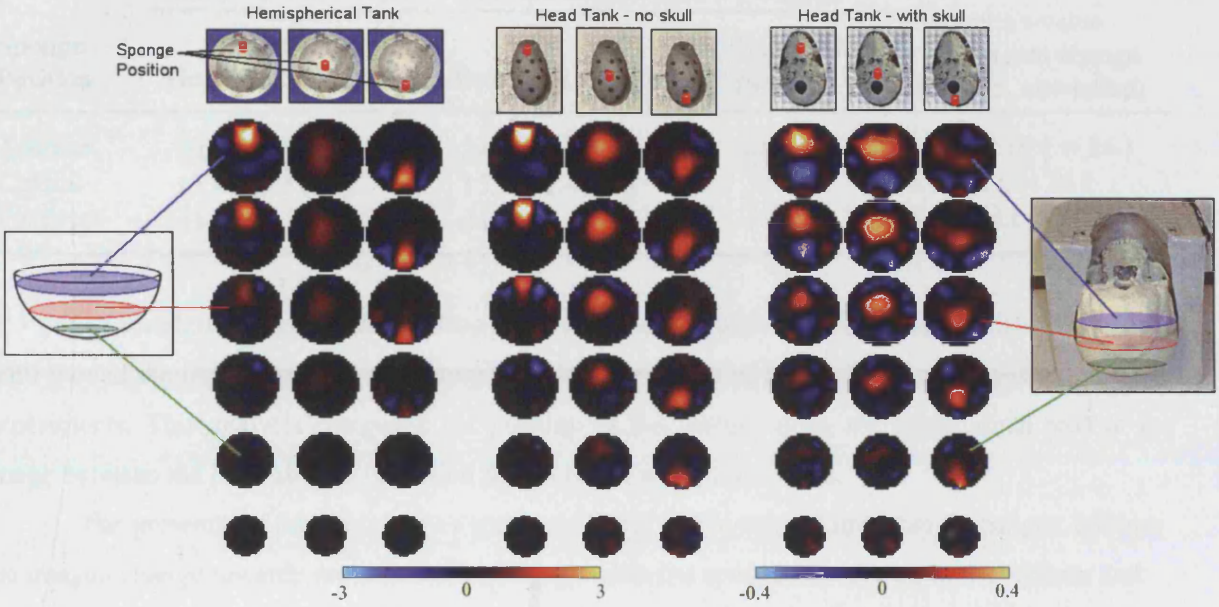

Figure 3.37 : Images of the sponge in the hemispherical and head-shaped tanks
Images of a sponge placed inside the hemispherical tank (left), the head tank without the skull (middle) and the head-tank with the human skull (right). Each column represents a different sponge position (indicated top left). Impedance increases, due to the sponge, are seen in each image. The averaged localisation error for all 3 sponge positions imaged within the skull was 14.5% of the tank diameter, compared to the average error in the head-shaped tank without the skull of 6.5% and 5.9% in the hemispherical tank. The presence of the skull reduced the size of the imaged impedance change by an average factor of 6.4, which is the reason for using a different scale for these images.

The presence of the skull significantly increased the localisation error obtained for the anterior and posterior positions of the sponge ($p<0.01$, two-tailed t-test, d.f. 26 and 30 for anterior and posterior comparisons, respectively, see Table 3.9). The localisation errors of the centrally positioned sponge were not significantly different from each other for all 3 tank simulations ($p>0.05$ for all comparisons, one-tailed t-test). The head shape alone did not affect localisation error, as the errors between the head shaped tank without the skull were not significantly different from those within the hemispherical tank for comparisons of all 3 sponge positions ($P>0.05$, one-tailed t-test,

d.f. 26, 26, and 30 for anterior, central and posterior comparisons, respectively). In the head-shaped tank the skull reduced the amplitude of the imaged impedance change by a factor of 8.2, 5.5 and 5.6 for anterior, central and posterior positions, respectively (0).

Table 3.9 Comparison of localisation error along the longitudinal axis of the head tank, with or without the skull

Sponge Position	Average position, expressed as % image diameter from the image centre. Positive values are anterior. (no. of images)			Student's t-value * significant change (P< 0.05, one-tailed)
	Head tank, no skull	Head tank + skull	Expected position	
Anterior	30.7 ± 0.4 (12)	24.4 ± 1.3 (16)	28.8	0.0002* (d.f. = 26)
Central	15.6 ± 0.5 (12)	13.1 ± 1.4 (16)	3.0	0.07 (d.f. = 26)
Posterior	-31.6 ± 1.2 (16)	-19.9 ± 5.3 (16)	-31.3	0.98* (d.f. = 30)

As the skull increased localisation error, a further analysis was performed to determine if the skull moved the imaged impedance change towards the centre of the skull, as suggested by previous experiments. This analysis compared the position of the sponge along the longitudinal axis of the image between the head shaped tank with the skull and without the skull.

The presence of the skull had a significant effect on the imaged impedance changes, moving the imaged change towards the centre of the image when the sponge was placed in the anterior and posterior positions of the tank (P<0.05, one-tailed t-test, d.f 26 and 30 for anterior and posterior comparisons, respectively, Table 3.9). No difference was seen comparing the sponge in the central position of the tanks (P>0.05, one-tailed t-test, d.f = 26).

Table 3.10 Localisation error in the EIT images of the sponge in the tank phantoms

Tank simulation	Average localisation error for each sponge position, expressed as % of image diameter (no. of images).		
	Anterior	Central	Posterior
Hemispherical	3.5 ± 0.3 (16)	10.7 ± 1.5 (16)	3.4 ± 0.4 (16)
Head shape, no skull	4.3 ± 0.6 (12)	13..3 ± 0.4 (12)	3.1 ± 0.9 (16)
Head shape + skull	10.3 ± 1.8 (16)	14.5 ± 1.8 (16)	18.7 ± 5.1 (16)

3.3.3.3 The effect of noise correction on image localisation

In order to test the noise correction procedure used on the adult EIT data, progressive simulated noise correction was performed on up to 100/258 measurements of EIT data acquired of a sponge in both anterior and posterior positions within the skull in the head-shaped tank. The reason for using the sponge data was that the signal to noise ratio (SNR) was similar to that obtained from the adult EIT data, which was 0.9 for the sponge data compared with 0.7-1.6 for the adult EIT data. The noise corrected data were reconstructed using the Transpose and SVD_62 algorithm (Figure 3.38).

Visual inspection of the images demonstrated that noise correction up to a maximum of 100/258 (39%) of measurements, does not affect image localisation. However, the size of the peak impedance change was reduced with progressive noise correction and became less well defined. These results indicate that in the adult EIT data, noise correction of up to 20 % of impedance measurements from the raw data should not have caused a significant effect on the EIT images, and therefore the noise correction procedure does not account for the mislocalisation of adult impedance changes.

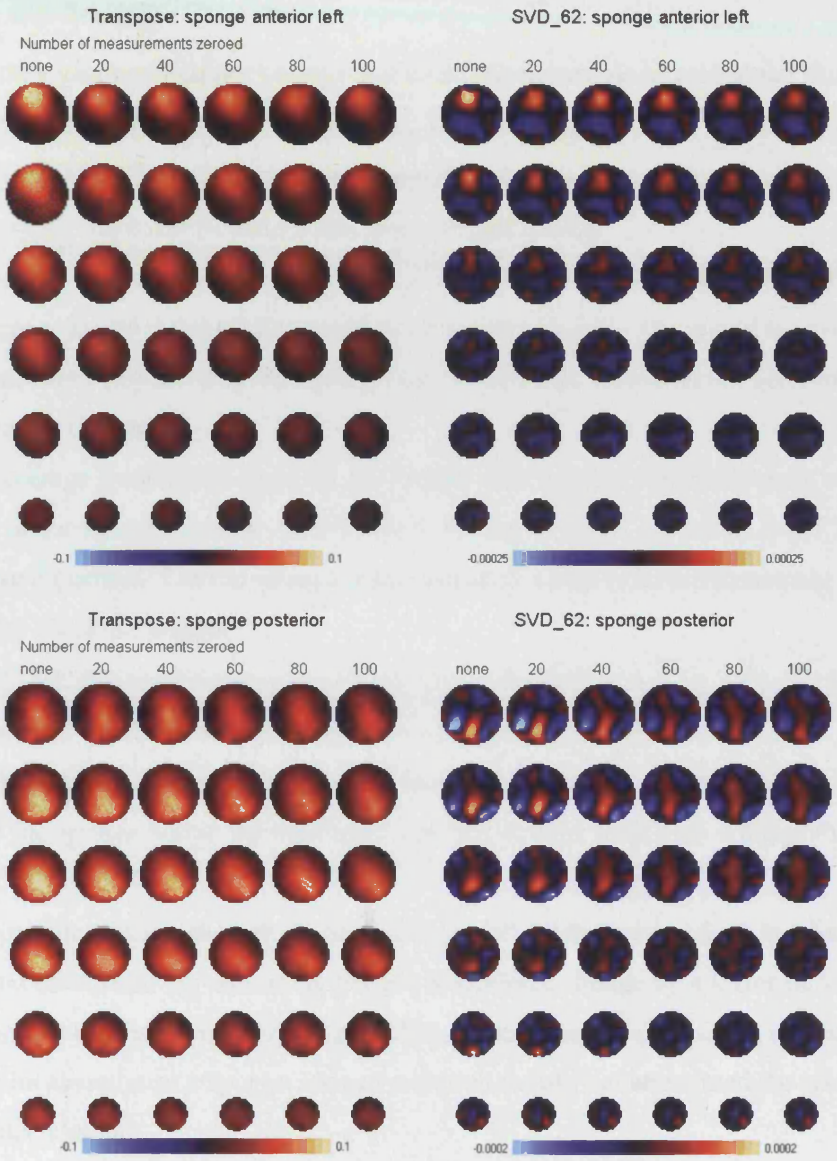

Figure 3.38 Effect of noise correction on Transpose and SVD_62 images of the sponge
Images of the sponge in two positions within the skull in the head-shaped tank are shown: a left-anterior position (top) and posterior-central position (bottom). These are reconstructed with the Transpose (left) and SVD_62 (right) algorithms. The raw data was randomly noise corrected prior to reconstruction (Section 3.2.4.2). Progressive levels of noise correction are indicated at the top of each image column. Different scales are used for images reconstructed by the Transpose and SVD_62 algorithms; these are arbitrary units as neither algorithm had been calibrated to a known impedance change.

The effect of progressive noise correction was similar for both algorithms and both sponge positions: it reduced the magnitude of the impedance change, but had little effect on its localisation. The conclusion from this experiment is that up to 20% (52/258) of electrode measurements could be eliminated from the data without a significant effect on image localisation of a small, physiologically sized, impedance change produced by a sponge. Noise correction in the adult EIT studies is unlikely to be the cause of the failure to localise impedance changes to the expected cortical area.

3.3.4 Results summary

A head shaped tank was successfully created that could accommodate a real human skull. Skull resistivity in 0.2% saline at 23 °C was 20.8 kΩ.cm. The resistivity of 0.2 % saline was 212 Ω.cm, with a resistivity contrast ratio of the skull to saline of 98:1. This tank was used to assess the ability to detect small impedance changes and assess image quality:

1) A sponge, with an impedance increase of 12% compared to saline produced small impedance increases inside the skull that could be detected with EIT. The signal to noise ratio in the raw impedance data produced by the sponge was 0.9 and was similar to the SNR of the adult EIT data acquired in Chapter 2.

2) The average localisation error for the Perspex rod imaged within the skull, expressed as a percentage of the image diameter, was 6.9-8.8% for the SVD_62 algorithm and 9.7-10.6% for the Transpose algorithm. For the sponge within the skull a higher localisation error was seen of 10.3-18.7% for SVD_62 images.

3) The FWHM of the Perspex rod imaged within the skull was 55 ± 21% and 34 ± 15% of the image diameter for the Transpose and SVD_62 algorithms, respectively.

5) The head-shape had no significant effect on the position of the impedance change, when images of the sponge within the hemispherical tank and the head-tank without the skull were compared.

6) The presence of the skull in the head-tank significantly increased the localisation error of the sponge and attenuated the size of the imaged impedance change by a factor of 5.6-8.2.

7) Progressive noise correction of up to 39% of the impedance data, had no qualitative effect on image localisation of a sponge imaged within the skull, but attenuated the size of the imaged impedance change.

3.4 Discussion

3.4.1 Summary of results

These experiments demonstrate that: 1) Large and small impedance changes can be imaged and localised within the human skull, even though the head was modelled as a homogeneous sphere in the reconstruction algorithm, 2) The geometry of the head does not increase localisation error, and 3) The presence of the human skull significantly increases localisation error towards the centre of the tank and attenuates the size of the imaged impedance change by a factor of 5-8.

Importantly, these results suggest an upper limit of the localisation error due to the skull, of up to 20% of the image diameter. This suggests that the use of an homogenous spherical model of the head in the reconstruction algorithm contributes to, but is not entirely responsible for, the localisation errors detected in the human EIT images.

3.4.2 Adequacy of the head-tank to simulate the head

The head tank attempted to simulate two main properties of the human head: the head-shape and the presence of the skull.

The head shape was based on a model which was built up around the human skull, with a scalp thickness obtained from MRI measurements of scalp thickness and facial features which included the nose, face, jaw and neck which were distant from the EIT electrodes. As such, the shape of the head-tank was an accurate representations of the human head and it contained a realistic scalp thickness between the EIT electrodes and the human skull placed within the tank.

In order to assess the adequacy of skull in the head-tank to simulate the presence of the skull in-vivo, a consideration of the relative resistivity ratio of the scalp:skull:brain needs to be made for published values in the literature and the resistivity of the different components in the head tank (Table 3.11). The value of scalp resistivity, 2.5-3.3 kΩ.cm, was obtained from impedance measurements of human skin at 40 kHz which had been layer stripped to remove the capacitative stratum corneum (Yamamoto and Yamamoto 1976). The value of human brain resistivity, 0.35-0.39 kΩ.cm measured at 50 kHz, was obtained at neurosurgery with a two-electrode technique (Lattikka *et al.* 2001), calibrated in a known resistivity solution of saline; these values agree with in-vivo measurements of animal brain resistivity (Van-Harreveld and Ochs 1956; Ranck 1963). The skull resistivity value, 6.7 kΩ.cm, was measured in post-mortem skull (Oostendorp *et al.* 2000). A similar value for skull resistivity, of 7.5 kΩ.cm, has also been obtained in a cleaned dried skull soaked 0.9% saline (Law 1993). These values are approximately

a third of the skull resistivity in 0.2% saline measured in this Chapter. However, it is likely that the skull resistivity measured in this chapter is that of the skull in life. The main reason for this, is that bone resistivity is related to the resistivity of the saturating solution (Kosterich *et al.* 1984). The skull resistivity measured in this Chapter, of 20.5 kΩ.cm, was measured in 0.2% saline which has a resistivity of 212 Ω.cm. In vivo, the equivalent saturating solution of the skull is comprised of cellular bone-marrow, blood and connective tissue. Blood alone has a resistivity of 140-230 Ω.cm (Geddes and Baker 1967), a range that overlaps 0.2% saline. Therefore the skull in vivo is likely to have a similar resistivity to that measured in this chapter. The underestimates in the two published studies of skull resistivity are due to the use of lower resistivity saturating solutions: 1) The value of 7.5 kΩ.cm was measured with human skull soaked in 0.9% saline which has a resistivity of 50 Ω.cm (Law 1993) and is much lower than that of blood, 2) In the second study, human skull was excised at post-mortem, frozen then thawed prior to resistivity measurements (Oostendorp *et al.* 2000); the effect of freezing acts to lyse cellular tissue, reducing the high resistivity intracellular component of the tissue by disruption of cell membranes and the release of intra-cellular fluid and electrolytes into the extra-cellular fluid. The resistivity of the effective bathing solution of this skull specimen would therefore approximate that of 0.9 % saline, which is again much lower than that of blood and underestimates true skull resistivity. After consideration of the methodology of these two studies, I believe that the skull resistivity of 20.5 kΩ.cm, measured in this Chapter, is a close approximation to the resistivity of the human skull in life.

Using the 20.5 kΩ.cm value of skull resistivity and the published measurements of abraded skin (~=scalp) and brain resistivity, the resistivity contrast of scalp:skull:brain is approximately 1.2:55:1, with a corresponding tank resistivity ratio contrast of 1:97:1. As such the tank represents a reasonable approximation, within a factor of 2, to the resistivity contrast provided by the skull in the human head and therefore results obtained by the head-tank can be used to make inferences about the effect that the presence of the skull has on EIT images obtained from the head.

Table 3.11 . Comparison of resistivities of the components of the head tank with human tissues.

Head tissue (Study)	Resistivity of tissue (measurement fr equency)	Equivalent head-tank component	Resistivity of head-tank component (Mean±SD)	Resistivity ratio of tissue to head-tank component
Unabraded skin (Gabriel *et al.* 1996)	2.5-3.3 kΩ.cm (40 kHz)	0.2% saline	0.212 ± 0.003 kΩ.cm	12:1
Abraded skin (estimate for scalp impedance) (Yamamoto and Yamamoto 1976)	0.45 kΩ.cm (40 kHz)	0.2% saline	0.212 ± 0.003 kΩ.cm	2:1
Skull (Oostendorp *et al.* 2000)	6.7 kΩ.cm (10 kHz)	Skull in 0.2% saline	20.5 ± 2.0 kΩ.cm	3:1
Brain (Lattikka *et al.* 2001)	0.35-0.39 kΩ.cm (50 kHz)	0.2% Saline	0.212 ± 0.003 kΩ.cm	2:1

3.4.3 Explanation of head-tank factors that affect EIT image quality

3.4.3.1 Effect of head shape

There was no effect of head shape on localisation error as the localisation errors of the sponge within the head-tank were not different to those obtained within the hemispherical tank. Therefore the errors in the human images are unlikely to be caused by the head shape.

3.4.3.2 Effect of the skull

On the size of impedance changes within the skull

The skull had a predictable effect on the size of the imaged impedance changes; it reduced their magnitude by a factor of 5-8. This is caused by the high resistance path imposed by the skull to the applied current, which is shunted through the low resistance path provided by the saline in the scalp layer of the head-tank phantom. As the current density inside the skull is reduced compared with the head tank without the skull, then the impedance change, produced by the sponge, is reduced. The size of reduction of the current density within the skull is related to the resistivity contrast of the skull to the surrounding tissues (Rush and Driscoll 1968; Gibson *et al.* 2000). In this study, the contrast ratio of the head-tank layers of scalp:skull:brain was 1:97:1, compared to

1.2:55:1 estimated for similar layers in-vivo, therefore I would expect a reduced attenuation of the skull for in-vivo EIT studies, as a smaller contrast ratio produces less attenuation of the impedance change within the skull in computer simulations (Gibson *et al.* 2000).

On image localisation

The effect of the skull on image localisation was to move the object towards the centre of the tank by up to 20% of the image diameter. This is likely to be the upper limit of localisation error produced by the skull, when data from the human head is reconstructed with an algorithm based on a homogeneous sphere model. As this is a predictable error, then a radial correction factor could be applied to the images to correct for localisation towards the centre of the image, although the size of such a corrections would be dependent on the resistivity contrast of the skull to the scalp, which may have a large amount of inter-subject variation and therefore be impractical to apply uniformly to all subjects. An alternative solution is to reduce the localisation error due to the skull by including realistic information about the resistivities of the head in the calculation of the sensitivity matrix used in the reconstruction algorithm. This could be done in two ways: 1) Either by using a 3 sphere head model which would give a more realistic representation of the current distribution in the human head than a homogenous sphere model (Rush and Driscoll 1968) or 2) By the use of a realistic finite element model of the human head (Gibson *et al.* 2000). The finite element model method has several advantages over a 3 sphere analytical model, in that complex information can be incorporated, such as the head shape, the presence of conductivity holes in the skull, the resistivities of different tissue layers of the head and potentially information about tissue anisotropy. The disadvantage of the finite element method is in the difficulty of its implementation compared to an analytical solution.

Despite the errors produced by the skull, it would seem that the upper limit of localisation error is still less than 20% of the image diameter and therefore not sufficient to explain mis-localisation of impedance changes in the human head away from the cortical area expected to be stimulated by the experimental paradigms. Although additional errors are probably present in the human images, from differences in the head not modelled in the head tank, such as the electrode-skin interface or the anisotropy of the head, it is not likely that these would cause a greater error than that caused by the skull.

It is unlikely that tissue anisotropy has a greater effect on the production of errors than that of the skull, as the resistivity contrast of 98:1 between the skull and saline in these tanks is likely to be higher than resistivity contrasts due to tissue anisotropy or between different tissues other than the skull. For example the resistivity contrast between two dissimilar tissues, the grey

matter and cerebro-spinal fluid, is approximately 7:1 (Lattikka *et al.* 2001). The high impedances at the electrode-skin interfaces may contribute to localisation error by the introduction of common mode errors (Boone and Holder 1996) which will reduce the magnitude of impedance changes measured at the scalp in an unpredictable manner. However, the effect of these errors are expected to be small, for the reasons discussed in the previous section.

3.4.3.3 Effect of head shape and skull on localisation: conclusion

The main contribution to the localisation error on images of impedance objects within the skull is due to the skull itself, whereas the head shape does not appear to contribute to localisation errors. The upper limit of these errors is 20 % of the image diameter, and the direction of the error is predictable and towards the centre of the tank; such errors are therefore insufficient to describe the larger localisation errors seen in the adult EIT studies. This may suggest that a factor not simulated in the head tank, such as skin impedance, affects localisation – although this seems unlikely that this would have a greater effect than that of the skull. More likely is that the adult EIT images are a representation of the true impedance changes within the head, but physiological factors contribute to mis-localisation.

3.4.4 Effect of reconstruction algorithm

The other question answered by this study is the question of the best reconstruction algorithm. This can be determined by either qualitative or quantitative criteria. From a qualitative point of view, the images produced by the SVD_62 algorithm produce impedance changes that are better defined, smaller and easier to localise than the Transpose algorithm. The disadvantage of the SVD_62 algorithm is the production of impedance artefacts of opposite magnitude to the impedance perturbation. It is possible that these artefacts contribute to some of the localisation errors in the human EIT images. The reason for the improvement with the SVD_62 algorithm is that it contains more information, the Transpose algorithm is equivalent to an SVD algorithm truncated at the first singular value. As successive singular values contain successive amounts of information, then truncation at 62 singular values provides better information in the image about the size and position of the impedance change (Gibson 2000).

From a quantitative point of view, similar conclusions are reached. The SVD_62 algorithm has a narrower FWHM, which enables it to localise two impedance changes within the skull, and the localisation errors are significantly smaller for the SVD_62 algorithm compared to the Transpose. From a qualitative assessment, the FWHM is a significant improvement in the images compared to the Transpose algorithm, however the improved localisation of 1-2 pixels in an image 32 pixels wide is a barely noticeable improvement. The quantitative assessment of the

impedance artefacts also agrees with the visual inspection of the images; the summed magnitude of the impedance change to impedance artefact was 540:1 and 2.7:1 for the Transpose and SVD_62 images, respectively and the ratio of the number of pixels due to the impedance change compared to artefact was 50:1 and 1.1:1, respectively.

From this there is an argument to use both algorithms in the reconstruction of human EIT data in which the location of the impedance change is unknown: the Transpose algorithm could be used to identify the predominant change in the image as this produces the least impedance artefact and the SVD_62 algorithm used to localise that change. If only one algorithm was to be used, the SVD_62 would be the most useful as it offers better spatial resolution and the peak impedance change image agrees between those produced by the SVD_62 and Transpose algorithms.

3.4.5 Effect of noise correction

The procedure of noise correction does not affect the image localisation of a small, 12% impedance change, produced by a sponge in the skull, with a similar signal to noise ratio in the raw impedance data compared to EIT data from the adult head. In the head-tank experiments up to 39% of measurements were subjected to simulated noise correction, compared to a maximum of 25% in the human data. It is therefore unlikely that the method of noise correction used on human EIT data affected localisation of the impedance changes within the human images. The ability to reduce the data set by 39% and obtain similar images implies a large degree of redundancy in the impedance data. It is possible that only a few measurements are required to give positional information about the location of the impedance change, and subsequent information helps to improve resolution and provide information about the magnitude of the change. These hypotheses were not formally assessed in these experiments, but could be tested in future studies.

One of the implications of information redundancy in the EIT data is that the resolution of EIT may not be improved by increased numbers of impedance measurements. If more electrodes are used, with closer spacing, the voltage measured between these electrodes becomes smaller and proportionally more noisy. At a certain stage, there is likely to be a compromise between the potential improvements to image quality through increased numbers of measurements and the degradation of images from increased measurement noise. The slow speed of the HP EIT system limited investigation into this, however the faster UCH Mark 1b EIT system would be capable of increased measurements during a smaller time interval so that future work could determine the optimum number of measurements and scalp electrodes.

3.4.6 Application of results to the EIT imaging of the real human head

The experiments from this chapter demonstrate that the current EIT system and reconstruction algorithms can image small changes within a human skull. This work also suggests that the use of an homogenous sphere model for the sensitivity matrix used in the reconstruction algorithm does not introduce large localisation errors when used on a real head shape, and that localisation errors due to the skull are relatively small and predictable. Therefore the results of these head-tank studies do not account for the poor localisation of impedance changes seen in the adult EIT images obtained in Chapter 2.

As the head-tank appears to be a good model of the head shape and the presence of the human skull, then the explanation of localisation errors in the human images must either be due: 1) Limitations of the head tank in modelling the human head (considered below), with factors present in the head that give rise to reconstruction errors, or 2) If the head-tank is a good model for the human head, then it is likely that physiological factors, such as multiple and multi-focal stimulus related impedance changes, account for poor localisation in the adult EIT images, especially as the EIT system has a low resolution and would be unable to independently resolve multiple impedance changes. Although the image of two Perspex rods was similar to the superposition of the images obtained with a single Perspex rod in either of the two positions (Figure 3.36), this only demonstrates what happens with impedance changes of the same size are summated, if both impedance increases and decreases were to occur in the head then these may cancel and lead to mis-localisation.

Limitations in the head-tank as a model of the human head may produce larger localisation errors in human EIT data than in head-shaped tank data. Obvious differences not modelled in this tank are the capacitative qualities of the skin, the anisotropy of tissues or the presence of a conductive layer of CSF between the skull and the brain. However, the largest resistivity difference between the homogenous spherical reconstruction model and the human head is the skull, which introduced a relatively small error in the head-tank images compared to the localisation errors present in the adult EIT images; it would therefore seem unlikely that other factors would have a larger effect on image localisation, but until future models can address limitations of the head-tank, then the possible effects of skin capacitance, tissue anisotropy and the CSF layer should still be considered as a possible source of error which may contribute to poor image localisation in the adult EIT images.

The final possibility that would affect the human EIT images is the presence of reconstruction artefacts, which were clearly demonstrated in the head-tank images on the introduction of a single impedance change. Their presence may well have an adverse effect on

image localisation in the human EIT data. If these artefacts are dependent on the location of the impedance change, then a reproducible change would be expected to produce a reproducible artefact. If the artefact is large enough it could be identified as the significant impedance change in the image and result in a localisation error.

3.4.7 Future work

Future work should be aimed at improving the head tank model and the reconstruction algorithm. In this study there was no attempt to simulate the resistance and capacitance of the scalp, the presence of which could introduce larger localisation errors in human EIT data. In the head tank the skull introduced localisation errors which may be reduced by the introduction of realistic resistivity information into the head model used in the reconstruction algorithm. At the time of writing, there has been recent success by members of the UCLH EIT in using a realistic FEM model of the human head to reconstruct head and tank data (Bagshaw *et al.* 2003), which appears to improve the localisation and reduce reconstruction artefacts in the EIT images. Once this algorithm is fully tested, then it is likely to be used in the reconstruction algorithm to reconstruct subsequent EIT data from tank and human studies. Other future work could extend the head model to incorporate more realistic tissue resistivities in order to try to simulate the capacitance of skin. Since the time of these experiments, this has been partially achieved by using marrow skin to simulate the capacitance of human skin, with conductive alginate to simulate the scalp, although the results of these studies were only able to use a headset of 21 scalp electrodes, with a different measurement protocol (Tidswell *et al.* 2003).

The work in the next chapter aims to simplify the human EIT studies by testing EIT in neonates. It is possible that neonatal EIT may produce better localisation in the images due to physical factors, such as the lower resistivity of the neonatal skull – which would result in less image distortion with the use of a spherical reconstruction algorithm model, and that the physiological impedance changes in the neonatal brain may be less complex and more focal than in adults due to the relative immaturity of the neonatal nervous system.

Chapter 4: Functional EIT in Neonates

4.1 Introduction

4.1.1 Purpose of neonatal studies:

The adult EIT studies demonstrated that EIT could be used to measure impedance changes from the head during sensory stimulation and motor activity; however the adult images were noisy and impedance changes were not localised to the expected area of cortex stimulated by the experimental paradigms. In contrast to this, in the head-shaped tank, the ability of the EIT system and algorithm to localise single impedance changes was proved. This implies that the localisation errors in the adult images are now either due to errors between the head and the reconstruction algorithm which were not modelled in the head tank, or due to multiple physiological impedance changes in the head that could not be resolved by the current EIT system.

The aim of this chapter was to determine whether EIT produced similar changes in neonates, and whether there was improved image localisation of these changes. Near infra-red studies (Meek *et al.* 1998) and fMRI studies (Yamada *et al.* 1997; Martin *et al.* 1999; Anderson *et al.* 2001; Born *et al.* 2002; Erberich *et al.* 2003) in infants have demonstrated that similar changes of blood flow and blood volume occur in the neonatal brain in response to stimulation. This indicates that neonatal brain impedance should change during stimulation due to increased blood volume in active cortex. However, the size of the volume of brain activated in infants is expected to be smaller than that in adults, which may reduce the magnitude of the impedance change to a level below the sensitivity of EIT. In contrast to this, the EIT system should be more sensitive to changes in the neonatal brain due to lower neonatal skull resistance (McArdle *et al.* 1988; Gibson *et al.* 1997) compared to the adult; this is due to the neonatal skull composition which is largely cartilaginous, thinner and less calcified than the adult's. I have not been able to find a value for neonatal skull resistivity in the literature, however the thickness of a neonatal skull can be measured from CT scan data: if adult skull resistivity is 20.5 kΩ.cm over a 6mm thickness (Chapter 3), and neonatal skull 2mm thick (from CT data) then this would decrease the resistance of a unit area of neonatal skull by a factor of 3 compared to the adult if the neonatal skull had a similar calcified composition. An additional reduction of resistivity would be expected from the more cartilaginous nature of neonatal skull, if human articular cartilage has a resistivity of 150 Ω.cm (Hasegawa *et al.* 1983), which gives a ratio of adult skull resistivity to articular cartilage of 137:1, then it is likely that the resistivity of neonatal skull is well below that of the adult's. The possible

benefit of the lower neonatal skull resistivity, is that as there will be less attenuation of the impedance change measured on the scalp. This in turn may improve the accuracy of the EIT images, due to increased signal to noise and also as a result of less error between the neonatal head and the homogenous sphere algorithm, compared to the errors between the algorithm and the adult head.

The methods used in the neonatal study are similar to the adult EIT methodology, but differs in three main respects: 1) A new faster EIT system was used to acquire the EIT data, which will be detailed in the methods section of this chapter, 2) Different stimulation paradigms were used in the study, in order to account for the developmental and behavioural nature of the neonate, and 3) Due to the use of a smaller array of 21 scalp electrodes, compared to 31 in the adult EIT studies of Chapter 2, a new reconstruction algorithm was used and validated.

4.1.2 Background to stimulus paradigms used in the neonatal EIT study

4.1.2.1 Overview

Although a number of different cognitive, motor or sensory paradigms could have been used in the adult EIT studies, there are restrictions on stimulus paradigms that are suited to neonatal functional imaging. The criteria for the choice of stimulus paradigms for use in this neonatal study were: 1) Evidence from other functional imaging modalities that neuronal activity or blood flow changes occur during the use of such a stimulus paradigm and 2) Ease of use of the stimulus paradigm, minimisation of discomfort to the neonate and parent acceptability.

On this basis, the electrical stimulation of the wrist used in adults was not used as it was a potentially uncomfortable, and likely to wake the infants, so producing crying and movement artefact. The stimulus paradigms chosen for the neonatal studies were an 8Hz flash visual stimulus provided by commercially available LED goggles, and a passive-motor stimulus in which either wrist was flexed and extended at 1.5Hz for up to 25s. The evidence that justifies the use of such stimuli in infants is now briefly discussed.

4.1.2.2 Visual Stimulation in Neonates

The cortical response to the effect of visual stimulation has been measured in neonates by several techniques using either a flash or a checkerboard stimulus. Visual evoked potentials (VEPs), measured with single channel EEG, have been detected over the visual cortex by studies which used light flashes (Hrbek and Mares 1963; Harding *et al.* 1989) or required the infant to observe a checkerboard pattern reversing at different frequencies (Sokol 1978; Harding *et al.* 1989). In a direct comparison of these stimuli in the same infants (Harding *et al.* 1989) the cortical potentials measured with flash stimulation are 1.2 to 2.5 times larger than those produced by a checkerboard.

Similar stimuli produce a haemodynamic response, as detected with fMRI in sedated infants with flash stimulation (Born *et al.* 1998), (Yamada *et al.* 1997), (Martin *et al.* 1999) and by Near Infra-Red Spectroscopy (NIRS) in unsedated infants in response to a multi-coloured moving circle stimulus (Meek *et al.* 1998).

These studies suggest that either a checkerboard stimulus or a flash stimulus would produce visual cortical activation and therefore be suitable for the neonatal EIT study. I decided on the use of a flash stimulus, for several reasons:

1) Ease of use: although it was possible to sit a neonate in front of a Checkerboard screen for several minutes (attempted in pilot studies) in practice it was much easier to use a flash stimulus which was independent of the neonate's attention.

2) There is a larger evoked response amplitude provoked by flash stimulation. As visual responses in monkeys indicate that a larger neural response to stimulation is correlated with a larger blood flow response, as measured by simultaneous fMRI and intra-cerebral local field potentials (Logothetis *et al.* 2001), then it was possible that flash stimulation would produce a larger impedance response for the neonatal EIT studies

The flash stimulus was provided by LED goggles adapted from a commercial EEG system (Micromed, Italy). A flash frequency of 8Hz was chosen as this had been demonstrated in adults to produce the largest BOLD signal in adults (Kwong *et al.* 1992; Singh *et al.* 1999). This decision was based on adult data, as no equivalent study has yet been performed in neonates. The advantage of the LED goggles chosen for the stimulus is that they also met the criteria for ease of use; they could be attached to infants using a soft felt mask and remained in place throughout the duration of the experiment

4.1.2.3 Passive motor stimulation in neonates

Passive motor stimulation was used as the second stimulus in the neonatal EIT study. This was designed to produce sensory stimulation of the wrist joint in order to produce a response in the contralateral sensory-motor cortex.

In previous neonatal studies, two main approaches to sensory stimulation have been used. The first approach is electrical stimulation of the median nerve at the wrist (Hrbek *et al.* 1968; Hrbek *et al.* 1972) or posterior tibial nerve in the leg (Pike *et al.* 1997) to produce somatosensory evoked potentials (SEPs) over the contralateral sensori-motor cortex. The second approach is to use passive motor movements around a limb joint. In adults, this approach produces similar BOLD-fMRI changes in the contralateral sensorimotor cortex to active, self-controlled motor activity (Holloway 2000). In neonatal NIRS, passive motor movement of the knee (Isobe *et al.* 2001) and

of the elbow (Hintz *et al.* 2001) have demonstrated that such stimuli increase blood volume over the contralateral and, to a lesser extent, over the ipsilateral cortex to the limb stimulated.

From consideration of these studies I decided to use a passive motor task in the neonatal EIT studies as this was:

1) An acceptable stimulus to the parents and relatively gentle so would not startle the infant (this was important as the startle response would cause movement and possibly respiratory artefact, and change the state of alertness of the neonate with potential effects on cerebral blood flow)

2) Demonstrated to change blood flow and volume in NIRS studies (Hintz *et al.* 2001; Isobe *et al.* 2001).

3) An easy task to perform.

The passive motor paradigm used in this study consisted of a passive flexion/extension of the wrist at a frequency of 1.5 Hz. The wrist was chosen, as was much easier to manipulate than the larger limb joints when the infant was swaddled and seated on my lap for the duration of the experiments.

4.1.3 Reconstruction issues with the neonatal EIT data

A new 3D reconstruction algorithm was used to take account of the reduced number of scalp electrodes used to acquire EIT data in the neonates, 21 electrodes compared to 31 in the adult EIT studies. The reason for a reduced electrode number was based on several issues which concerned: 1) The minimisation of handling of the neonates, 2) The smaller head size of the neonate, and 3) The practicality of reducing the chance that movement of the neonate would dislodge electrodes.

The new neonatal reconstruction algorithm was similar to the adult reconstruction algorithm, in that it was based on an identical spherical model of the human head, but with a reduced electrode number. This algorithm was validated prior to use on neonatal impedance data. This algorithm was tested on a new simulation of the human head, which consisted of a saline filled human skull, covered in conductive alginate - to simulate the scalp, and the vegetable skin of a large marrow - to simulate the impedance of skin (Tidswell *et al.* 2003). In these studies the algorithm correctly imaged an impedance object in several separate locations within the marrow-tank phantom. The results of this work validated the new algorithm and electrode protocol for use in the human neonates. In this work, the optimal truncation of the images was with 60 singular values; however similar quality images were obtained from the head-simulation with 40 and 50 singular values.

In addition, in order to improve image quality, a spatial noise reduction method was applied to the images using a 2D, 9-pixel width, median filter. Median filters are used in image

processing in order to preserve the features in an image while noise is removed (Niblack 1986). In order to demonstrate its suitability to EIT images, the same filter was applied to data acquired from the marrow-tank head-phantom data (Tidswell *et al.* 2003): in this study, the application of the median filter preserved the image changes made by a Perspex rod, and image noise, particularly electrode artefact, was removed. In theory, it is not appropriate to apply a 2D filter to 3D data; however due to the higher resolution in the x and y dimensions of the EIT images than in the z-dimension a 3D filter in the z-direction would have corresponded to a slice width of 2 which would not have produced any additional spatial smoothing in the z-direction. Therefore a 2D median filter was used, and applied individually to the image slices.

4.1.4 Purpose of Neonatal Study

The purpose of the neonatal study was to determine whether EIT could detect impedance changes, expected from changes of blood flow and blood volume, in the areas of cortex stimulated by the chosen stimulus paradigms.

The secondary purpose was to image these changes and, as in the adult EIT chapter, determine the localisation of stimulus related impedance changes with respect to the areas of cortex expected to be stimulated by such paradigms.

4.2 Methods

4.2.1 Overview

Nine healthy, term infants were recruited and each connected to the new Mark 1b UCLH EIT system (Tidswell *et al.* 2001; Yerworth *et al.* 2002) by a set of 21 EEG scalp electrodes through which four 3D EIT images were acquired every second. Consecutive images were acquired during periods of rest which alternated with 25 second periods of either a visual or passive motor stimulus. The raw data and the reconstructed images were analysed for impedance changes during the stimulation period compared to the baseline data.

4.2.2 Subjects and Consent Procedure

Each of the nine infants were recruited from either the postnatal unit or the neonatal unit at University College Hospital, London. One was my son. The studies were performed at a corrected gestational age of 36-44 weeks and the infants had no neurological problems at the time of the studies. One infant had had neonatal seizures in the premature period which had resolved 6 weeks prior to the EIT study - no cause was found for the seizures, despite intensive investigation, and the infant was normally developed at the time of the study.

Each infant was recruited by informed consent through a discussion with one or both parents. It was made clear to them that 1) EIT was an experimental technique, 2) They did not have to consent to the study, and 3) Refusal to enter the study would not affect either the mother's care or their infant's care.

The experimental procedure and the use of a small electrical current to make the impedance measurements was discussed in full to the parents, prior to consent. Further information was provided on an information sheet. Infants were recruited once the parents understood the information and were willing for the EIT study to take place, indicated by their signature on a consent form. This study was approved by the Joint UCL/UCLH Committees on the Ethics of Human Research

4.2.3 Equipment

4.2.3.1 Mark 1b UCLH EIT System

Impedance data was recorded by the newly developed Mark 1b UCLH EIT system (Yerworth *et al.* 2002). This system provided a portable, fast, and medically safe 32-channel EIT system, fully

programmable from a laptop PC which also controlled the acquisition of EIT data and stored it for offline analysis.

4.2.3.2 EIT system components

The Mark 1b UCLH EIT system (Figure 4.39) was specifically designed for imaging the human head and met the relevant safety standards (BS 5724, IEC 601-1). It consists of a small headbox attached to the infant by a set of 21 silver/silver chloride EEG electrodes and connected by a 3m lead to the EIT baseunit.

The headbox contained the current source for the impedance measurements and the multiplexer circuits, which selected the combinations of four scalp electrodes used for each impedance measurement.

The baseunit contained the power supply for the headbox, the impedance measurement circuits and the 8-bit microprocessor unit which was programmed to operate the EIT system's electronics.

The laptop PC , a Hi-Grade AS8300 Pentium 500 MHz notebook running Windows98 (www.higrade.com), was connected to the EIT system by: 1) A digital serial interface and 2) An analogue voltage interface.

The digital serial interface between the PC and the EIT system was used to communicate the measurement settings, download the electrode measurement protocol files and to start data acquisition.

The analogue interface transferred the voltage measurement data from the UCLH system to the PC. The voltage measurement was amplified in the UCLH system to between 3-4V and converted to a 12-bit digital signal by the analogue to digital (A/D) converter PCMCIA card (analog input range –5 to +5V, Computerboards PCM-DAS 16/330, Measurement Computing, www.computerboards.com). The PC ran programs written in the HPVee visual software suite (Hewlett Packard Ltd, www.hp.com) to control the EIT system, the A/D conversion of the impedance measurements and storage of this data to the hard drive. The data was stored for later analysis.

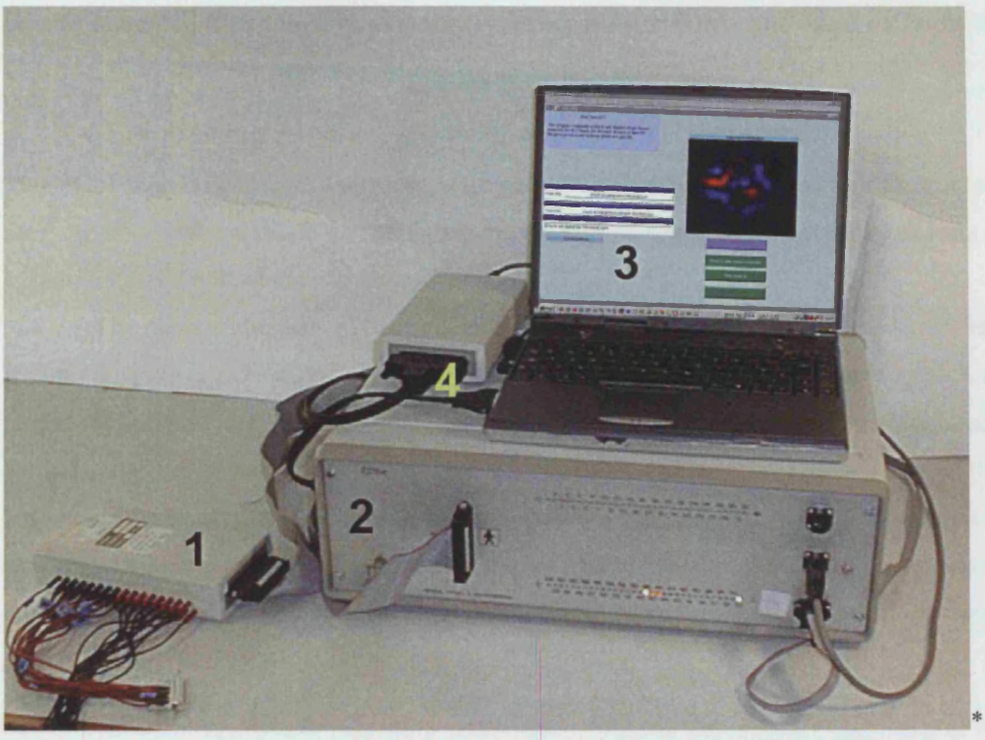

Figure 4.39 UCLH Mark 1b EIT system.
This illustrates the size of the complete EIT system used to acquire neonatal data. Components are: 1) Headbox on 5m cable, positioned near the neonate during the experiment, in which 21 EEG scalp electrodes are plugged, connecting the baby to the headbox. 2) Baseunit which contains the power supply, the microcontroller board and the majority of the electronics, 3) Laptop PC to control the EIT system and the stimulus timing. 4) Connector box between UCLH system and the PCMCIA data acquisition card.

4.2.3.3 Impedance Measurements

Impedance measurements were made in a similar manner to the HP based EIT system used for the adult and head-tank studies. As a reduced set of 21 electrodes was used for the neonatal EIT studies, the number of impedance measurements for each image was reduced to 187. Each measurement was made through a different combination of four electrodes selected from the 21 scalp electrodes: two were used to inject a 38.4kHz alternating current across the head and two were used to measure the voltage produced on the scalp by that current. In order to measure the peak voltage at each measurement which represented the magnitude of the impedance, measurements were made at a previously calibrated phase angle which compensated for the phase angle introduced by the capacitance of the electrode-skin interfaces and the head. The optimal phase angle was determined for each electrode combination by a calibration program run prior to each set of experiments. This program also set the gain of the amplifier in the EIT system, to amplify the measured scalp voltage into the ±5V dynamic range of the 12-bit A/D converter.

Signals measured from the head were usually between 10-100 mV, and could be amplified by a factor of 10 to 8000 for output to the analog to digital converter on the laptop PC.

4.2.3.4 Comparison of UCLH Mark 1b and HP EIT systems

The UCLH and HP based EIT systems were similar in that they both used four electrodes to measure impedance across the head; however, the lack of several medical safety aspects of the HP system rendered it unsuitable for use in infants.

The main advantages of the UCLH Mark 1b system are that: 1) It is medically safe: it isolates the patient from mains electricity and contained safeguards to prevent current levels above the safety limits set out in British Standards 5724, 2) It is fast: four images were acquired each second compared to one image in 25 s with the HP based EIT system, 3) It is portable: the baseunit and the laptop PC could be positioned up to 3m away from the infant while the headbox was positioned within 80 cm of the infant. This allowed a great deal of flexibility in the positioning of the infants so that EIT data could even be acquired while infants were asleep in their cots or in their parent's arms.

The single advantage of the HP-EIT system compared to the UCLH system was the lower level of baseline noise. Noise, measured on the head-tank, was 0.05% and 0.1 % of the baseline impedance for the HP-EIT and UCLH-EIT systems, respectively. However the 100-fold speed increase of the UCLH-EIT system could be effectively used to reduce random noise by a factor of 10, which more than compensated for the increased measurement noise of the system.

4.2.3.5 Electrodes and skin preparation

Twenty-one silver/silver-chloride electrodes, of 1 cm diameter, were placed around the scalp using a the 10-20 system of EEG electrode placement (Binnie *et al.* 1982). A reduced electrode set, compared to the adult EIT studies, was used due to the restriction of head size.

Each electrode site was prepared by rubbing the skin with abrasive gel on a cotton wool bud to reduce the electrode/skin impedance, and the EEG electrodes applied with a conductive paste (Ten20 conductive EEG paste and Nuprep Abrasive Skin Prepping Gel both products of D.O.Weaver and Co. 565-C Nucla Way, Aurora, CO 80011, USA). Electrode impedance was assessed at the drive electrodes by a calibration program in HPVee on the controlling computer. High electrode/skin impedances were corrected by re-abrasion of the skin and re-application of the electrode or a complete replacement of the electrode. The electrodes were secured to the scalp with either pieces of gauze, surgical tape (3M Micropore Surgical Tape, www.3m.com), or an elasticated head net. Electrode application took approximately 40 minutes in each infant and electrodes were sterilised by autoclave between infants.

4.2.3.6 Stimulator Goggles

Visual stimulation was produced by commercially available LED goggles used for EEG evoked response studies (Micromed, Italy, Figure 4.40). The goggles were triggered from the laptop PC via an optically isolated USB interface (ActiveWire USB, www.ActiveWireInc.com) connected to a self-built, battery operated timer circuit which delivered an 8 Hz, 1.2 ms pulse to the goggles. The intensity of the flash produced was 6 lumens, sufficient to be seen clearly through closed eyelids.

Figure 4.40 Neonatal EIT Study.
A neonate with the LED visual stimulator goggles. The EIT headbox is positioned close to the neonate (right side of the picture), which is connected to the baseunit (out of picture) via the grey lead. The 21 EEG scalp electrodes are attached to the infant with EEG electrode paste and held in place with an elasticated head net, these electrodes are connected to the appropriate inputs of the EIT headbox.

4.2.4 Stimulation Paradigms

During data acquisition, each infant was sat in either the examiner's or the parent's arms. If infants could not settle then they were swaddled with a blanket to minimise movement during the study. Continuous EIT images were acquired during a block design experiment that was 10-12 minutes long and consisted of 10-15 repetitions of a 15-25s stimulus interspersed with periods of baseline (no stimulus). Stimuli were either 1) Visual stimulation (4 infants) with LED goggles, at 8 Hz, with

a luminosity of 6 lumens or 2) Passive motor (6 infants), achieved by the examiner gently flexing and extending the right or left wrist. Up to three sets of experiments were usually acquired in each infant, dependent on the state and activity of the infant. The ideal state was an infant in quiet sleep or awake and settled which minimised movement and movement related artefact. Results were obtained from one infant with both visual and motor experiments.

4.2.5 Raw data analysis

4.2.5.1 Baseline Correction

The data was processed offline by programs written in Matlab (MathWorks inc. USA). Each experiment was segmented into its component 10-15 stimulus blocks. The baseline at the end of each stimulus block overlapped with the next stimulus block. After segmentation the data was corrected for baseline drift by a least squares, linear fit to the baseline data. The baseline was defined as the first 15 seconds and the last 15 seconds of a stimulus block; which allowed a 15 second recovery period after stimulus cessation for any impedance change to return to the baseline, pre-stimulus values (Figure 4.41). The baseline correction procedure was applied separately to each electrode combination in each stimulus block in each subject.

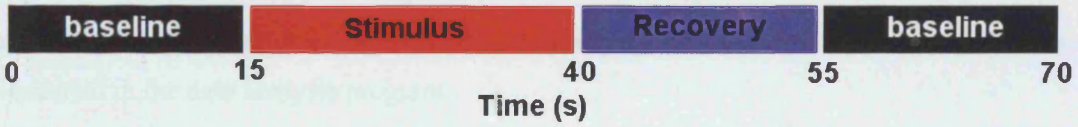

Figure 4.41 Time course of a stimulus paradigms:
The first and last 15s of data (black baseline) were used for baseline correction of the data. The stimulus was presented between 15-40 seconds and a 15 s recovery period was allowed for the impedance change during stimulation to return to baseline levels. The baseline period at the end of this block overlaps with the next block and becomes the baseline for the next stimulus presented.

After baseline correction, the impedance data were expressed as a percentage change from the mean baseline. Experiments in which the subject moved excessively, i.e. throughout the 10 repeated stimuli, were excluded from further analysis. Significant impedance changes were defined as those electrode combinations in which the impedance changed during stimulation by more than 2 standard errors of the mean (2SEM). Peak impedance changes from each subject were recorded and were defined as the electrode combination with the most significant change, i.e. with the highest signal to noise.

4.2.5.2 Noise Correction:

The baseline corrected impedance data, expressed as percentage change from baseline impedance, was analysed and displayed in Matlab. The data was then corrected for levels of noise which exceeded specific exclusion criteria:

1) Baseline noise greater than 1 % of baseline impedance.

2) Median filter of noise 'blips', defined by 1-2 consecutive data points which exceed the baseline by 1% and returned to baseline. These data points were replaced by the median value of two data points either side of the noise blip.

3) Elimination of movement artefact that produced large deviations or non-linear baseline drift of the impedance data which exceeded 1% of the baseline impedance.

The noise correction procedure was performed semi-automatically with slightly less strict criteria, then the data was manually stepped through and corrected further if required, using the criteria outlined above. This procedure was followed for each experiment in each subject. If the impedance data met the criteria for exclusion, they were either filtered to remove the noise blip or the data for that electrode combination was set to a value of zero so that it would not be reconstructed.

The probable reason for the noise blips was that the output impedance across the head, occasionally exceeded the optimal output impedance of the current source. This resulted in the occasional noise spike, which could be corrected by a spike detection routine and median filter implemented in the data analysis program.

Comparison of data between the experimental groups was performed using a two tailed t-test. Differences were significant if the probability of no difference was less than 0.05%.

4.2.5.3 Calculation of electrodes with significant impedance change

The number of electrode combinations in which a significant impedance change was detected was assessed from a visual analysis of the baseline and noise corrected EIT data, imaged as a surface plot in Matlab (Figure 4.47, Figure 4.48). For each experiment, the data at each electrode combination was averaged for the repeated presentations of the stimuli. The averaged impedance data for each electrode combination was displayed with the timecourse on the x-axis, and each electrode combination stacked on the y-axis, sorted by the size of the impedance change during stimulation. Each experiment was viewed at the same impedance scale with limits of $\pm$ 0.1% of the baseline impedance. From this surface plot of the data, the number of measurements with a change of more than 10 seconds during stimulation, and greater than 0.05% of the baseline impedance could be measured. The number of electrode combinations which demonstrated such impedance changes, expressed as a percentage of 187 measurements, were 37.6 $\pm$ 3.5 % for the visual and

38.7 ± 4.7 % for the motor experiments. There was no statistical difference between the different stimulation paradigms.

4.2.5.4 Method of assessing timecourse of impedance changes

The timecourse of the impedance changes was calculated in a program written in Matlab. For each experiment the impedance changes during stimulation were sorted by size and it's significance. Changes were considered significant if more than 90% of the data in a 15 second period during stimulation was more than two standard errors from the baseline impedance (see Figure 4.43-4.9).

The largest significant impedance decreases and impedance increases were analysed for the timecourse of the impedance change. The rise time was defined as the time taken after the onset of stimulation for the impedance to change by more than 2SE from the baseline impedance, and the time taken after stimulus onset to reach 80% of the peak impedance change was also measured.

The time taken to return to baseline was assessed from a visual analysis of the raw data: the averaged data from an experiment was displayed as a surface plot (Figure 4.47, Figure 4.48) with the impedance data from each of the 187 measurements stacked on top of each other (y-axis), sorted by the size of the impedance change during stimulation. Each was viewed on a colour scale, with limits at ±0.1%, and the time taken for the maximum impedance changes to return to within 0.1% of the baseline impedance was recorded for the experiments.

4.2.5.5 Method of assessing signal and noise

Baseline and noise corrected impedance data were selected for analysis in each experiment. Noise was calculated from the baseline data, by a program written in Matlab, as the standard deviation of impedance from baseline in each electrode, averaged across experiments, and then averaged for all electrode combinations. The average noise for each experiment was averaged for all neonates to give the average noise for both motor and visual stimulation experiments.

The calculation of signal was also performed on noise corrected data. Signal was calculated for each electrode combination as the average impedance change from baseline during the duration of the stimulus. This was averaged across repetitions of the experiment in a neonate for each electrode combination. Then the 10% of electrode combinations with the highest absolute impedance change were selected for each experiment in each neonate, and these were averaged to give a measure of the signal in that neonate.

4.2.5.6 Method of assessing reproducibility of impedance responses

For the visual experiments, data was analysed visually to examine the raw corrected impedance data for the largest impedance increase and decrease in each experiment. Where there had been a repetition of the experiments, e.g two runs of the same experimental paradigm in one patient, the

same electrode combination was compared between the two runs and displayed side by side. In one subject (Co) three experimental runs of visual stimulation were performed, two that used an 8Hz flash rate for the visual stimulus and one run that used a 2Hz visual stimulus. Although the data from the 2Hz flash frequency experiment in this patient was not used for the raw data and image analysis, this data was used to show the reproducibility of the impedance response in this patient.

4.2.6 Image Analysis:

4.2.6.1 Reconstruction and effect of SVD value on image quality

EIT images of neonatal functional activity were produced with a similar reconstruction algorithm used to construct the adult EIT data in chapter 2. The algorithm consisted of a forward solution produced analytically from a homogenous sphere model of the head and inverted by singular value decomposition (Tidswell *et al.* 2001). Images were reconstructed using 40,50, or 60 singular values. The algorithm differed to that used in the adult, in that a new electrode protocol file and new electrode position file was required, due to the reduced number of scalp electrodes and electrode measurements.

Images were reconstructed from the noise corrected impedance data for each stimulus presentation in each experiment in each subject. Images were only reconstructed from a stimulus presentation in which less than 20% of the impedance measurements had been rejected on the grounds of noise. To reduce image noise, data was averaged over periods of 5 seconds, and images reconstructed from the time-averaged data. For a 70 s experiment (15s baseline, 25s stimulation, 15s recovery, 15s baseline), with impedance measurements made at 3Hz, the final set of reconstructed images comprised of 14 images (3 baseline, 5 stimulus, 3 recovery, 3 baseline), each image reconstructed from the average of 15 data points from a 5 second period.

Each image consisted of 6 transverse slices through the head; each slice was represented by an image of 40 by 40 pixels. As there were only 6 transverse image slices, the z-dimension (cranial-caudal) was therefore represented by fewer pixels than in either the x (left to right) or y (front to back) dimensions. On a 38 cm diameter head, assuming that the head shape imaged approximated the shape of a hemisphere, these 40 pixels represented a distance of 12 cm diameter in the x and y-directions, and approximately 6 cm in the z-direction. The dimensions of each voxel (3-dimensional pixel) was therefore a cuboid of 0.3 x 0.3 x 1 cm in the x, y and z dimensions, respectively.

4.2.6.2 Effect of SVD truncation level on image quality

To assess the qualitative effect of SVD truncation on the neonatal images, three truncation levels were used to reconstruct the images obtained during visual stimulation; these truncation levels were at 40, 50 and 60 singular values. The images were assessed qualitatively for the size of the peak impedance change and the amount of electrode artefact seen around the perimeter of the image.

4.2.6.3 Image processing - median image filter

A preliminary inspection of the image data revealed that the images were noisy with small artefacts around the edge of the images. Such electrode artefacts are also seen in images of tank data, and are thought to represent errors of electrode positioning and electrode modelling between the point electrodes in the analytical forward model and the 1cm diameter electrodes in the head and tank data (Barber and Brown 1988).

A median filter, designed to smooth out spatial noise (see Introduction for more details), was applied to each image after reconstruction, then these filtered images were averaged and thresholded. These filtered and averaged images were compared to the original raw, averaged images in a side-by-side comparison for 40, 50 and 60 singular values and analysed for the correct localisation of impedance changes.

4.2.6.4 Image analysis

For each infant, the filtered or unfiltered images from each stimulus presentation were averaged. This produced a time series of images, representing the mean impedance change for that stimulus in that infant. The images were analysed visually for impedance changes with the same time-course as the stimulus. If such changes were identified, they were assessed for localisation in the expected cortical region for that stimulus paradigm. The expected cortical regions for an impedance change were defined as:

1) Visual: an impedance change in the posterior quadrant of the lower 4 slices of the images.

2) Motor: an impedance change in the lateral quadrant of the upper 4 slices of the images, contralateral to the side of the hand moved.

4.3 Results

4.3.1 Raw data analysis

Data, suitable for image reconstruction, was obtained from 9/9 neonates. As one neonate had both visual and motor studies performed there were 4 infants who provided visual data sets and 6 infants who performed motor experiments (5 infants had both right and left motor stimulation, one infant with right motor stimulation only). The following results are summarised in Table 4.12.

Both impedance increases and impedance decreases were seen in all the experiments (Figure 4.42). Peak impedance increases, expressed as a percentage change from the baseline impedance, were 0.8 ± 0.2 % and 0.6 ± 0.1 % and peak decreases were –1.0 ± 0.4 % and -0.5 ± 0.1 % for visual and motor responses respectively. There was no significant difference comparing the peak increases of the motor and visual experiments ($p=0.85$, d.f. = 23), but there was a significantly more impedance decreases in the visual experiments ($p<0.05$, d.f. = 23).

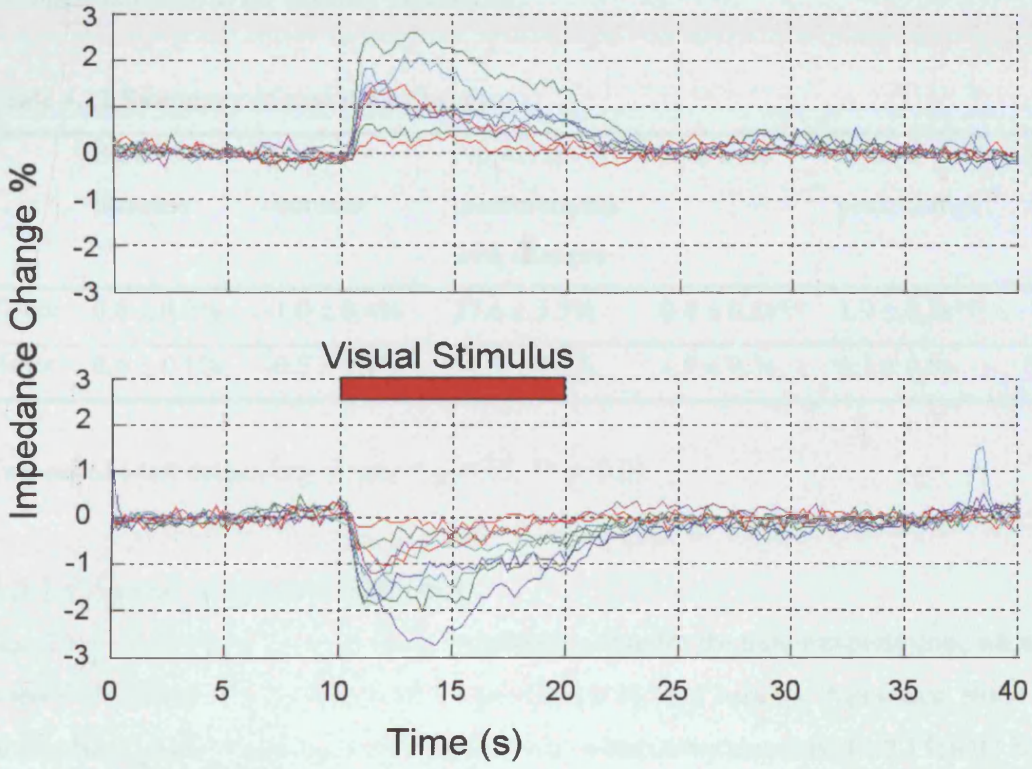

Figure 4.42 Example of impedance changes during visual stimulation in one subject
The timecourse of impedance changes during visual stimulation are presented in one subject. Data is displayed from two selected electrode combinations to demonstrate impedance increases (top) and impedance decreases (bottom). The period of visual stimulation with the LED goggles is indicated by the red rectangle. The different traces in each graph represent each of 9 repeated

stimuli presentations in the same subject. Reproducible changes are seen during stimulus presentation, with a wide variation in signal between the traces.

4.3.1.2 Electrodes with significant impedance change

The number of electrode combinations which demonstrated such impedance changes, expressed as a percentage of 187 measurements, were 37.6 ± 3.5 % for the visual and 38.7 ± 4.7 % for the motor experiments. There was no statistical difference between the different stimulation paradigms.

4.3.1.3 Timecourse of impedance changes

For visual and motor evoked responses respectively, the rise times (time from impedance change from stimulus onset) were 0.6 ± 0.1s and 1.9 ± 0.3s, the times to reach 80% of the maximum impedance change were 1.9 ± 0.2s and 6.1 ± 0.8s and the times taken to return to baseline were 7.5 ± 0.8s and 7.1 ± 0.5s (Table 4.12). Visual impedance changes occurred significantly faster than motor evoked impedance changes ($p<0.01$ for both the rise time and the time to 80% of the peak change), but there was no significant difference in the time it took for the visual and motor responses to return to the baseline impedance.

Table 4.12 Summary of raw data changes

	Peak Increase	Peak decrease	Proportion of measurements with changes	Rise time	Time to 80% peak change	Decay time
Visual	0.8 ± 0.2%	-1.0 ± 0.4%	37.6 ± 3.5%	0.6 ± 0.1s**	1.9 ± 0.2s**	7.5 ± 0.8s
Motor	0.6 ± 0.1%	-0.5 ± 0.1%*	38.7 ± 4.7%	1.9 ± 0.3s	6.1 ± 0.8s	7.1 ± 0.5s

Two-tailed t-test comparing means: * $p<0.05$, ** $p<0.01$

4.3.1.4 Signal to Noise in the data

Signal was slightly higher in the visual experiments than for the motor experiments, which were, respectively (Mean ± SD), 0.32±0.19 % and 0.25 ± 0.16 % of baseline impedance. Noise was similar between the visual and motor experiments, which were respectively, 0.15±0.02 % and 0.15±0.04 % of baseline impedance. Signal to noise ratios were therefore, for visual and motor experiments respectively, 2.0±1.0 and 1.7 ± 0.9 (Table 4.13).

Table 4.13 Signal and noise in the raw data

	Signal	Noise	Signal: Noise
	Mean±SD (Range) – Signal and noise expressed as % of baseline impedance		
Visual	0.32 ± 0.19 % (0.09-0.57)	0.15 ± 0.02 % (0.12-0.20)	2.0 ± 1.0 (0.6-3.4)
Motor	0.25 ± 0.16 % (0.09-0.60)	0.15 ± 0.04 % (0.08-0.22)	1.7 ± 0.9(0.6-3.8)

4.3.1.5 Reproducibility of the baseline corrected impedance changes

As this is a visual analysis, the baseline corrected impedance for the largest impedance increases and decreases for each subject is shown in Figure 4.49 to Figure 4.55. This shows that the impedance responses were reproducible in the same electrode combination in each experiment in each subject. Where there were repetitions of the experiment in the same subject (separated in time by 10-20 minutes), the same electrode combination is shown, again demoshowed similar impedance changes to the first experimental run. In the patient in which three experiments were obtained, with two runs of 8Hz flash visual stimulation and one run of 2Hz visual stimulation, the same electrode combinations showed similar impedance changes between the three different experiments.

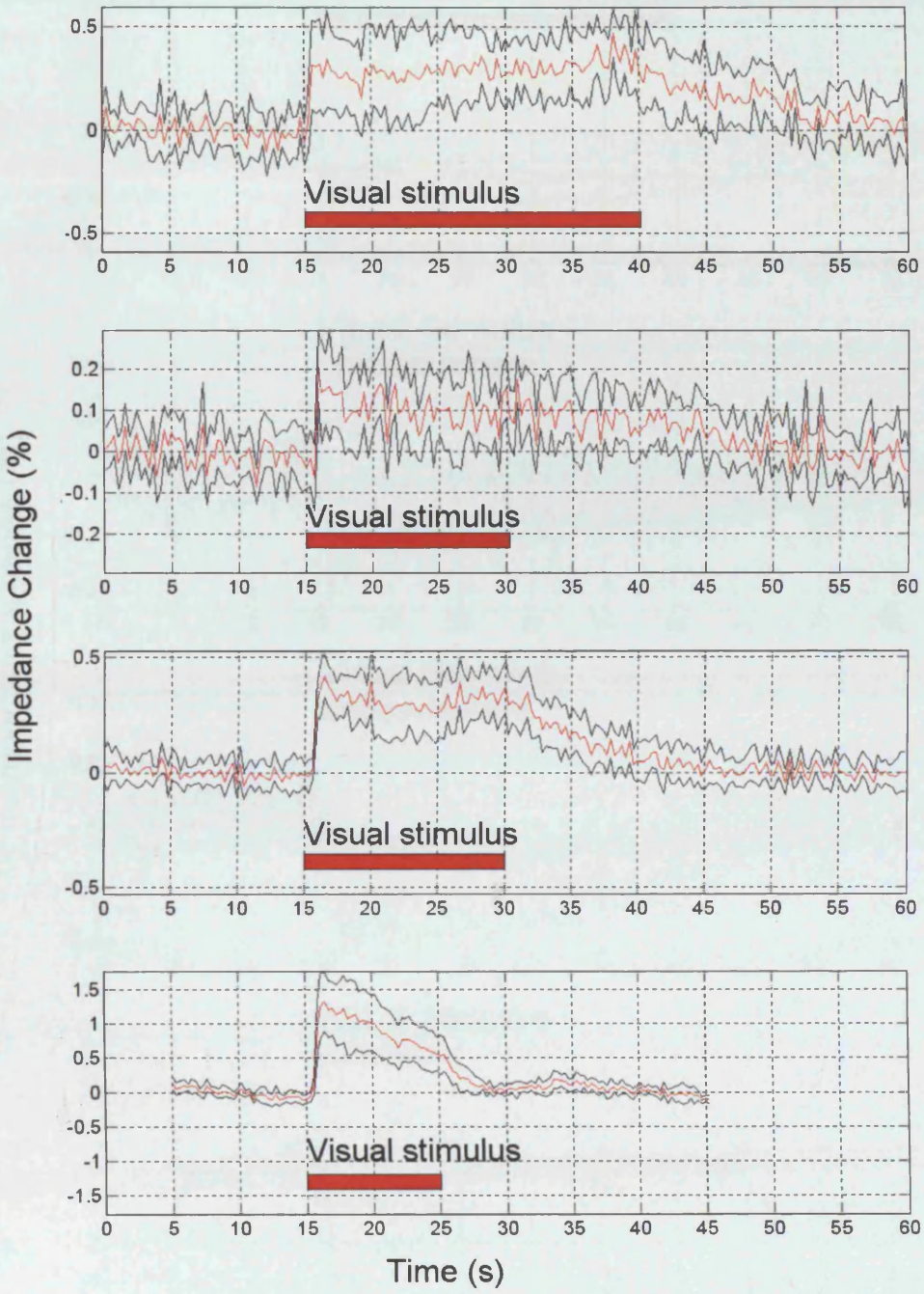

Figure 4.43 Typical impedance increases from the visual experiments
Each graph represents the timecourse of the average impedance increase for data acquired during repeated stimuli presentations in a selected electrode combination. The four graphs represent data selected from the four different subjects. Mean (red) ± 2 Standard Errors (black) are shown, with the stimulus duration indicated by the red rectangle. The impedance changes are similar in shape between subjects, despite a variation in the stimulus duration. Impedance changes are only seen during stimulation and return to baseline impedance after stimulus cessation.

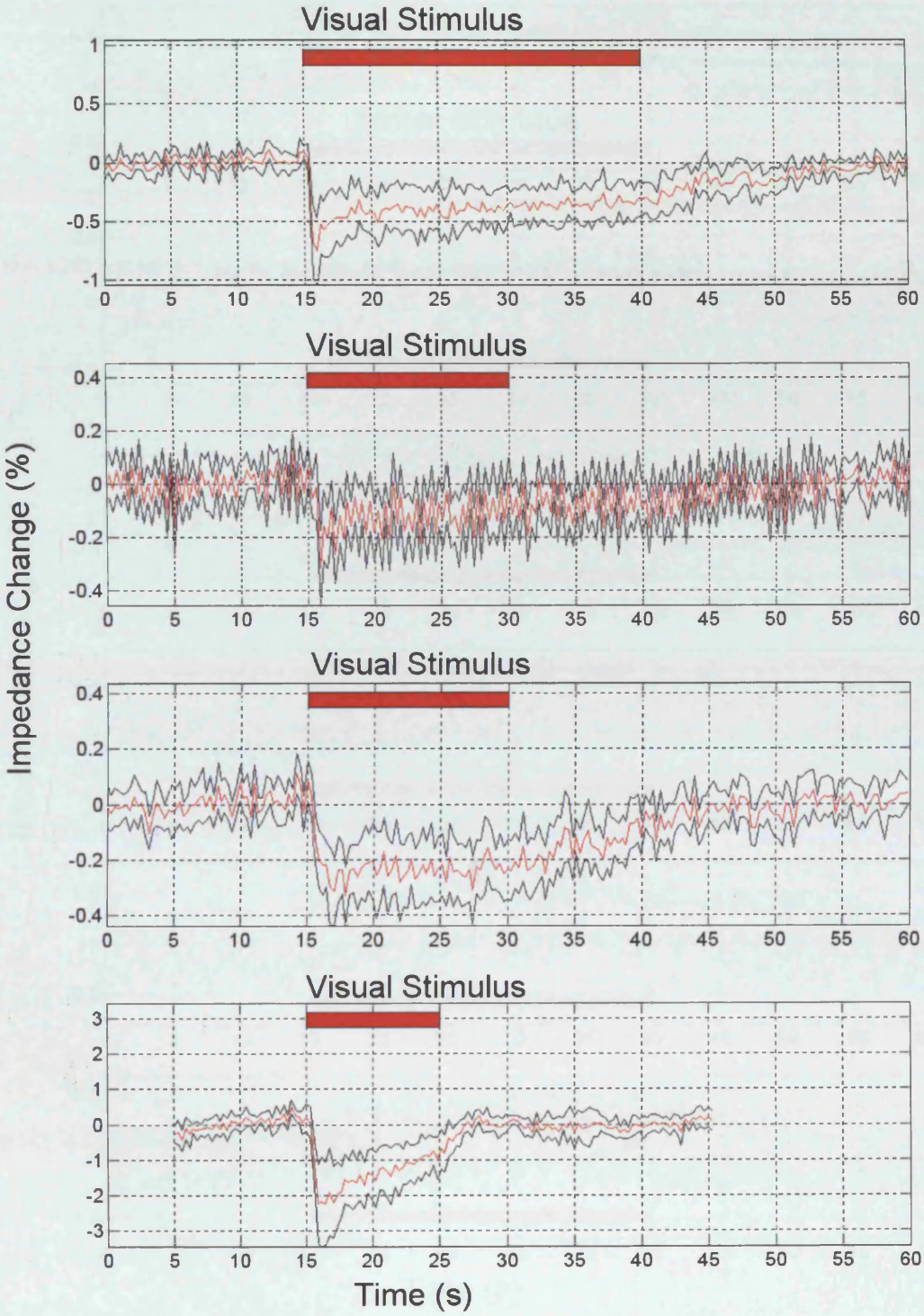

Figure 4.44 Typical impedance decreases from visual experiments
Average peak impedance decreases for visual stimulation in each of the four neonates. Data shown is the average (red) and 2SE (black) of impedance data obtained from repeated trials of stimuli presentation. Each graph represents the data from one electrode combination from each of the four subjects.

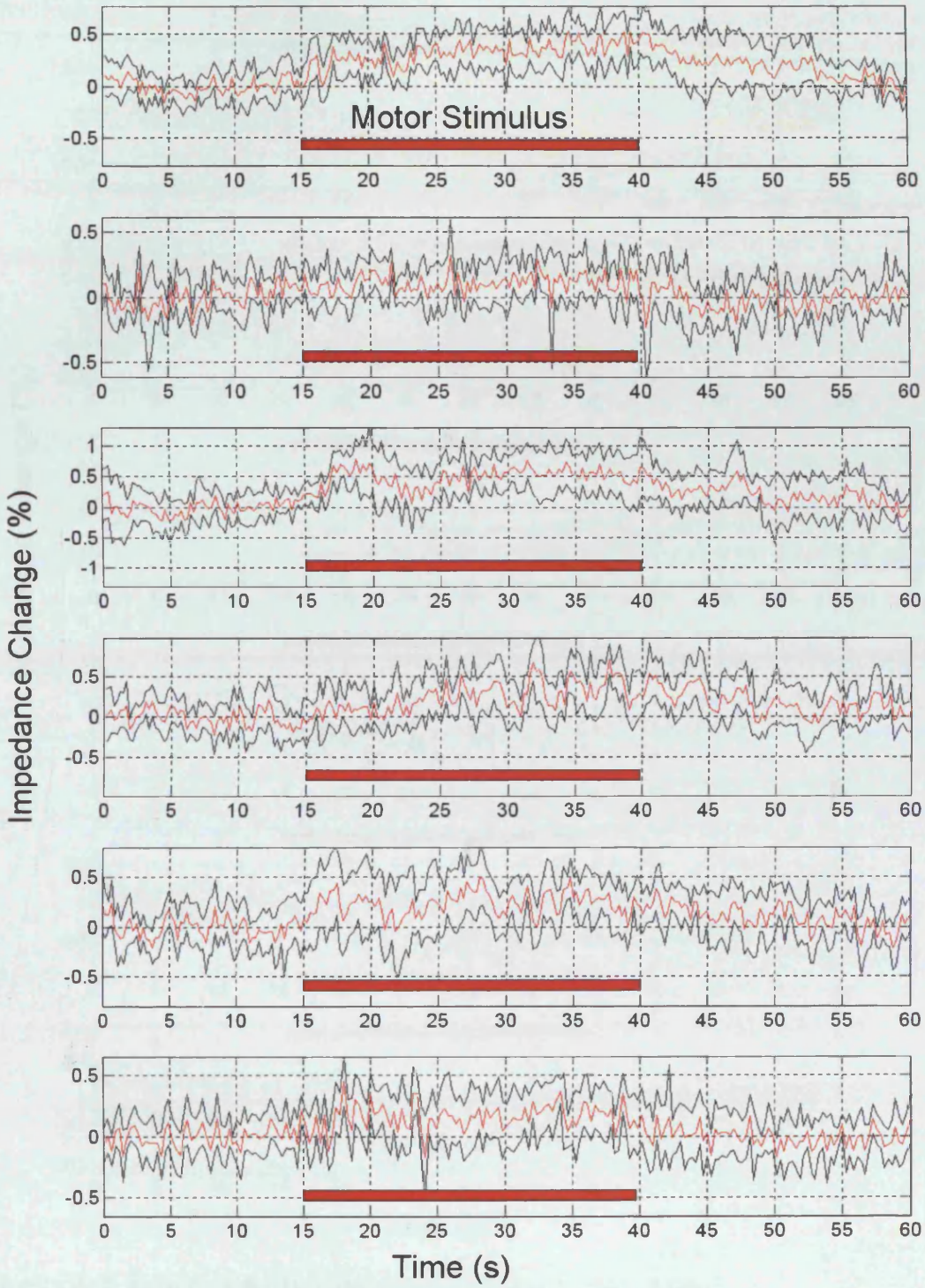

Figure 4.45 Typical impedance increases from motor experiments
Average peak impedance increases for motor stimulation in each of six neonates. Data shown is the average (red) and 2SE (black) of impedance data obtained from repeated trials of stimuli presentation. Each graph represents the data from one electrode combination from each of the six subjects.

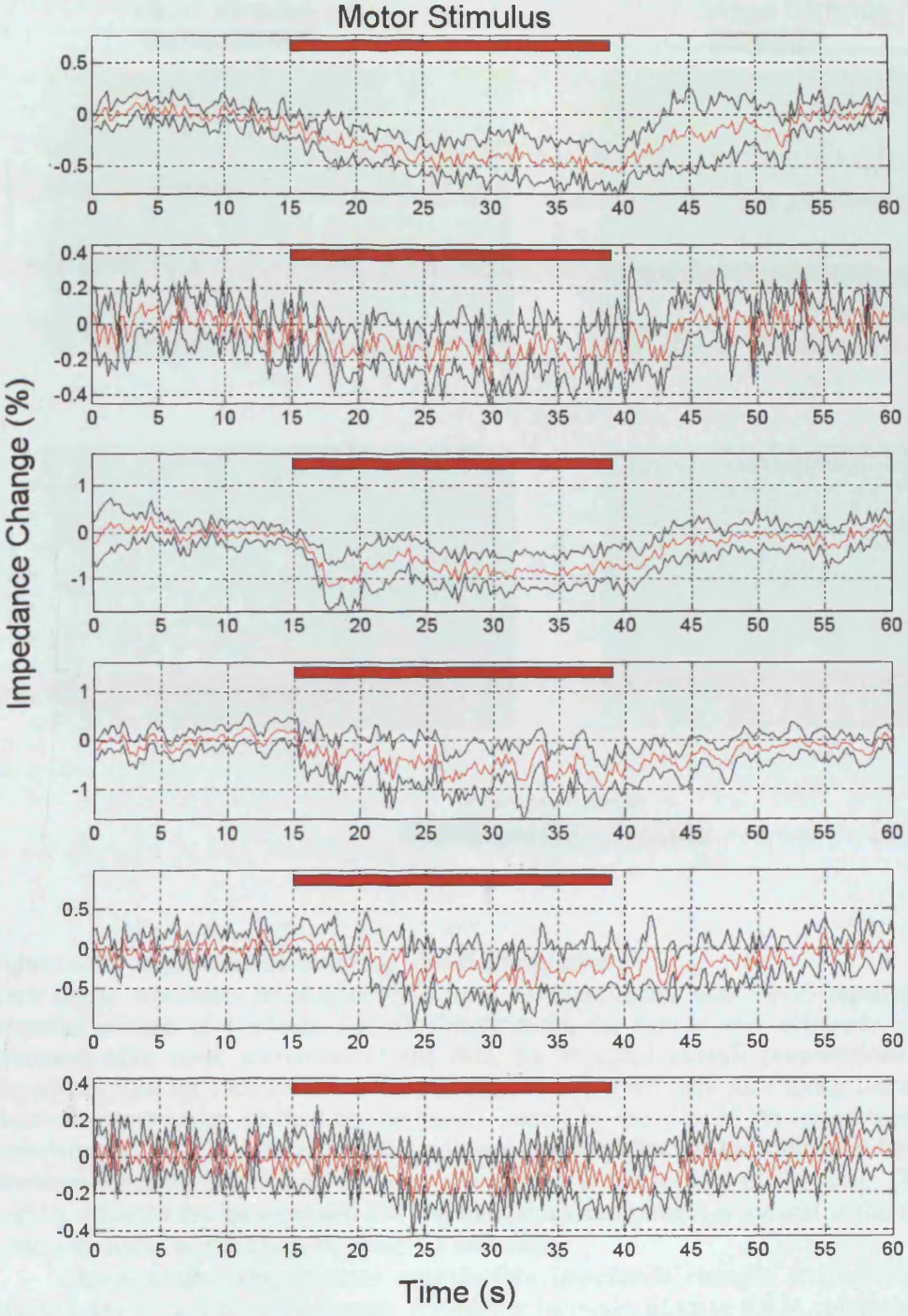

Figure 4.46 Typical impedance decreases from motor experiments
Average peak impedance decreases for motor stimulation in six neonates. Each graph represents the mean (red) and 2SE (black) of the repeated trial data from one electrode combination from each of the six subjects.

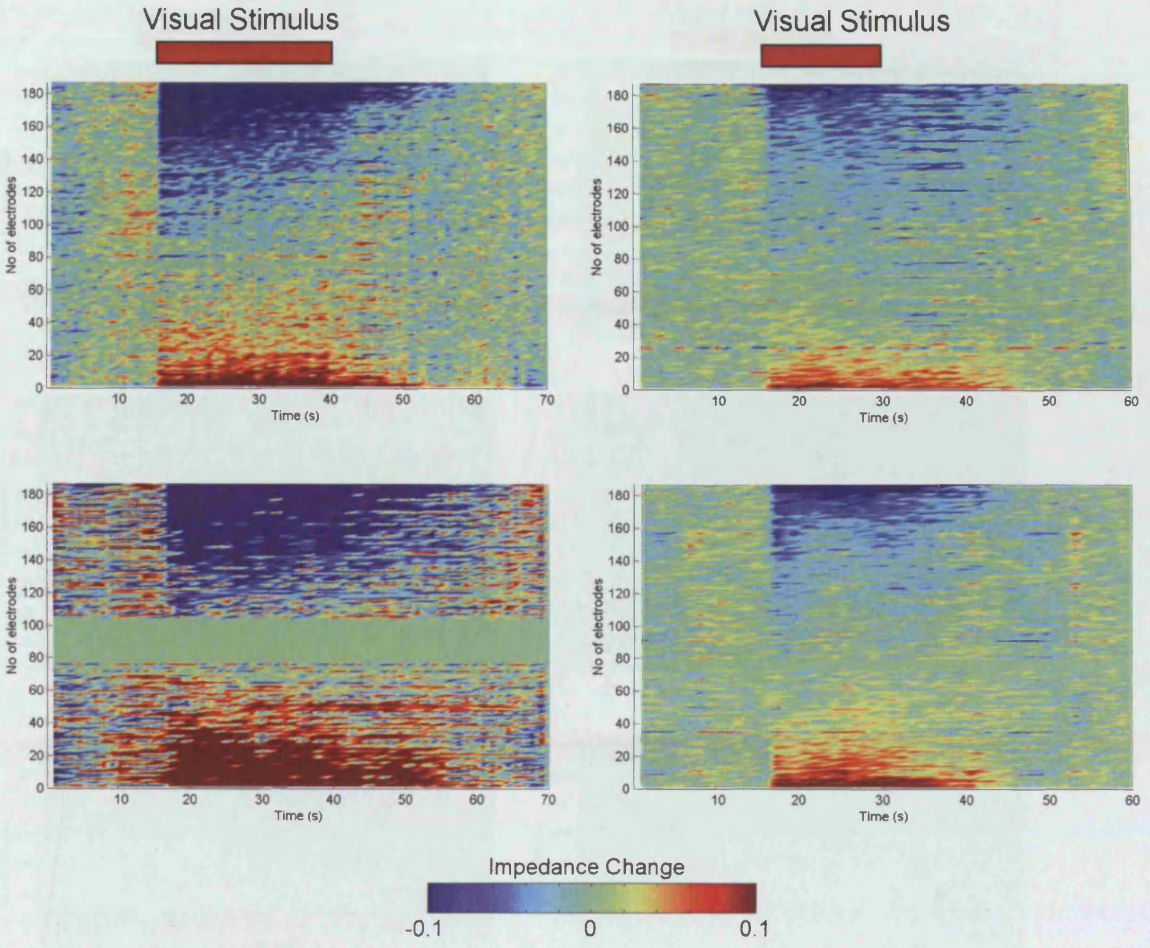

Figure 4.47 Impedance data during visual stimulation.
Each image represents impedance data from an experiment, with 10-15 repetitions of a visual stimulus, in each of 4 infants. For each experiment, the data at each electrode combination was averaged, after noise correction of the data, for repeated stimuli presentations. The averaged impedance data for each electrode combination is displayed with time along the x-axis, and each electrode combination stacked on the y-axis, sorted by the size of the impedance change during stimulation at time 15-40s in the left side images and 15-30s for the right side images. The noise corrected data, set to zero, appear as a green band in the middle of the data. The time scale is slightly different for the right and left columns. Each experiment is viewed at the same impedance scale with limits of ± 0.1% of the baseline impedance.

Each subject demonstrates reproducible impedance changes during visual stimulation (indicated at the top of each column). Impedance increases of up to 0.8 % and decreases of up to – 1.0% are measured in many of the electrode combinations. The timecourse of the changes are similar to that seen with fMRI, with a rise time of 0.6 ± 0.1s after the onset of stimulation and a decay to baseline time of 7.5 ± 0.8s after the cessation of stimulation.

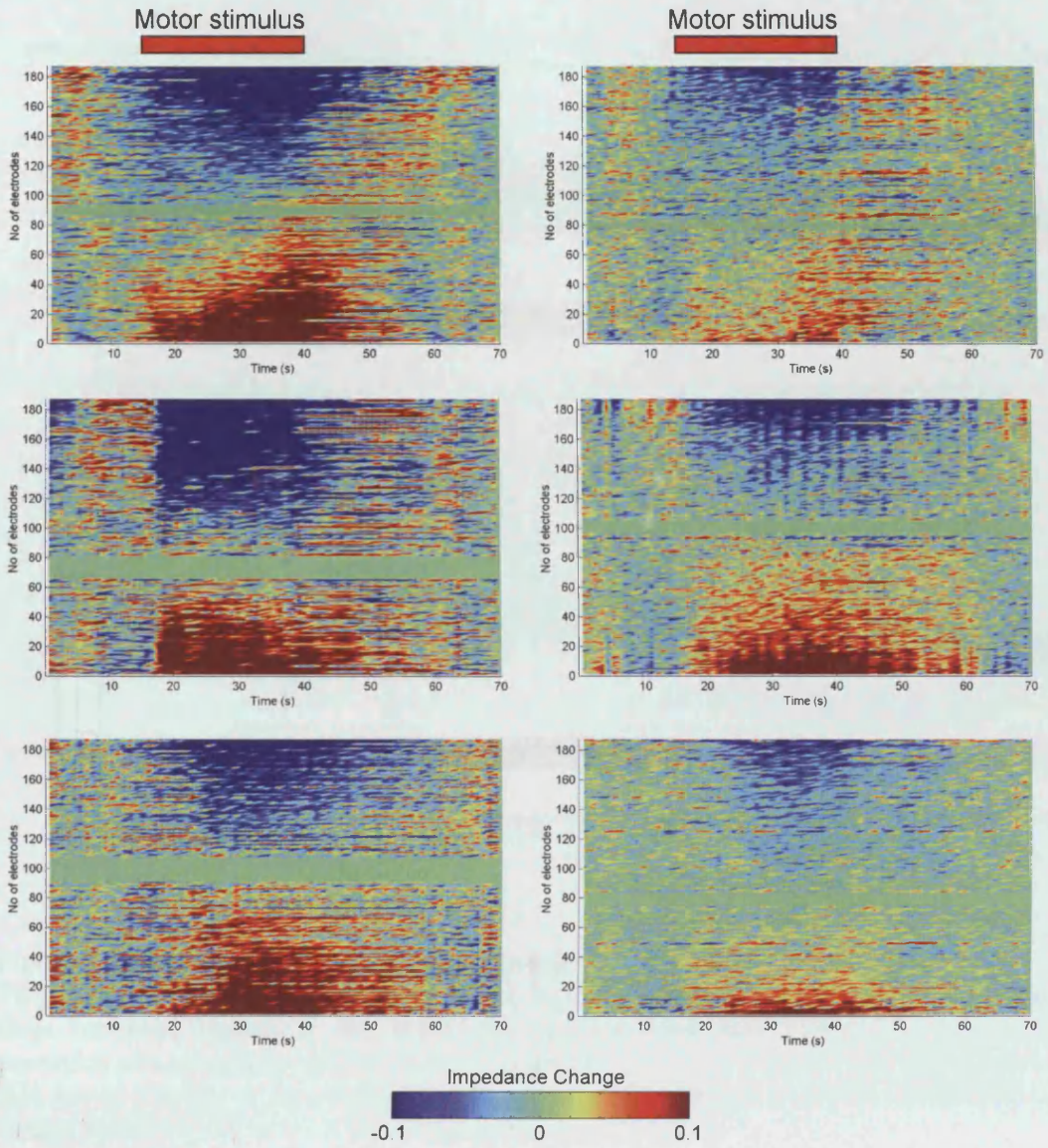

Figure 4.48 Surface plot of impedance data from motor stimulation

Noise corrected impedance data from 6 infants during motor stimulation of either hand. Each image represents an experiment with 10 repetitions of motor stimulation in one subject; if results were available from right or left hand stimulation in an infant, then only the larger changes are shown in this figure. For each experiment, the data at each electrode combination was averaged, after noise correction of the data, for repeated stimuli presentations, between 15-40s. The averaged impedance data for each electrode combination is displayed with time along the x-axis, and each electrode combination stacked on the y-axis, sorted by the size of the impedance change during stimulation. The green band in the middle represents the noise corrected data, set to zero. Each experiment is viewed at the same impedance scale with limits of ± 0.1% of the baseline impedance.

Each subject demonstrates reproducible impedance changes seen during the timecourse of the motor stimulation (indicated at the top of each column). Both impedance increases of up to 0.6% and decreases of up to –0.5% are measured in many of the electrode combinations. The timecourse of the changes are similar to that seen with fMRI, with a rise time of 3.9±0.3s after the onset of stimulation and a decay to baseline time of 7.0±0.5s after the cessation of stimulation.

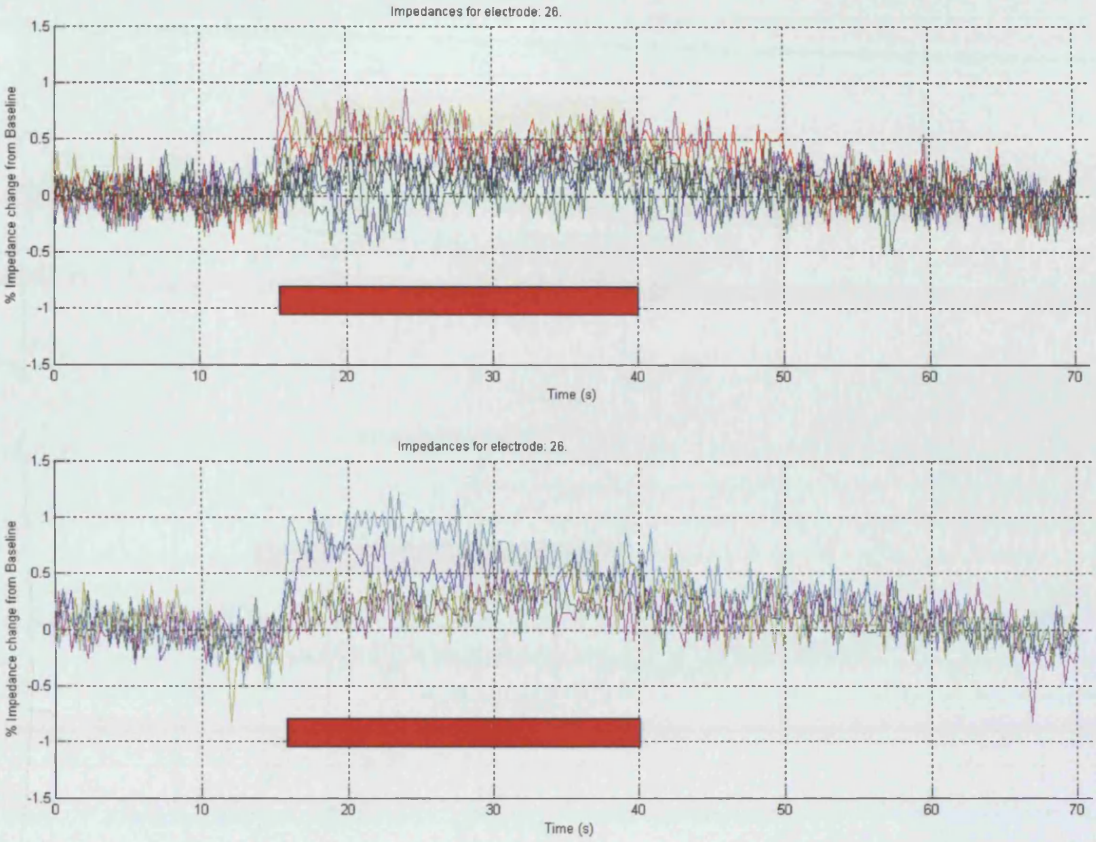

Figure 4.49 Impedance increases for Infant Ti
Two consecutive experiment runs are shown (first run top) with the timecourse of the baseline and noise corrected impedance data shown for identical electrode combinations; impedance data is expressed as a percentage change from the baseline impedance (y-axis). The timecourse of the 25s 8Hz visual stimulus is indicated by the red bar. Although noisy, a clearly reproducible impedance change following the timecourse of the visual stimulus is seen.

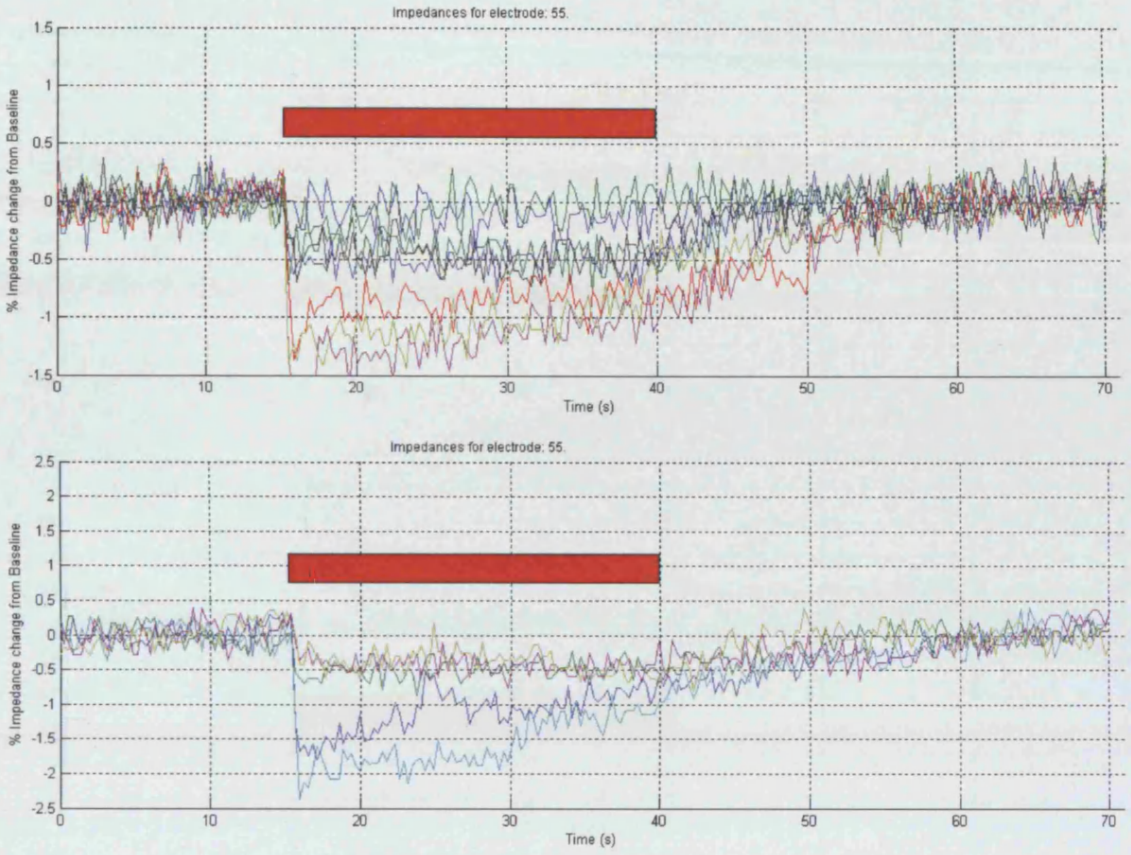

Figure 4.50 Impedance decreases for Infant Ti
Two consecutive experiment runs are shown (first run top) with the timecourse of the baseline and noise corrected impedance data shown for identical electrode combinations; impedance data is expressed as a percentage change from the baseline impedance (y-axis). The timecourse of the 25s 8Hz visual stimulus is indicated by the red bar. A clearly reproducible impedance decrease following the timecourse of the visual stimulus is seen, albeit with a fairly wide range in the magnitude of the response between different stimuli. In the bottom trace the stimuli in each run are clearly seen and correspond to a different colour: Stimulus 1 – dark blue, Stimulus 2 – green, Stimulus 4 – light blue, Stimulus 5 purple and Stimulus 6 – yellow (NB: Stimulus run 3 deleted due to noise). The variability is not clearly explained by habituation, but may indicate a variation in the size of the response to a variable state of arousal in the infant.

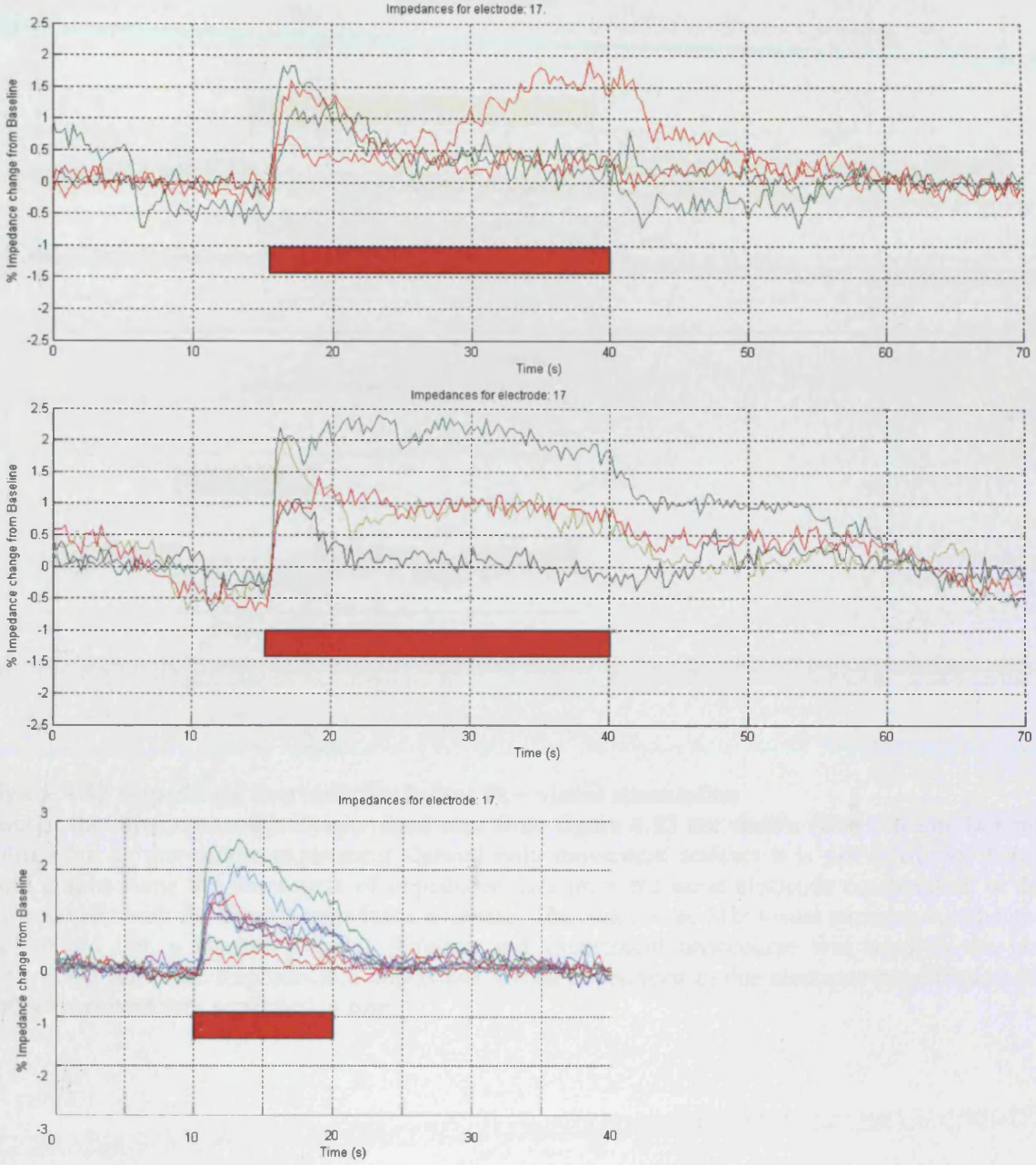

Figure 4.51 Impedance increases for Infant Fc – visual stimulation
Three consecutive experiment runs are shown (first run top) with the timecourse of the baseline and noise corrected impedance data shown for identical electrode combinations; impedance data is expressed as a percentage change from the baseline impedance (y-axis). The timecourse 8Hz visual stimulus is indicated by the red bar, a shorter stimulus duration and experiment timecourse was used in the third experiment (bottom). Reproducible impedance increases are seen in this electrode combination for all three experiment runs separated in time, indicating a strong reproducibility, and again (compared with infant Ti) clear variation in the magnitude of the responses are seen between successive stimuli.

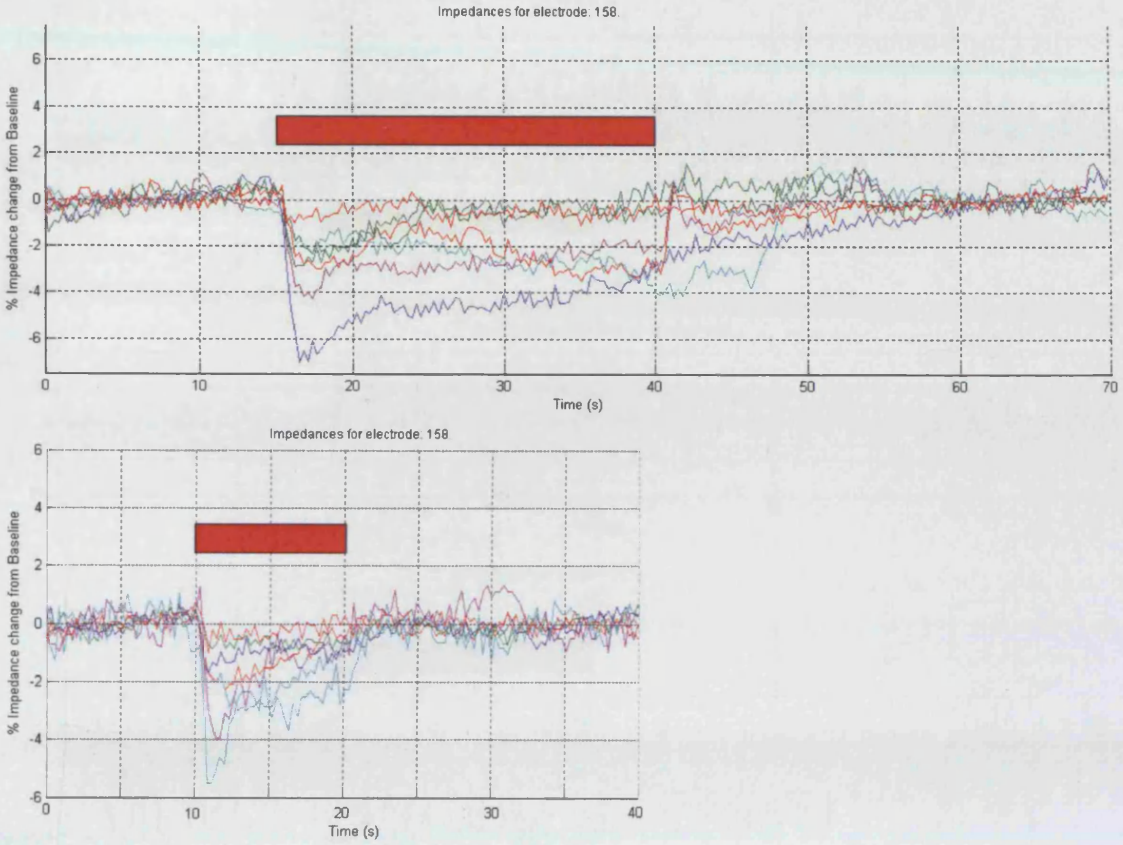

Figure 4.52 Impedance decreases for Infant Fc – visual stimulation
Two of the three consecutive experiment runs from figure 4.52 are shown (first run top, last run bottom but as the middle experiment showed only movement artefact it is not illustrated here). Both graphs show the timecourse of impedance data from the same electrode combination in the same subject with the biggest impedance decrease. The timecourse 8Hz visual stimulus is indicated by the red bar, a shorter stimulus duration and experiment timecourse was used in the last experiment (bottom). Reproducible impedance increases are seen in this electrode combination for both experiment runs separated in time.

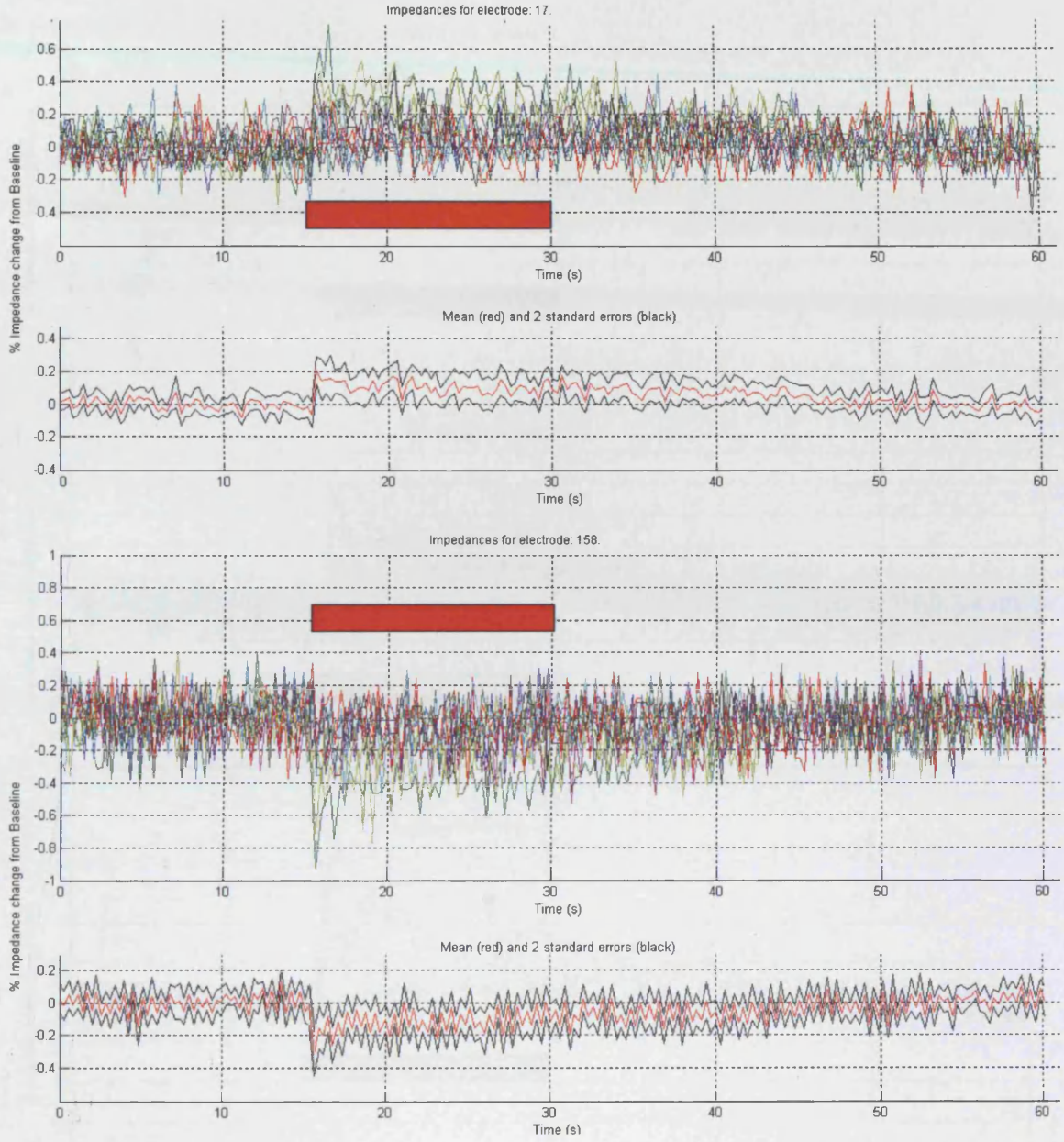

Figure 4.53 Largest impedance increase and decrease from Infant Mu – visual stimulation
In this subject, only one experiment run had data which was unaffected by movement artefact, so only the largest impedance increase and decrease from the one experiment run is shown (timecourse of the 8Hz visual stimulus indicated by the red bar), and as the size of the change is small in this infant, the mean and 2SE of the impedance change is shown below. Again reproducible impedance increases and decreases are visible that follow the timecourse of the visual stimulus.

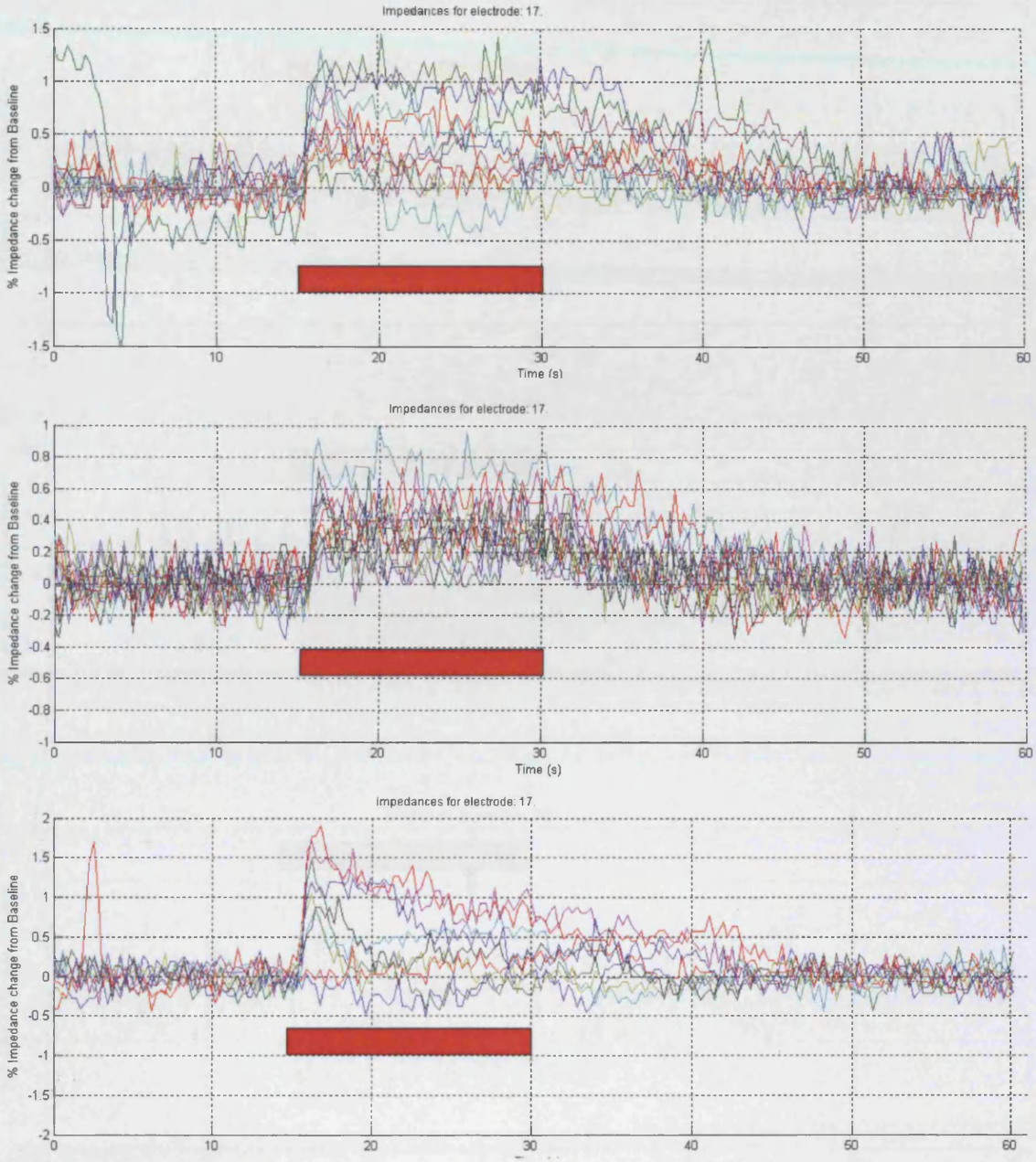

Figure 4.54 Impedance increases for Infant Co – Visual stimulation
The impedance changes at the same electrode combination showing the largest impedance increase are shown from three experiment runs, with the timecourse of visual stimulation indicated by the red bar. Top and middle graphs show the response to 8Hz visual stimulation, with the bottom graph showin the response to 2Hz visual stimulation. A reproducible increase in impedance is measured in all three experiments, although the plateau of the impedance response to 2Hz visual stimulation appears to be not as prolonged as that seen during 8Hz visual stimulation.

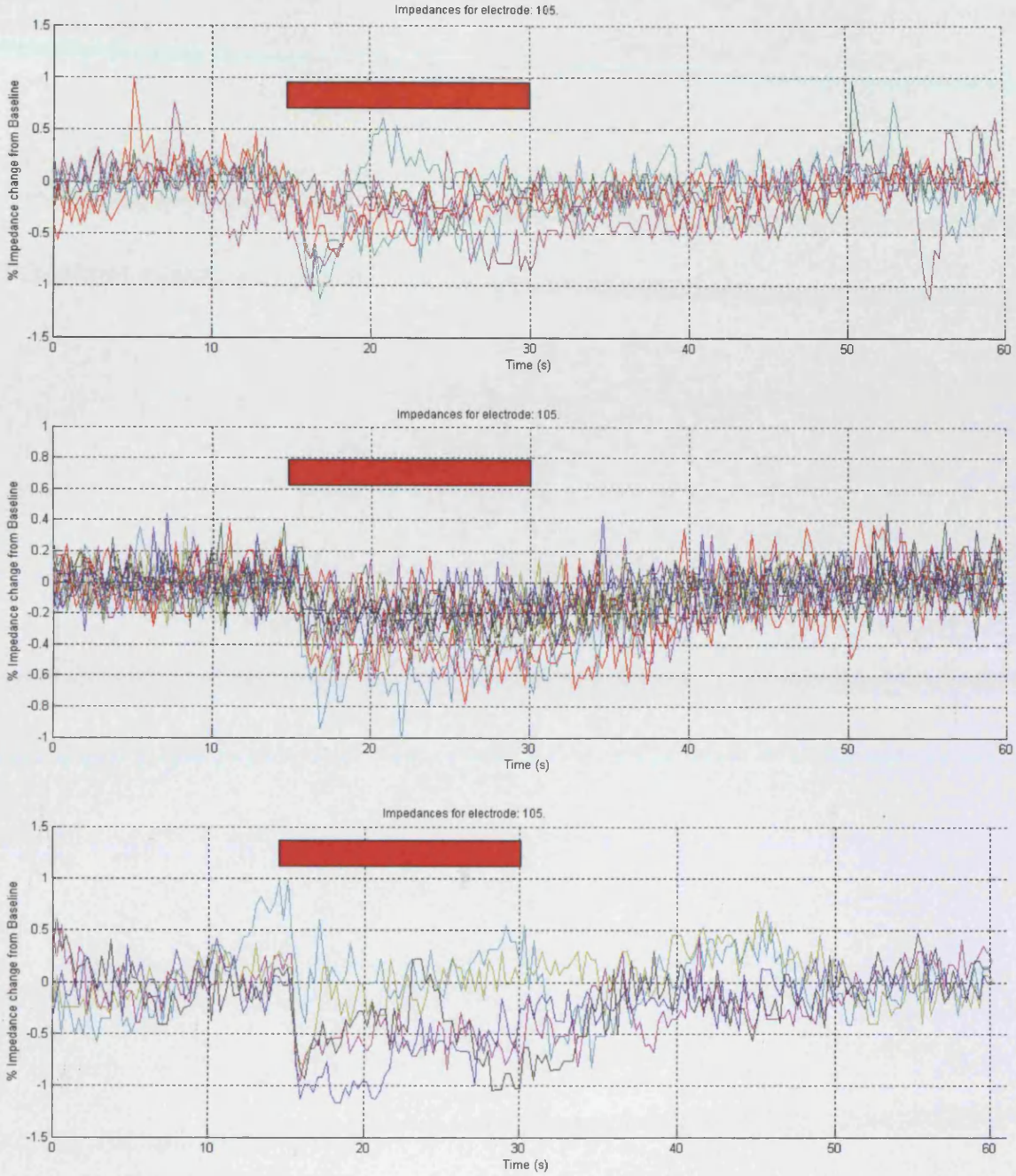

Figure 4.55 Impedance increases for Infant Co – Visual stimulation
The impedance response at the same electrode combination is shown for the largest impedance decrease, again from three experiment runs with top and middle graphs showing the response to 8Hz visual stimulation, and the bottom graph the response to 2Hz visual stimulation. A reproducible decrease is measured in most of the runs of all three experiments.

Image data

4.3.1.6 Effect of SVD value on visual images

Visual images (Figure 4.56) demonstrated that the predominant impedance change(s) were consistent between singular values, within each experiment. However, with increasing singular value, high frequency spatial noise was introduced in the images, particularly around the perimeter. In addition the use of 60 singular values in three of the subjects (Ti, Fc and Co) introduced an impedance increase near the centre of the images.

4.3.1.7 Effect of median filter on visual images

The median filter reduced the spatial noise in the images, particularly by reduction of high spatial frequency noise at the image edges (Figure 4.56). The main impedance changes in the images were preserved when the filtered and unfiltered images were compared side by side. These findings were similar to that found with an identical filter used in EIT data obtained from a marrow/head-tank simulation of the human head (Tidswell *et al.* 2003).

These results indicated that reconstruction with an inverted sensitivity matrix truncated at 40 singular values and then filtered with a 9 pixel width median filter led to preservation of the dominant impedance changes and reduction in spatial noise. Therefore images reconstructed and filtered in this manner were used for the subsequent image analysis of both the visual and motor neonatal images.

4.3.1.8 Image analysis

Visual Stimulation

Four sets of images were reconstructed from the 4 neonates (Figure 4.58). All of these had stimulation related impedance changes. Three of the subjects had small impedance decreases present over the region corresponding to the area of the visual cortex. In all 4 subjects a larger impedance decrease was seen over the area of the frontal cortex.

When the images obtained during visual stimulation in all 4 neonates were averaged, a total of 48 stimuli, (Figure 4.57) and thresholded to show changes significantly different from baseline at $p<0.05$, several changes were seen which were temporally associated with the visual stimulus. The largest magnitude change was an impedance decrease over the frontal area, a large area decrease was present in the right lateral side of the images, and a significant impedance decrease present over the area of the visual cortex.

Motor Stimulation

In all, eleven sets of images were reconstructed from the 6 neonates (Figure 4.60 to Figure 4.65). Of these, five neonates had images of both right and left handed stimulation and one neonate had images for right handed stimulation only (due to excess noise and movement during the left hand experiment). 8/11 of these images demonstrated impedance changes with the same timecourse as the stimulation. Of the 8 stimulus related impedance changes 6 had impedance changes in the contralateral quadrant to the hand stimulated and were considered to be correctly localised; of these three were impedance increases and three impedance decreases.

Group average images of either right or left hand stimulation were also analysed. These consisted an average of all stimuli and all subjects for either left or right hand stimulation paradigms (Figure 4.59). Both sets of images demonstrated lateralised changes. Left sided stimulation produced an inferior impedance increase and a superior impedance decrease over the contralateral cortex. The superior impedance decrease was more closely related with the area of the right motor cortex. In addition an impedance decrease was seen in the inferior image slices on the left. The averaged images of right hand stimulation produced two changes: a small posterior impedance decrease over the approximate region of the visual cortex and a larger impedance decrease in the contralateral side of the image to stimulation, over the region of the left sensorimotor cortex.

Qualitatively, the images were noisy with multiple stimulus related impedance changes. Frequently, no single impedance change stood out from the images. Additionally, the visual and motor images had a different symmetry, with a front-back symmetry for visual and right-left asymmetry for motor images.

Table 4.14 Summary of stimulus related changes in the neonatal EIT images

	Images with change during stimulus	Change over expected area
Visual (n=4)	4	3 (3 decreases)
Motor Left (n=5)	2	2 (1 decrease)
Motor Right (n=6)	6	4 (2 decreases)
Total (n=15)	12	9 (6 decreases)

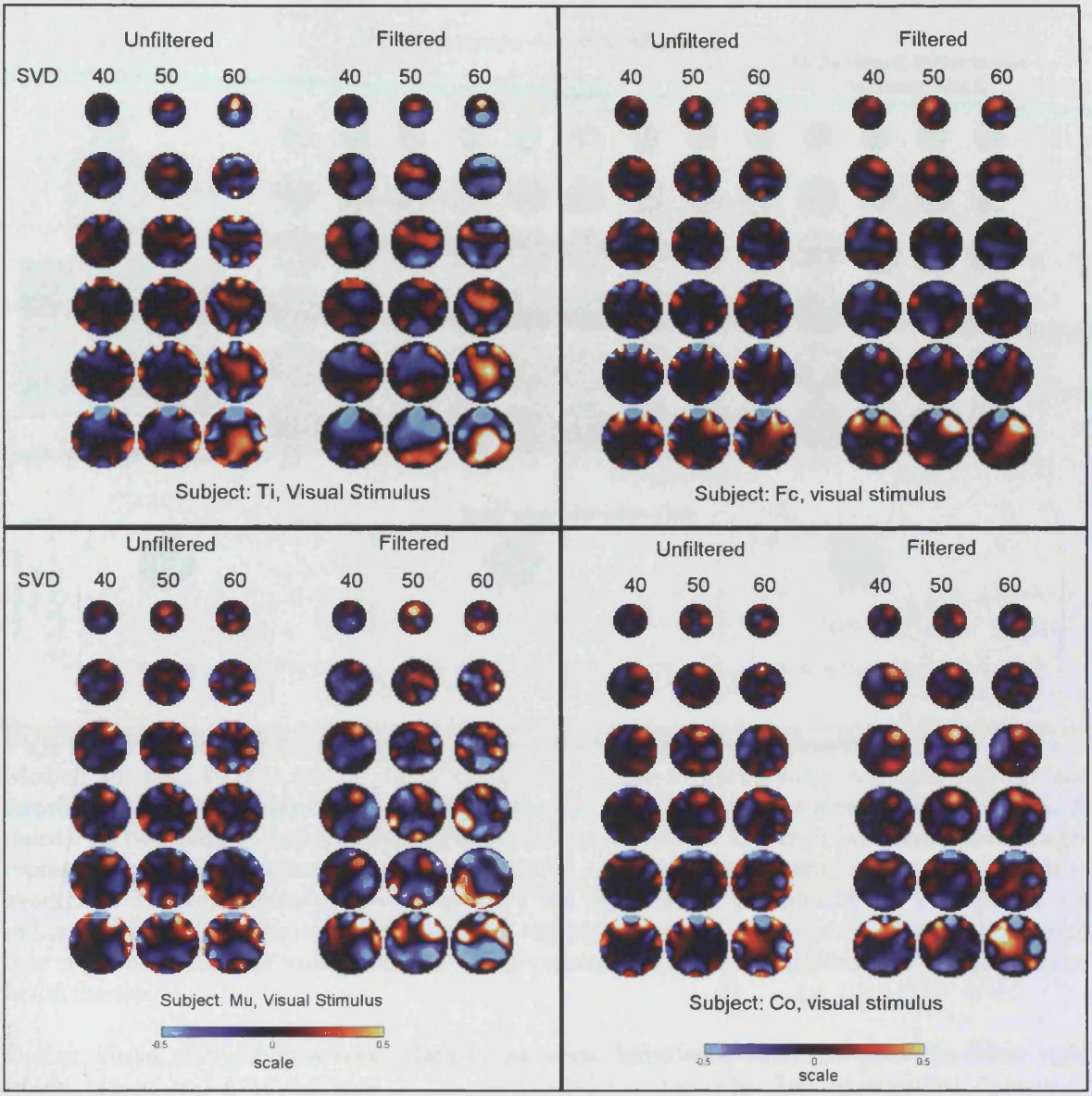

Figure 4.56 Effect of SVD value and Median filter on the reconstructed images.
Each box contains images acquired from each subject during visual stimulation. In each box there are 6 images: the 3 images on the left demonstrates the effect on the images of the singular value used to truncate the inversion of the sensitivity matrix. The 3 images on the right represent the same images filtered with a 2-dimensional median filter of width 9 pixels, in an attempt to reduce spatial noise.

From a qualitative assessment of the images, the effect of increasing SVD values increases the spatial noise in the images, but in general the main features of the images are preserved particularly the impedance decreases at the front of all the images. The effect of the median filter also preserves the main feature of the image, whilst reducing spatial noise. Therefore the images used for analysis of the EIT data were those with the least spatial noise: i.e. images produced with a singular value level of 40 and images which were median filtered.

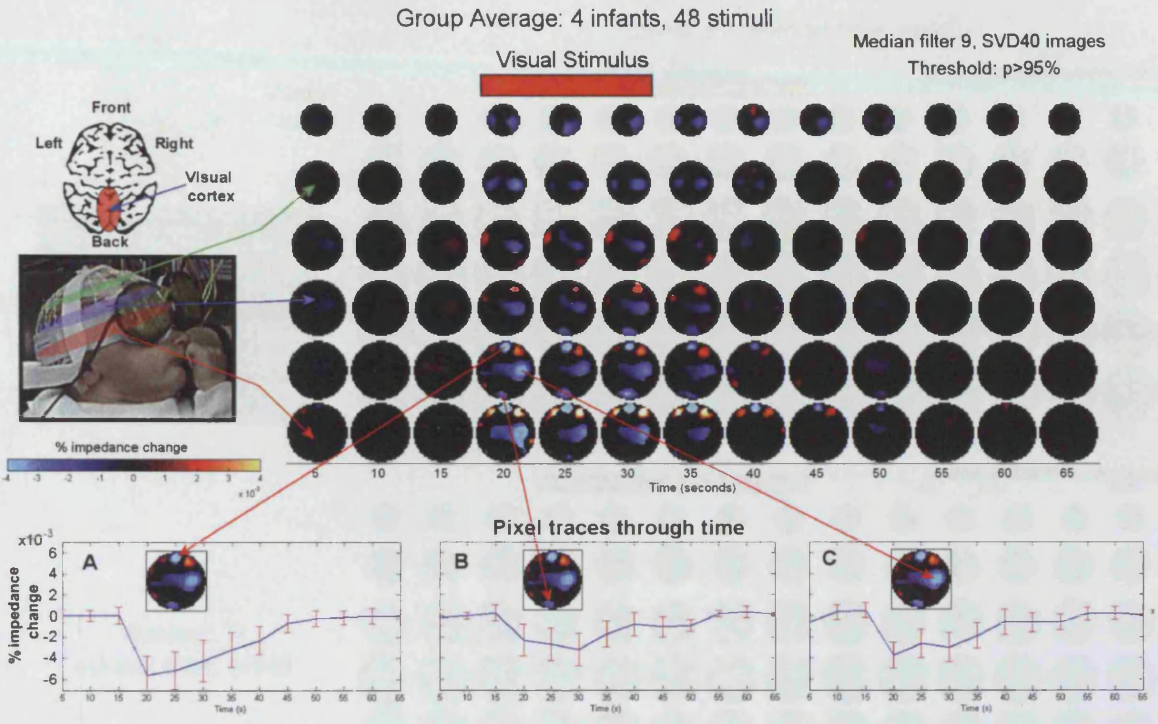

Figure 4.57 Visual EIT Images, group average of 48 stimuli from 4 neonates.
Median filtered, SVD40 images from 48 stimuli in four neonates were averaged together and thresholded to demonstrate changes which were more than 2SE from the mean (p value of 95%, 2-tailed). As two subjects had stimulation periods of 25s and two of 15s, then two consecutive images representing 10s stimulation were removed from the neonates with 25s stimulation periods prior to averaging. The orientation of the images and the approximate position of the slice planes are indicated by the diagrams on the left. Each column represents the image for averaged data acquired over a period of 5s. The visual stimulus was presented between 15-30s, illustrated by the stimulus bar at the top.

During visual stimulation several changes are seen: impedance decreases over the front, right lateral region and over the area of the visual cortex posteriorly. The symmetrical impedance decreases either side of the impedance change at the front are probably artefactual as a result of the large impedance decrease between them.

The timecourse of the three significant impedance decreases are shown: A - anterior change, B- posterior change and C - right lateral change.

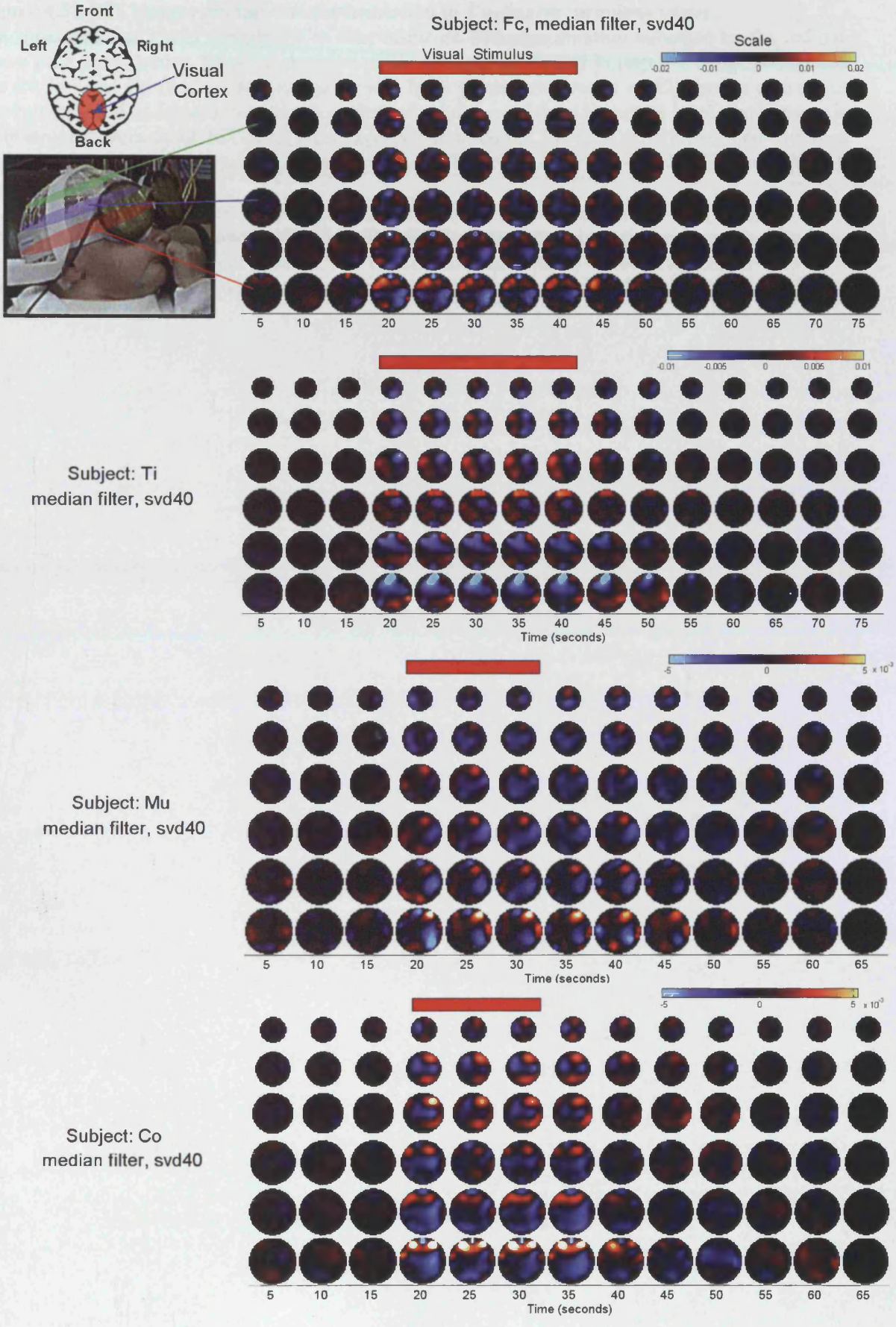
Front
Left
Right
Visual
Cortex
Back
Subject: Fc, median filter, svd40
Visual Stimulus
Scale
-0.02 -0.01 0 0.01 0.02
5 10 15 20 25 30 35 40 45 50 55 60 65 70 75
-0.01 -0.005 0 0.005 0.01
Subject: Ti
median filter, svd40
5 10 15 20 25 30 35 40 45 50 55 60 65 70 75
Time (seconds)
-5 0 5 x 10^-3
Subject: Mu
median filter, svd40
5 10 15 20 25 30 35 40 45 50 55 60 65
Time (seconds)
-5 0 5 x 10^-3
Subject: Co
median filter, svd40
5 10 15 20 25 30 35 40 45 50 55 60 65
Time (seconds)

Figure 4.58 EIT images during visual stimulation in 4 neonates (previous page)
EIT time-series of visual stimulation in four neonates. Stimulus duration indicated by the red bar above each image series. Stimulus duration of 25s for subjects Fc and Ti (top two image series) and 15s for Mu and Co (bottom two image series). Each column represents an EIT image of 6 slices through the head, indicated by diagram on the left, and viewed from above the head. Each image is reconstructed from 5s of EIT data, the images median filtered for each experiment then averaged for repetitions of the stimulus in each subject. The images are un-thresholded to show all impedance changes.

Although the images are noisy, impedance changes are seen that occur with the same timecourse as the visual stimulus. All four subjects demonstrated an impedance decrease at the front of the head. Three subjects, Fc, Ti and Co, had stimulus related impedance changes over the region of the visual cortex, which remained after thresholding at the $p<0.05$ level (thresholded images not shown).

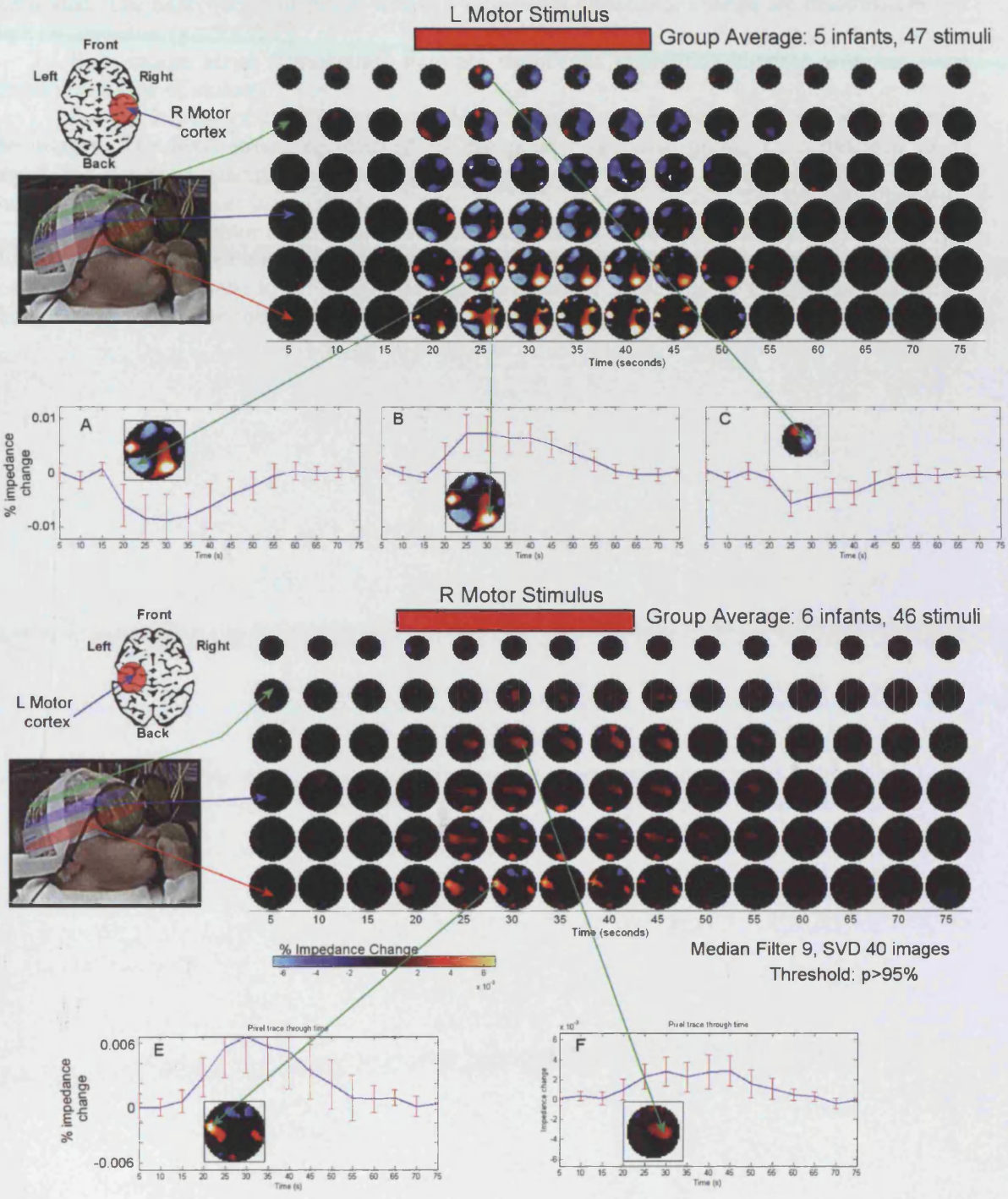

Figure 4.59 Group average images for Left and Right motor stimulation
EIT images from left (Top) or right (Bottom) motor paradigms were averaged from all infants. The timecourse of the stimuli, between 15-40s, is indicated at the top of each set of images. The images were thresholded after averaging to display only those pixels which significantly differed from baseline. The images on the left help to spatially orient the images, and demonstrate the approximate area of the expected impedance change in contralateral motor cortex to the hand

stimulated. The timecourses of pixels within a significant impedance change are illustrated below each image series (graphs A-F).

Both image series demonstrate multiple significant impedance changes with the same timecourse as the stimulus.

For the left motor experiments, impedance changes are seen in the left and right sides of the images. The pixel group represented by the pixel timecourse graph, C, correspond to an impedance decrease near to the area of the right motor cortex. This change is smaller than the changes seen in the lower image slices.

For the right motor experiments, two main significant impedance changes are seen. However, the impedance increase on the left, although on the same side as the contralateral motor cortex, is positioned in the lower image slices and is therefore too low in the head to account for a change in the left motor cortex.

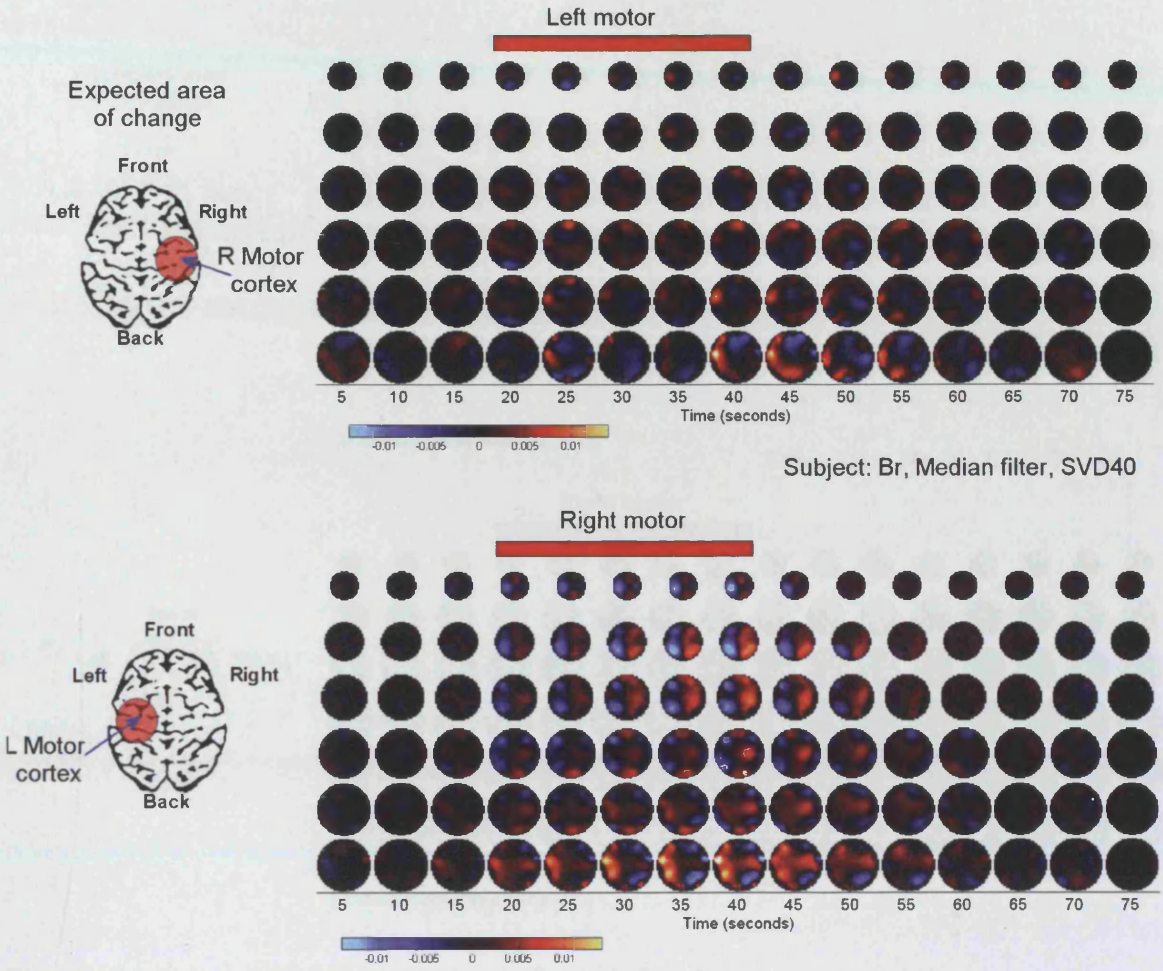

Figure 4.60 Left and Right motor stimulation in infant Br
Time-series of EIT images in subject Br, orientated as the average motor images (Figure 4.59). Left hand moved (top) and right hand moved (bottom).

Top image series, left hand stimulation - no stimulus related impedance changes are imaged.

Bottom image series, right hand stimulation - several stimulus related impedance changes are present. Of these, only the impedance decrease in the upper 3 rows are near the region of the left motor cortex.

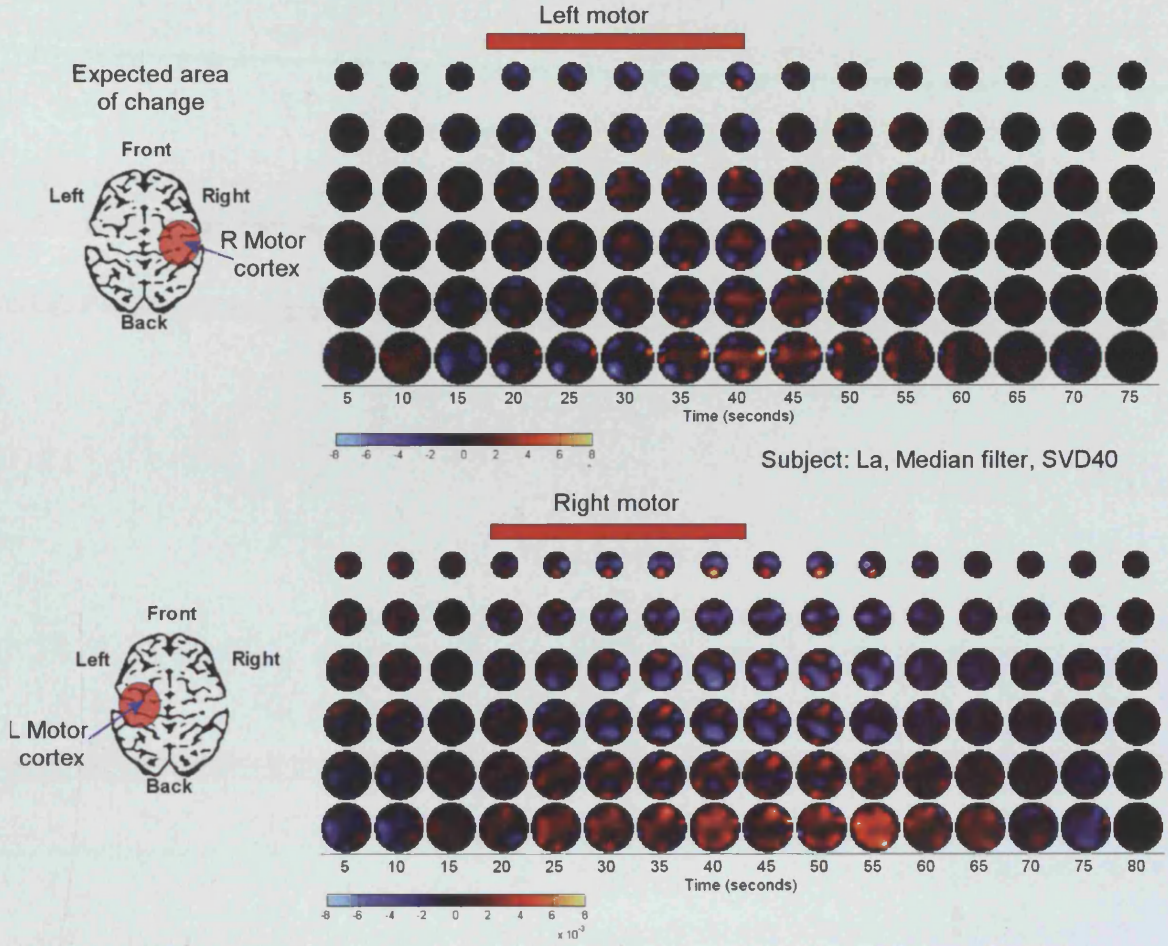

Figure 4.61 Left and Right motor stimulation in infant La
Time-series of EIT images in infant La. The period of left and right hand stimulation is indicated by the stimulus bars at the top of each set of images. These images demonstrate:

Top image series, left hand stimulation – no stimulus related impedance changes

Bottom image series, right hand stimulation – an impedance decrease is seen posteriorly in 3rd-4th rows of image slices. This is not in the region of cortex expected to be stimulated by movement of the right hand.

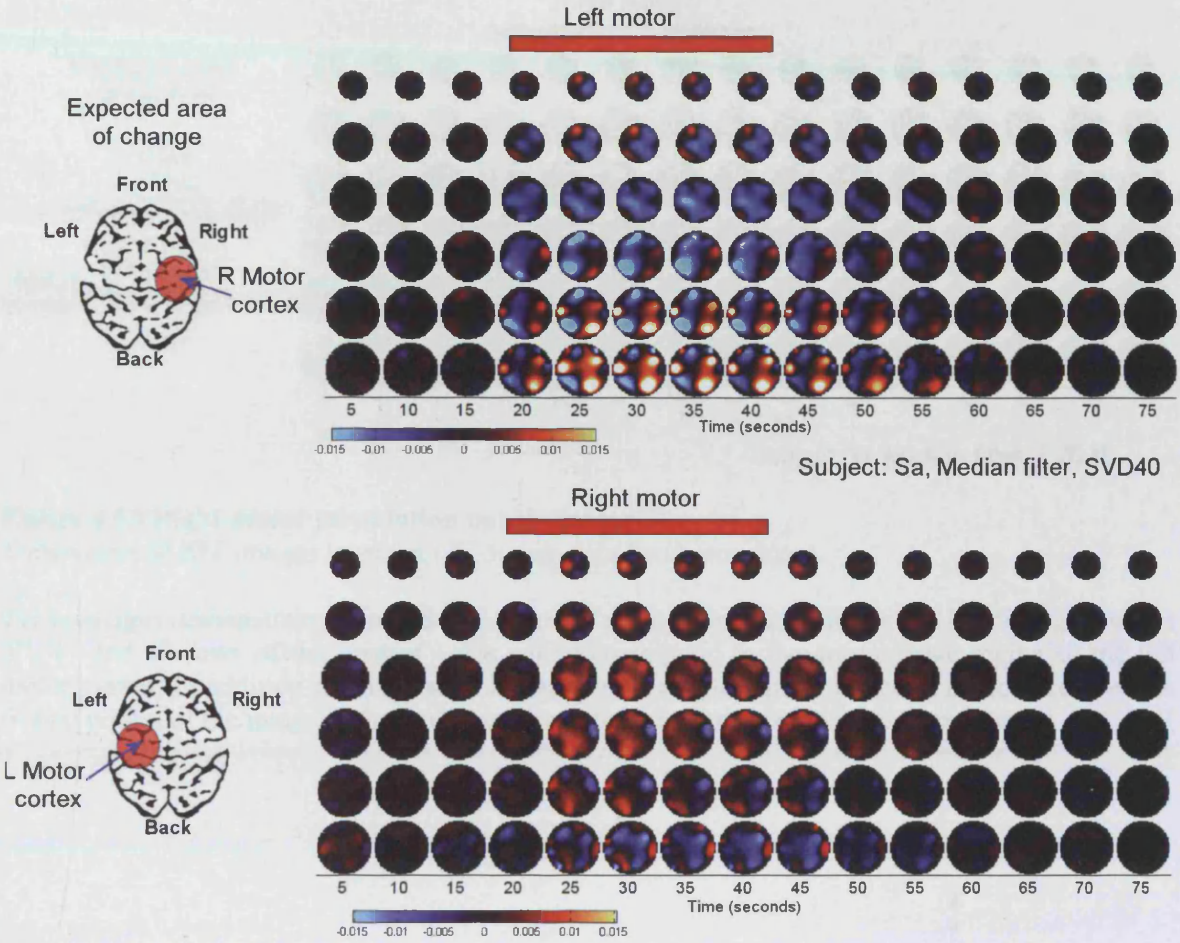

Figure 4.62 Left and Right motor stimulation in infant Sa
Time-series of EIT images in subject Sa. These images demonstrate:

Top, left hand stimulation – multiple impedance related changes are imaged. In the bottom 3 rows of images: an increase in the right side of the images (which is too low for the right motor cortex) a decrease in the left side of the images. In the top two rows there is a smaller impedance decrease in the approximate region of the right motor cortex.

Bottom, right hand stimulation –An impedance increase is imaged on the left side, in the top 3 rows of images, which would correspond to the region of the left motor cortex; these changes are correctly localised. An impedance decrease is imaged on the right side of the lower 3 rows of image slices.

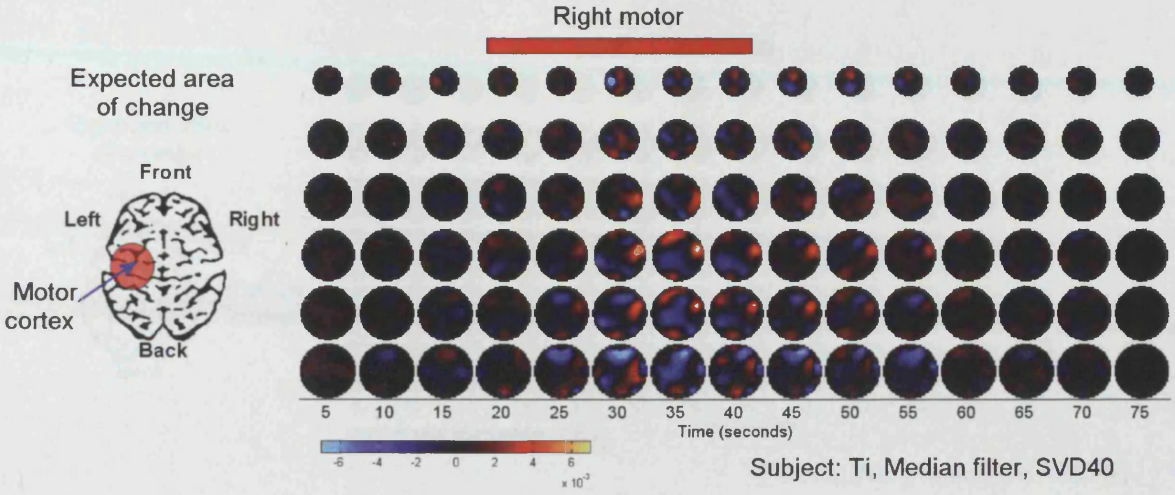

Figure 4.63 Right motor stimulation only in infant Ti
Time-series of EIT images in subject Ti during right hand movement.

These images demonstrate an impedance decrease during stimulation in the left lateral region of the 3rd, 4th and 5th rows of the images - this would correspond to the approximate region of the left motor cortex. In addition an impedance increase on the right and an impedance decrease over the frontal region of the images can also been seen with a similar timecourse to stimulation.

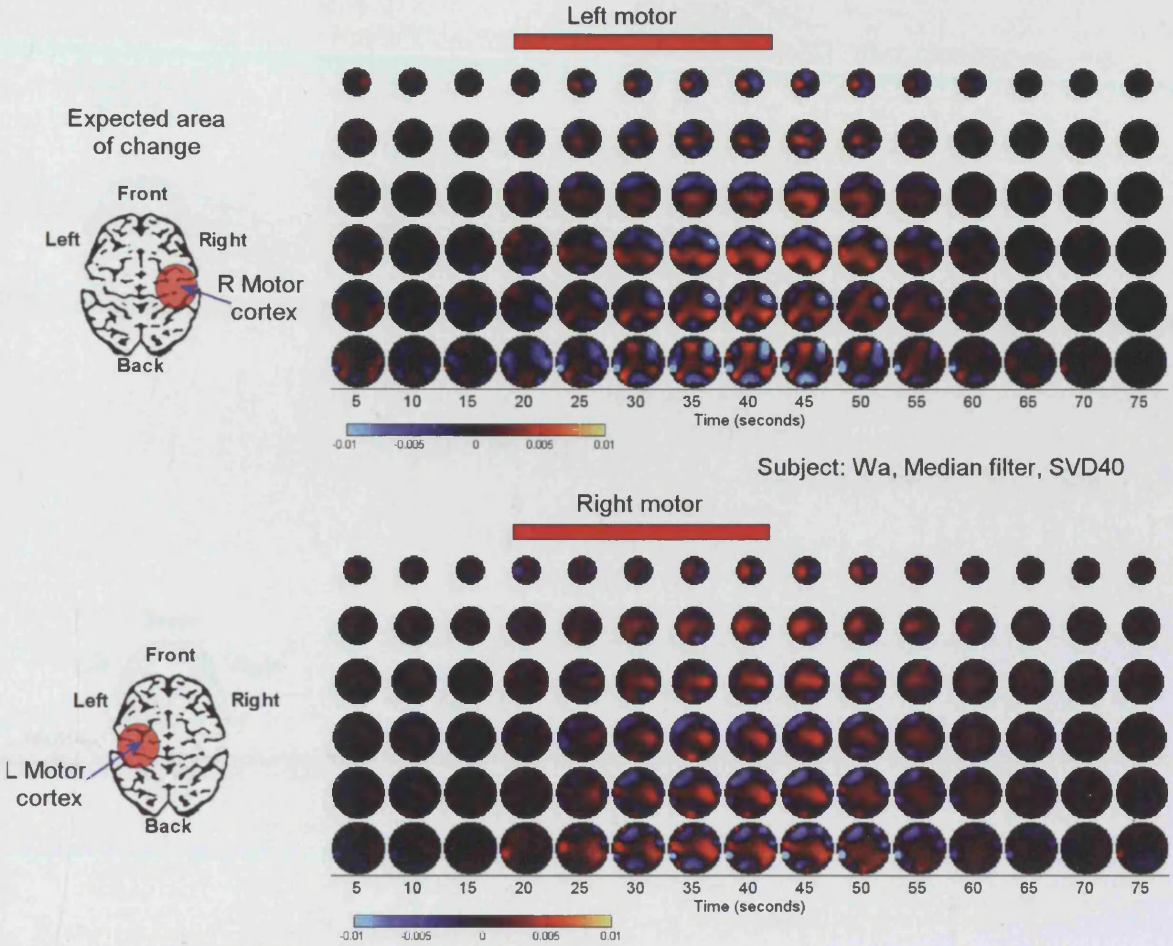

Figure 4.64 Left and Right motor stimulation in infant Wa
Time-series of EIT images in subject Wa. These images demonstrate:

Top, left hand stimulation – multiple stimulus related impedance changes are present: an impedance increase on the right side of the images which corresponds to the right motor cortex. A similarly sized impedance decrease is seen in the left side of the images.

Bottom, right hand stimulation – the predominant change is of an impedance increase in the right side of the images. In addition a smaller impedance decrease is present in the left lateral-frontal areas of the images, particularly in the 4th and 5th rows of the images, which are too anterior to lie within the left motor cortex. .

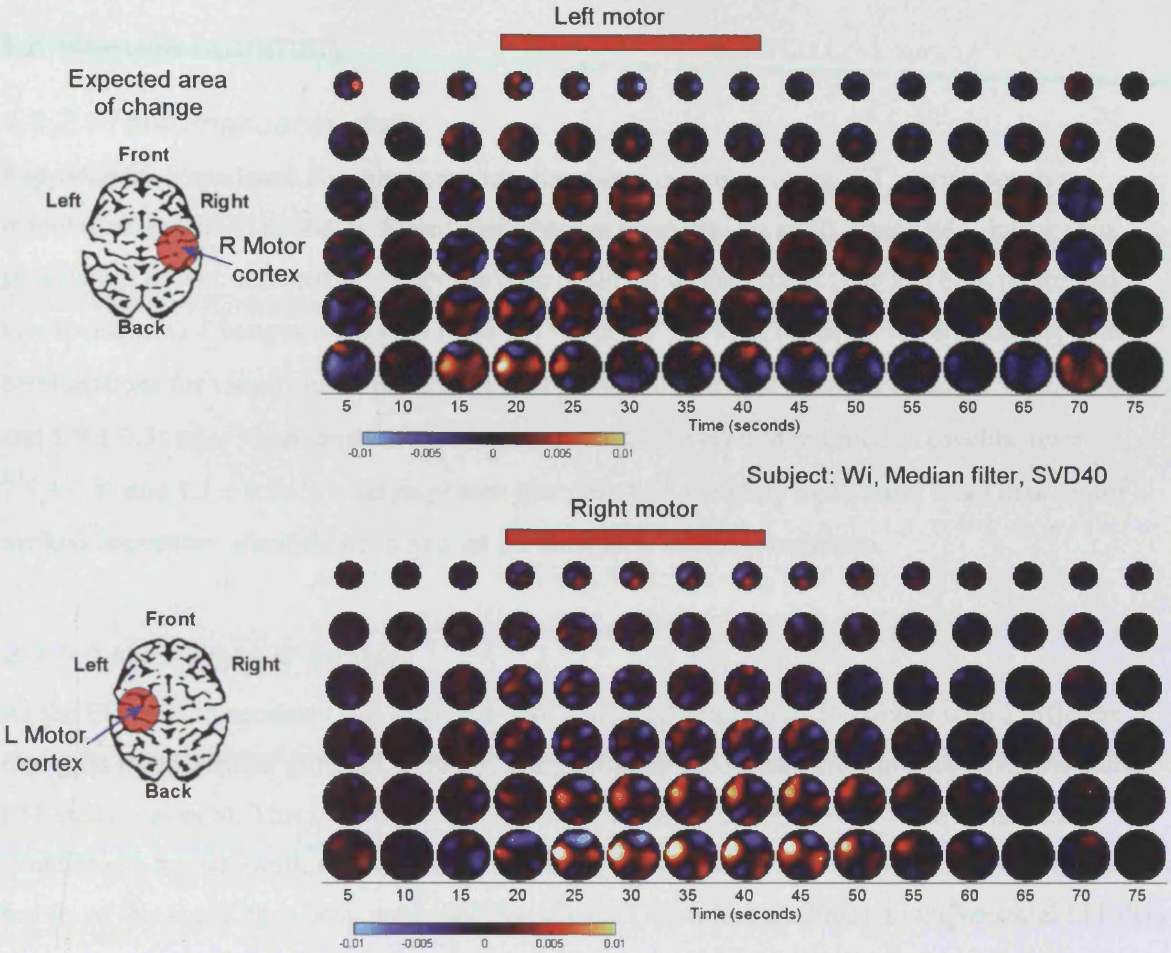

Figure 4.65 Left and Right motor stimulation in infant Wi
Time-series of EIT images in subject Wi These images demonstrate:

Top, left hand stimulation – noisy images. No stimulus related change.

Bottom, right hand stimulation – a stimulus related impedance increase is present in the left lateral-area of the images, particularly in the 4th, 5th and 6th image rows. These changes are correctly localised to the region of the left motor cortex. In addition a smaller impedance decrease is seen in the frontal area of the images.

4.3.2 Results summary

4.3.2.1 Raw impedance data

Reproducible impedance changes in the raw data were recorded, using EIT, during sensory stimulation in human neonates. Significant changes were present in all 9 neonates, during visual stimulation in four and passive motor movements in six of the infants (one had both motor and visual changes). Changes were seen in 38 ± 4 % and 39 ± 5 % of the scalp impedance electrode combinations for visual and motor experiments, respectively. The changes commenced 0.6 ± 0.1s and 1.9 ± 0.3s after visual and motor stimulation, respectively and returned to baseline over 7.5 ± 0.8s and 7.1 ± 0.5s. Visual responses therefore had a slightly more rapid onset than motor evoked impedance changes, but a similar duration after stimulus cessation.

4.3.2.2 Neonatal EIT images

As the EIT data in neonates was obtained with a reduced head set of electrodes with a different electrode measurement protocol, then a slightly different reconstruction algorithm than the adult EIT study was used. This has been calibrated in data acquired from a realistic head-phantom containing a human skull, with marrow (vegetable skin) used to simulate the properties of skin. The results of this study have been published elsewhere (Tidswell *et al.* 2003). In the neonatal EIT data the images were reconstructed with this algorithm, truncated at 40 singular values, with the resultant images median filtered to reduce spatial noise. Stimulus related impedance changes were seen in 4/4 visual and 8/11 motor experiments, however these images were noisy and generally had more than one stimulus related impedance change. Of those multiple changes, a stimulus related impedance change was seen over the area of the visual cortex in 3 subjects and over the area of the contralateral motor cortex to the hand stimulated in 6 motor experiments. Thresholded averages of all the images demonstrated contralateral impedance increases to the hand stimulated, and for the visual experiments a significant impedance decrease over the area of the visual cortex. Again multiple, stimulus related impedance changes were seen even after thresholding.

4.4 Discussion

4.4.1 Overview of results

This is the first demonstration that impedance changes can be reliably and reproducibly measured in neonates during visual or motor activity. Although these changes were clearly reproducible in the raw impedance data, the images were disappointing, as the images failed to demonstrate a clear, localised impedance change to the area of cortex expected to demonstrate an impedance change in response to the stimuli. In a similar manner to the adult EIT images, some of the impedance changes did co-localise to these areas, but as the changes were not unique in the images, such co-localisation may have arisen by chance, rather than as a result of the EIT system to accurately image an impedance change in either the visual or motor cortex.

In the sections that follow I will discuss: 1) The evidence supporting neonatal cortical impedance changes, with regard to their probable mechanism and consideration of possible confounding artefacts, 2) The time course of the neonatal impedance responses to stimulation with respect to both adult EIT changes and other neonatal functional imaging modalities, and 3) The technical problems associated with the neonatal EIT images such as poor localisation, and the level of image noise which required filtering and optimisation of the truncation threshold for the neonatal reconstruction algorithm.

4.4.2 Impedance changes

4.4.2.1 Are neonatal impedance changes physiological or artefact?

Possible sources of artefact

The most likely source of artefact in EIT data is from movement. If this was to be responsible for the impedance changes, which have a timecourse that is related to the duration of the stimulus, then likely movement artefact would arise from head movement in response to the stimuli, eye movement, eye blinking or muscle activity from the forehead or scalp.

Close observation of the neonates during the studies did not identify perceptible changes in head movement during the majority of the stimuli; where such movement was observed, artefact was present in the raw impedance data and eliminated under the pre-determined noise elimination criteria (Section 4.2.5.2). Other smaller movements of the forehead or scalp during visual or motor stimulation were also not observed, although blinking underneath the LED goggles remains a possibility as this would have been obscured.

If movement artefact had been present, then the likely time points at which it would have occurred is during the onset or offset of stimulation. In addition, artefact would be expected to be increased during visual stimulation, as neonates have a tendency to react to bright light by blinking, brow furrowing and head movement away from the light source. These expectations were not present in the raw data: 1) Visual and motor responses produced a similar sized signal, 2) The timecourse of both motor and visual stimulus related impedance changes demonstrated a gradual return to baseline impedance after stimulus cessation, whereas the return to baseline from movement artefact would have been expected to be more rapid after stimulus cessation, 3) Impedance responses returned to baseline after stimulus cessation: this is unexpected from movement artefact as movement changes electrode impedance by causing small shifts in electrode which do not subsequently return to baseline, and 4) The timecourse of the impedance responses were similar between experiments in the same neonate, and also between neonates – this pattern would be unexpected from movement artefact which would be expected to show a wider variation between subjects and also habituation between consecutive stimuli in the same subject.

Evidence for physiological impedance changes

The stimulus related timecourse of the impedance changes is strong evidence for a physiological mechanism of impedance change in the neonatal brain. These responses demonstrated a slight delay in onset, peaked within a few seconds of stimulus onset, and showed a decay to baseline impedance after stimulus cessation. In addition there were similarities in the timecourse of the respective visual and motor responses in the neonates tested, with differences in the timecourses of the visual and motor responses when compared to each other. This is again supportive of a common physiological mechanism between different neonates, although why there was a faster onset of the visually evoked impedance changes compared to motor evoked responses needs to be considered.

The probable reason this delay in the motor responses, which commenced 1.9 ± 0.3s after motor stimulation compared to 0.6 ± 0.1s after visual stimulation, may arise from two mechanisms: 1) The onset of visual stimulation was immediate (triggered by the computer) whereas a reaction time delay (with an estimated maximum latency of 1.0s) was present in the onset of the motor stimulus (the time between the presentation of a prompt on the computer to the time taken to initiate the hand movement) and 2) A possible slower build up the physiological impedance change in the somatosensory/motor cortex than in the visual cortex.

Conclusion

After consideration of possible artefacts, and consideration of the impedance timecourse and similarity between neonates, the most likely mechanism of the impedance changes measured in this study is that of a physiological impedance change. The likely physiological origin of these changes is considered in the next section.

4.4.2.2 Likely origin of neonatal impedance changes

Possible source of impedance changes in the scalp

Stimulus related changes in scalp impedance were not ruled out in the neonatal studies as they were in adults (Chapter 2). Ideally, neonatal scalp impedance should have been measured, however this would have necessitated an extended 3-4 hour experiment which I considered unacceptable to the infant. However, the neonatal impedance responses are similar to the adult responses, and as adult scalp impedance was measured and did not change during stimulation, it is therefore unlikely that changes in scalp impedance were responsible for the impedance changes in the neonatal studies.

Evidence for the origin of impedance changes within the brain

The delayed timecourse of the neonatal impedance responses, in relation to stimulus onset and cessation, is similar to the timecourse of changes in regional cerebral blood volume (rCBV), measured with Near Infra-Red studies (Meek *et al.* 1998; Hintz *et al.* 2001), however the onset of these changes are faster than the changes of regional cerebral blood flow (rCBF) measured with fMRI studies (Yamada *et al.* 1997; Born *et al.* 1998; Martin *et al.* 1999; Martin *et al.* 2000; Yamada *et al.* 2000; Born *et al.* 2002). Both types of study have used similar motor and visual stimulation paradigms to those used in the neonatal EIT studies. Support for the hypothesis that impedance changes are a result of changes in rCBV, as a result of increased neuronal activity are now considered.

Evidence for increased neural activity during stimulation

The support for increased electrical activity in the neonatal brain in response to somatosensory and visual stimulation, is provided by studies which have examined the development of the evoked response in neonates. Visual evoked potentials have been recorded over the occipital cortex in infants from 32 weeks gestation to either flash stimuli, similar to the visual stimulus in this neonatal EIT study (Hrbek and Mares 1963; Hrbek *et al.* 1972) or using patterned stimuli, such as checkerboards (Sokol 1978; Harding *et al.* 1989). Somatosensory evoked potentials have also been

recorded in neonates, using measurement electrodes over the contralateral somatosensory cortex to record potentials produced by stimulating the peripheral nerves of the arm or leg (Hrbek *et al.* 1968; Desmedt and Mai 1970; Hrbek *et al.* 1972). The passive motor paradigm used in this study should also stimulate a similar contralateral somatosensory area; evidence that supports this is derived from an fMRI study in adults that compared the passive motor response of the fingers to electrical nerve stimulation of the median nerve at the wrist (Holloway 2000); similar areas of activation were produced by both the passive motor and electrical stimulation paradigms.

From this evidence, the stimuli in the neonatal study would be expected to increase neural activity in the visual and contralateral somatosensory cortex, for visual and passive motor stimuli, respectively. An impedance change would be expected in these areas, if blood volume changes occurred in these areas as a result of this activity.

Evidence for vascular changes during stimulation

Evidence for the neonatal cortical vascular response to stimuli is provided by neonatal functional imaging studies, using either fMRI, PET or NIRS. Some of this evidence has been discussed in Chapter 1, and in this Chapter in Section 4.1.2 in the context of the choice of stimulus paradigms for use in this study.

Briefly, evidence from neonatal fMRI studies, has demonstrated that negative BOLD responses generally occur in response to visual (Yamada *et al.* 1997; Born *et al.* 1998; Martin *et al.* 1999; Martin *et al.* 2000; Yamada *et al.* 2000; Born *et al.* 2002) or auditory stimuli (Anderson *et al.* 2001). However positive BOLD responses have been detected in unsedated infants in response to speech (Dehaene-Lambertz *et al.* 2002), and in sedated infants in response to 2 Hz visual flash stimuli and passive motor stimulation of the hands (Erberich *et al.* 2003). The only PET neonatal functional imaging study (to my knowledge) also supports the hypothesis of rCBF increase during visual stimulation (Tzourio-Mazoyer *et al.* 2002), with increased visual cortical blood flow during visual stimulation, although it is not possible to assess the timecourse of the rCBV changes with PET. NIRS studies of visual (Meek *et al.* 1998), auditory (Sakatani *et al.* 1999; Zaramella *et al.* 2001), olfactory (Bartocci *et al.* 2001), speech (Pena *et al.* 2003) and motor stimulation (Hintz *et al.* 2001) have demonstrated that increased blood flow and volume occur during stimulation in activated cortex, with an increased concentration of deoxygenated haemoglobin (deoxy-Hb) in the activated cortex (presumably due to increased oxygen extraction by the neonatal cortex); this increase in deoxy-Hb concentration is therefore likely to account for the negative BOLD response recorded in some studies.

Therefore the results of neonatal fMRI and PET studies are consistent with the hypothesis that rCBF is increased during sensory stimulation in activated areas of cortex. In addition the

results of NIRS studies provide evidence that rCBV is also increased with a faster onset of rCBF associated BOLD changes (see below). This change in rCBV would provide the physiological mechanism for an impedance change due to the increased volume of lower resistivity blood compared to higher resistivity cortex.

Comparison of the impedance timecourse to other functional imaging modalities

Some support for the hypothesis that neonatal cerebral impedance change is related to changes of blood volume is indirectly provided by a comparison of the timecourse of the neonatal impedance responses with the timecourse of fMRI-BOLD and NIRS signals.

The neonatal impedance response to visual stimulation was a change that occurred 0.6s after stimulus onset, peaked at 1.9s and decayed to baseline over 7.5s. This compares to the BOLD response in infants during visual stimulation, in which onset is within 3 seconds of the stimulus onset, and peaks by 6 seconds (Yamada *et al.* 2000). Similar BOLD responses are recorded with speech presentation to unsedated neonates, with a delay of 3-7 seconds between speech onset and the onset of a BOLD response (Dehaene-Lambertz *et al.* 2002). The rapid onset of the impedance response is therefore faster than the rCBF response, so the impedance response is not directly related to the change in rCBF, however the faster onset of the impedance response is more in agreement with studies of blood volume change recorded by optical imaging techniques in the exposed human and animal brain. In these studies a rapid response, due to an increase of blood volume, occurs within the first 0.5s due to somatosensory stimulation in the adult (Sato *et al.* 2002), and visual stimulation in the cat (Malonek *et al.* 1997). In the latter study, blood volume and blood flow were recorded simultaneously by optical imaging and laser Doppler flowimetry, respectively. This study found that an increase in blood volume preceded the rise in blood flow by over a second; the theoretical explanation for this was that neural activity dilated cortical blood vessels first, which then facilitated a passive increase in blood flow. This finding may explain why the impedance response in infants is faster than the BOLD response during similar stimuli. Further support that the faster impedance change is due to a change in rCBV is supported by NIRS studies of blood volume change during visual stimulation. The timecourse of these changes are more in agreement with the neonatal impedance data than the BOLD fMRI studies, and demonstrate that blood volume increases within a second of visual stimulation in neonates and peaks at 3-5s during a 10 second stimulus (Meek *et al.* 1998). The peak of the NIRS rCBV response is slightly slower than the neonatal impedance response (mean of 2s), but faster than the rCBF peak response measured by BOLD. These findings support a closer correlation of the impedance response with a mechanism of change in rCBV.

Once the impedance changes have risen to a peak, the impedance change plateaus for the duration of the stimulus, then returns to resting baseline levels over a period of 5-15 seconds. This return to baseline time is similar to that of the fMRI-BOLD response in neonates in response to a speech stimulus, in which BOLD signal returns to baseline in 12-15s (Dehaene-Lambertz *et al.* 2002), and a similar response measured in monkeys to visual stimulation (Logothetis *et al.* 2001), illustrated in Figure 4.66.

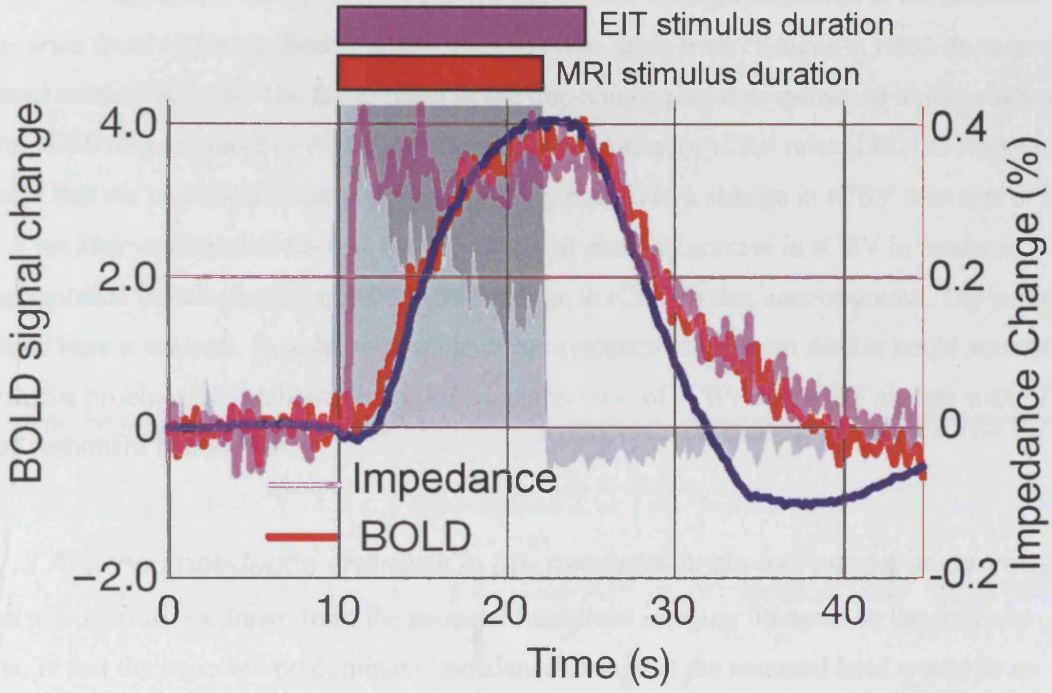

Figure 4.66 Comparison of BOLD-fMRI and impedance responses to visual stimulation
BOLD-fMRI data obtained in monkeys during visual stimulation with a checkerboard (red line), the blue line indicates a modelled BOLD response (from (Logothetis *et al.* 2001)). The light grey graph indicates the neuronal spike measured simultaneously in the area of the visual cortex with the BOLD response.

Superimposed on the graph is the time course of the average impedance change measured during neonatal visual stimulation in an experiment that had a stimulus duration of 15s (pink line). Note that the stimulus differs between the experiments, 12s for the BOLD-fMRI stimulus and 15s for the neonatal EIT experiment.

The impedance response in neonates has a much faster onset than the BOLD-rCBF response and shares the faster onset of NIRS studies that have measured changes in rCBV in neonates in response to visual stimulation. The impedance response plateaus after an initial peak and then returns to the baseline with a similar physiological decay to the BOLD response. This comparison indicates that the impedance change is not a direct consequence of the haemodynamic change of rCBF that produces the BOLD change.

Conclusion: Impedance responses are due to changes in rCBV

The evidence presented from neonatal and some animal studies provide support for 1) A synchronised increase in neural activity during somatosensory or visual stimulation, and 2) An increases in CBF and CBV in the visual cortex during flash visual stimuli and in the contralateral motor/somatosensory cortex during passive motor movements, and 3) A CBV increase that has a similar timecourse to the impedance changes measured in neonates. These studies provide indirect experimental support for the hypothesis that the impedance changes measured in the neonatal studies arise from within the brain and are most likely to arise from changes in rCBV in response to increased cortical activity. The faster onset of the impedance response measured in this chapter, and the NIRS measurement of rCBV compared with the onset of rCBF related BOLD response indicates that the impedance change is more directly related to a change in rCBV than that of blood flow. A possible explanation for this may be an initial passive increase in rCBV in neonates through cortical vessel dilation, preceding the change in rCBF to that area of cortex. The evidence presented here is indirect. In order to provide direct evidence subsequent studies could attempt to address this problem by simultaneous NIRS measurements of rCBV and rCBF change with EIT of evoked responses in neonates.

4.4.2.3 Are the impedance changes in the neonatal brain increases or decreases

One of the conclusions drawn from the neonatal functional imaging literature in the previous section, is that the expected predominant impedance change in the neonatal head would be an impedance decrease due to increased regional cerebral blood volume (rCBV). This was found for the images of the visually evoked impedance responses, and reflected the predominant impedance decreases present in the raw impedance data (Figure 4.47). However, in some of the motor studies, and in the group average of the motor responses, impedance increases were seen in the contralateral area to passive motor stimulation which is not expected from the hypothesis of increased rCBV in the activated cortical area. The presence of impedance increases in the motor studies reflect a larger proportion of impedance increases present in the raw impedance data when compared to the visual evoked response data (see Figure 4.47 and Figure 4.48). The presence of both impedance increases and decreases in both the raw impedance data and the reconstructed EIT images suggests that both directions of impedance change are present in the brain, and their likely mechanisms will therefore be considered further.

Explanation for impedance increases during stimulation

Impedance increases are not expected from the hypothesis of increased rCBV in activated cortex. If the impedance increases are assumed to be real then possible explanations for the impedance increases are that either rCBV is decreased in those areas – but this hypothesis contradicts the evidence from NIRS studies, or that increased rCBV occurs due to activation but the impedance decrease produced is countered by a much larger impedance increase produced by either CSF shunting away from the area of increased cortical volume, or cell swelling at physiological levels of stimulation. The evidence that the impedance increases are real or are due to reconstruction artefact will now be considered.

Evidence that impedance increases are real

The main evidence that the impedance increases in the images are real is the presence of significant numbers of electrodes which recorded impedance decreases in the raw impedance data. These raw data increases are of a similar size, timecourse, and present in similar numbers of electrodes to the impedance decreases (from visual inspection of surface plots of the impedance data). This may suggest that the impedance increases are real. However from tank studies, I know that both impedance increases and decreases can be produced by a single impedance change (as discussed in Chapter 2, Section 2.4.2).

An example of data from the head-tank is discussed to illustrate the changes seen with a single impedance change. In this example, EIT data from the head-shaped tank, with the skull in place, was acquired with the Perspex Rod (a large impedance increase) inserted just inside the periphery of the skull and then in the centre of the skull. The acquisition of this data is described in Chapter 3. In the raw impedance data, both impedance increases and decreases (>0.1% of baseline) are detected, with the ratio of increases to decreases of 3:1 with the Perspex rod just inside the periphery of the skull and 18:1 with the rod in the centre of the skull. In contrast to this data, the neonatal studies demonstrate a 1:1 or 2:1 ratio of impedance decreases to increases. These findings seem to suggest that the neonatal impedance changes may not be due to just a single impedance decrease and indicates that both impedance increases and decreases may occur in the neonatal brain. However, as there are many differences between the neonatal head and the head-shaped tank, the inference made from this comparison should be regarded with uncertainty.

If it is then likely that impedance increases occur in the neonatal data, as suggested by the raw impedance changes, then the physiological mechanisms that contribute to impedance increases are most likely to be due to areas of decreased rCBV, or possibly be due to physiological cell

swelling or an increase of rCBV but a shunt of CSF away from the area of cortex. These possible mechanisms, and evidence supporting them, will be addressed in turn.

In adults there is supportive evidence from PET, to suggest that cerebral blood flow decreases in frontal and parietal areas during visual stimulation (Mentis *et al.* 1996; Mentis *et al.* 1997; Mentis *et al.* 1998). However, no corresponding evidence from PET or NIRS exists to support blood flow and volume decreases in infants. The lack of this data may be due to a lack of studies, as it is unethical to perform functional PET in infants unless there is a clinical indication for such a study. Although NIRS has not detected blood volume decreases, the limited coverage of the brain by NIRS has therefore led to studies which have investigated areas of brain likely to show increased activation; therefore the lack of demonstration of blood volume decreases may be an effect of under sampling of the neonatal brain, or due to rCBV decreases occurring in deeper brain structures, to which NIRS is insensitive. There may be support for rCBF decreases from fMRI studies of cortical function; for example, negative BOLD responses have been detected in the visual cortex during visual stimulation (Yamada *et al.* 1997; Born *et al.* 1998; Martin *et al.* 1999; Yamada *et al.* 2000; Born *et al.* 2002), ipsilateral motor cortex to passive hand movements (Erberich *et al.* 2003) and in the auditory cortex during click presentation (Anderson *et al.* 2001). The main problem is that the BOLD response is an indirect measure of blood flow, as changes in the BOLD signal are inversely related to the concentration of deoxyhaemoglobin. A negative BOLD response may therefore occur due to decreased blood flow, an increase in blood volume of deoxygenated venous blood, or increased oxygen extraction by the brain, and as discussed previously, NIRS supports the theory that the BOLD decreases occur due to increased oxygen extraction by the brain , despite increased rCBF and rCBV in the activated area of brain (Meek *et al.* 1998).

There is a similar lack of evidence for cell swelling, discussed in Chapter 1 and 2, as a possible mechanism of impedance change during increased neuronal activity. The proposed mechanism is that cell swelling may occur for two reasons: 1) Neuronal cells take water in from the extra-cellular space with the inward movement of sodium during depolarisation, and 2) The outward movement of potassium from the active neurones increases potassium concentration in the ECF, which enters the glial cells along with water, reducing the extra-cellular space volume. The net result is a decrease in the volume of the conductive extra-cellular space, which would result in an impedance increase, as the majority of conduction occurs through the extra-cellular space. However, the evidence that cell swelling occurs during increased neural activity has only been demonstrated convincingly in animal models of epilepsy (Holthoff and White 1996), during electrical stimulation of the hippocampus in the cat (Rector *et al.* 1997) and electrical stimulation

of the avascular optic nerve (MacVicar *et al.* 2002). There is also evidence that probable cell swelling occurs, as demonstrated by intrinsic optical signal changes, in chemically induced depolarisation and electrical stimulation in isolated guinea pig cortical slices (Lipton 1972) during depolarisation of the squid nerve axon (Cohen *et al.* 1972) and possibly detected in the human motor cortex at neurosurgery, along with changes due to blood flow and volume, during motor movements (Haglund *et al.* 1992; Sato *et al.* 2002). These studies all suggest that cell swelling occur, but do not give an indication of how much and therefore I cannot calculate whether this would have an appreciable effect on regional cerebral impedance.

The final possible cause of an impedance increase in activated cortex, is the possibility that there are changes in the thickness of CSF surrounding the cortex. This theory was first suggested in relation to optical tomography (Firbank *et al.* 1998), but equally such changes would have a significant effect on cortical impedance, and possibly exceed the impedance decrease produced by a change in blood volume. The principle of such a change is that there is an increase in rCBV in the activated cortex, if this lies near the cortical surface, then there will be a small increase in the regional cortical volume which may cause a shift of the cortex into the CSF space which surrounds the cortex. This would shunt low resistivity CSF away from that cortical area, and as CSF has a third of the resistivity of blood, then the overall impedance change for that cortical area would be an increase. Again there is no hard evidence that these changes occur, but it is useful to consider all possibilities.

So in concluding this section, it is likely, considering the impedance increases seen in the raw data, that impedance increases occur in the neonatal brain. The most likely cause of such changes is to be due to blood volume decreases in areas of relatively low neuronal activity (as seen in adult PET studies), however CSF thickness changes may also be a likely candidate for impedance increase – particularly in the areas of brain expected to be activated by stimulation, and cell swelling is also a possible, but unproven mechanism for impedance increase in neuronally active cortex.

Evidence that impedance increases are due to artefact

The possibility still exists that many of the changes in the EIT images are due to artefact. This is supported by evidence from EIT in tank studies, in which images of a single object show a large impedance change, and additional artefacts of an opposing impedance change. It is easy to identify the correct impedance change, as the localisation of the object is known, but this *a priori* knowledge is not available for the neonatal images and this presents a problem as to which changes represent real impedance change and which changes are artefact. As the neonatal images are generally of poor quality with multiple, small impedance changes, it is difficult to isolate a single

change and be certain that the change has been produced by an underlying physiological event and does not represent an artefact of the reconstruction process.

These artefacts may arise due to noise around a combination of electrodes, or due to reconstruction errors produced by using a simplified head model in the reconstruction algorithm. In addition other factors may contribute to image artefact, such as stimulus related impedance changes due to eye, forehead or scalp movements. Close observation of the neonates during the EIT studies did not identify significant movement of the forehead during visual or motor stimulation, although blinking underneath the LED goggles during visual stimulation would have been obscured. However, I believe it is unlikely that movement artefact had a significant contribution to the impedance changes measured for two main reasons: 1) Movement related artefact should be more pronounced during visual stimulation, as blinking and brow furrowing in the neonate is a reflex response to stimulation with bright lights, however the size of impedance changes between the motor and visual stimuli were similar and no significant facial or scalp movement was observed during the motor studies, 2) The timecourse of the impedance changes demonstrated a gradual return to baseline impedance after stimulus cessation which is more in keeping with a physiological impedance change in the brain due to changes of rCBV, than a stimulus related artefact which would be expected to cease much sooner after stimulus cessation.

4.4.3 Comparison of the neonatal impedance timecourse to adults

The impedance time course in infants during visual and motor stimulation had both a more rapid onset than that of adults, and a more rapid return to baseline impedance. A direct comparison with motor data can be made, in which the neonatal and adult impedance changes were, respectively, 1.9s and 7.1s for impedance change onset, and a decay to baseline impedance of 7.1s and 36s. The differences between the adult and neonatal impedance changes are difficult to explain. In part some of the difference may reflect errors in calculating the timecourse of the adult EIT data due to a slower EIT acquisition speed, and the lack of accurate timing in the adult EIT studies between stimulus onset and image acquisition. Although these factors may contribute to a slower adult response time, the difference in the return to baseline time is difficult to explain. It is possible that some of the prolongation of the return to baseline impedance in adults reflects the longer stimulus duration used in those experiments, which was 75 s and 15-25s for adult and neonatal stimuli, respectively. It is feasible that a prolonged cerebrovascular response can be expected from a longer duration stimulus.

As the cause of these differences cannot be resolved using existing data, then further work would be recommended to investigate the differences between adult and neonatal impedance change timecourses. This would require a repetition of some of the adult EIT studies with identical

equipment, the UCLH-EIT system, and identical stimulus paradigms to those used in the neonatal experiments. This work would help to determine whether the differences in the impedance timecourses were due to different experimental technique or are due to an underlying difference in physiology.

4.4.4 Technical Issues

4.4.4.1 Issues that affect localisation accuracy

Despite the convincing raw impedance data changes, and the evidence that supports a vascular mechanism for these changes, the main issue that remains is in regard to the poor quality of the EIT images, which demonstrated multiple impedance changes and both a lack of consistent localisation of impedance changes between subjects, and a lack of localisation to the expected area of cortex stimulated. In addition, in the motor studies, there was a lack of symmetry of the EIT images acquired during right hand or left hand stimulation in the same infant. There is therefore no evidence from this study that EIT in neonates produced better localisation of impedance changes than in adults, despite the hypothesis that the spherical reconstruction model is a better approximation to the neonatal head, due to a thinner and less calcified skull, than the adult's (Gibson *et al.* 2000; Tidswell *et al.* 2001).

The implication of these findings is that the EIT images are affected by either, or a combination of, physiological noise or technical noise: 1) Physiological noise would be represented by the presence of multiple, multi-focal impedance changes that cannot be independently localised by the EIT, or by multiple changes that affect the localisation of the expected impedance change, and 2) Technical noise implies impedance changes in the images that are produced by either measurement errors, such as stray capacitance effects, or reconstruction errors. It is important to try to separate these, as localisation inaccuracies produced by technical noise could theoretically be resolved by improved instrumentation, data analysis techniques or improved reconstruction methods, however if the images are a representation of the true 'noisy' physiological state of the neonatal brain during stimulation, then improvements may only be brought about by improved stimulus paradigms, if improvements are possible at all.

Evidence for physiological noise

Evidence for physiological noise has been provided by PET, fMRI and NIRS studies of both adults and neonates. In such studies, multiple areas of the brain have been demonstrated to be subject to blood flow changes during visual or motor stimulation.

For visual stimulation, in 2 month old infants, complicated face stimuli produce increased blood flow in the frontal cortex as well as the expected area of the visual cortex (Tzourio-Mazoyer *et al.* 2002) when compared to stimuli produced by patterns of flashing light emitting diodes. Although the frontal changes occurred with more complex stimuli, the baseline condition was also an active visual stimulus, so the possibility exists that the frontal cortex was activated to a lesser extent with LED stimulation. If frontal cortex blood flow increases occur during visual stimulation in infants, then this may account for the consistent finding of stimulus related impedance decreases in the frontal parts of the neonatal EIT images cortex. Similar frontal cortical changes have been demonstrated to occur during simple visual stimuli, using PET in adults (Mentis *et al.* 1996; Mentis *et al.* 1997; Mentis *et al.* 1998), in which decreased rCBF was present over wide areas in the frontal and parietal cortices during visual stimulation, which was related to the frequency of the visual stimulus.

Further evidence for multi-focal BOLD changes are seen with motor stimulation in adults, in which ipsilateral changes are seen as well as the expected contralateral sensori-motor cortices (Nirkko *et al.* 2001)(Figure 4.67). In neonates, NIRS evidence exists for both contralateral and ipsilateral increases of blood volume during a passive knee flexion/extension stimulus (Isobe *et al.* 2001), with the ipsilateral changes a third of the size of the contralateral response. If such changes occurred in the unsedated infants in this study, then significant stimulus related and bilateral impedance decreases would be expected in the EIT images. In this EIT study, this occurred in 3 infants: infants Sa (Figure 4.62) and Wa (Figure 4.64) during left motor stimulation, and in infant La during right motor stimulation (Figure 4.61) and may represent the bilateral stimulation of the sensorimotor cortices but this still does not explain the lack of symmetry between right/left motor paradigms in these infants.

Evidence that this expected right/left symmetry may not exist in neonates has been provided by a neonatal fMRI study (Erberich *et al.* 2003), using a very similar passive hand-motor paradigm to that used in the neonatal EIT studies. This fMRI study demonstrated that 1) There was a lack of symmetry between right and left hand stimulation in several infants studied, and 2) That not all BOLD responses were seen in the expected area of the contralateral motor-sensory cortex. In this study, during left hand stimulation 3/6 neonates had contralateral motor cortex BOLD increases, 5/6 had contralateral BOLD decreases and some also had ipsilateral BOLD decreases (see Figure 4.68, for an example). In contrast to this, passive motor stimulation of the right hand demonstrated BOLD changes in contralateral sensory-motor cortex in only 2/6 infants, with changes seen in the other 4/6 infants in the mesial frontal region, possibly related to the early

supplemental motor area. An example of the asymmetry of the neonatal BOLD responses demonstrated in this paper is illustrated in Figure 4.68.

Taken together, this evidence strengthens the hypothesis of a physiologically noisy brain, in which blood flow changes occur over wide areas of cortex in response to relatively simple stimuli. The advantage for fMRI is that many of these changes can be screened out by the use of thresholding, as signal from each voxel is relatively independent of signal in voxels further away. However, with EIT, due to the low resolution, these multiple changes cannot be independently resolved (as seen from the tank studies in Chapter 3), which may merge together and produced the relatively noisy EIT images seen. Physiological noise is therefore very likely to account for the noisy EIT images, and therefore affect image localisation – due to the difficulty of identifying a single significant impedance change in the images.

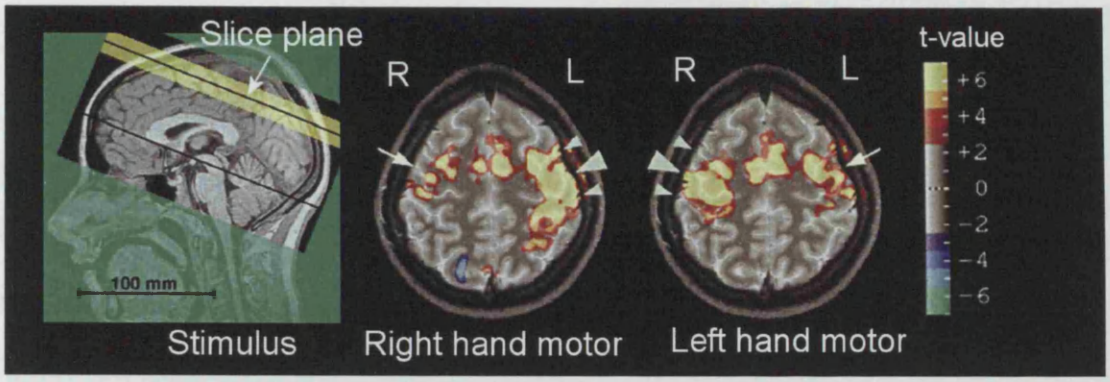

Figure 4.67 Illustrative fMRI example of bilateral adult BOLD changes during an active motor task of each hand. (Adapted from a paper by Nirkko et al (Nirkko *et al.* 2001))
These images shows the significant BOLD changes during an active motor, finger-thumb oppositions task obtained in one subject. The diagram on the left indicates the slice plane of the images, the fMRI on the left (middle image) demonstrates bilateral BOLD changes during right hand movements, and the fMRI on the right (right image) demonstrates similar, but reversed bilateral BOLD changes produced during left hand movements.

These images demonstrate that large areas of brain are bilaterally stimulated by a unilateral motor task, even when the images are thresholded. The implication of such changes on EIT studies, is that the bilateral responses would be expected to produce a bilateral impedance change and not necessarily the single contralateral change that we expected during the neonatal, and adult, EIT studies of motor activity. As a side note, the fact that these images are thresholded hides smaller, less reproducible and therefore less significant changes that may occur elsewhere in the brain. Such changes would also affect the EIT images.

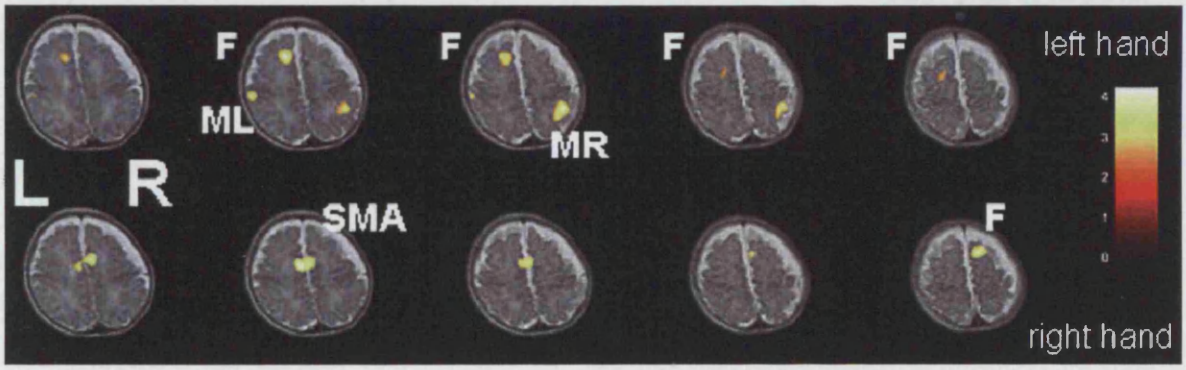

Figure 4.68 Example of neonatal BOLD differences to passive motor stimulation of the left (top) and right hand (bottom) in the same neonate. Adapted from (Erberich *et al.* 2003)
These images show the thresholded increase of BOLD signal (yellow) detected in the neonatal brain to passive motor stimulation. In the top row of the images, left hand stimulation produces an increased BOLD signal in contralateral motor cortex, an area in the contralateral frontal region and ipsilateral parieto-occipital region. However the images of right hand stimulation are asymmetrical, and show no motor cortex stimulation, but BOLD increases in mesial frontal and frontal areas.

These findings illustrate two points: 1) That multi-focal blood flow changes occur in the neonatal brain in response to a simple passive motor stimulus and 2) Asymmetrical BOLD, and rCBF changes may be produced by the same stimuli in each hand. These findings from neonatal fMRI may help to explain why multiple changes were seen in the neonatal images, and why there was a lack of EIT image symmetry in a comparison of images obtained with right or left hand passive motor stimulation in the same neonate.

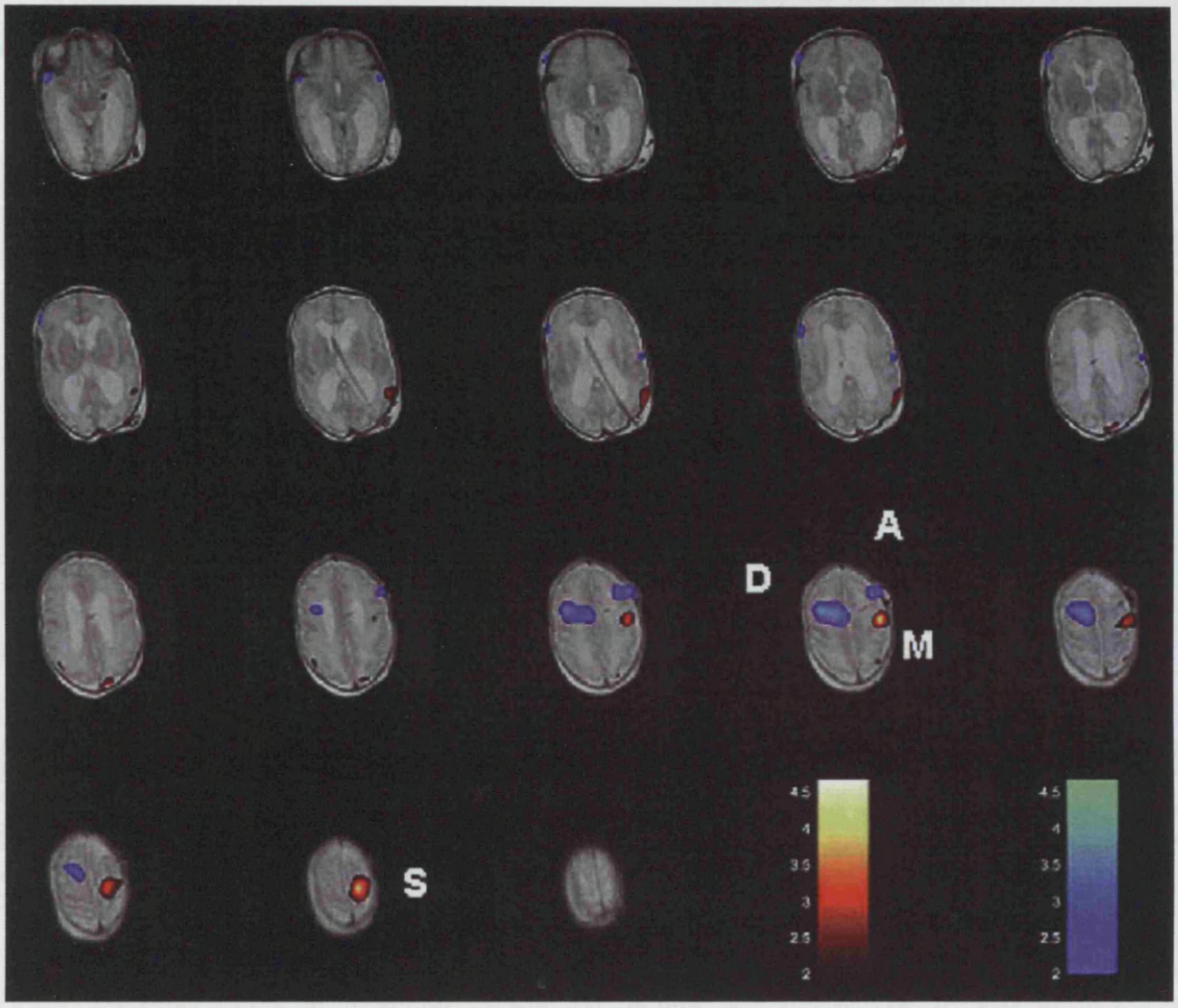

Figure 4.69 Example of multifocal neonatal BOLD changes during left hand passive motor stimulation. Adapted from (Erberich *et al.* 2003)
A 34 week neonate was imaged during passive left hand motor stimulation (similar to that used in the neonatal EIT study). BOLD increases are shown in red and probably indicate a region of increased rCBF in the contralateral motor area (M) and somatosensory area (S). BOLD decreases, represented by blue, are probably related to decreased rCBF in the ipsilateral cortex and right frontal cortex. Note that only BOLD signal changes above a certain statistical threshold are shown, and there are likely to be less significant, but real BOLD signal changes present elsewhere in the images.

This study illustrates that multifocal, and opposing changes of BOLD signal occur, which are likely to represent multifocal changes in rCBF and rCBV. The presence of which is likely to produce multiple impedance changes that cannot be resolved independently by the current EIT system.

Evidence for technical noise

Technical issues that may have affected the neonatal EIT images to account for the noisy images seen could have arisen from the EIT equipment and leads, or from the data processing, or from the image reconstruction, including the truncation threshold used and the image filtering. The question to ask is whether there was a greater amount of noise, or lesser amount of signal in the neonatal data, than in either the adult EIT data or the head tank EIT data of a sponge.

There was no evidence that noise was higher in the neonatal data than in the adult data. Baseline noise for visual and motor experiments, respectively, was in the adult 0.17 % and 0.14 %, and in neonatal data 0.15 % and 0.15 %. As 20 data points were averaged to provide the neonatal data for reconstruction, this effectively reduces the noise by a factor of 4.5, then the noise in the raw data used to reconstruct images is much less than in the adult data.

There was no evidence that signal was reduced in the neonatal data compared to the adult EIT data. Signal in the visual and motor experiments, respectively, was in the adult 0.23 % and 0.23 %, and in neonatal data 0.32 % and 0.25 %.

Compared to sponge data, acquired in the head tank within the skull, signal was 0.05 %, with noise 0.06 %, with a signal to noise ratio (SNR) of 0.9. In comparison, the average SNR for the neonatal studies was, visual and motor experiments respectively, 2.0 (range 0.6-3.4) and 1.7 (range 0.6 – 3.8). As adequate images were obtained with sponge data, with a low SNR compared to the neonatal data, it would therefore seem unlikely that high noise, or low signal solely accounts for the relatively poor image quality seen in the neonatal EIT images. Data processing also seems an unlikely factor, as not only were identical processing performed on adult, tank and neonatal data, the data processing of the neonatal data, due to the higher frequency of data acquisition, served to reduced noise reconstructed into the images.

The likely candidate for technical issues affecting the quality of the neonatal EIT images, is once again the reconstruction algorithm, which again brings up the differences between the simplified model of the head as a sphere and the neonatal head. Evidence that this model is even worse at being a simulation of the neonatal head compared to the adult head, arises from the reduced truncation threshold of 40 singular values, compared to 62 in the adult, required to reduce high frequency spatial noise in the neonatal images. As was seen in Section 4.3.1.6, the effect of an increased truncation level of the sensitivity matrix, from 40, 50 and 60 singular values, was to increase spatial image noise. This noise was predominant around the periphery of the images, but at 60 singular values impedance changes in the images were affected. These results determined the truncation threshold at 40 singular values for all the neonatal EIT images, in order to minimise

spatial noise. This truncation level was lower than the 62 singular values used for the adult EIT images, and the probable reasons for this difference are:

1. The neonatal study used a reduced number of 21 scalp electrodes compared to the adult experiments which used 31. This reduced the number of theoretically independent surface impedance measurements to 187, from which I would expect there to be a reduction in the number of independent basis images produced by SVD; this probably accounted for some of the reduced truncation threshold.

2. The neonatal data required a lower singular value truncation threshold, as the truncation threshold is dependent on a combination of measurement noise and the size of the errors between the reconstruction model and the properties of the object the EIT data is acquired from (Avis and Barber 1994; Gibson 2000). I have shown that the noise in the raw EIT data is similar to that of the adults, and that the noise in the averaged data used to reconstruct the images is even less; the corollary of this is that it is not measurement noise that accounts for the reduced truncation threshold, but differences between the head model (a sphere) and the neonatal head. One of the main reasons for this may be the presence of large conductive 'holes' in the neonatal skull, which are the sutures and the fontanelles – a fibrous tissue connecting the bony plates of the neonatal skull. These fontanelles and sutures are illustrated in Figure 4.70. As these conductive gaps in the skull will act to shunt electric current through them, then this may account for a large error between the neonatal head and the spherical reconstruction model that assumes homogenous conductivity of an applied current.

The combination of these two factors would account for the reduced truncation threshold required by the neonatal EIT images. It should be mentioned here that there currently exists no satisfactory analytical way in which the truncation threshold can be calculated, when applied to physiological data. Much of the theoretical work used in SVD truncation uses computer generated EIT data (Breckon 1990), and in this thesis optimisation of SVD truncation has used data obtained from realistic tank phantoms. The selection of the optimum truncation threshold for 3D EIT of the head is outside the scope of this thesis, but is certainly a major project for future work.

The final technical issue to be discussed is that of the median image filter that was applied to the images. The effect of the median filter was tested on images of visual stimulation reconstructed with 40,50 and 60 singular values which were compared to non-filtered images. The median filter was effective at reducing the high frequency spatial noise, but preserved the larger and stimulus related impedance changes. As the filter did not affect localisation of the impedance changes, it would not have contributed to localisation error.

In concluding this section, I have demonstrated that there is no evidence that there is higher noise or lower signal in the neonatal raw impedance data to account for the poor localisation of the impedance changes in the EIT images, or the presence of image noise. I therefore think it is likely that the most significant technical contribution to the image noise/mislocalisation of impedance changes in the neonatal EIT images is that produced by the use of a simplified forward model in the calculation of the reconstruction algorithm, and the use of such a reconstruction algorithm on data acquired from the neonatal head.

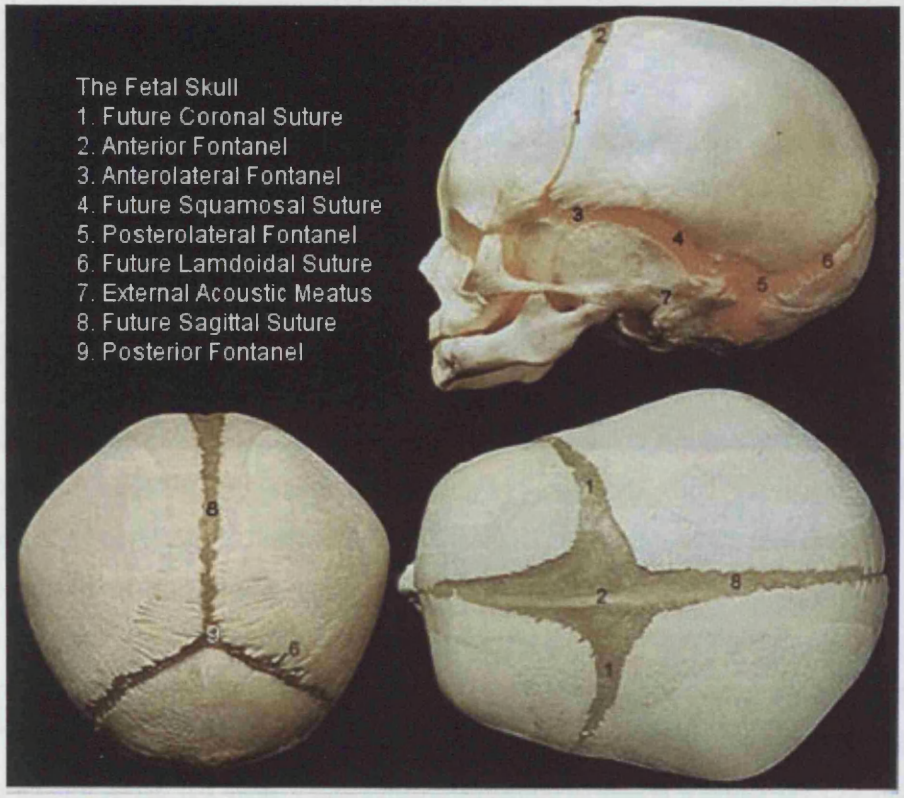

Figure 4.70 Images of the foetal skull (uncertain gestation, probably 28-32 weeks)
These images of a foetal skull, although of uncertain gestation, indicate the positions of the gaps in the neonatal skull which are expected to act as low resistance current paths.

The skull bones themselves are very flexible, due to the lack of mineralisation of the bone, and therefore will have a lower resistivity than the adult skull. In the gaps between these bony plates there is a non-calcified membrane which will have a lower resistivity than the skull. These will act to shunt current, and distort the current path expected from the forward model; this will probably lead to reconstruction errors.

Areas where there is likely to be current shunting are in the anterior (2) and posterior (9) fontanelles and the future sagittal (8) and coronal (1) sutures..

4.4.5 Conclusions

The main findings from the neonatal EIT studies are that reliable impedance changes can be detected from the neonatal scalp as a result of sensory stimulation. The timecourse of these changes correlate closely with neonatal blood volume changes measured with NIRS and with neonatal BOLD changes measured with fMRI. It is therefore highly probable that these impedance changes are a direct result of blood volume changes within the neonatal cerebral cortex, produced as a result of sensory stimulation. A possible contribution to these impedance changes may be made from physiological cell swelling and CSF shunting away from the active cortex, although these must remain unsupported hypotheses, as there is no evidence that these changes occur under physiological levels of stimulation. Although additional contributions from changes of scalp impedance or movement artefact may occur, I believe that these are likely to be small or negligible, as the timecourse of the impedance changes is closely related to cerebral vascular changes measured with other imaging modalities in neonates.

Unfortunately, EIT images did not reproducibly localise these impedance changes to the areas of cortex expected to be activated by the stimulation paradigms. This failure of localisation may be due to physiological factors, such as multiple areas of impedance change which EIT cannot independently localise, or unexpected areas of rCBF and rCBV in the neonatal cortex – both of these factors are supported by functional imaging data, some of which was performed using fMRI of similar neonatal passive motor studies. However, it is more likely that there are reconstruction issues that need to be improved in order to improve the EIT images. Likely reconstruction errors are due to the use of an 'incorrect' reconstruction algorithm which is based on a highly simplified model of the human head, with possible additional errors from non-optimum selection of the truncation of the sensitivity matrix. The presence of the impedance changes in the raw data are encouraging, but clearly much work is needed to assess whether the EIT localisation can be improved before EIT could be considered as a useful imaging modality.

Future work needs to be aimed at improving the reconstruction model, used in the forward problem. The use of a homogenous resistivity, spherical model of the head in the reconstruction algorithm and its problems was discussed in the adult EIT chapter. Similar problems apply to the neonate, in that the model does not account for the different resistivities and anisotropies of the tissues in the head: the skin, the scalp, the skull, the CSF and the brain. The differences between the head and the model will give rise to reconstruction errors, which may produce localisation errors of the imaged impedance changes.

In some respects the homogenous spherical model is more closely related to the neonatal head, than in the adult, as the neonatal skull resistivity is estimated to be smaller than the adult and

closer to the resistivity of the surrounding brain (Gibson *et al.* 2000). However there are still conductive gaps in the neonatal skull, in the areas of the sutures and the fontanelles, which will have a very low resistance and act as large shunt paths for the applied current (Figure 4.70). This will distort the path of currents in the head, from the expected current paths in the homogenous spherical forward modes, and the differences between the two may result in higher reconstruction errors than that seen in the head-tank with an adult skull or in the adult EIT data. This may explain why there is little improvement in the image quality of the neonatal EIT images compared to that of the adult.

Ideally to test the effect of the sutures and fontanelles, a neonatal head phantom study should be performed, with a neonatal skull. Unfortunately, our laboratory did not possess such a skull and these studies could not be performed. An alternative method would be to use a realistic model of the neonatal head, using a finite element model constructed from neonatal MRI data. The use of such a model may decrease reconstruction errors and possibly improve image localisation by a reduction in the number of impedance changes imaged. As this project has demonstrated that impedance changes can be measured, then if improvements to image reconstruction can be made and images produce consistently localised changes, then it would be likely that EIT would find a use in functional imaging studies of both normal and abnormal neonatal brain activity.

Chapter 5: Improved Adult Reconstruction Algorithm

5.1 Introduction

The results from both the adult and neonatal EIT chapters indicated that promising raw impedance data changes were obtained, but that the EIT images were noisy, and localised impedance changes to areas outside the area of cortex expected to be stimulated by the various visual, motor and sensory paradigms. In the conclusion of both these chapters, one of the main suspected contribution to probable image errors was the use of a homogenous sphere model of the head in the forward model used to calculated the reconstruction algorithm, and the use of such a reconstruction algorithm on data acquired from a real head.

Since the EIT work in both adults and infants, presented in this thesis, progress has been made in the UCLH EIT group in the production of a more realistic forward model of the head. At the time of writing this chapter a Finite Element Model (FEM) of the adult human head had been constructed, from real anatomical data obtained from the MRI of an adult head (Bagshaw *et al.* 2003). As the aim of this model was to reduce reconstruction error in the EIT images, this needed testing on real EIT data.

The purpose of this chapter was to test whether using a realistic model of the human head in the forward model, produced improvements in the reconstructed EIT images. This model, known as the FEM model, was tested on: 1) EIT data from the head-shaped tank with the skull – acquired in Chapter 3, in order to test whether a known impedance change within a skull could be imaged with the FEM based algorithm, and 2) The adult EIT data - acquired in Chapter 2, in order to test whether the FEM based algorithm improved localisation of significant changes in the adult EIT images.

In this chapter I will briefly recap the data acquisition, the methods of how the head model was made, how the forward model was solved and how images were reconstructed and compared to the original EIT data. The FEM head model used in the reconstruction process is credited to Dr Andrew Bagshaw, Andrew Tizzard and Dr Richard Bayford; the rest of the work in this Chapter is my own.

5.2 Methods

5.2.1 Construction of the finite element head mesh

The purpose of the head model was to incorporate realistic geometry and contain separate resistivity information about the different tissue layers in the head. This involved the construction of a 4-layer FEM of the head, which represented the anatomical tissues of the brain, CSF, skull and scalp (Bagshaw *et al.* 2003).

Anatomical data was obtained from an MRI scan of the adult head. The transverse slices obtained from the scan were imported into a graphical package, and segmented into 4 compartments: 1) Scalp, 2) Skull, 3) CSF and 4) Brain. The process of segmentation required a person (Dr Bayford) to draw around each tissue surface in each MRI slice. As the outline of each surface was too complex for the finite element package generator, the surface outlines were smoothed by a non-uniform rational B-spline (NURB) interpolation technique.

The finite element model of the head was generated from the manually segmented images by a computer program called I-DEAS (EDS, Missouri, USA), an engineering package designed to model stress or temperature. As thermal modelling requires information about temperature conductivity, then the values assigned to elements of the finite element mesh were also suited for electrical conductivity.

There were three steps in the generation of the FEM head model from the segmented MRI images: 1) Volume construction - in which the volumes of the skull, skull, CSF and brain were created from interpolation between the layers identified in adjacent transverse MRI images. 2) Finite element mesh generation - in which the program was used to create a finite element model (FEM) of the different layers. 3) Assignment of different resistivity values to each layer in the finite element mesh.

The final stage was the production of the sensitivity matrix from the FEM head model. This was done with a program that used the FEM to simulate current application at simulated 'scalp electrodes' and measurement of scalp voltage at 'voltage electrodes'. From these simulations, the sensitivity of each node in the FEM was calculated.

Volume construction

The segmented, volume model of the head was created using a variety of techniques. Most of the information was obtained from the segmented MRI slices, where for each transverse MRI slice the surface outline of, for example, the brain, was interpolated between adjacent MRI scans. The final

result was a volume of the head, which was then further smoothed in order to enable it to fit snugly into other adjacent layers of the head, for example the skull had to fit without gaps between the scalp and CSF layers, otherwise gaps would lead to large errors in the model. Some of the structural information of the head, such as the neck and jaw, which were not included in the MRI scans, were modelled from anatomical images obtained from the Visual Human Project (http://www.nlm.nih.gov/research/visible/visible_human.html).

Mesh generation

From the segmented volume model of the head, I-DEAS created a finite element mesh. This mesh consisted of linear tetrahedral elements which connected each point or node in the head volume model to its neighbours. The size of the model was 104, 000 elements. This meant that some layers, such as the skull and CSF, only contained two layers of elements, which may introduce errors in the model. Although it would be possible to increase the number of elements by making the elements smaller, which would theoretically increase the accuracy of the model, the problem with increased element numbers is the exponential increase in computational time required to solve the model.

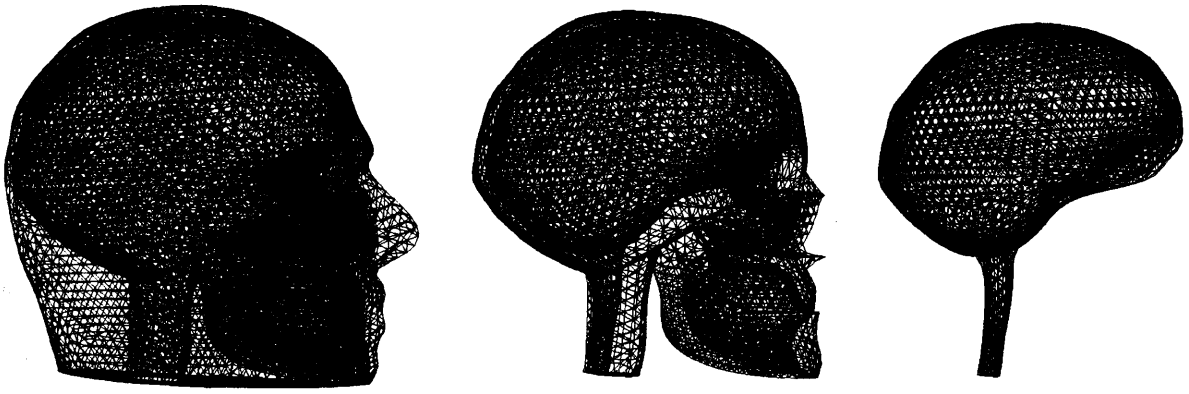

Figure 5.71 Finite element meshes of the human head
Different finite element meshes of the scalp and facial tissues (left), the skull (middle) and the brain (right) are shown (CSF layer not shown), which were created from segmented MRI images, and converted into volumes in the I-DEAS package. The mesh elements are tetrahedral in structure, connecting 4 points within a certain volume. As each element in a layer can be assigned a different resistivity value, then a computer program can 'solve' the model by calculating the current distribution in the model for each point of current injection. This information can be used to assign the sensitivity matrix for the head, used to reconstruct EIT images.

Resistivity assignment

Once the FEM model of the head was complete, the different layers were assigned different resistivity values, to simulate the resistivity of the scalp (230 Ω.cm), skull (5500 Ω.cm), CSF (56 Ω.cm) and brain (400 Ω.cm). These values were taken from the literature (Geddes and Baker

1967; Yamamoto and Yamamoto 1976; Kosterich *et al.* 1983; Kosterich *et al.* 1984; Lattikka *et al.* 2001).

The justification for the use of these resistivity values, and their accuracy in the simulation of *in vivo* tissue resistivities will be examined in the discussion.

Calculation of the sensitivity matrix, and its inversion

The completed FEM mesh, with assigned node resistivities, had points defined on the scalp surface which corresponded to the 31 EEG electrodes placed on the adult scalp for acquisition of the EIT data. Then the FEM mesh and a file containing these electrode positions, were exported into a computer program, called TOAST (time resolved optical absorption and scattering tomography), developed by the optical tomography group at UCLH (Hebden *et al.* 2002). This program produced a solution for the FEM model, which was used in the reconstruction algorithm. Briefly, the solution of the FEM mesh simulated the application of a current at two electrodes, and calculated the contribution of each node (within the FEM volume) towards the scalp surface potential. This level of contribution at each node is also known as the sensitivity. These sensitivities were calculated for each node in the FEM model, for the different combinations of current injection and voltage measurement electrodes used to make each of the 258 scalp impedance measurements made for the adult and head-tank EIT data. The final solution was expressed in the form of the sensitivity matrix, **A** (equation 1).

The sensitivity matrix also relates small changes in the conductivity of each node to a voltage change produced at the scalp for a constant current. This is the EIT forward problem, in which scalp voltage changes, $\Delta\mathbf{V}$, are related to conductivity changes, $\Delta\boldsymbol{\sigma}$, by Poisson's equation:

1) $$\Delta\mathbf{V} = \mathbf{A}\,\Delta\boldsymbol{\sigma}$$

As EIT measures changes in voltage, and needs to solve the equation to produce images of conductivity change, then the sensitivity matrix needs to be inverted. This was inverted by singular value decomposition (SVD) with a truncation level of 70 singular values. This truncation threshold was used as the 70^{th} singular value has a contribution to the image corresponding to 0.0013-0.004 of the maximum singular value for all the matrices used and as such corresponds to the level of noise present in the raw adult impedance data which was 0.0015 of the baseline impedance (Bagshaw *et al.* 2003). The inverted matrix was then used to reconstruct the tank and human EIT data.

5.2.2 Acquisition of EIT data

5.2.2.1 EIT of a Perspex rod in the head-tank with a skull

These details are from Chapter 2 Section 3.2.4.2. Briefly, a Perspex rod, of 20 mm diameter and 20 mm height, was inserted within the skull in the head-shaped tank, in a solution of 0.2 % saline. An equivalent volume of saline to the Perspex rod was removed. The Perspex rod was suspended by a support constructed from 2 wooden sticks, 1 mm diameter, fastened at right angles by a small Araldite mould, this was inserted through the foramen magnum and manoeuvred into the desired position. Because the support had a small, but measurable impedance, this was eliminated from the reconstructed images by a comparison of the EIT data acquired with the support and Perspex rod in the tank to the baseline EIT data obtained with the support in an identical position. The difference between these conditions was reconstructed into EIT images.

The Perspex positions were: 1) Anterior-posterior in the midline longitudinal axis, moved in 2cm increments, and 2) Left to right in 2cm increments, going along a transverse axis which was perpendicular to a line connecting the vertex of the skull and the centre of the foramen magnum.

5.2.2.2 EIT of adult human evoked responses

The visual, motor and somatosensory evoked responses were imaged by the FEM method. The acquisition of this data, the paradigms used and the methods used to process this data prior to reconstruction are described in the methods section of Chapter 2. The baseline and noise corrected EIT data for each experiment in each subject was then reconstructed by multiplication of the data by the FEM reconstruction algorithm.

5.2.3 Reconstruction of EIT data

Reconstruction of the EIT data was similar for both the head-tank and adult EIT data. The noise corrected impedance data for each timepoint in each experiment in each subject (or Perspex rod position) was multiplied by the FEM reconstruction algorithm (the inverted sensitivity matrix).

As the reconstructed images represented a series of points corresponding to the position of each element or node of the FEM mesh, and as these nodes were irregularly spaced, this produced problems for the rapid visualisation of the image data. In order to simplify the image data, the FEM images were interpolated (or rasterised) onto a 3-D, regularly spaced voxel grid by a program written by myself in Matlab. The 20,000 irregularly spaced nodal elements in each image were rasterised onto a grid of 71x51x69 voxels, 3 mm^3 in size, which represented the anterior-posterior, transverse (right-left) and cranial-caudal axes of the head, respectively.

For the tank images, no further processing was required. For the human images, each set of experiments for each subject was averaged to produce a mean and standard error image – from which the images could be averaged to exclude voxels that were not significant on a t-test performed on a per voxel basis. The averaging, thresholding and image display was all performed by programs (written by myself) in Matlab.

5.2.4 Image analysis

5.2.4.1 Analysis of tank EIT data

The FEM and SVD62 images of the Perspex rod in each position were compared by visual inspection to determine whether the Perspex rod was visualised similarly or more accurately in the FEM images.

5.2.4.2 Analysis of human EIT data

The human EIT images, reconstructed with the FEM reconstruction algorithm, were thresholded at a $P<0.05$ level, and displayed. The images during the visual and motor stimuli were assessed for the presence of a significant impedance change (which remained after thresholding) in the appropriate are of the image. The appropriate image area was defined as the posterior quadrant for the visual stimuli, and the superior quadrant of the image contralateral to the hand stimulated for the motor and somatosensory stimuli. These areas were similar to those defined for the images reconstructed by the SVD_62 algorithm in Chapter 2.

5.2.5 Results

5.2.6 EIT images of a Perspex rod in the head-tank

The Perspex rod localisation within the skull, was similar between the FEM and SVD_62 images (Figure 5.72 and Figure 5.73). It was imaged as an impedance increase in all the images; surrounding impedance decreases (image artefact) were seen in both the FEM and SVD_62 images.

Image artefact was seen in both sets of images, defined as either 1) Electrode artefact – small impedance changes which alternate between impedance increases and decreases and are seen on the boundary of the image and 2) Image artefact - defined as the impedance changes produced in the image of opposite magnitude to the actual impedance change, and usually surround the main impedance change in the images. Visual assessment of the image quality suggested that there was less electrode artefact and less impedance artefact in the FEM reconstructed images that for the SVD_62 algorithm images (Figure 5.72 and Figure 5.73). The most striking improvement was a reduction of the electrode artefact with the FEM images.

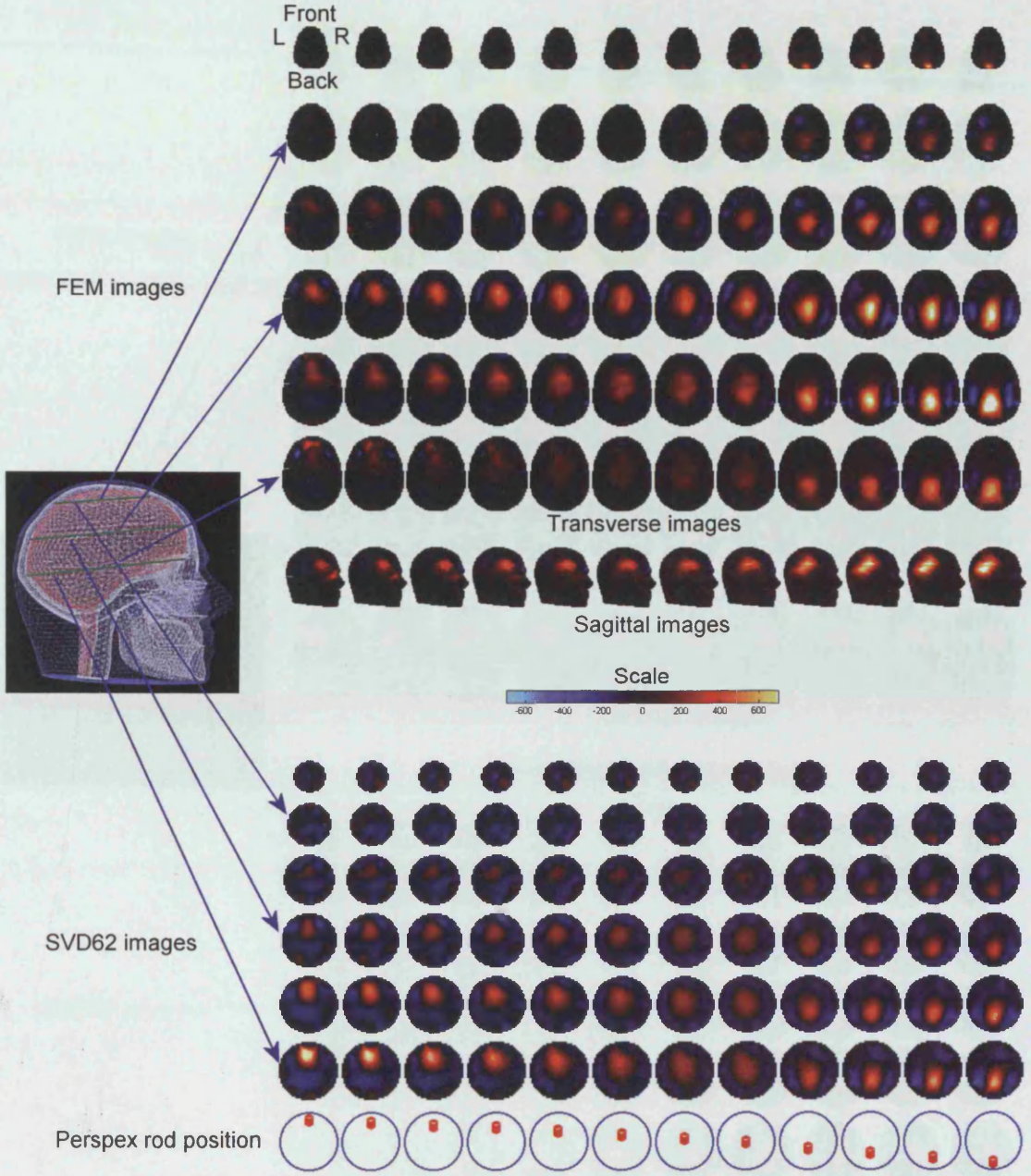

Figure 5.72 EIT images of a Perspex rod in the head tank: anterior-posterior movement
Images of the Perspex rod were reconstructed with algorithms based on a FEM forward model (top) and spherical model (SVD62, bottom). Each column represents images of one position of the Perspex, indicated by the bottom row of images. Each image consists of 6 transverse slices through the head-tank as indicated by the diagram on the left. The Perspex rod is seen as an impedance increase (red/yellow) in the images, moving from front to back.

The Perspex rod was localised in a similar position with both algorithms, with slightly less image artefact (blue) seen with the FEM based algorithm. These images demonstrate that localisation with the FEM algorithm is similar to the SVD_62 algorithm, with an improvement in image quality, as judged by reduced electrode and impedance artefact.

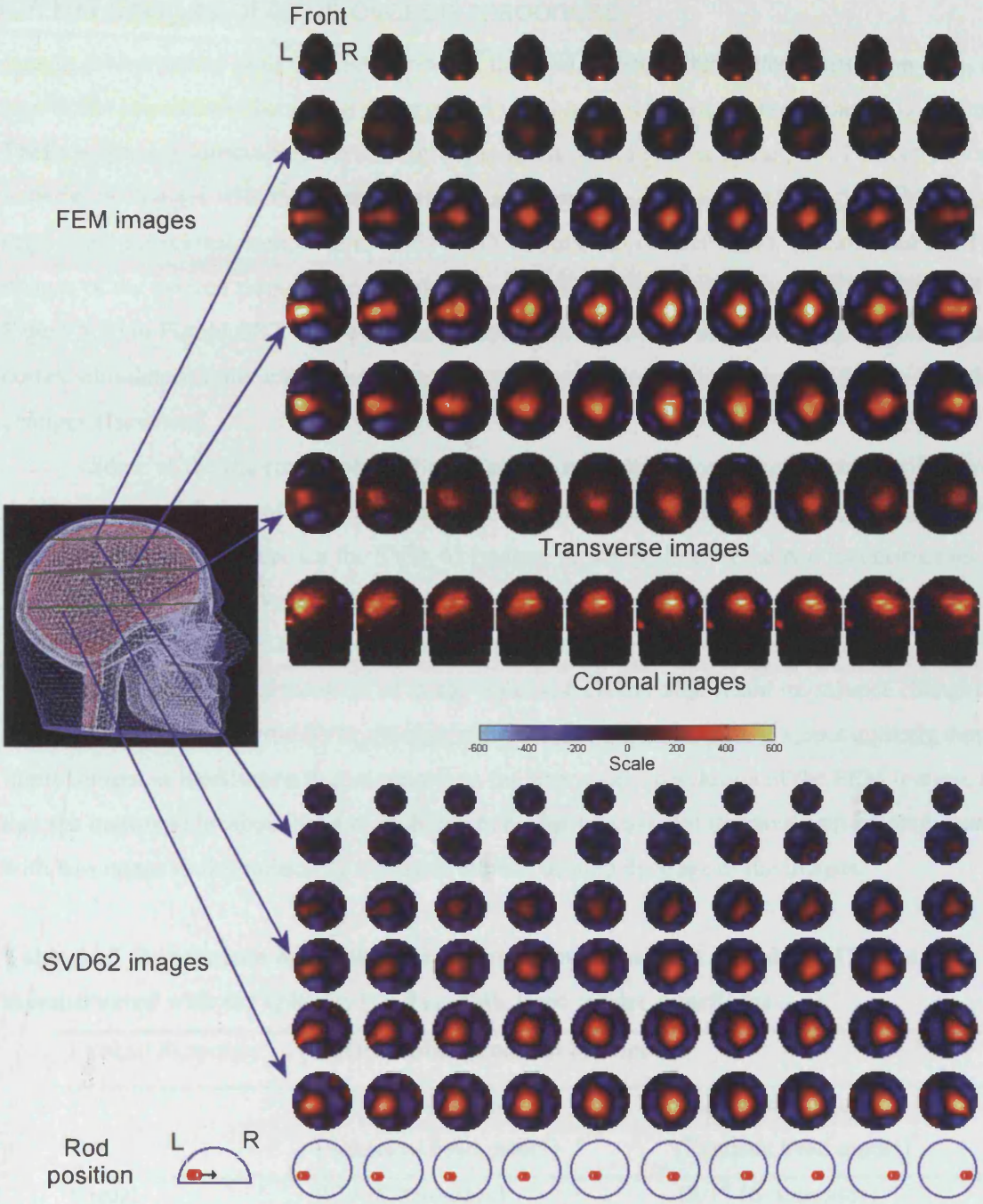

Figure 5.73 EIT images of a Perspex rod in the head tank: left to right movement
Images of the Perspex rod were reconstructed with algorithms based on a FEM forward model (top) and spherical model (SVD62, bottom). Each column represents images of one position of the Perspex, indicated by the bottom row of images. Each image consists of 6 transverse slices through the head-tank as indicated by the diagram on the left. The Perspex rod is seen as an impedance increase (red/yellow) in the images, moving from left to right.

The Perspex rod was localised in a similar position with both algorithms, with slightly less image artefact (blue) seen with the FEM based algorithm. These images demonstrate that localisation with the FEM algorithm is similar to the SVD_62 algorithm, with an improvement in image quality with a reduction of electrode and impedance artefact.

5.2.7 EIT images of adult evoked responses

Images reconstructed with the FEM model of the head demonstrated better localisation of significant impedance changes to the expected image area, when compared to the SVD_62 images. These results are summarised for the various stimulus paradigms in Table 5.15. Correctly localised impedance changes with the same timecourse as the stimulus were found in 38/51 FEM images (18 impedance decreases) compared to 19/51 SVD_62 images (10 decreases). Thresholded FEM images of the evoked responses which were considered to be correctly localised are shown in Figure 5.76 to Figure 5.87. However, these changes were not just exclusive to the expected area of cortex stimulated, some images which contained correctly localised changes had other impedance changes elsewhere.

Some of the improved localisation of significant impedance changes was possibly due to the improved resolution of the FEM images in the z-dimension (cranial-caudal), which was 69 slices, compared to 6 slices for the SVD_62 images. A comparison of the two reconstruction algorithms, with an equivalent 6 slices in the z-dimension for the FEM algorithm corresponding to the 6 slices of the SVD_62 algorithm, are shown for the visual evoked responses in Figure 5.74. This shows a general improvement of image noise and clearer significant impedance changes for the FEM algorithm than the SVD_62 algorithm. From this comparison, it seems unlikely that the improvement in localisation is due entirely to the improved z-resolution of the FEM images, and that the improved localisation is more likely to be due to a general improvement in image quality, with less image noise, especially electrode artefact around the edge of the images.

Table 5.15 Comparison of localisation of significant changes in the adult EIT data reconstructed with the spherical and realistic head model algorithms

Evoked Response	Total number in correct location	
	SVD 62 algorithm (Spherical head model)	FEM model algorithm (Realistic head model)
Visual	9/13 (5 decreases)	12/13 (6 decreases)
Right motor	6/13 (3 decreases)	13/13 (8 decreases)
Left motor	2/7 (1 decrease)	6/7 (3decreases)
Right somatosensory	1/10 (1 decrease)	5/10 (1 decrease)
Left somatosensory	1/8 (0 decreases)	2/8 (0 decreases)
Total	19/51 (10 decreases)	38/51 (18 decreases)

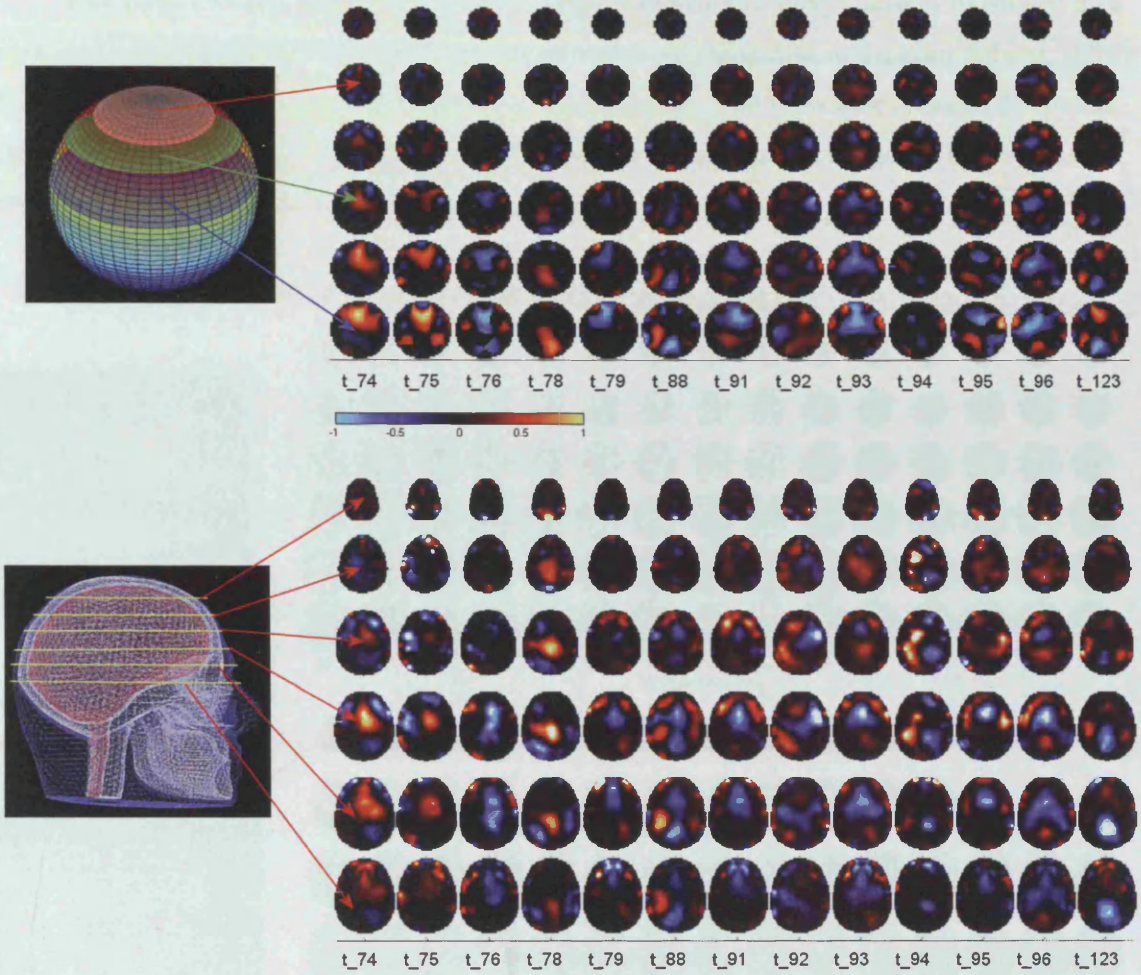

Figure 5.74 Like-for-like comparison of FEM and SVD_62 images of visual responses
These sets of images represent one of the images during visual stimulation in each of 13 different subjects. The images are averaged for repetitions of the stimulus in each subject, and thresholded at 2 standard errors.

The top image set was produced from data reconstructed with the spherical head model reconstruction algorithm (SVD_62). The bottom set of images, with the finite element model (FEM) algorithm, were sliced at the equivalent levels used for the SVD_62 algorithm in order to demonstrate that the improved image quality was not just due to an improved resolution of the FEM images in the cranial-caudal axis of the head.

The predominant features in both sets of images are preserved between the two algorithms. Although localisation was improved with the FEM model algorithm, the images still contain noise. There is reduced electrode noise around the periphery of the FEM images and impedance changes appear better localised, in comparison to the SVD_62 images, in which many of the impedance changes appear smeared across the image.

An example of how the FEM algorithm helps to reduce EIT image noise is illustrated by a comparison of the visual evoked responses imaged with both algorithms in the same subject, shown in Figure 5.75. There was a general improvement to the image quality, with less electrode artefact around the edge of the images, and increased localisation of impedance changes to the expected area of cortex stimulated.

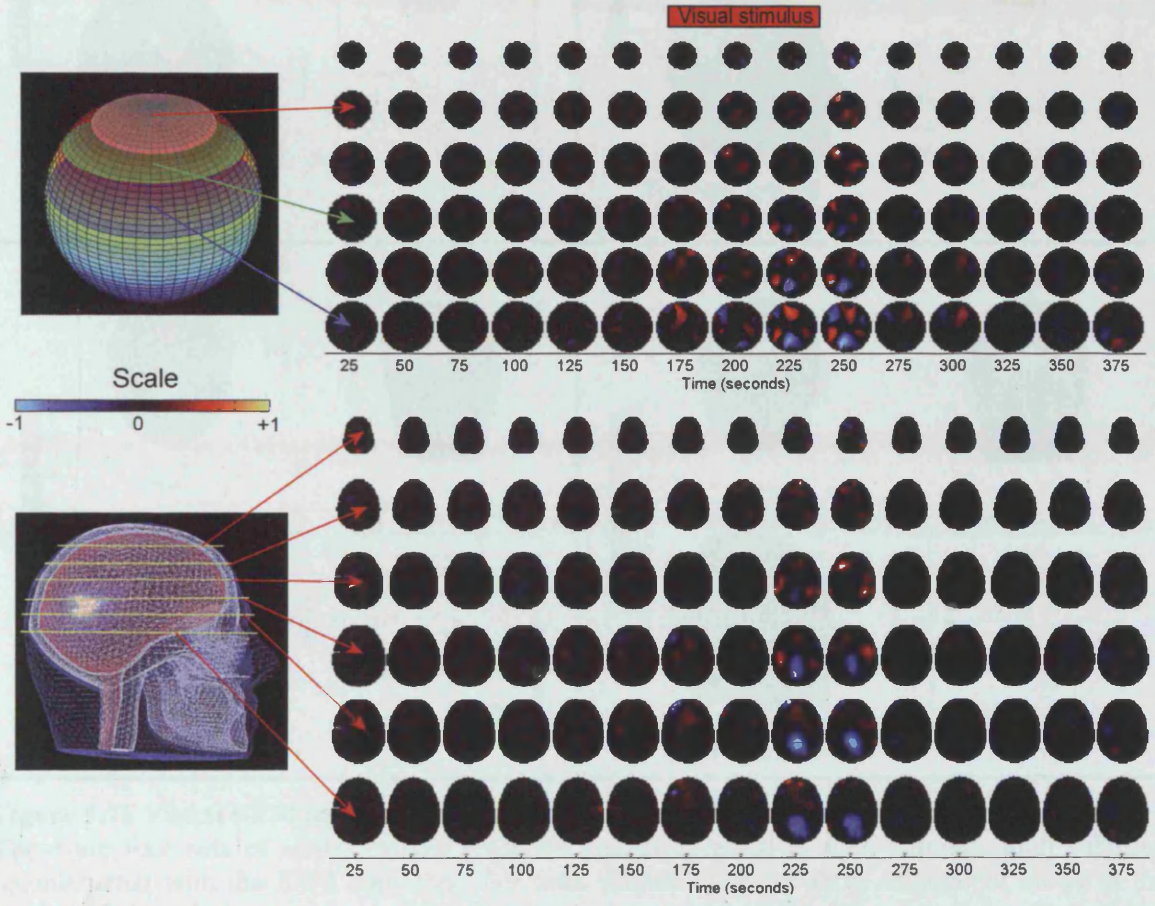

Figure 5.75 EIT image time series of visual activity, reconstructed with different algorithms
These time series of EIT images, of visual stimulation in one subject, are reconstructed by the SVD_62 algorithm (top), which uses a homogenous spherical model of the human head, and the FEM model of the head (bottom series of images). The FEM head model is pictured on the left, with the superimposed impedance change during visual stimulation. This picture indicates the level at which each of the transverse slices of the images are displayed. The red bar at the top indicates the period of visual stimulation. The images are the average of 6 experiments, and are thresholded to show impedance changes with mean values more than 2 standard errors from the baseline.

Both series of images demonstrate an impedance decrease in the region of the visual cortex. However the top series of images have multiple impedance changes, so it is difficult single out the change over the visual cortex. In the images reconstructed with the FEM head model, the predominant change is an impedance decrease over the area of the visual cortex; other impedance changes are present but are much smaller.

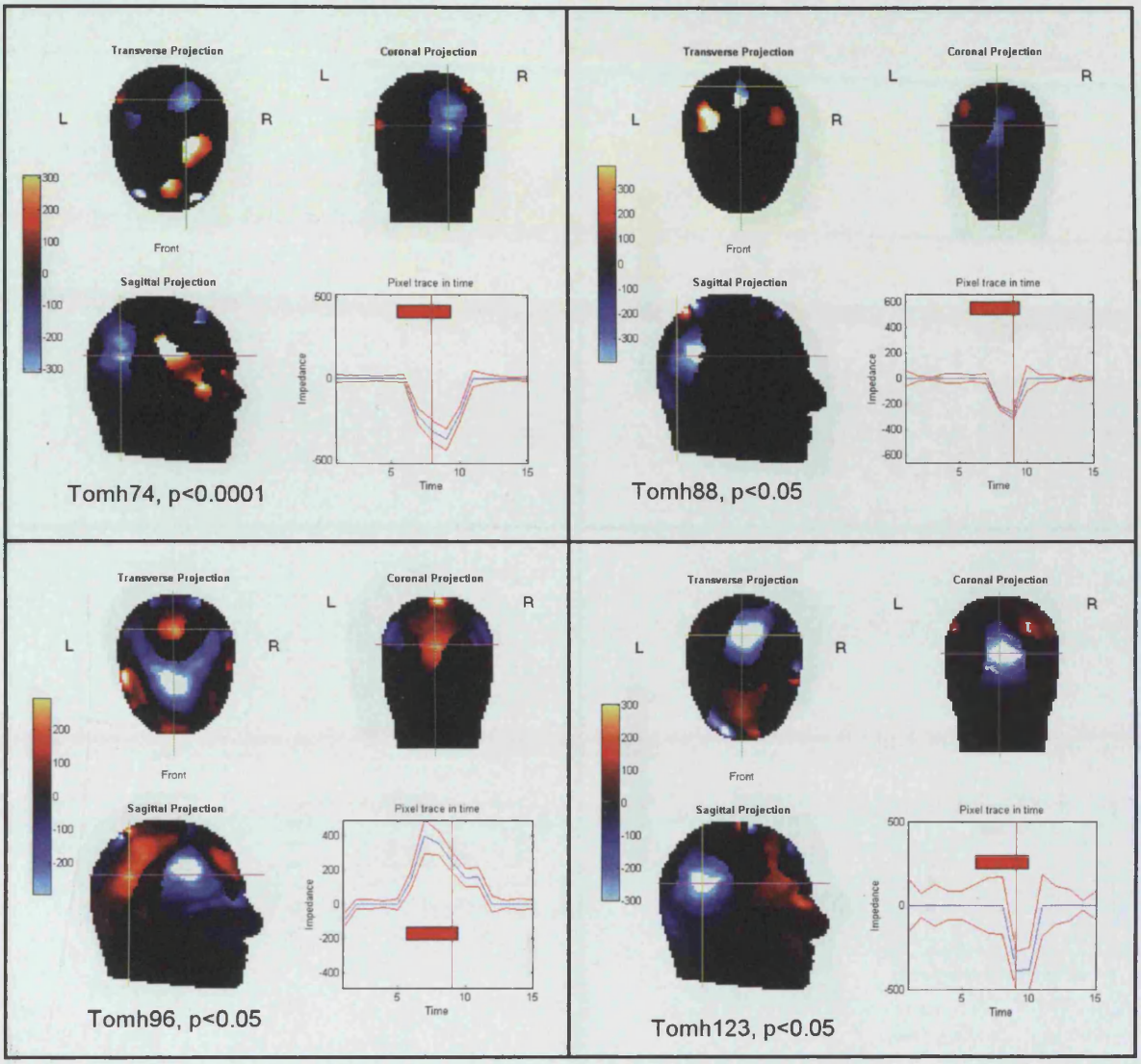

Figure 5.76 Visual FEM images (1)

These are four sets of visual evoked response images obtained in four different adult subjects, reconstructed with the FEM algorithm. For each subject there are three orthogonal views of the head, and the relative positions of the head sections are indicated by the crosshairs. The subject number and the threshold level of the images are indicated at the bottom of each set of images.

The timecourse of the impedance (mean±SE) at the voxel centred on the cross hairs is indicated by the lower right graph in each subject. Impedance is indicated on the y-axis. Time is indicated on the x-axis in image frames, with each frame representing 25s. The timecourse of the visual stimulus and the timepoint of the image are also indicated in this graph, by the red horizontal bar and red vertical line, respectively.

Spatially large, and statistically significant impedance changes, with the same timecourse as the visual stimulus are seen in all four subjects over the region of the visual cortex. Three show impedance decreases in blue (tomh74, tomh88 and tomh123), with one an impedance increase in red (tomh96). Other impedance changes are imaged elsewhere in the images in all four subjects.

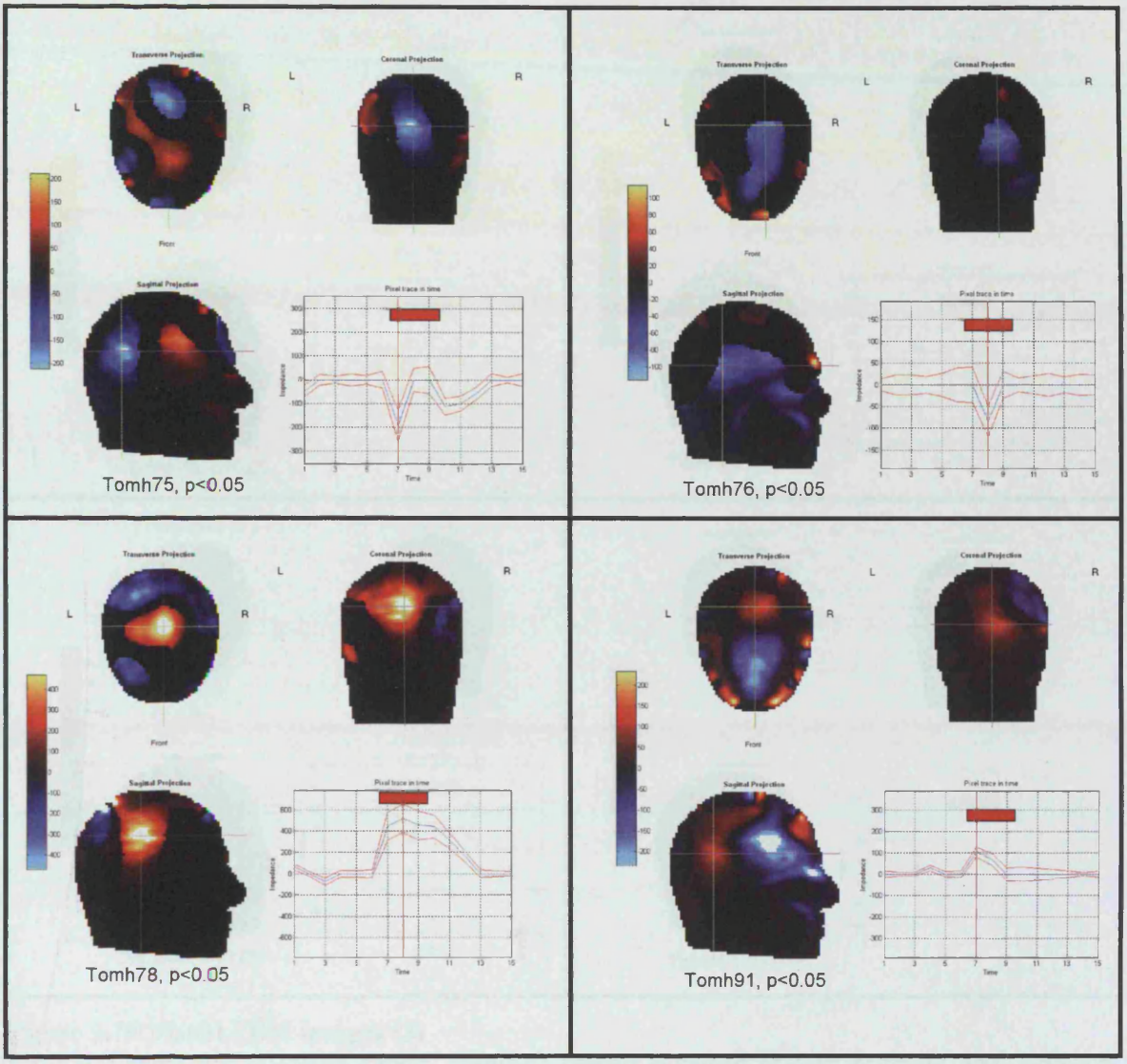

Figure 5.77 Visual FEM images (2)
These are four sets of visual evoked response images obtained in four different adult subjects, reconstructed with the FEM algorithm. For each subject there are three orthogonal views of the head, and the relative positions of the head sections are indicated by the crosshairs. The subject number and the threshold level of the images are indicated at the bottom of each set of images.

The timecourse of the impedance (mean±SE) at the voxel centred on the cross hairs is indicated by the lower right graph in each subject. Impedance is indicated on the y-axis. Time is indicated on the x-axis in image frames, with each frame representing 25s. The timecourse of the visual stimulus and the timepoint of the image are also indicated in this graph, by the red horizontal bar and red vertical line, respectively.

Spatially large, and statistically significant impedance changes, with the same timecourse as the visual stimulus are seen in all four subjects in the posterior quadrant of the images, near the region of the visual cortex. Two show impedance decreases in blue (tomh75 and tomh76) and two show impedance increases in red (tomh78 and tomh91). Other impedance changes are imaged elsewhere in the images in all four subjects.

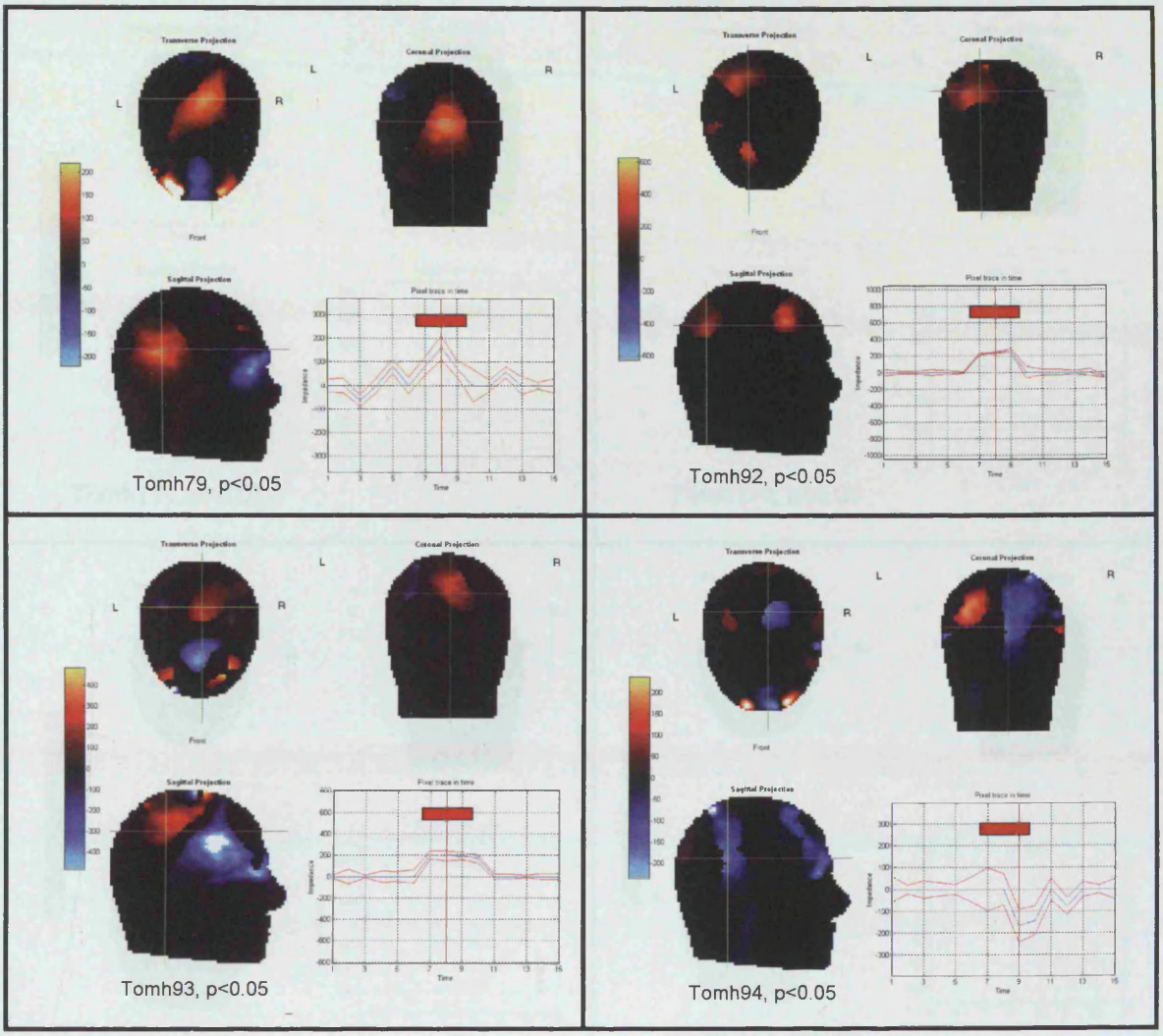

Figure 5.78 Visual FEM images (3)
These are four sets of visual evoked response images obtained in four different adult subjects, reconstructed with the FEM algorithm. For each subject there are three orthogonal views of the head, and the relative positions of the head sections are indicated by the crosshairs. The subject number and the threshold level of the images are indicated at the bottom of each set of images.

The timecourse of the impedance (mean±SE) at the voxel centred on the cross hairs is indicated by the lower right graph in each subject. Impedance is indicated on the y-axis. Time is indicated on the x-axis in image frames, with each frame representing 25s. The timecourse of the visual stimulus and the timepoint of the image are also indicated in this graph, by the red horizontal bar and red vertical line, respectively.

Spatially large, and statistically significant impedance changes, with the same timecourse as the visual stimulus are seen in all four subjects in the posterior quadrant of the images near the region of the visual cortex. Three show impedance increases in red (tomh79, tomh92, tomh93) and one a blue impedance decrease (tomh94). Other impedance changes are imaged elsewhere in the images in all four subjects.

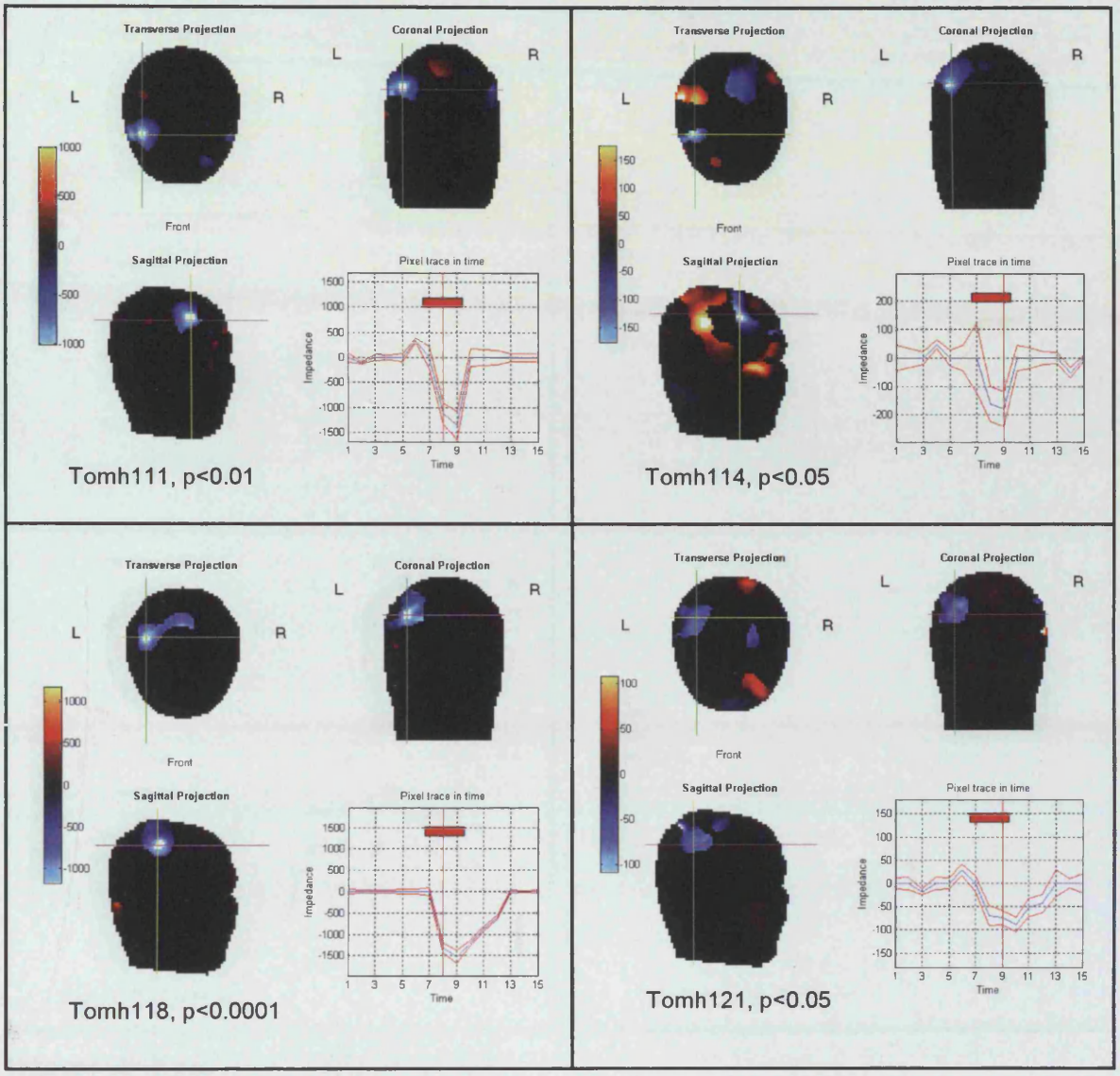

Figure 5.79 Right motor FEM images (1)
These are four sets of right motor evoked response images obtained in four different adult subjects, reconstructed with the FEM algorithm. For each subject there are three orthogonal views of the head, and the relative positions of the head sections are indicated by the crosshairs. The subject number and the threshold level of the images are indicated at the bottom of each set of images.

The timecourse of the impedance (mean±SE) at the voxel centred on the cross hairs is indicated by the lower right graph in each subject. Impedance is indicated on the y-axis. Time is indicated on the x-axis in image frames, with each frame representing 25s. The timecourse of the visual stimulus and the timepoint of the image are also indicated in this graph, by the red horizontal bar and red vertical line, respectively.

Spatially large, and statistically significant impedance decreases (blue) are seen over the quadrant of the images contralateral to the hand moved, which corresponds to the approximate region of the contralateral motor cortex. These changes all have the same timecourse as the motor activity.

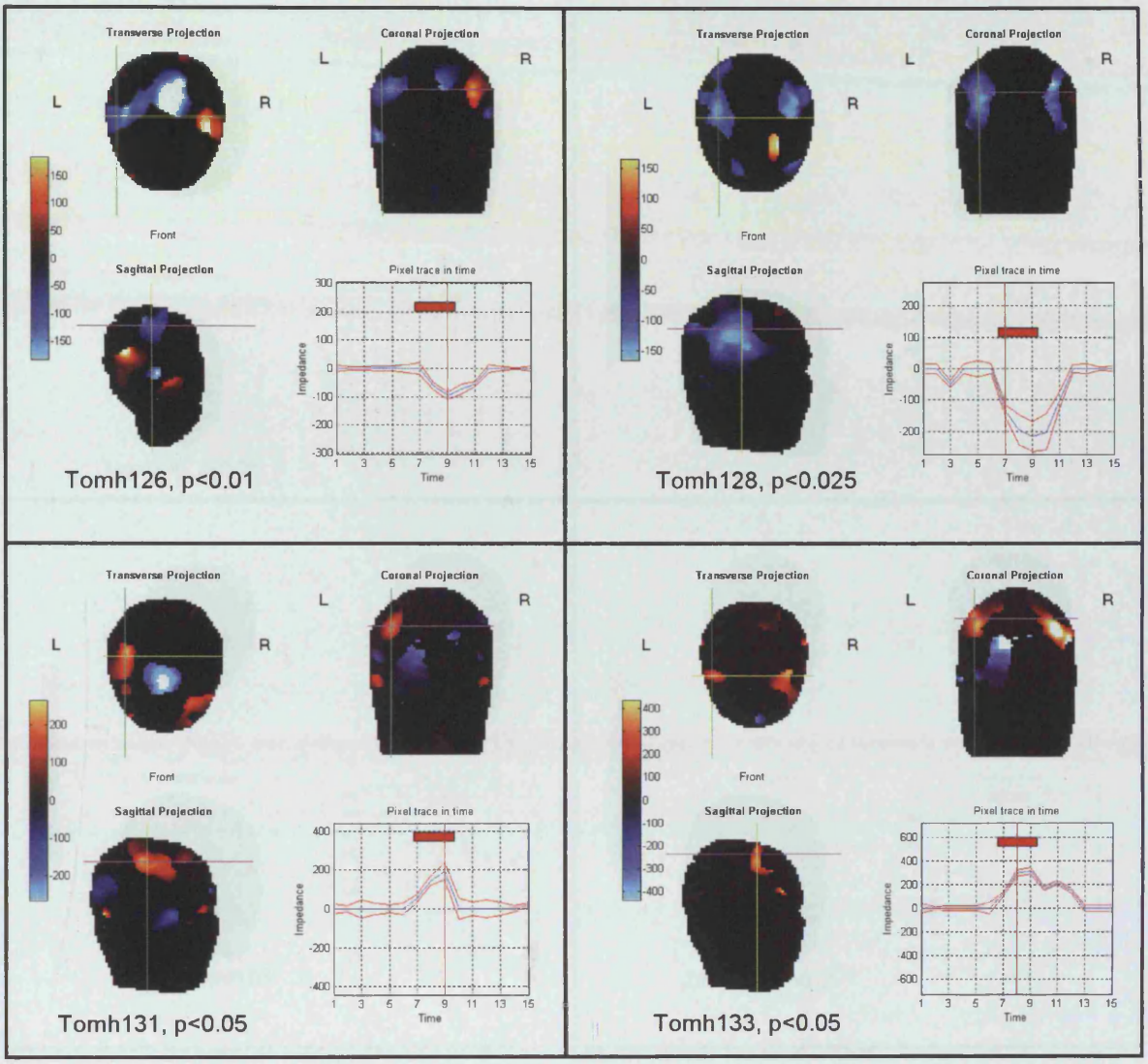

Figure 5.80 Right motor FEM images (2)
These are four sets of right motor evoked response images obtained in four adult subjects, reconstructed with the FEM algorithm. For each subject there are three orthogonal views of the head, and the relative positions of the head sections are indicated by the crosshairs. The subject number and the threshold level of the images are indicated at the bottom of each set of images.

The timecourse of the impedance (mean±SE) at the voxel centred on the cross hairs is indicated by the lower right graph in each subject. Impedance is indicated on the y-axis. Time is indicated on the x-axis in image frames, with each frame representing 25s. The timecourse of the visual stimulus and the timepoint of the image are also indicated in this graph, by the red horizontal bar and red vertical line, respectively.

Spatially large, and statistically significant impedance changes, with the same timecourse as the motor activity are seen in all four subjects over the region of the contralateral motor cortex. Significant decreases (blue) are seen in two subjects (tomh126 and tomh128) and increases (red) in two (tomh131 and tomh133).

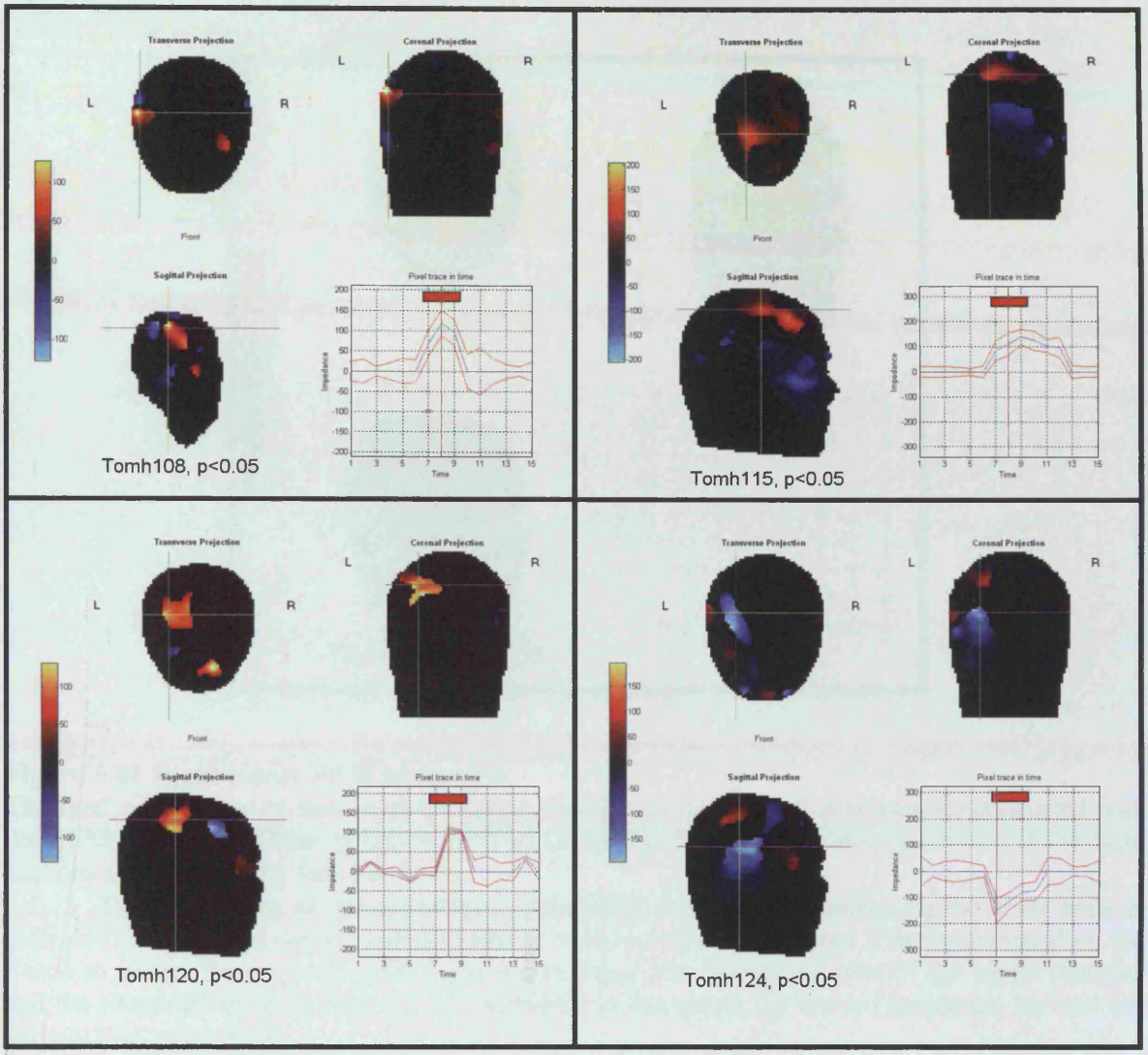

Figure 5.81 Right motor FEM images (3)
These are four sets of right motor evoked response images obtained in four different adult subjects, reconstructed with the FEM algorithm. For each subject there are three orthogonal views of the head, and the relative positions of the head sections are indicated by the crosshairs. The subject number and the threshold level of the images are indicated at the bottom of each set of images.

The timecourse of the impedance (mean±SE) at the voxel centred on the cross hairs is indicated by the lower right graph in each subject. Impedance is indicated on the y-axis. Time is indicated on the x-axis in image frames, with each frame representing 25s. The timecourse of the visual stimulus and the timepoint of the image are also indicated in this graph, by the red horizontal bar and red vertical line, respectively.

Statistically significant impedance changes, with the same timecourse as the motor activity are seen in all four subjects in the contralateral quadrant of the image to the hand stimulated which corresponds to the approximate region of the contralateral motor cortex. Significant decreases, blue changes, are seen in one subjects (tomh124), and impedance increases (red) in three subjects (tmh108, tomh115 and tomh120).

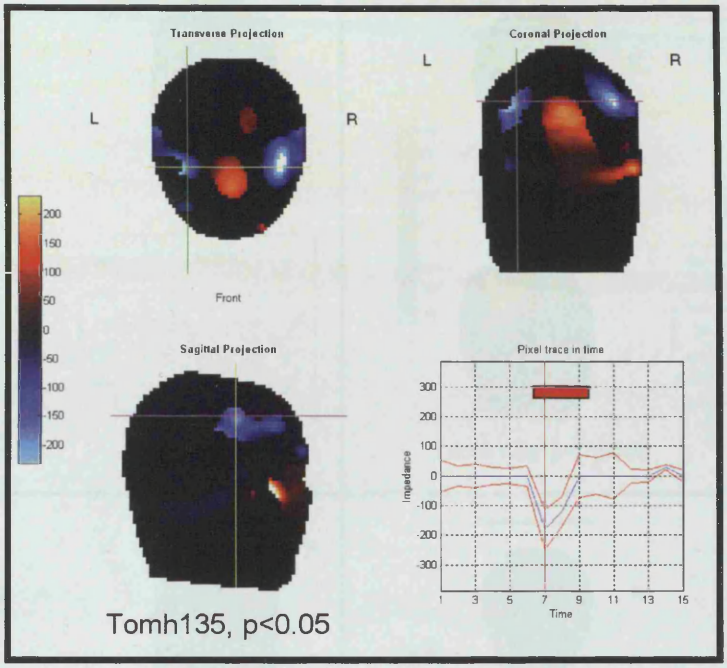

Figure 5.82 Right motor FEM images (4)
The final right motor evoked response image obtained in one subject is shown, reconstructed with the FEM algorithm. Three orthogonal views of the head, and the relative positions of the head sections are indicated by the crosshairs.

The timecourse of the impedance (mean±SE) at the voxel centred on the cross hairs is indicated by the lower right graph. Impedance is indicated on the y-axis. Time is indicated on the x-axis in image frames, with each frame representing 25s. The timecourse of the visual stimulus and the timepoint of the image are also indicated in this graph, by the red horizontal bar and red vertical line, respectively.

A statistically significant impedance decrease (blue) is seen, with the same timecourse as the motor activity, in the left side of the image corresponding to the area of the contralateral motor cortex to the hand moved. A significant decrease is also seen in the ipsilateral motor cortex region on the right, with an impedance increase (red) in the fronto-central part of the image.

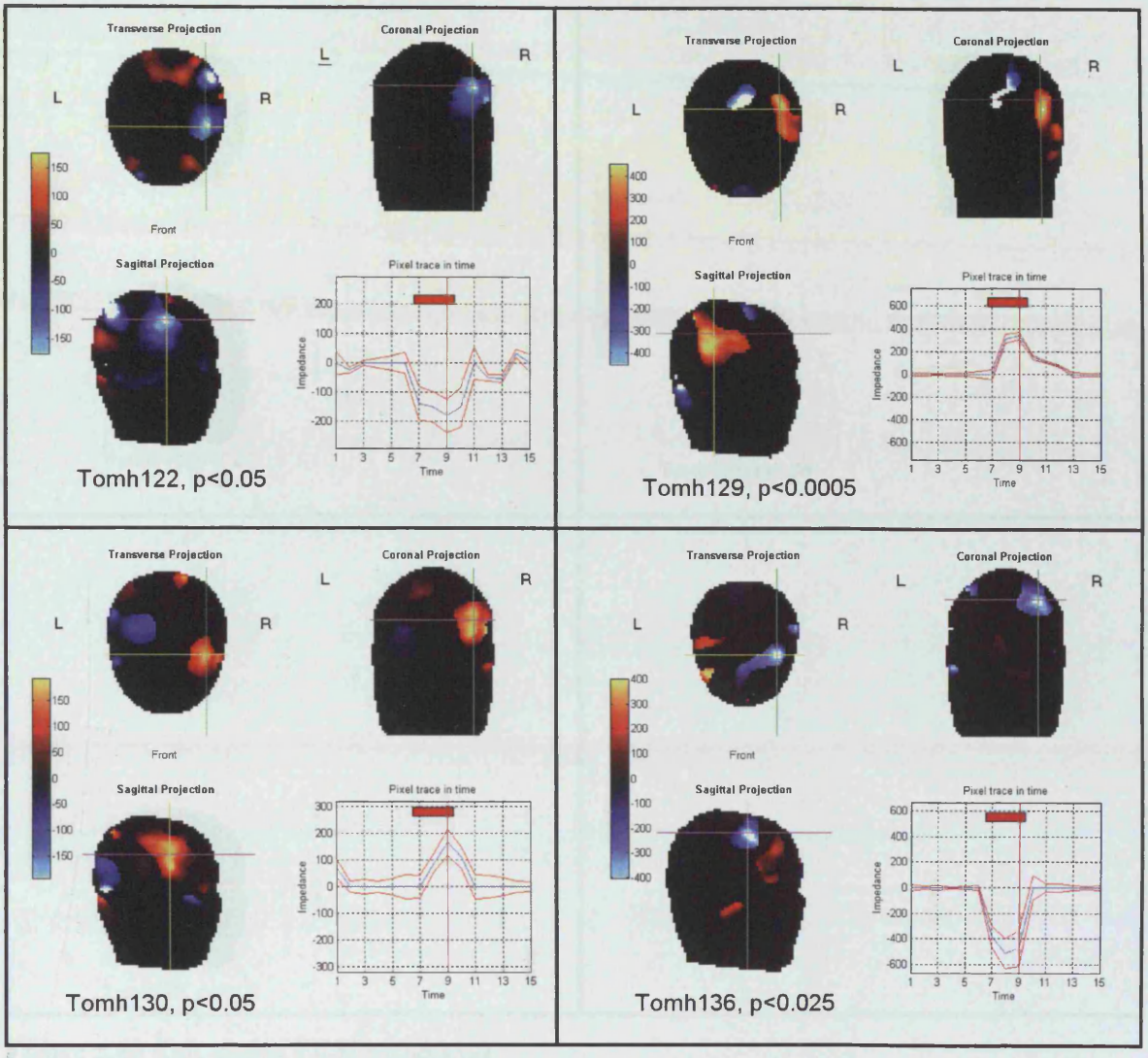

Figure 5.83 Left motor FEM images (1)

These are four sets of left motor evoked response images obtained in four different adult subjects, reconstructed with the FEM algorithm. For each subject there are three orthogonal views of the head, and the relative positions of the head sections are indicated by the crosshairs. The subject number and the threshold level of the images are indicated at the bottom of each set of images.

The timecourse of the impedance (mean±SE) at the voxel centred on the cross hairs is indicated by the lower right graph in each subject. Impedance is indicated on the y-axis. Time is indicated on the x-axis in image frames, with each frame representing 25s. The timecourse of the visual stimulus and the timepoint of the image are also indicated in this graph, by the red horizontal bar and red vertical line, respectively.

Spatially large, and statistically significant impedance changes, with the same timecourse as the motor activity are seen in all four subjects over the region of the right motor cortex, contralateral to the hand stimulated. Both significant impedance increases in red (tomh129 and tomh130) and decreases in blue (tomh122, tomg136) are seen. Smaller impedance changes are imaged elsewhere in all four subjects.

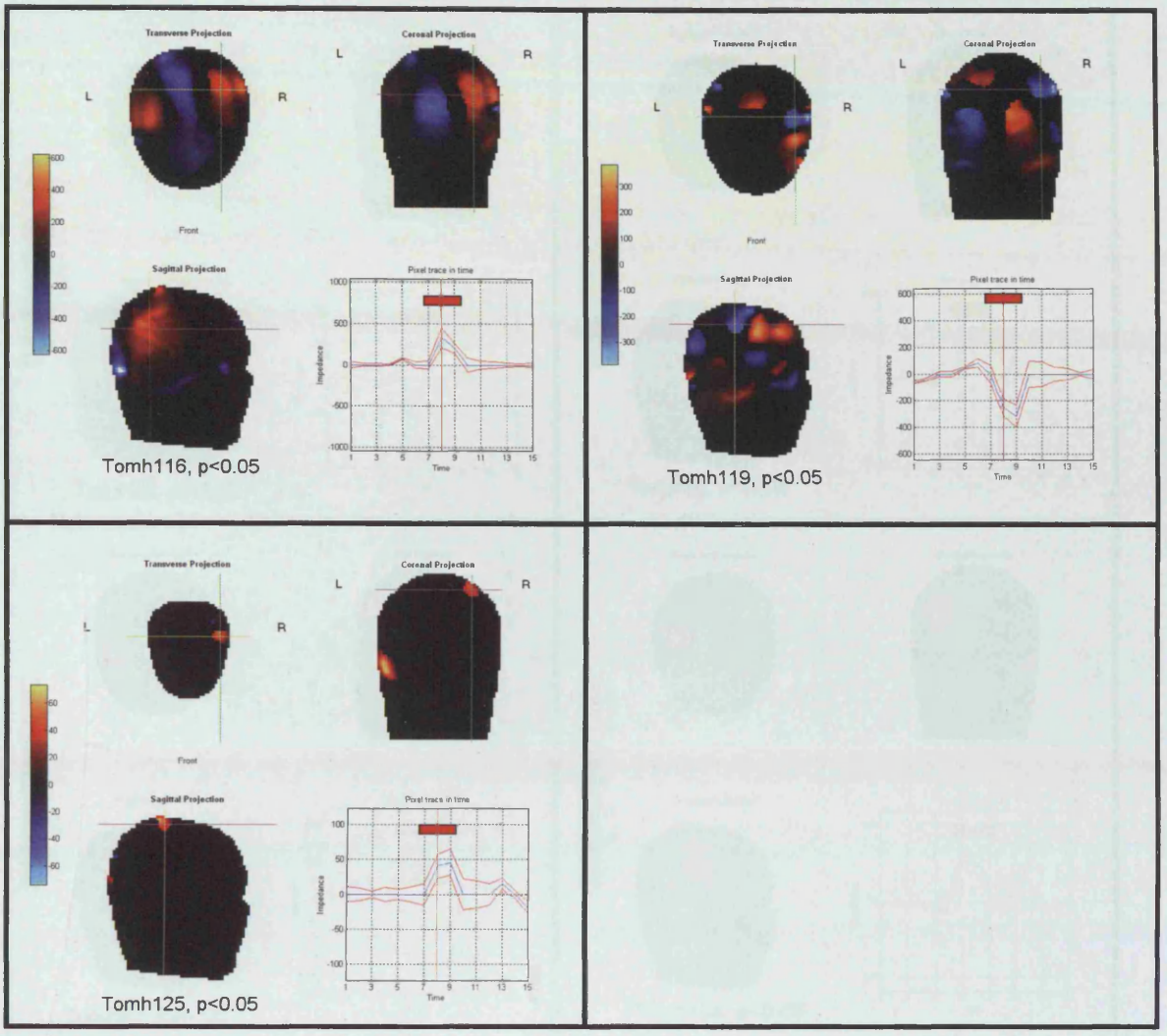

Figure 5.84 Left motor FEM images (2)

These are three sets of left motor evoked response images obtained in four different adult subjects, reconstructed with the FEM algorithm. For each subject there are three orthogonal views of the head, and the relative positions of the head sections are indicated by the crosshairs. The subject number and the threshold level of the images are indicated at the bottom of each set of images.

The timecourse of the impedance (mean±SE) at the voxel centred on the cross hairs is indicated by the lower right graph in each subject. Impedance is indicated on the y-axis. Time is indicated on the x-axis in image frames, with each frame representing 25s. The timecourse of the visual stimulus and the timepoint of the image are also indicated in this graph, by the red horizontal bar and red vertical line, respectively.

Statistically significant impedance changes, with the same timecourse as the motor activity are seen in all three subjects over the region of the right motor cortex, contralateral to the hand moved. Both significant impedance increases in red (tomh116 and tomh125) and a decrease in blue (tomh119) are seen. Smaller impedance changes are imaged elsewhere in all three subjects.

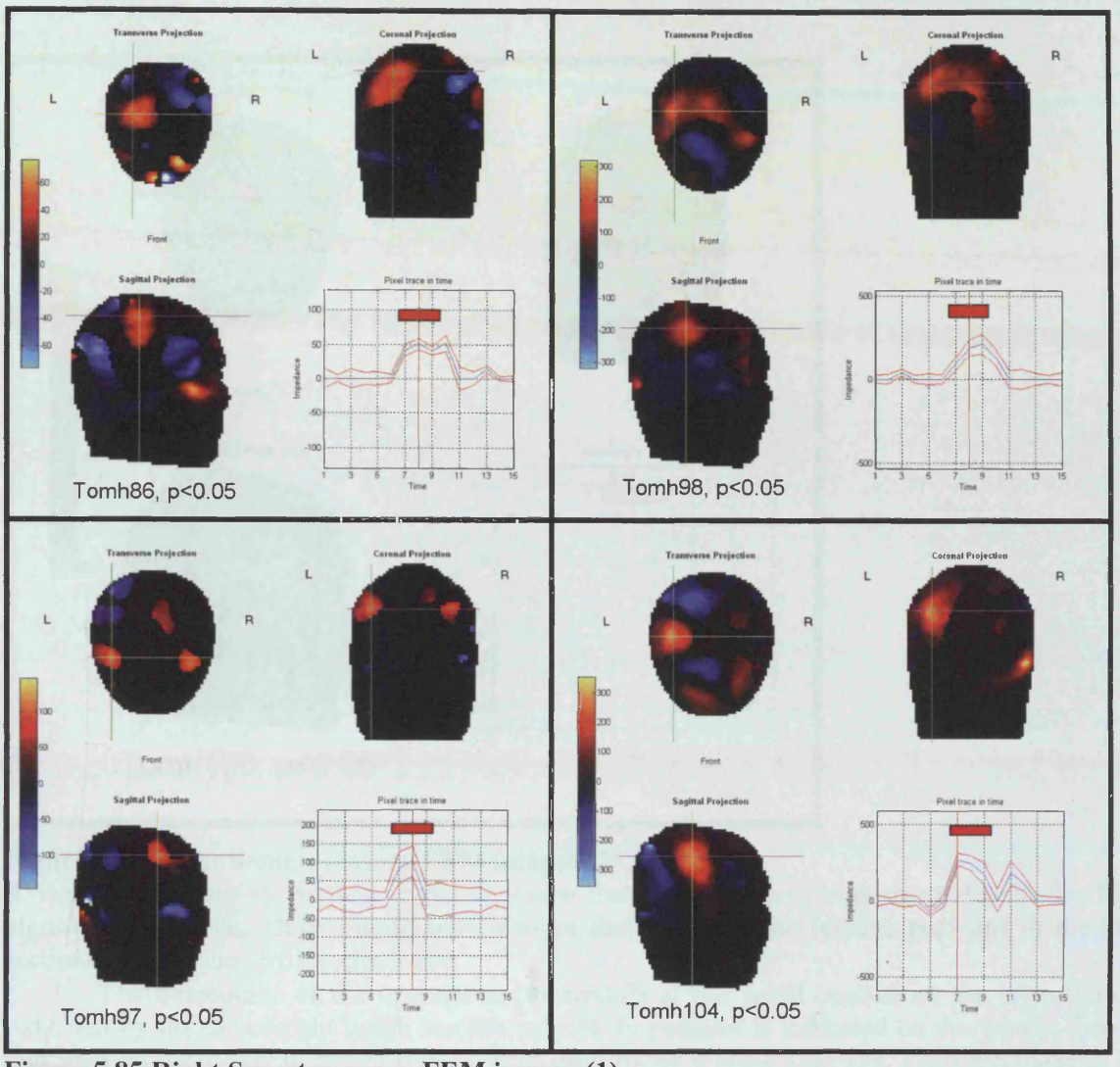

Figure 5.85 Right Somatosensory FEM images (1)

These are three sets of right somatosensory evoked response images obtained in four different adult subjects, reconstructed with the FEM algorithm. For each subject there are three orthogonal views of the head, and the relative positions of the head sections are indicated by the crosshairs. The subject number and the threshold level of the images are indicated at the bottom of each set of images.

The timecourse of the impedance (mean±SE) at the voxel centred on the cross hairs is indicated by the lower right graph in each subject. Impedance is indicated on the y-axis. Time is indicated on the x-axis in image frames, with each frame representing 25s. The timecourse of the visual stimulus and the timepoint of the image are also indicated in this graph, by the red horizontal bar and red vertical line, respectively.

Statistically significant impedance increases (in red), with the same timecourse as the somatosensory stimulus, are seen in all four subjects over the approximate region of the right somatosensory cortex, contralateral to the hand stimulated. Smaller impedance changes are imaged elsewhere in all three subjects.

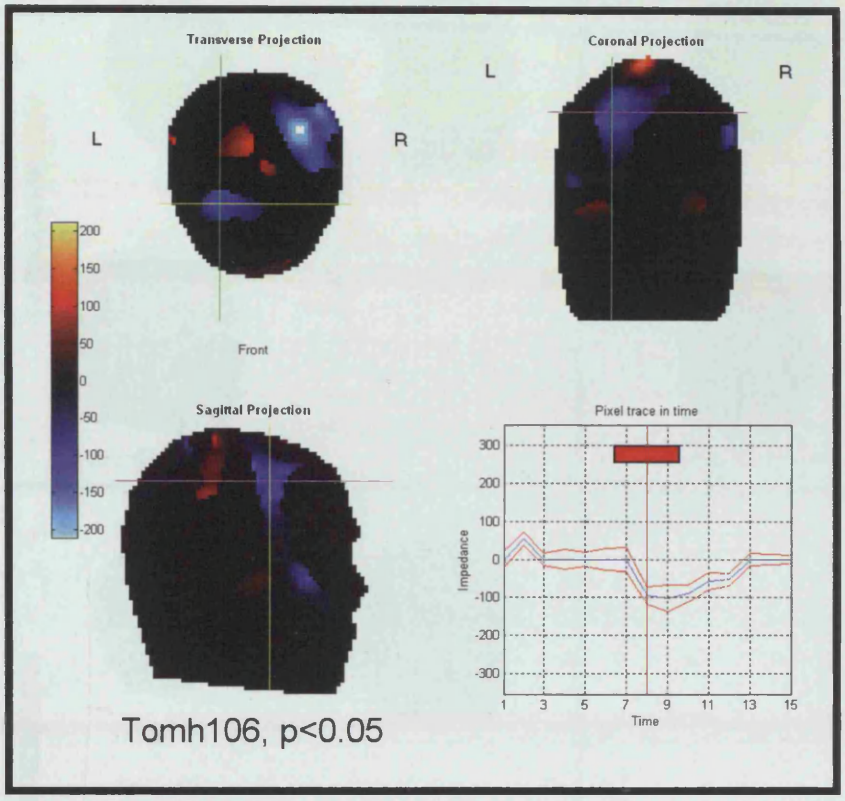

Figure 5.86 Right Somatosensory FEM images (2)
A right somatosensory evoked response image from one subject, reconstructed with the FEM algorithm, is shown. Three orthogonal views of the head, and the relative positions of the head sections are indicated by the crosshairs.

The timecourse of the impedance (mean±SE) at the voxel centred on the cross hairs is indicated by the lower right graph in each subject. Impedance is indicated on the y-axis. Time is indicated on the x-axis in image frames, with each frame representing 25s. The timecourse of the visual stimulus and the timepoint of the image are also indicated in this graph, by the red horizontal bar and red vertical line, respectively.

A statistically significant impedance decrease (in blue), with the same timecourse as the somatosensory activity, is seen over the approximate region of the right somatosensory cortex, contralateral to the hand stimulated. Other significant impedance changes are seen elsewhere in the image.

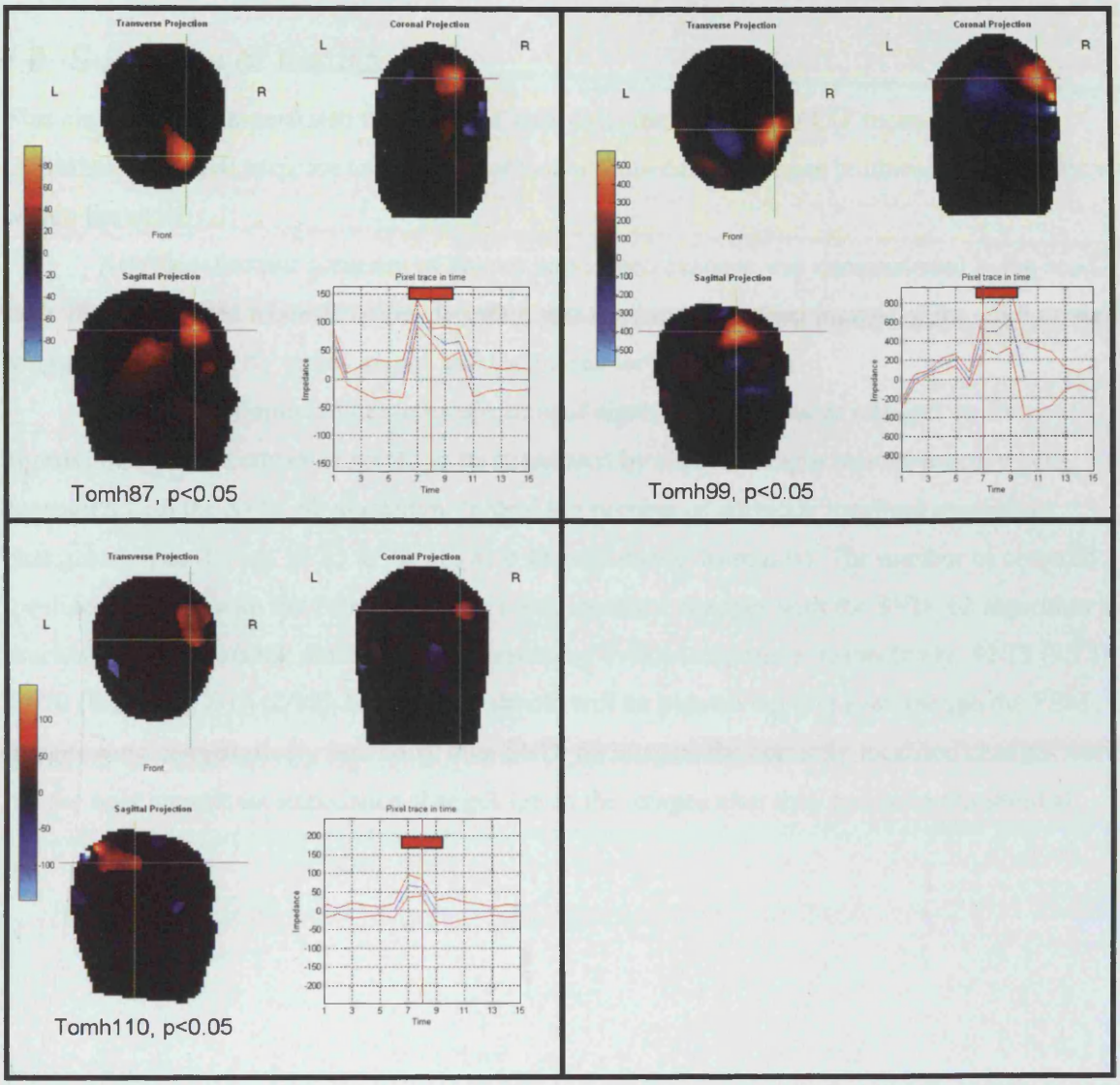

Figure 5.87 Left Somatosensory FEM images

These are three sets of left somatosensory evoked response images obtained in three different adult subjects, reconstructed with the FEM algorithm. For each subject there are three orthogonal views of the head, and the relative positions of the head sections are indicated by the crosshairs. The subject number and the threshold level of the images are indicated at the bottom of each set of images.

The timecourse of the impedance (mean±SE) at the voxel centred on the cross hairs is indicated by the lower right graph in each subject. Impedance is indicated on the y-axis. Time is indicated on the x-axis in image frames, with each frame representing 25s. The timecourse of the visual stimulus and the timepoint of the image are also indicated in this graph, by the red horizontal bar and red vertical line, respectively.

Statistically significant impedance increases (in red), with the same timecourse as the somatosensory stimulus, are seen in all three subjects. However, only two of these were present in the contralateral quadrant of the image to the hand stimulated (tomh99 and tomh110), and were considered as a correctly localised impedance change to the right somatosensory cortex. The impedance change in tomh87, although a significant stimulus related impedance change, was considered to be too anterior to be considered as correctly localised.

5.2.8 Summary of results

This chapter has demonstrated that, in head-tank data, the FEM based EIT reconstruction algorithm, produced accurate localisation of known impedance changes produced by a Perspex rod within the skull.

After localisation accuracy of known impedance changes was demonstrated in the head-tank, the FEM based reconstruction algorithm was used to reconstruct images of the adult evoked responses, produced by visual, motor and somatosensory stimulation.

A dramatic improvement in localisation of significant impedance changes to the approximate area of cortex expected to be stimulated by each paradigm was achieved, when compared with the SVD_62 algorithm. In total the number of correctly localised impedance changes increased from 19/51 to 38/51 (with 18 impedance decreases). The number of correctly localised changes with the FEM algorithm (with localised changes with the SVD_62 algorithm in brackets) was, for visual, motor and somatosensory evoked responses, respectively, 12/13 (9/13), 19/20 (8/20) and 7/18 (2/18). However, it should still be pointed out that even though the FEM images were comparatively less noisy than SVD_62 images, the correctly localised changes were not the only significant impedance changes left in the images after they had been thresholded.

5.3 Discussion

This chapter has demonstrate an improvement in the images of adult evoked responses, reconstructed with the first EIT reconstruction algorithm to use realistic geometrical and resistivity information about the human head. The images reconstructed with the FEM algorithm in this chapter produced: 1) Improvements in localisation of impedance changes, particularly with motor and somatosensory evoked responses, 2) Improved resolution along the cranial-caudal axis of the head which may have aided improved localisation of changes, particularly in somatosensory and motor cortices which lie near the apex of the head, and 3) Improved image quality with reduced electrode artefact and possibly reduced impedance artefact.

However, despite these improvements, the EIT images can still be criticised, as they remain noisy, i.e. they still contain multi-focal impedance changes, and the correctly localised impedance changes are both of a positive and negative magnitude, contrary to what is expected by a model that assumes that impedance should decrease, based on the evidence that blood volume should increase in the area of activated cortex.

The aim of this section is to examine 1) How accurate the FEM model is as a model of the human head, 2) Whether the improvements in localisation are real, 3) Why there are still impedance increases and decreases in the expected areas, and why there is residual noise in the images, and 4) Areas of future work for the FEM reconstruction algorithm.

5.3.2 Accuracy of the FEM head model

5.3.2.1 Overview

The FEM head model improves upon the homogenous sphere model of the human head used in the SVD_62 algorithm , used in Chapters 2 and 3 to reconstruct adult and tank EIT data, in the separation of different tissue layers of the head, into scalp, skull, CSF and brain, and the assignment of realistic resistivity information to each layer. In addition the FEM model also incorporated a realistic head shape. The head-tank work of Chapter 3 demonstrated that the main contribution to the localisation error of an impedance change within the tank, was the presence of the skull, whereas the effect of head-shape had no significant contribution to localisation errors. It is therefore likely that the improved images produced by the FEM based algorithm were due to the use of realistic resistivity of the separate tissue layers in the head. The accuracy of resistivity values used in the FEM model will now be considered further.

5.3.2.2 Accuracy of tissue resistivity used in the FEM model

The layers of the FEM head model were assigned different resistivity values, to simulate the resistivity of the scalp (230 Ω.cm), skull (5500 Ω.cm), CSF (56 Ω.cm) and brain (400 Ω.cm). These values were taken from the literature (Geddes and Baker 1967; Yamamoto and Yamamoto 1976; Kosterich *et al.* 1983; Kosterich *et al.* 1984; Lattikka *et al.* 2001). However not all of these values were from direct measurements of human tissues, as some were interpolated from animal studies. Therefore possible errors between the resistivity values assigned to the FEM head model and the values of resistivity *in vivo* may exist, the evidence for which will be examined for each tissue layer.

Scalp resistivity

The scalp resistivity value of 230 Ω.cm was based on data of measurements of human skin, which was stripped of the highly capacitative stratum corneum by repeated use of adhesive tape (Yamamoto and Yamamoto 1976). In this paper, the human skin was modelled as having two compartments which contributed to the overall skin resistivity, 1) The stratum corneum which is the superficial skin layer and is composed of many layers of skin cells, which provide the waterproof coating of the skin; this layer has a very high resistivity and also a high capacitance due to the multiple layers of cells, and 2) The granular skin layer, which lies underneath the stratum corneum and is of a much lower resistivity and has a negligible capacitance.

This paper calculated the resistivity of the granular layer of skin, underneath the stratum corneum, at 230 Ω.cm at 50 kHz. This probably represents a fairly accurate value of scalp resistivity, which is made up of skin, blood vessels, muscles and connective tissues, similar to the components present in the granular skin layer. This resistivity may be inaccurate underneath the scalp electrodes used to inject current, because the scalp skin also has a highly capacitative surface produced by the scalp's stratum corneum. However, in the adult EIT studies, the area of scalp under each electrode was abraded with an abrasive paste to reduce the stratum corneum, then the resistivity of the FEM scalp is also likely to be an accurate reflection of the resistivity of the scalp under each electrode in the adult EIT studies. One caution is that there are likely to be variable errors, between the FEM model and each subject, as the level of skin abrasion may have varied between subjects.

Skull resistivity

The most likely source of resistivity error in this current FEM model is in the assignment of a low resistivity value for the skull of 5500 Ω.cm. This value was obtained from bone resistivity measurements of cleaned rat femur soaked in 0.9 % saline (Kosterich *et al.* 1983; Kosterich *et al.*

1984). This value of skull resistivity is similar to measurements made in the human skull of 6700 Ω.cm measured in post-mortem skull (Oostendorp *et al.* 2000) and 7500 Ω.cm in a cleaned dried skull soaked 0.9% saline (Law 1993). However both these studies had weaknesses, discussed in Chapter 3, Section 3.4.2., due to either the preparation of the skull specimen, or due to the use of too low a resistivity bathing solution, such as 0.9% saline. I believe that the value of skull resistivity that I measured in Chapter 3, of 20,500 Ω.cm when soaked in 0.2 % saline, lies closer to the *in vivo* skull resistivity, as the resistivity of 0.2% saline is closer to that of blood, which perfuses the skull. Therefore the value of skull resistivity used in the FEM model may be as low as 25 % of the real skull resistivity value, and this needs to be considered for future FEM head models.

CSF resistivity

The CSF resistivity, of 56 Ω.cm, assigned to the FEM model was interpolated for the resistivity value of human CSF of 65 Ω.cm, measured at 25 °C (Geddes and Baker 1967), presumably extracted by lumbar puncture. A lower resistivity value was assigned to the CSF of the FEM model in order to account for the fact that CSF *in vivo* is at body temperature of 37 °C. This correction was applied based on an approximate 2% increase of resistivity for each degree C drop in temperature, extracted from brain impedance measurements made in rabbits (Van-Harreveld and Ochs 1956). Therefore the resistivity value assigned to the CSF in the FEM head model is likely to be a very accurate reflection of CSF resistivity *in vivo.*

Brain resistivity

The resistivity of the brain in the FEM model was assigned a value of 400 Ω.cm, based on direct measurements of human brain resistivity at a measurement frequency of 50 kHz in vivo, made at neurosurgery (Lattikka *et al.* 2001). In this study brain resistivity varied between grey matter and white matter, which were 391 Ω.cm (range 194 to 501 Ω.cm in 8 patients) and 351 Ω.cm (range 331 to 477 Ω.cm in 5 patients), respectively. The assigned resistivity value to the brain compartment of the FEM model therefore is very close to direct resistivity measurements made of the brain, although individuals may have grey matter resisitivites that differ by up to 25% of the assigned value.

Conclusion of assigned tissue resisitivites

After consideration of the assignment of tissue resisitivites to the different layers of the FEM model, the scalp, CSF and brain resistivities are likely to be accurate representations of *in vivo* tissue resistivities, although inter-subject variation, as seen with direct measurements of brain

resistivity in humans (Lattikka *et al.* 2001), will produce variable errors. The largest error is likely to have been an underestimate of the skull resistivity in the FEM model, which may lead to residual localisation errors in the FEM EIT images. The size of these errors are likely to be much smaller than those produced by the use of the homogenous spherical model of the head used in the SVD_62 reconstruction algorithm. The upper limit of localisation error produced by the use of the homogenous sphere algorithm, when used on EIT data acquired from the head-tank has been determined as 20% of the image diameter (Tidswell *et al.* 2001), therefore residual errors due to an underestimate of skull resistivity in the FEM head model are likely to be much smaller than this, although the size of residual error is not yet known. Correction of the low estimate of skull resistivity in the current FEM model of the head, should be performed for future iterations of the FEM head model.

5.3.2.3 Accuracy of head shape used in the FEM head model

The FEM head model used a realistic head shape obtained from MRI data in a single adult. However the reconstruction algorithm, based on this FEM model, was then applied to EIT data acquired from a number of subjects, each of which would have had a different head shape. Therefore errors could have arisen in the images, due to the error between the head shapes used in the model and the head shape of each subject.

Fortunately, evidence from the head tank data, shown in Chapter 3, indicated that significant localisation errors were only introduced by the presence of the skull in the head tank. In addition, a more detailed study has looked at the effect of head-shape directly by a comparison of EIT images acquired of an object two different tank phantoms: 1) The head-tank and 2) A hemi-spherical tank which more closely resembled the spherical head model used to reconstruct the EIT data (Tidswell *et al.* 2001). This study showed no significant effect of head shape on localisation of the impedance change in the reconstructed images from the hemispherical and head tanks. From the evidence of this study, it is unlikely that significant localisation error should be produced by the use of a particular head-shape in the FEM model when used to reconstruct EIT data obtained from slightly different head-shapes.

The effect of different head shapes is therefore unlikely to have had a significant effect on localisation errors, however the advantage of using the realistic head shape in the FEM based reconstruction algorithm, is that the appropriate areas of the head were much easier to visualise in the head-shaped images, when the assessment of the localisation of significant impedance changes in the images was performed.

5.3.2.4 Evidence for real improvement

I believe that there was a dramatic qualitative improvement in the EIT images with the use of the FEM reconstruction algorithm. There was suppression of electrode noise at the peripheries of the images (which were apparent in the SVD_62 images) and in addition the impedance changes left after thresholding were clearer (possibly due to improved resolution of the images along the cranial-caudal axis of the head). This subjective improvement in image quality has also been demonstrated by a comparison of several different observers, both for head-tank data and some of the adult EIT images (Bagshaw *et al.* 2003). In the same paper the FEM algorithm was demonstrated to have better resolution, as determined by measurements of the FWHM of known impedance changes in head-tank data.

The subjective improvement in image quality has also been borne out by the improvements in image localisation of significant impedance changes in the adult evoked response images shown in this chapter. The number of correctly localised changes with the FEM algorithm (with localised changes with the SVD_62 algorithm in brackets) was, for visual, motor and somatosensory evoked responses, respectively, 12/13 (9/13), 19/20 (8/20) and 7/18 (2/18), with largest improvements seen with motor and somatosensory evoked impedance changes.

The improvement for motor and somatosensory responses are probably related to the position of the motor and somatosensory cortices, which lie in the superior part of the head, adjacent to the skull. In the SVD_62 images, this represented the top 2 image slices which often contained electrode artefact and had a very small pixel area when compared to image slices more inferior in which visual evoked response changes were seen. In comparison, the FEM images represent the approximate areas of the motor/somatosensory cortices by approximately 15-20 image slices. This improvement in resolution has probably allowed: 1) Clearer visualisation of impedance changes in the top image slices and 2) Clearer separation of electrode artefact (which was reduced in the FEM algorithm) from the stimulus related impedance changes of the head. This combined with an improvement in resolution of impedance changes seen in tank work (Bagshaw *et al.* 2003), has enabled real improvements of identification of significant impedance changes in the somatosensory and motor cortices, which has led to the improved localisation of changes with the FEM algorithm.

The final evidence for an improvement of the FEM images, is the difference in the SVD truncation level used in the inversion of the sensitivity matrix produced by the FEM and spherical head models, which were 70 and 62 singular values, respectively. The truncation level for the SVD_62 algorithm was limited by the amount of noise introduced into the reconstructed EIT images; higher truncation levels introduced higher levels of image noise. However the SVD value

obtained for the SVD_62 algorithm was much lower than that expected by the level of noise in the raw impedance data (the expected range was around 70 singular values), and it was thought that it was errors between the homogenous sphere algorithm and the human head that was the cause of the introduction of image noise (Gibson 2000). The higher level of truncation for the FEM algorithm corresponded more closely to the level of noise present in the raw impedance data (Bagshaw *et al.* 2003), which suggests that less error was present between the FEM model and the human head than with the homogenous sphere model of the head. In addition the higher truncation threshold used for the FEM model algorithm produced qualitatively less image noise in the reconstructed images. As both algorithms were used on identical data, the reduced FEM image noise was not due to improved signal to noise in the EIT data, which again suggests that EIT image errors are minimised by the use of an accurate reconstruction model for the head. The benefit of the higher SVD truncation threshold, is that more signal from the raw impedance data is reconstructed into the images, which, in addition to reduced image noise, has led to improved image quality and image localisation.

5.3.2.5 Evidence against real improvement

In contrast, there is much less evidence that the FEM algorithm has not improved image quality. However, one argument against a significant improvement produced by the FEM images is that there has not been a like-for-like comparison of FEM and SVD_62 images, as the resolution of the SVD_62 EIT images was 40x40x6 (voxels in longitudinal, transverse and cranial-caudal directions, respectively) compared to 71x51x69 for the FEM algorithm.

The significant compression of image data along the cranial caudal axis (69 slices for the FEM images, compared to 6 slices for the SVD_62 images) was chosen for the SVD_62 images, due to the limits of computer hardware and data storage at the time of the adult EIT work. In retrospect this was probably an error, as the reduced resolution has probably contributed to a failure to localise impedance changes in the superior image slices, particularly in areas of the motor and somatosensory cortices. This failure may be due to 1) Decreased resolution, so more difficult to identify a significant change, and 2) Aggregation of pixels which contain electrode noise and impedance signal from the evoked response. Therefore, in order to reliably demonstrate that the FEM algorithm has improved image localisation, then it should have been compared to SVD_62 images of a similar resolution. It is unlikely that this work will be performed, as the image quality improvement seen with the FEM images will ensure that FEM algorithms of the head are used exclusively in future EIT work. Despite the lack of a direct comparison, I attempted to perform this in Figure 5.74, by comparing SVD_62 images of visual evoked responses with FEM images sliced in the same areas corresponding to the SVD_62 image slices, which demonstrated a qualitative

reduction in image noise and improvement in the imaged impedance changes with the FEM algorithm, which again suggests that part of the improvement in image localisation is linked with the use of an accurate forward model of the head in the reconstruction algorithm, rather than all the improvement linked with improved resolution.

5.3.3 Discussion of problems in the FEM images

Despite improvements of the FEM images and a much improved localisation of significant impedance changes to the expected cortical area, two main problems with the FEM EIT images remain: 1) Multiple significant impedance changes were present in many images, and 2) Correctly localised impedance changes were still increases or decreases, in contrast to the expectation of impedance decreases from the hypothesis that blood volume changes in activated areas of cortex.

Presence of multiple impedance changes

The problem of multiple impedance changes was discussed extensively at the ends of both the adult and neonatal EIT chapters (Chapters 2 and 4, respectively). The main conclusions from these chapters was that the presence of multiple impedance changes in the EIT images is likely to be due to the presence of multiple impedance changes in the head, with or without impedance artefact produced by these impedance changes, with a probable contribution of image errors introduced by the use of a homogenous sphere algorithm on EIT data acquired from the head.

Some of the image errors produced by the spherical head model in Chapter 2 have probably been reduced by the FEM algorithm. This is supported by 1) A qualitative improvement in the images in which less electrode artefact and image noise is generally seen, 2) A quantitative improvement in the resolution of impedance changes in FEM images on head-tank data (Bagshaw *et al.* 2003), and 3) The higher SVD truncation threshold used to invert the sensitivity matrix for the FEM forward model compared to the spherical forward model indicates an improvement of image errors. Despite these improvements, some image errors remain as not all electrode artefact has been abolished from the reconstructed images, and, from the head-tank images shown in Figure 5.72 and Figure 5.73, it is apparent that artefacts, of opposite sign to the main impedance change, are still present in the EIT images. Therefore, some of the stimulus related impedance changes are likely to be represented by impedance artefact and will in part contribute to multiple impedance changes in the images.

The other likely contribution to multiple image changes is the presence of multiple impedance changes within the brain, proposed in the discussion sections of Chapter 2 and Chapter 4. There is supportive evidence from some functional imaging literature to support multiple areas of blood flow change in both adults (Mentis *et al.* 1996; Mentis *et al.* 1997; Mentis

et al. 1998; Nirkko *et al.* 2001) and in neonates (Isobe *et al.* 2001; Erberich *et al.* 2003). These papers have been discussed in Chapter 4, so the arguments supporting multiple impedance changes will not be re-iterated here. It is worth mentioning that many functional imaging papers average changes across groups of subjects, in which case multiple areas of activation with wide inter-subject variation will not be apparent on the final thresholded images. This was not possible to perform with the FEM EIT images of the adult evoked responses for two reasons: 1) The localisation of the impedance changes varied slightly in the approximate area of the cortex expected to be stimulated by the paradigms, and as there is no method of co-registering the images (as performed for fMRI and PET studies), then these inter-subject variations would have produced no significant change on statistical analysis of the combined images, and 2) The impedance changes imaged were both impedance increases and impedance decreases, which would have resulted in cancellation of the impedance signal between subjects and again produced no significant change on a statistical analysis of the images for all subjects with a particular stimulus paradigm.

In conclusion, despite improvements of localisation, multiple impedance changes remain in the images which are significant and related to the timecourse of the impedance changes. These imaged changes are likely to be either impedance artefact of opposite sign to the actual impedance change within the head, or that they represent multiple, real impedance changes within the head – for which there is supportive evidence from some of the neuroimaging literature. One of the main problems for the interpretation of the EIT data, is whether the imaged change in the area of cortex expected to be stimulated is a real physiological change, or the chance occurrence of an artefactual impedance change which just happens to be in the correct area.

I think it is unlikely that the impedance changes have occurred in the correct area of the images purely by chance, as a large proportion of the motor and somatosensory and visual evoked images with a significant stimulus related change have that change in the right area, in addition, for the motor and sensory studies, these changes are present in the contralateral area to the hand stimulated and are either not apparent, or much smaller, in the ipsilateral cortical area. If these images changes had appeared by chance, due to the presence of multiple impedance changes in the images, then I would have expected that an equal number of images would have shown changes in either the contralateral and ipsilateral sensorimotor areas. As this was not the case, then it is highly unlikely that the presence of multiple imaged impedance changes produced the correct localisation in the FEM images, although I accept that a small proportion of correctly localised changes may have been produced by artefact produced by a real impedance change elsewhere in the head.

Presence of impedance increases and decreases

The EIT images produced by the FEM head algorithm when used on the adult evoked response data, improved image localisation of significant impedance changes, to 38/51 images. Of these changes 18 were impedance decreases, which can easily be explained from the neuroimaging evidence that both blood flow and blood volume increase in the active area of cortex, and as blood has a lower resistivity than the brain, a local cortical impedance decrease is produced (See Chapters 1, 2 and 4 for more discussion).

However 20 of these impedance changes were increases, which is not immediately accounted for by the hypothesis that cortical blood volume is increased in activated cortex. One argument is that these impedance increases are not real, but represent impedance artefacts of opposite sign to a stimulus related impedance decrease elsewhere in the head. Although this may account for some of the correctly localised impedance changes, I do not believe it accounts for the majority of the correctly localised changes as: 1) There is a bias in the motor and somatosensory studies for the impedance increases to be correctly localised and are therefore unlikely to arise by chance, and 2) There are not an equal number of impedance increases in the opposite side of the head, which again should be expected by the chance production of impedance artefact from a randomly placed impedance change within the head. As there is no proof to either confirm or exclude the correctly localised changes as real or artefact, I will not take this discussion much further, but assume from the high number of correctly localised impedance increases that these changes are real and reflect a physiological phenomenon in the area of activated cortex.

If we assume that these correctly localised impedance increases are real, then a plausible mechanism for their genesis needs to be proposed. Previously, in Chapters 2 and 4, it has been suggested that increased cortical impedance can be explained by several mechanisms 1) Decreased blood volume in the activated cortical area – which is highly unlikely when nearly all the evidence of both the adult human and animal functional imaging literature supports an increase in regional cortical blood flow and volume in response to activation, 2) Cell swelling – for which there is no definite evidence from either human or animal studies during physiological levels of stimulation (although cell swelling does occur in extremes of neural activity such as epilepsy (Andrew and MacVicar 1994)), 3) Decreased cortical temperature – again unlikely as cortical temperature changes in humans occur over minutes of stimulation (Yablonskiy *et al.* 2000) and would not produce the timecourse of the adult impedance changes, and 4) CSF changes over the area of activated cortex.

It is the last proposed mechanism, that of CSF volume change, that is most likely to account for the impedance increases, and as this would be produced under the condition of an

increase in cortical blood volume, then this mechanism is entirely consistent with the findings from the neuroimaging literature, and the results of EIT changes in rabbits (Holder *et al.* 1996). To understand how CSF volume change over the area of activated cortex, the resistivity of the relevant tissues, the brain, blood and CSF need to be known, which are 400 Ω. cm, 150 Ω.cm, and 56 Ω.cm, respectively. If regional cerebral blood volume (rCBV) is increased due to increased neural activity, then the area of affected cortex will undergo an impedance decrease due to the presence of an increased volume of blood of lower resistivity than the surrounding cortex. However, if the increased rCBV pushes that area of cortex outwards into the thin layer of CSF that surrounds the brain, an equivalent volume of low resistivity CSF will be displaced away from the area of activated cortex. As CSF has a lower resistivity than that of blood, then the overall impedance for the volume that contains the activated cortex, increased rCBV and the displaced CSF will be an impedance increase. The reason that this may occur in some subjects and not in others may be related to how near the cortical surface the change in rCBV occurs in response to stimulation and whether the activated area of cortex is adjacent to the CSF layer, or buried within a cortical gyrus. As yet there is no evidence to support this hypothesis, although possible experiments designed to measure this effect may be possible in future work (which will be discussed in the concluding chapter of this thesis).

5.3.4 Conclusions

The reconstruction algorithm based on the finite element model of the human head has been demonstrated to work on head-tank EIT data and has also been demonstrated to improve image localisation when applied to the adult evoked response impedance data, in addition to an improvement of image noise. Most of these improvements are likely to be due to the incorporation of realistic anatomical and resistivity information in the four main tissue layers of the head, as from head-tank work in Chapter 3, the presence of the skull produced the largest localisation errors in the EIT images.

The FEM model has not totally cleared up the impedance images (and was not expected to), as multiple impedance changes remain in the images and these changes consist of both impedance increases and decreases. These findings can be explained by feasible mechanisms of physiological impedance change, both in the area of cortex stimulated and elsewhere in the images, and some of these explanations have support from the neuroimaging literature. There still remains image artefact in the head-tank images reconstructed with the FEM algorithm, which are likely to be present in the adult FEM images, but despite this a significant improvement in the localisation of impedance changes was achieved when compared to the reconstruction algorithm based on a model of the head as a homogenous resistivity sphere.

Despite some of the remaining problems with the EIT images reconstructed with the FEM algorithm, it is important to recognise that this is the first working FEM model of the head used to reconstruct the EIT data and there are still improvements that can be made. These improvements consist of adjustments of the skull resistivity to a value that I believe more closely represents that of the human skull *in vivo*, finer FEM meshes, FEM modelling of the electrodes where current injection takes place, incorporation of white matter and ventricular CSF within the brain compartment of the FEM head model, and finally the application of a FEM head mesh to the neonatal head. Even though there are all these improvements that can, and probably will, be made, I have been greatly encouraged by the results of this chapter, in particular with the improved localisation of impedance changes in adult EIT evoked response data, produced by this reconstruction algorithm based on an early FEM head model.

Chapter 6: Discussion

6.1 Progress Made During This Work

This thesis has described the first work that has detected impedance changes from the human head during evoked brain activity. It is worth reviewing whether this thesis has met the objectives laid out in the introduction of Chapter 1. These were:

1. The primary objective to determine whether scalp impedance measurements could detect the cerebral impedance changes during brain activity.

2. The secondary objective was to determine whether these changes could be reconstructed into images and be localised to the expected areas of cortex stimulated.

The work in Chapter 2, demonstrated that, for the first time, that human brain activity produced reproducible, stimulus related impedance changes that could be detected with scalp impedance measurements. These changes had a similar timecourse to haemodynamic changes detected with fMRI and NIRS, and I demonstrated that as these changes did not arise from the scalp directly, the changes were likely to have arisen from changes of cerebral impedance. I also demonstrated the first 3-dimensional EIT images of human brain activity, reconstructed from these changes. However, localisation of significant impedance changes to the expected area of cortex stimulated was only demonstrated in a third of the experiments, and the EIT images were noisy. A possible reason for this was that the reconstruction algorithm, based on a forward solution which modelled the head as a sphere of uniform resistivity, produced reconstruction and localisation errors when applied to the head, which was head-shaped and contained a highly resistive skull.

In Chapter 3, I developed a tank-phantom that simulated some of the properties of the human head, notably the head shape and the presence of a real human skull. This was designed to validate the reconstruction algorithm, based on the spherical model of the head, when used to reconstruct data acquired from a head shape with or without the presence of the skull. These studies indicated that although the spherical reconstruction algorithm was sufficient to image small impedance changes within the skull, a localisation error of up to 20% of the image diameter was introduced by the presence of the skull. Although these findings did not account for all the localisation errors seen in the adult EIT images, they indicated that some of the image errors were due to reconstruction errors introduced by the difference between the forward model and the head-shaped tank with the skull. The conclusion from this work was that the reconstruction algorithm needed a more accurate

forward solution, and that it was likely that part of the difficulties encountered in localising an impedance change due to brain activity could have been due to the presence of multiple impedance changes within the brain which could not be independently localised with EIT.

In Chapter 4, I extended the use of EIT to imaging neonatal brain function. It was possible that the neonate would reduce reconstruction errors, as the neonatal skull resistivity is low and therefore the homogenous spherical forward model is a more accurate simulation of the neonatal head than that of the adult. The neonatal studies also offered the chance of imaging functional activity in a potentially less physiologically complex brain. The results of these studies were similar to that of Chapter 2, in that reproducible impedance changes could be measured during visual and passive motor stimulation in the neonate. The EIT images were an improvement over the adult EIT images, in that two-thirds of the images demonstrated a correct localisation of the impedance changes.

In Chapter 5 , the adult evoked response impedance data, obtained in Chapter 2, was reconstructed with the first EIT reconstruction algorithm, produced by my colleagues, from a FEM model of the adult head. This produced a dramatic improvement in the localisation of the impedance changes to the region of the cortical area expected to be stimulated by each paradigm. In addition there was a general improvement of image quality. Although this improvement was in part due to the increased resolution of the FEM images along the cranial-caudal axis of the head, it was also in part due to improved localisation and a reduction of image errors produced by the FEM algorithm, when compare to images reconstructed with the SVD_62 reconstruction algorithm used in Chapter 2. I believe that the improvement in image localisation seen in this chapter has boosted the credibility of EIT, in that it now seems more capable of being able to image impedance changes in the human head.

In the work in this thesis, I have developed the use of EIT and obtained the first measurements from adult and neonatal subjects. In addition, the work in neonates has proved that EIT is a viable, bedside neuroimaging method. Although the EIT images could be improved further, this research indicates that EIT will be detect the much larger impedance changes associated with abnormal brain pathology such as those produced by seizures, stroke and in the newborn, hypoxic-ischaemic damage. EIT would therefore be used to provide useful, bedside clinical information about the brain, which is currently unattainable with existing neuroimaging technologies.

6.2 Conclusions and Future Work

6.2.1 Mechanisms of the cerebral impedance changes

This work has demonstrated that impedance changes can be measured from the human head during sensory and motor activity. Both impedance decreases and increases were observed. As the changes did not arise from the scalp (Chapter 2, (Tidswell *et al.* 2001)), the likely source of the impedance changes is the brain, and the likely mechanism due to increased blood volume (Section 2.4.1.2 and Section 4.4.2.3) as a consequence of increased blood flow to supply extra oxygen to the region of the brain which undergoes an increase of neural activity (Hoge *et al.* 1999; Hoge and Pike 2001; Logothetis *et al.* 2001). Support for this hypothesis is also derived from the timecourse of the impedance changes, which resemble the timecourse of regional cerebral blood volume changes measured with NIRS (Meek *et al.* 1995)(Section 4.4.2.2). However, if this hypothesis is correct, I would only expect to see impedance decreases in the EIT images. This would be predicted from the results of other studies, particularly the rabbit EIT studies (Holder *et al.* 1996), and human PET (Mazziotta and Phelps 1984; Fox *et al.* 1986; Chugani *et al.* 1987), fMRI (Kim *et al.* 1993; Ogawa *et al.* 1993; Schneider *et al.* 1993) and NIRS (Kato *et al.* 1993; Villringer *et al.* 1993; Meek *et al.* 1995) studies of brain function. As blood has a lower resistivity than the surrounding brain, an increase in rCBV will decrease impedance.

The findings of impedance increases in the EIT images are not explained by the hypothesis of increased rCBV alone and are one of the main areas where the changes found in the EIT images of both the adult and neonatal studies differ from those expected from an examination of the functional imaging literature. Explanations for impedance increases are either: 1)Physiological: due to decreases in rCBV, increases in cell swelling (discussed in Chapter 2, section 2.4.1.2 and Chapter 4, section 4.4.2.3) or contributions from changes in CSF volume over the area of cortex that undergoes increased rCBV (discussed in Chapter 2, section 2.4.1.2), or 2) Reconstruction artefacts (discussed in Chapter 3, section 3.4.4, Chapter 4, section 4.4.2.3 and Chapter 5, section 5.3.3).

Despite many possible confounding factors that may be present in the EIT images, I believe that the main source of impedance change in the human head is due to increased rCBV in the area of activated cortex, and that this mechanism accounts for most of the correctly localised impedance decreases and impedance increases (via a shunt of CSF away from activated cortex) seen in the EIT images. A contribution to some of the correctly localised impedance changes is likely to exist from impedance artefact, but does not account for the majority of the changes

imaged, and in addition a theoretical contribution from cell swelling to the overall impedance change should be considered.

I propose that the resolution of the underlying mechanism of cerebral impedance changes could be achieved with multi-frequency EIT. During the final stages of this thesis, work by Rebecca Yerworth in collaboration with Medical Physics at UCL and Sheffield, has produced a multi-frequency EIT system intended for neuroimaging. This system, the UCLH Mark 2, can be used to measure impedance at a wide range of frequencies from 2 kHz to 1.6 MHz.

If the evoked response experiments were repeated using this equipment, then the time course of impedance changes produced by changes in blood volume or cell swelling could be separated out, in addition to changes of local CSF. This is because changes in blood volume would be expected to be relatively frequency invariant in comparison to changes in cell swelling, which would have a greater effect at low frequencies, but a reduced effect at high measurement frequencies. Blood flow changes may have some frequency variance, while CSF changes should be frequency invariant. It may then be possible to try to identify these different frequency dependent or independent responses by the use of multi-frequency EIT Further functional imaging experiments with this system, could therefore provide information about the underlying mechanism of the impedance changes, which the experimental work in this thesis has been unable to address.

6.2.2 Improvements to experimental design

Improvements to the experimental design would either be in the design of the experimental paradigms used to produce the impedance changes, or improvements to the EIT equipment in order to reduce noise

Improvements to concentration during the experiments

Part of the reason for poor localisation, may have been due to the experimental design. This consisted of the presentation of a stimulus or motor movement within a baseline period in which the subject did nothing for several minutes. This might have failed to control the concentration of the subjects during the baseline conditions. If the subjects became drowsy during the baseline condition, then a reduction in CBF and an impedance increase would be expected, from studies of blood flow and impedance during sleep. PET studies in humans, performed during the onset of sleep, have demonstrated that CBF is reduced (Braun *et al.* 1997), and in rats, intracortical electrodes have detected impedance increases of up to 20% during sleep (Ranck 1966). If these occurred during the baseline condition, and were suddenly reversed during the stimulus condition (as the subject awoke), then this could have introduced impedance changes which were not related to the stimulus, and therefore cause localisation failure of the impedance change in some subjects.

If further functional imaging studies were to be performed with EIT, then I would suggest shortening the period of each experiment in order to reduce the possibility of sleep, which is now a possibility with the faster Mark 1b and Mark 2 UCLH EIT systems. In addition, in order to maintain concentration, I would develop a fixation task for the subjects, i.e. to visually track a moving dot on a screen during baseline and stimulus conditions, in order to maintain their attention; as the task would be performed continuously during the experiment, task related impedance changes would remain constant throughout the duration of the experiment, and only stimulus related impedance changes imaged.

Improvements to electrode placement and design

One improvement that could be made is to the electrodes. Various headnets have been developed for use in EEG, to enable the rapid application of a large number of electrodes to the human head. An example is the Geodesic net (Tucker 1993; Csibra *et al.* 2000; Johnson *et al.* 2001), which has been used for high density mapping of evoked responses in adults and in neonates. The potential advantage that a head-net would offer is that it would enable increased numbers of EIT electrodes to be applied to the head, and allow for increased numbers of scalp impedance measurements, which may improve resolution of EIT with the cost of increased noise in the individual impedance measurements. An additional advantage of reduced electrode movement and improved electrode position placement may also be achieved with such electrodes.

6.2.3 Improved EIT image reconstruction

Improvements to forward model

Additional improvements to the forward model could be made to improve image reconstruction and reduce reconstruction errors. In Chapters 2 and 4, the inaccurate localisation of impedance changes in the adult and neonatal EIT studies may have been due to the use of a spherical model of the head in the reconstruction algorithm. In Chapter 5, an improvement in the correct localisation of impedance changes was achieved through the use of a reconstruction algorithm based on a FEM model of the head and included realistic information about geometry, tissue layers and tissue resistivity.

In the future, I expect that more information will be incorporated into the FEM models. Obvious areas of improvement are realistic electrode models, so that current application to the head is solved more accurately than with the FEM model in Chapter 5, in which point electrodes were assumed. In addition there could be improved separation of the brain compartment of the FEM to separate the grey and white matter from the brain (which have slightly different electrical

properties (Ranck 1963; Lattikka *et al.* 2001)) and include the intra-cerebral CSF spaces. The resolution of the FEM model could be increased, as computing power increases, in order to reduce potential errors from unequal FEM elements, and finally the FEM could incorporate information about tissue anisotropy in order to realistically simulate the different resistivities of tissues in different orthogonal planes. The work I would like to do, is to reanalyse the neonatal EIT data with a FEM reconstruction model of the neonatal head which incorporates information about the fontanelles, which are effectively low resistivity holes in the neonatal skull, to see if subsequent improvements in image localisation are achieved.

Improvements to inverse solution

One criticism of the use of SVD in the inversion of the sensitivity matrix is that the optimal truncation level had to be determined by an analysis of the EIT images reconstructed at different SVD truncation levels (Chapter 2 and 4). Although this method used predetermined criteria, such as the presence of image noise and the presence of electrode artefact to exclude truncation levels which were too high, I feel that some method of automating the truncation level is required. As the truncation level is dependent on the combined error from the noise in the raw EIT data, and the errors between the forward model and the head (Breckon 1990; Gibson 2000), then I would expect that as the forward model is improved, a higher truncation value would be required, and the selection of an optimal truncation level would be limited by the noise in the data, and computational error. As the noise in the data can be determined, then this would be the ideal method of setting the optimal truncation level. Although this seemed to be improved with the FEM reconstruction algorithm in Chapter 5, where the truncation level did correlate with the noise in the raw data, some noise was still present in the EIT images so there is some residual error left that may be improved by an examination of the optimal method used to invert the sensitivity matrix.

Optimising electrode placement

In addition to improvements in the forward and inverse solutions, a more fundamental cause of error may well be in the errors produced in the placement of the scalp electrodes, which realistically probably vary by up to 1cm from the ideal electrode placements, and therefore electrode placement errors exist between the human head and the solution of the forward model.

It may well prove to be very time-consuming and impractical to accurately localise each electrode, unless a standardised head net array was used. However, it should be possible to measure the effects of electrode placement error by using the FEM model and introducing random electrode placement errors, in order to measure what effect this would have on the reconstructed images.

This could be performed in two ways, either using artificial computer generated data, with the FEM mesh, with random errors of electrode placement and determine the image errors produced by a reconstruction model with idealised electrode positions, or data could be acquired from the head tank, from which the electrode positions are known, and used different reconstruction algorithms, each with a different level of electrode position error, and determine the effect of these errors on image quality at different truncation levels.

If electrode placement error has a significant effect on the image quality, then it would be worthwhile to pursue a method that minimises these errors. In contrast, if the small electrode placement errors have little effect, then EIT of the head could continue to use EEG electrodes placed on by the 10-20 system, and use a standardised electrode model in the forward solution of the reconstruction algorithm.

6.2.4 Future applications of EIT

The demonstration that EIT can detect changes in the human brain during functional activity has paved the way for an extension of the use of EIT. The impedance changes measured during functional activity (2-5%) in rabbits (Holder *et al.* 1996) is smaller than the 10% impedance increases changes produced during epilepsy (Rao *et al.* 1997), 100% impedance increases during spreading depression (Boone *et al.* 1994) and the 150-200% increases measured during ischaemia in cats, rabbits and lambs (Van-Harreveld and Ochs 1956; Hossmann 1971; Gunn *et al.* 1997). As the functional activity impedance changes have now been demonstrated to be detected using EIT with scalp electrodes, it is very probable that EIT can detect the larger impedance changes associated with brain pathology.

Imaging epilepsy

As a result of the work in this thesis, further funding has enabled the EIT research to be developed to image epilepsy (Figure 6.88) (Bagshaw *et al.* 2003). This work has enabled EIT to be performed simultaneously with EEG, by the development of EEG hardware and software filters to remove the EIT artefact from the EEG trace. Although the work is in its early stages, current work has demonstrated that impedance decreases can be imaged in the area of a seizure, usually before seizure onset, which is confirmed independently by the simultaneous EEG and video findings. The advantages of using EIT are that it can provide 3-dimensional images of the seizure activity at the bedside during prolonged telemetry. This is not possible with any other neuroimaging method. The findings of increased blood flow during seizures have been confirmed in other studies, which have fortuitously been using imaging during a random seizure event using MRI in adults (Salek-Haddadi *et al.* 2002) and during PET imaging of neonates (Perlman *et al.* 1985; Borch *et al.* 1998). If EIT

telemetry of seizures proves effective, then this could revolutionise the imaging of seizures prior to neurosurgery. In addition EIT could be used for prolonged monitoring of seizures in both adult and neonatal care, in order to optimise therapeutic strategies designed to suppress seizure activity and to prevent secondary, seizure related brain damage.

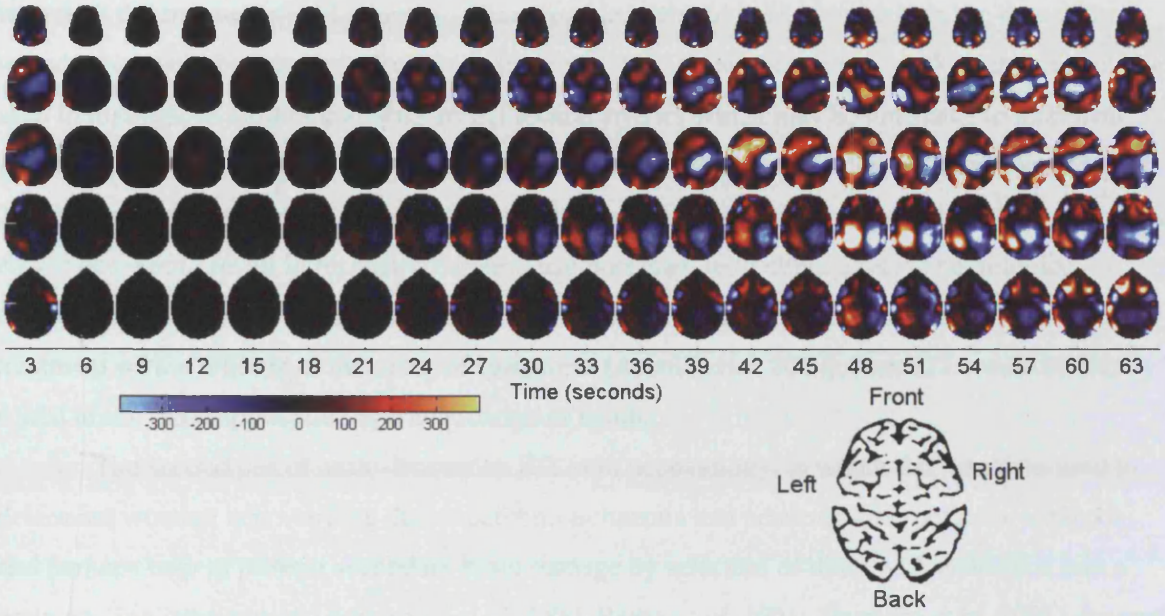

Figure 6.88 EIT images of right temporal seizure activity
This series of images was acquired in a man with right temporal lobe epilepsy, who was investigated with EEG telemetry to determine the location of his seizures (Bagshaw *et al.* 2003). As part of a current research project, EIT images were acquired at the same time as the EEG. These images were reconstructed with the FEM head model algorithm. Each column represents 3 seconds of data, averaged and reconstructed into one EIT image. The images are displayed as a time series, with the time in seconds labelled on the x-axis.

The images demonstrate a progression of an impedance decrease (blue) over the region of the right temporal lobe, which starts at 21seconds, and increases in size throughout the image series. At 52 seconds, the patient pressed the alarm button, as he was aware of the onset of a seizure, this was accompanied by the presence of rhythmic delta activity over the T6 electrode, which corresponds to the area in the image of the impedance decrease. The epileptic activity gradually increased in amplitude over the next 20 seconds, then generalised, at which point the video demonstrates generalised tonic-clonic seizure activity. The impedance decreases in the area of the subsequent seizure was likely to be due to increased CBF and CBV in the affected area of cortex. Although it seems strange that the haemodynamic response precedes increased neural activity in seizures, there is additional evidence from fMRI that this occurs (Salek-Haddadi *et al.* 2002). These images are provided by the courtesy of, and from the work of my colleagues Matthew Sparkes and Dr Andrew Bagshaw.

Imaging stroke and cerebral ischaemia

The development of the new multi-frequency EIT system raises the possibility that EIT can image stroke. Although other methods are very good at imaging stroke, such as CT and MRI, the advantage of EIT is that it could be used very early in stroke to determine whether the stroke was due to an ischaemic infarction or due to an intracerebral bleed. The difference between these is that infarction, due to arterial blockage would produce a cell swelling impedance change that would vary with the measurement frequency, whereas a bleed would have blood within the tissue whose impedance would be relatively frequency invariant. The importance of this work, is that it could be used to distinguish strokes that arise from blocked arteries which may be amenable to treatment with thrombolytic therapy, given to dissolve the clot and restore cerebral blood flow (Arnold *et al.* 2002). However it is important to exclude cerebral haemorrhage, as thrombolysis given under these conditions would result in increased cerebral haemorrhage, with either a worse neurological outcome or death. As it is important to distinguish between these two conditions, and give the treatment within 6 hours of the onset of symptoms (Arnold *et al.* 2002), then EIT would be ideally suited to the rapid application and acquisition of results.

The second use of multi-frequency EIT is in neonatology, in which EIT could be used to determine whether cell swelling due to cerebral ischaemia had occurred after perinatal asphyxia, and perhaps help to prevent secondary brain damage by selection of those with ischaemia into a brain cooling intervention (Azzopardi *et al.* 2000; Battin *et al.* 2001; Thoresen *et al.* 2001). Several studies have demonstrated that such impedance or cell swelling changes occur during ischaemia in animals (Van-Harreveld and Ochs 1956; Hossmann 1971; Holder 1992; Gunn *et al.* 1997; Miyasaka *et al.* 2000) and it is likely that these changes could be detected with EIT. In fact, it is not so important to *image* these changes, the information could be just as useful if an index of cell swelling could be obtained. This would therefore remain a useful clinical application of EIT, even if the problems with image localisation of impedance changes within the brain cannot be resolved.

Neonatal Seizures

As EIT has been demonstrated to be able to detect small changes due to functional activity, then it may be used to detect changes in blood flow or volume which occur during neonatal seizures (Perlman *et al.* 1985; Borch *et al.* 1998). The maximum changes of cerebral blood flow detected in adults during visual stimulation is 30% (Hoge *et al.* 1999); however neonatal seizures change rCBF by 50-130% (Borch *et al.* 1998). If there is a similarly sized increase in cerebral blood volume, then neonatal seizures would be expected to produce much larger impedance increases than functional activity, although the vascular impedance change may be offset by the impedance increase

expected from seizure associated cell swelling (Lux *et al.* 1986; Andrew and MacVicar 1994). The two opposing impedance changes may result in a reduction in the magnitude of the impedance change in the EIT images, or possibly cancel each other. The indication from EIT of epilepsy (Van-Harreveld and Schade 1962; Rao *et al.* 1997) and functional imaging in the exposed cortex of rabbits (Holder *et al.* 1996) is that seizures produce impedance increases, which suggests the effect of cell swelling predominates. In contrast to these studies, pilot data from EIT of seizures, currently performed by our group at King's hospital, London, indicates that the impedance changes in humans are impedance decreases and which probably reflect increased blood volume during seizure activity. These early adult studies are encouraging and indicate that it should also be possible to image seizures in the newborn with EIT.

The advantage of using EIT to detect neonatal seizures is that it would provide 3D information from the whole of the brain, compared to EEG which limited to the detection of surface electrical activity. In addition, if real-time images of seizures are available at the cotside, this would enable clinicians to diagnose clinically silent seizures without the need for specialist interpretation of the EEG. The goal of such monitoring would be to improve seizure detection, which would lead to improved seizure treatment and hopefully a better neurological outcome.

Role of EIT in the detection of neonatal ischaemic brain damage

Much larger impedance changes occur during and after hypoxic-ischaemic brain damage, as demonstrated by direct cortical impedance measurements in experimental animal models of ischaemia (Hossmann 1971; Williams *et al.* 1991; Holder 1992; Gunn *et al.* 1997). Typically, the change in impedance is of the order of 100%-200% of the baseline cortical impedance, much higher than 5% changes associated with functional brain activity (Holder *et al.* 1996). Impedance changes of this magnitude should be easily detected by EIT, which would enable EIT to monitor energy failure after perinatal asphyxia.

The main barrier to using EIT to detect asphyxia related changes is that EIT is only suited to imaging the difference of changes between a baseline and activation state. This approach is suited to functional imaging and seizure imaging, however the baseline state prior to asphyxia is in utero and cannot be measured. The alternative is to develop EIT to become a static imaging method, to provide information about cell swelling in order to apply potentially neuroprotective treatments such as brain cooling (Azzopardi *et al.* 2000; Battin *et al.* 2001; Thoresen *et al.* 2001). Work is in progress to develop a new EIT system which may be able to provide static information by the use of different simultaneous current frequencies. If successful, temporally static images of the impedance difference between different current frequencies may be used to indicate cell swelling. The mechanism which allows this to work is that low frequency currents would measure

a high impedance with cell swelling compared to normal brain as the current would have less of the highly conductive extra-cellular space to pass through. In contrast, at high frequencies, the difference between normal brain and a brain with cell swelling is reduced as current can also pass through the cell membranes. The frequency impedance difference would then enable an EIT spectroscopy image to be reconstructed of the level of cell swelling. At the moment, such a multi-frequency system has been developed, and preliminary EIT spectroscopy images of vegetables within saline filled tank phantoms have been produced. This is exciting work, but several refinements need to be made before it is used in humans.

If successful, EIT spectroscopy could also provide information about the severity of the ischaemic insult, and therefore may find a role in prognostic prediction after perinatal asphyxia. The reason for this is that the time course of the impedance change will vary, depending on the length of the hypoxic-ischaemic insult. This is supported by animal evidence, in which DWI imaging was used to investigate cell swelling after cortical hypoxia-ischaemia in the rat (Miyasaka *et al.* 2000). In this study, 3 types of cell swelling was detected: 1) A transient cell swelling, in which cell swelling occurred during asphyxia and then returned to normal, pre-asphyxia levels. This finding was associated with short, 15 minute periods of hypoxia/ischaemia, 2) A Biphasic response: in which cell swelling occurred during asphyxia, returned to baseline values, then a secondary, delayed cell swelling occurred within 12 hours of the initial insult. This was associated with a medium, 30 minute duration hypoxic-ischaemic insult, and 3) Permanent cell swelling: associated with a long, 60 minute, ischaemic insult in which cell swelling occurred during hypoxia/asphyxia and does not recover after restoration of oxygen and blood flow. Similar changes have been detected with single channel impedance scalp measurements performed in a similar type of arterial occlusion study in rats (Holder 1992). If impedance can detect these changes over the first 12-24 hours after asphyxia, then it may provide cotside, prognostic information, due to an indication of the level of neuronal injury.

6.2.5 Final words

When I first started the work in this thesis, an optimistic estimate of the chance that I would measure impedance changes from the human head was given at 50%. I have now demonstrated that these changes can indeed be produced in adults and neonates during functional brain activity, and to the best of my ability, I have demonstrated that these changes are not artefacts due to changes of the skin and scalp impedance, but arise from the brain. I have also demonstrated, using phantoms of the head, that impedance changes can be imaged with some accuracy within the skull. In addition, with thanks to my colleagues, I have demonstrated that a more realistic head model used in the algorithm improved the EIT images. The two main questions that remain unanswered are:

1) What is the underlying cause of the imaged impedance changes, particularly the impedance increases which run counter to the results of neuroimaging studies with other methods which suggest that blood flow and blood volume is the main change produced during neural activity, and from this I would expect to only image impedance decreases, and 2) What is the cause of the mis-localisation of impedance changes, from the expected position of the stimulated brain activity, in up to a third of the studies.

Despite these unanswered questions, I believe that this research has been a major step forward for EIT of the head. At the start of my period of research, we were the only group in the world working on this problem. Thanks to the presentation and publication of the results in this thesis (Tidswell *et al.* 2001; Tidswell *et al.* 2001; Tidswell *et al.* 2001; Tidswell *et al.* 2001; Tidswell *et al.* 2001; Bagshaw *et al.* 2003), there has been increased interest in imaging the brain with EIT, and now there are several research groups, worldwide, partaking in brain EIT research. I look forward to their results, and the future results from our EIT research group at UCL. With further improvements, EIT looks set to become a viable clinical neuroimaging tool which is particularly suited to those areas in which a bedside monitor of both normal and abnormal brain function are required. Finally, and most importantly, I have thoroughly enjoyed my role in this work.

Appendix 1: Image Reconstruction

The reconstructed EIT images represent a spatially smoothed and low resolution image of the impedance changes within the head, in which the pixels are inversely related to the conductivity changes, $\Delta\sigma$. These conductivity changes are related to voltage changes measured at the scalp, ΔV, when a current is applied to the head. This relationship is expressed in matrix form by the equation:

(1) $$\Delta V = A\,\Delta\sigma$$

where **A** is known as the sensitivity matrix. The problem is to solve the equation to find $\Delta\sigma$, given the measured voltages, ΔV, which are proportional to the boundary impedance measurements. This was done by calculating the sensitivity matrix analytically for a model of the head as a sphere of uniform conductivity. The matrix was then inverted, by truncated singular value decomposition (SVD) in which the sensitivity matrix was decomposed into a series of orthogonal matrices, each associated with a weighting factor – a singular value (Golub and Loan 1996). However, as errors in the sensitivity matrix are emphasised by the inversion process and can severely distort the final images, these errors are suppressed by truncating the inversion process at a point before noise is introduced into the images. This threshold depends on the size of noise in the impedance data, the size of the errors in the sensitivity matrix and the numerical rank of the sensitivity matrix, determined by the number of independent impedance measurements (Breckon 1990; Gibson *et al.* 1999; Gibson 2000). For the human data, the number of independent measurements was determined by SVD. Of 258 electrode combinations used in this study, 255 appeared independent (Gibson 2000). However, a truncation threshold of 62 singular values was chosen, as this was appropriate for the level of noise present in the impedance data.

Once the inverted sensitivity matrix, A^{-1} is calculated, equation (1) can be rewritten:

(2) $$\Delta\sigma = A^{-1}\,\Delta V$$

from which the image of impedance change in the head can be calculated for any set of measured voltage changes.

Appendix 2: Medical Safety of EIT

2.1 Introduction

Although a study which specifically assesses the effects of the application of currents used in EIT (about 1 mA at 10 kHz and 5 mA at 50 kHz) has not been performed, there is a substantial body of work with similar currents applied to the brain or elsewhere in the body, from which deductions about safety may be drawn. Some of this work, in relation to EIT and in particular to the UCH EIT system as applied to neonates, are presented below.

Medical safety of the UCH EIT system

The electrical currents applied by the Mark 1b UCH EIT system, meet British Standards BS 5724 for electrical stimuli applied to the skin – i.e. 1 mA with applied current up to 1 kHz, rising linearly to a maximum of 5 mA at 50 kHz. The rationale of these criteria is to use a current which is roughly ten times less than the minimum which causes stimulation of nerves.

Theoretical sources of risk include those associated with the use of any mains powered appliance applied to the body, tissue heating due to the electric current, or neuronal stimulation. As the UCH Mark 1b EIT system applies an electric current at zero phase and stops current application at zero phase, this prevents a charge imbalance at the current injection electrodes which would otherwise produce an electrolytic effect at the electrodes. There should therefore be a negligible electrolytic effect with the EIT system, and electrolytic effects will not be discussed further.

Risk associated with use of an electrical appliance in general applied to the body.

The UCH EIT system has been designed and built in conjunction with the Medical Physics Department at University College London to meet the levels of medical safety set by British Standard (BS) 5724. It meets all the criteria for single fault conditions, current applied to the body, auxiliary and leakage currents and so, to the best of our knowledge, does not constitute any significant risk in this respect. The UCH EIT system passed medical safety tests, performed by a trained medical physicist, and was therefore approved for safe use in human subjects, both adult and neonatal.

Potential risk due to heating.

There are two possible areas of concern for the risk of heating: 1) The heating effect to the entire head, or 2) Where current density is maximal, and therefore the heating effect is maximal, underneath the current injection electrode.

The heating effects of EIT are small. The power relationship for an electrical current is the product of the resistance and the square of the current. With an applied current of 5 mA, it may be calculated that there is a maximal heating effect of 20 $mWcm^{-2}$ at the electrodes, assuming that the transimpedance of the head is 1kOhm; 100 $mWcm^{-2}$ is allowed by BS5724. The heating effect that this would have would be maximal in the neonate, as the head is much smaller than that of the adult. This amount of energy applied to a baby's head (estimated weight of a 3 kg baby's head = 500 g, given the specific latent heat of water as 4.2 $Jg^{-1}K^{-1}$, and assuming an even power distribution) would cause a temperature increase of approximately 0.05 °C/hour, less than temperature fluctuations due to physiological effects.

The local heating effects are limited by British Standards BS5724 to prevent local damage occurring at the sites where the electric current is applied to the body. The major determining factor for damage at the electrode skin interface is current density and it has been shown for current densities of 1mA mm^{-2} tissue damage does not occur. As we use a maximum current of 5mA spread over an electrode area of 1cm^2 (=100mm^2), the current density, therefore, does not exceed 0.05mA mm^{-2}, almost two orders of magnitude below the limit set by BS5724. At the current densities used by EIT, there will be undetectable tissue heating and no damage to the skin from local heating effects.

Potential risk due to neuronal stimulation.

Neuronal stimulation has been proposed to be the mechanism by which neural damage occurs, supported by evidence that neural damage produced by electrical stimulation can be prevented by blocking the nerves with lignocaine (McCreery and Agnew 1990). However, EIT, as used in the adult and neonatal studies, does not cause neuronal stimulation. Information about the energy required to provide neuronal stimulation and neuronal damage are available from both human and animal studies.

One study has tested the perception threshold, at which point neural stimulation leads to sensation, of electrical currents at different frequencies in 40 adults with electrodes applied to the skin. The 0.5 percentile perception threshold at frequencies of 10 kHz and 50 kHz is 7 mA and 50 mA respectively (Dalziel 1972), which is an order of magnitude larger than the currents used by EIT.

Even when suprathreshold electrical stimulation has been performed in humans, there is no evidence for significant local histological damage. The effects of cortical stimulation for pain relief in terminally ill adults has been studied. Intracortical neuronal stimulation at a frequency of 20 Hz and an amplitude of 6 V or less, for up to 3 months in 7 adults produced no neural damage assessed by histology for evidence of gliosis, parenchymal or neural reactions at the electrode tip (Baskin *et al.* 1986). The effects of cortical stimulation through sub-dural electrodes prior to resective neurosurgery has also been examined in 3 patients (Gordon *et al.* 1990). Intermittent stimulation at 50 Hz, with a charge per phase and charge density of up to 4.4 μC/phase and 57 μC/cm^2/phase respectively, was performed for a total duration of 30 minutes. Histological analysis for structural damage and gliosis revealed no difference between stimulated and non-stimulated areas of cortex under the electrode array .

The level at which chronic cortical stimulation produces damage with cortical electrodes, has been determined in several animal studies. Safety limits are expressed in units of charge per phase. In monkey cerebellum, a frequency of 10Hz and at charge per phase and charge density of 0.5 to 22 μC/phase and 7.4 to 300 μC/cm^2/phase respectively was applied for 205 hours. Neural damage, assessed by gliosis, collagen infusion, PAS staining and electron microscopy, was not present at a charge per phase and charge per phase density of 0.5 μC/phase and 7.4 μC/cm^2/phase respectively (Babb *et al.* 1977; Brown *et al.* 1977; Dauth *et al.* 1977). In cats the effects of continuous electrical stimulation using sub-dural electrodes on the cerebral cortex at a frequency of 50 Hz and at a charge per phase and charge density of 0.3-3 μC/phase and 30-300 μC/cm^2/phase respectively for 36 hours, has been investigated. There was no evidence of cortical damage assessed by light microscopy and electron microscopy or damage to the blood brain barrier in cats stimulated for 36 hours with a charge per phase and charge density of 0.3 μC/phase and 30 μC/cm^2/phase respectively (Agnew *et al.* 1975; Pudenz *et al.* 1975; Pudenz *et al.* 1975).

EIT uses a maximum charge per phase and charge per phase density of 0.05 μC/phase and 0.05 μC/cm^2/phase at scalp electrodes. These are respectively one and two orders of magnitude smaller than the limits determined above. However, the above experiments were performed with electrodes placed on the brain. EIT in the adult and neonatal experiments were performed with scalp electrodes. The effect of the scalp and skull reduces the charge density at the cortex substantially. Although the frequencies of stimulation used by these studies were much lower than that used in EIT (10-20 Hz compared to 50 kHz), at higher current frequencies a larger current is required to produce neuronal stimulation (Dalziel 1972). The only example of a routine, safe medical application of high frequency current is surgical diathermy which uses frequencies of 500 kHz and above with currents of up to 1 A, two orders of magnitude greater than that used in EIT.

Potential genotoxicity of low frequency electric fields.

Concerns for the harmful effects of electromagnetic fields have arisen from some controversial epidemiological studies which indicate an increased risk of cancers in people who have had exposure to electromagnetic fields from power lines over many years. A recent review (Lacy-Hulbert *et al.* 1998) has assessed these studies, 10 of which show no increased risk and 7 of which show a slight increased risk for some cancers. The review argues that in those studies which show a positive effect of electromagnetic fields on the increased relative risk of cancers, there are methodological problems such as small numbers, indirect calculations of electromagnetic fields and a lack of a dose response effect. One of the largest and most recent studies was the National Cancer Institute Study (Linet *et al.* 1997), where magnetic fields were measured in the houses of: 1) children with leukaemia and 2) matched controls, by technicians blinded to whether the house belonged to the case or control subject. This study showed no significant increased risk of leukaemia in children exposed to magnetic fields of >0.2 μTesla, (odds ratio (OR) = 1.53 with 95% confidence interval (CI) 0.91-2.56). One subgroup in this study (magnetic fields 0.4-0.5 μTesla) showed an increased relative risk on sub-group analysis (OR= 6.4 with 95% CI 1.30-31.73), but numbers in this group were small and there was no increased risk in the subgroup with exposures of >0.5 μTesla (OR=1.01, 95% CI 0.26-3.99) which would be expected if there was a dose response relationship between electromagnetic fields and the induction of leukaemia. The sub-group analysis was performed post-hoc and it is not clear from the paper that the sub-group analysis was Bonferroni corrected for multiple statistical tests. This large study does not support a significant leukaemic risk with long term exposure to high domestic electro-magnetic fields.

In addition to the epidemiological studies, there are numerous studies which look at the effects that 50-100Hz electrical fields, magnetic fields and a combination of the two have on biochemical reactions, cell cultures and animals within the laboratory (reviewed by Lacy-Hulbert, Metcalfe et al. 1998 and McCann, Dietrich et al. 1998)(Lacy-Hulbert *et al.* 1998; McCann *et al.* 1998). The majority of such studies show no effect of electromagnetic fields on genotoxicity, cancer promotion or biochemical reactions. Although some studies have shown an increase in chromosomal breakages, tumour growth and changes in biochemical reactions, several attempts to reproduce these positive electromagnetic field induced biological effects have failed. Both reviews conclude that there is no convincing evidence that electromagnetic fields at 50-100 Hz have genotoxic or tumour promoting potential, but that continued attempts should be made to reproduce studies which show positive effects.

Potential risk of affecting cerebral development.

Evidence for the absence of risk that electromagnetic fields have on human cerebral development derive from epidemiological studies which study the possible effects that electric blankets or heated water beds have on childhood malignancies or foetal abnormalities. The electromagnetic field exposure from such appliances is much greater than that with other household appliances due to the magnitude of the induced magnetic field (0.3-0.5 μTesla) and the proximity and duration the subject spends within that field (Dlugosz *et al.* 1992). If there is a risk from electromagnetic field exposure in humans, then we would expect these people to be at the greatest risk of developing abnormalities.

One report has studied the effects that electric blankets have on the developing foetus. This study found no effect of the use of electric blankets on the incidence of neural tube defects (odds ratio 0.9, 95% confidence interval 0.5-1.6), nor on the incidence of cleft lip (OR 0.7, 95% CI 0.3-1.3) or cleft palate (OR 0.8, 95% CI 0.3-2.1) (Dlugosz *et al.* 1992).Two further studies have looked at the incidence of brain tumours in association with such appliances. The first, a case-controlled questionnaire study which compared children with primary brain tumours (n=82) to population matched controls (n=164), found no increased risk of brain tumours with exposure to electric blankets (OR = 0.4, 95% CI 0.2-1.2) there were not enough cases exposed to water beds to comment on (McCredie *et al.* 1994). This finding was reproduced in a larger USA study (Preston-Martin *et al.* 1996) which compares 540 children with brain tumours and 801 control children. The risk of brain tumour occurrence in those with in utero exposure to electric blankets (OR 0.9, 95% CI 0.6-1.2) and heated water beds (OR 0.9, 95% CI 0.6-1.3) was not elevated, nor was the risk increased in children who used electric blankets (OR 1.0, 95% CI 0.6-1.7) or heated water beds (OR = 1.2, 95% CI 0.7-2.0).

On the basis of this evidence it is reasonable to conclude that there is no significant risk from long term electromagnetic field exposure at 50-60 Hz, either on cerebral development or the development of cancer. Given this, a reasonable view would be that there is no significant risk from electromagnetic fields at higher frequencies, as used by EIT, and applied over much shorter periods of time.

Possible hazards in applying scalp electrodes to neonates for EIT

One of the concerns of EIT in neonates is the use of handling in order to place scalp electrodes. As this was similar to the amount of handling a neonate is subjected to during an electroencephalogram (EEG). As EEG's are commonly used in sick full-term and preterm infants without risk, it is reasonable to assume that the handling of a neonate for an EIT study was just as

safe. All the neonatal studies were performed in healthy term infants, or preterm infants who were the term equivalent, by myself, a Paediatric Specialist Registrar. During the neonatal studies, I assessed they were all well and could tolerate the handling required for electrode application. In those who became hungry during the study, the study was paused for a feed, or discontinued. At no time was the experimental procedure allowed to interrupt the medical care of the neonate.

Previous and current use of EIT in neonates

An internationally recognised group in Medical Physics, at the Royal Hallamshire Hospital, Sheffield, has performed several pilot studies with EIT of chest function in neonates without any reported ill effects (Professor B.H. Brown, Head of Medical Physics, personal communication (Smallwood *et al.* 1999; Brown *et al.* 2002)). Other published studies have not performed EIT but cerebral impedance measurements through scalp electrodes in neonates: 1) measurement of cerebral blood flow during indomethacin infusions (Colditz *et al.* 1989); 2) a comparison of cerebral impedance measurements with ^{133}Xenon clearance (Colditz *et al.* 1988; Colditz *et al.* 1989) strain gauge plethysmography (Costeloe *et al.* 1984) as measures of global cerebral blood flow and 4) measurement of the changes of impedance which occur with intra-ventricular haemorrhage in preterm infants (Siddiqui *et al.* 1980). These studies used similar electrical currents and frequencies to those used in EIT and, to the best of our knowledge, caused no ill effects.

2.2 Conclusions

Although there is still a theoretical risk from the use of 50 kHz currents during EIT of adult and neonatal brains, to the best of my current knowledge, the UCL EIT group's existing experience with EIT and my reading of the published literature, this risk has been assessed to be negligible for the conditions in which EIT was used and the short periods of exposure. As an endpoint, the biomagnetic fields produced by EIT are much lower than the magnetic fields applied to neonates with MRI, and the heating effects of EIT are an order of magnitude less than the heating effect of cerebral ultrasound. Both of these techniques are used extensively for neonatal neuroimaging. I believe that EIT is as safe or safer than either neonatal MRI or ultrasound, both of which are considered very safe for use in neonates.

Appendix 3: Electrode Placement

Electrodes were placed around the scalp in positions based on the 10-20 International System of Electrode Placement. This is a standardised system which was developed to allow similar placement of electrodes across a wide variety of neurophysiological departments and to give good agreement between the electrode placement used between different studies.

The electrode positions used for the EIT studies had the requirement that good spatial impedance sampling of the head was needed. This, I felt, could have been achieved by a non-standard placement of electrodes, but this would have required the development of a technique to place the electrodes accurately and reproducibly, something the 10-20 system had already achieved. As the 10-20 system also met the requirement of good spatial sampling, and was something that could be reproduced in other EIT studies of the head, then the 10-20 system was chosen.

Initially it was felt that the 21 electrodes commonly used in the 10-20 system for routine EEG use was too limited for the adult EIT studies. Therefore 10 more electrode positions were chosen which were used in the acquisition of EIT data from the adult head. When the EIT studies were performed in neonates, several problems were found with 31 electrodes: 1) The application time increased, because the babies moved and electrodes had to be reapplied, although this was not an experimental problem the length of time of handling produced more anxiety in the parents who had consented to the study, and 2) Due to the size limitation of the neonatal head, there was a danger that electrical shorts could occur between adjacent electrodes from the electrode paste that oozed out from the electrode base. For these reasons, the number of electrodes used in the neonatal EIT studies were reduced to 21, and a different measurement protocol and reconstruction algorithm created.

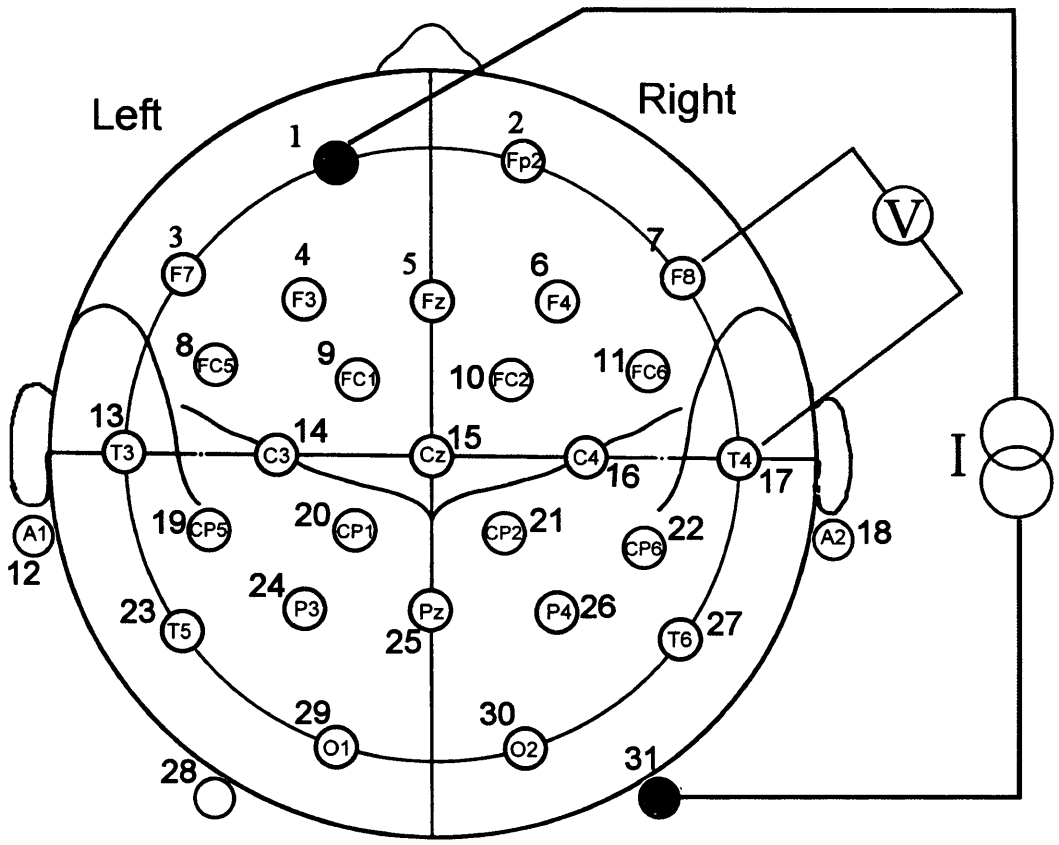

Figure 3.1 Adult placement of 31 scalp electrodes for EIT studies.
Each electrode is represented by a circle with a label inside that represents the name of the electrode according to the 10-20 system. The two posterior electrodes without labels on the inside are placed a third of the distance measured between A1 and A2, in a horizontal line below and parallel to the electrodes T5, O1, O2 and T6. The electrode numbers 1-31 on the outside of each electrode are the electrode numbers used in the EIT protocol file, *eeg31b_258.prt.*

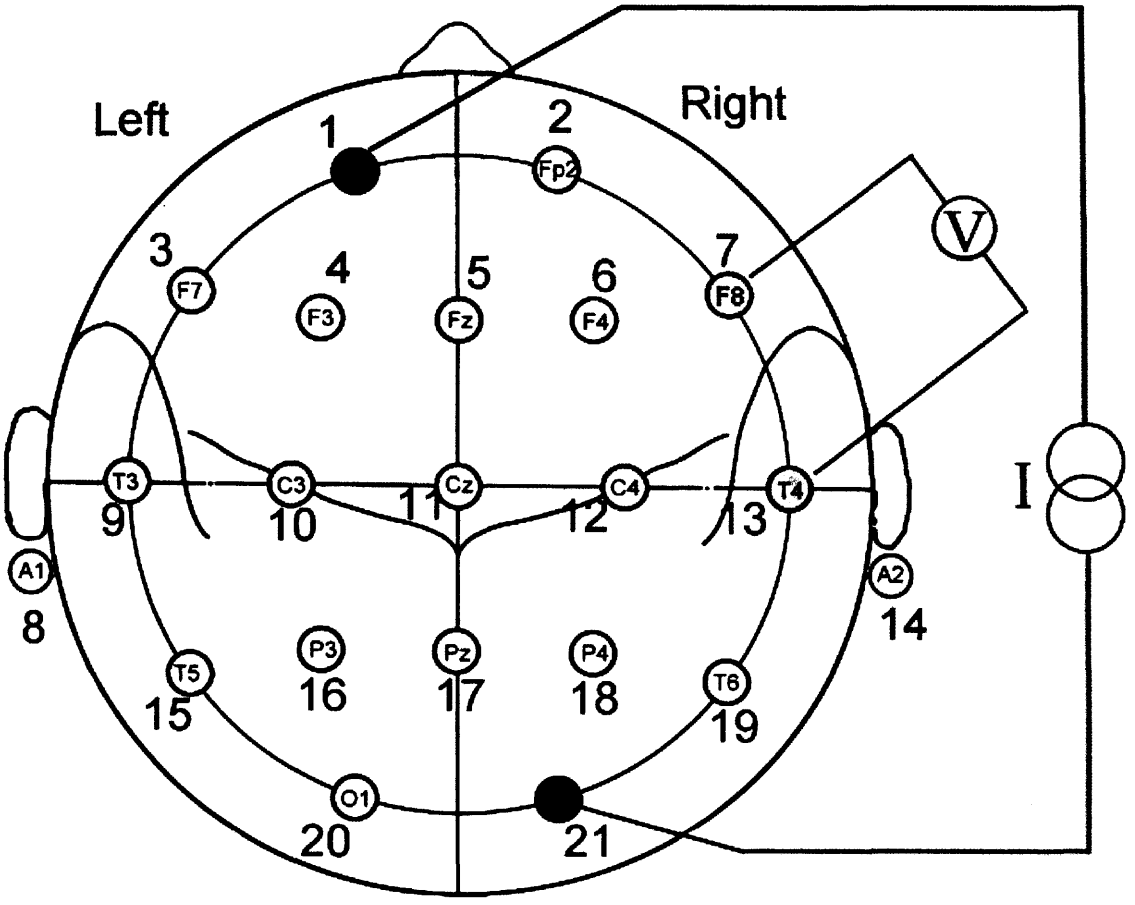

Figure 3.2 Scalp electrode placement for neonatal EIT studies.
Each electrode is represented by a circle with a label inside that represents the name of the electrode according to the 10-20 system. The electrode numbers 1-21 on the outside of each electrode are the electrode numbers used in the EIT protocol file, *eeg21_187.prt*. A reduced number of electrodes was used in the neonatal study to prevent electrode shorts and to reduce the amount of time spent in the electrode application for each neonate.

Appendix 4: Measurement of Scalp Impedance

4.1 Introduction

In the adult EIT studies, detailed in Chapter 2, an experiment was performed to exclude the contribution that the scalp impedance made to the transcranial impedance changes measured during sensory stimulation. This required the design of a set of electrodes which would be sensitive to changes in impedance just below the electrode. The electrode design was influenced by the results of a study which performed investigated the current distribution through the scalp layer and intracranial space of different patterns of current applied to the surface of a real human skull soaked in saline (Rush and Driscoll 1968). This demonstrated that two current injection electrodes placed diametrically across the scalp allowed approximately 45% of the current to enter the intracranial cavity, however if the electrodes were moved closer together, less current entered the skull, until an electrode separation gap of 5 cm or less. At very small electrode separations of less than 2 cm very little of the applied current passed into the head because it shunted through the scalp layer. The design of the electrodes in this study therefore aimed to minimise the current density which entered the brain underneath the electrodes, in order to be most sensitive to impedance changes within the scalp.

4.2 Methods

4.2.1 Scalp impedance electrode manufacture

The scalp electrode design is illustrated in Figure 4.3. The electrode spacing of the current injection electrodes was designed to be less than 2 cm in order to maximise current through the scalp and minimise current entry through the skull into the brain Each electrode block comprises 4 electrodes spaced 4 mm apart, current injected at the outer electrodes will travel through the scalp under the surface of the electrode block, the voltage produced by this current is measured by the inner electrodes and impedance calculated. As the scalp is the path of least resistance to the applied current then most of the it will be conducted through the scalp without penetration of the skull: therefore these electrodes should be insensitive to impedance change within the skull cavity and only sensitive to impedance change within the scalp under the electrode.

The electrode blocks were made from epoxy resin casts of a silicone rubber mould, with dimensions of 15 x 21 mm. The electrode face contained semicircular wells 5 mm deep in which silver ball electrodes, at the end of 0.5 mm silver wire, were inserted. Each wire was passed

through a hole in the well to the back of the electrode block and soldered onto 14 cm lengths of silicone wire which ended in 2 mm silver connector plugs. Electrodes were chlorided prior to experiments in sodium chlorocyanate (Haztab granules) solution which reduced the resting potential between electrodes in saline to less than 1 mV. The electrode wells were then filled with EEG conduction paste to maximise the surface area for electrode-skin contact. Impedance measurements were made with the HP EIT system at a frequency of 50 kHz, an applied voltage at the current injection electrodes of 1.0 V, ALC off and short integration time. Impedance was recorded at different electrodes by multiplexing the HP impedance analyser through the 4 scalp electrode blocks.

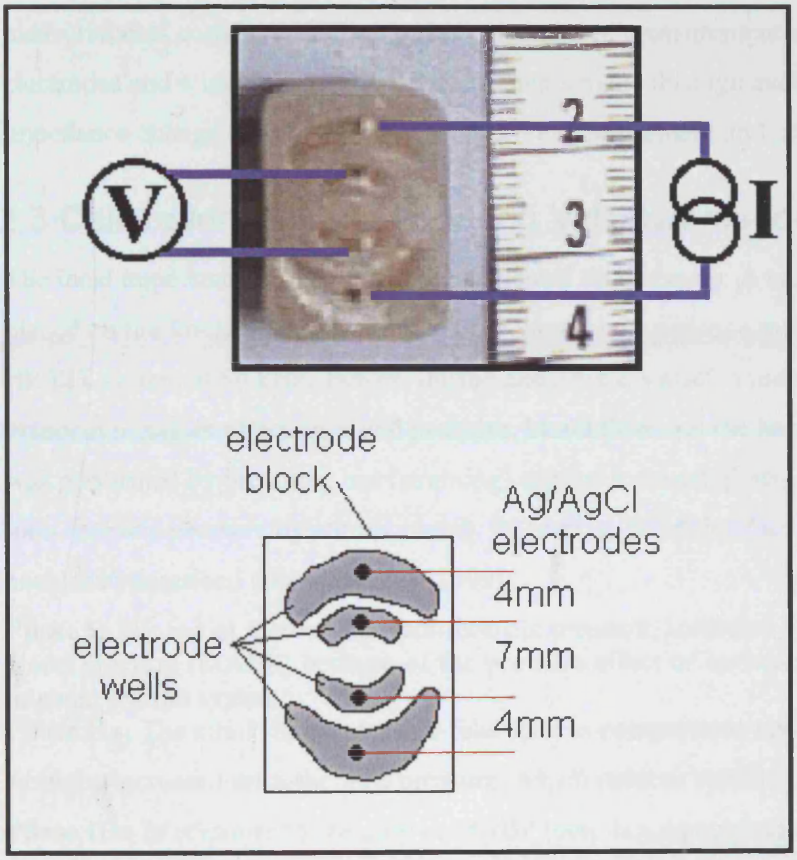

Figure 4.3 Diagram of scalp impedance electrode
Picture of the resin block which contained the 4 Ag/AgCl scalp impedance electrodes (top) with diagram (bottom). The electrode wells were filled with conductive paste prior to placement on the scalp. Four point impedance measurements were made by the application of a current through the outermost electrodes, ***I***, with a separation of 15 mm, voltage was recorded by the innermost electrodes, ***V***.

4.2.2 Calibration in tanks

The local impedance electrodes were calibrated in a saline filled tank. Four EEG and four scalp impedance electrodes were placed around the edge of a 10 cm diameter cylindrical tank, filled with 1 litre of 0.2 % saline: four EEG electrodes were placed in a polar drive arrangement and scalp impedance electrodes adjacent to each of these. Baseline impedance measurements were collected with the HP EIT system at a measurement frequency of 50 kHz, then measurements were made after a 0.5% impedance change was introduced in the tank by the removal of 5 ml of saline and replacement with 5 ml of distilled water. Each data set comprised of 100 measurements, 50 baseline and 50 of the impedance change, at each of 5 different electrode combinations. These measurements consisted of 1 polar drive impedance measurement made through the EEG electrodes and 4 local impedance measurements made through each scalp electrode. The impedance change recorded by the polar drive measurement and scalp electrodes were compared.

4.2.3 Calibration in humans during Valsalva manoeuvre

The local impedance electrodes were also tested on the scalp. A scalp impedance electrode was placed on the forehead of a healthy adult volunteer. Impedance measurements were made, with the HP EIT system at 50 kHz, before, during and after a Valsalva manoeuvre. The Valsalva manoeuvre has an effect on blood pressure, blood flow and the heart rate. The Valsalva manoeuvre was performed by breathing out (straining) against a closed glottis for 20 s, which increases the intra-thoracic pressure by approximately 40 mmHg. In adults, four phases of the Valsalva response have been described (**Dawson** *et al.* 1999):

Phase I: The initial increase in intra-thoracic pressure, leads to a transient increase in mean arterial blood pressure (MABP) because of the pressure effect of increased thoracic pressure on the intra-thoracic arterial system.

Phase IIa: The atrial filling pressure falls (due to compression and emptying of intra-thoracic veins from the increased intra-thoracic pressure) which reduces cardiac output and MABP.

Phase IIb: In response to the drop in MABP there is a compensatory constriction of peripheral arterial vessels and a compensatory increase in the force and rate of heart contraction. These have the combined effect of increasing the MABP.

Phase III: When the strain is released the MABP falls due to the sudden release of the intra-thoracic pressure on thoracic arteries. The MABP starts to increase again due to the increased cardiac output produced by improved venous filling of the heart in response to the drop in intra-thoracic pressure.

Phase IV: An overshoot in the MABP increase occurs because of the increased cardiac output against a high peripheral vascular resistance (produced by the arterial vasoconstriction in phase

IIb). The increased MABP stimulates arterial pressure receptors, which act to reduce cardiac output by a reduction in the heart rate and the force of ventricular contraction. The heart rate and MABP gradually return to baseline as normal arterial tone is restored.

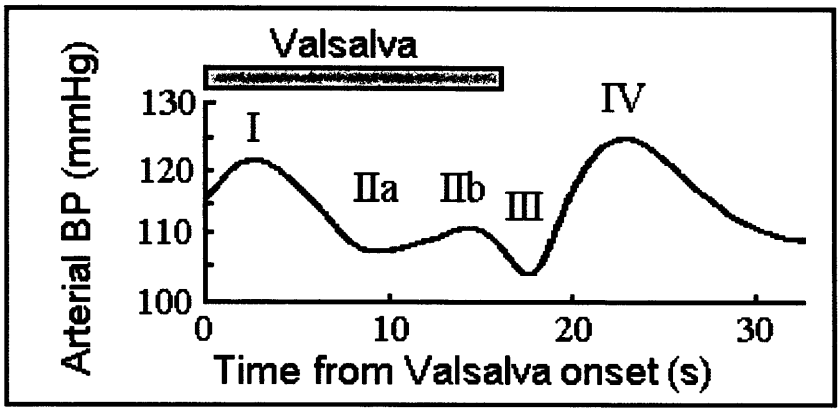

Figure 4.4 Effect of Valsalva on Arterial BP (from Dawson et al. 1999)
Effect of Valsalva on arterial blood pressure in 53 healthy adult volunteers. See text for description of the 5 phases shown (**Dawson** *et al.* 1999)

The predicted effect of the Valsalva on scalp impedance would be to increase scalp impedance due to reduced scalp blood flow and decrease impedance with increased scalp blood flow. However, changes in scalp blood flow are not easy to predict at all phases of the Valsalva manoeuvre, e.g. increased blood pressure would normally increase skin blood flow, but if the increased blood pressure is achieved by increased peripheral vascular resistance produced from blood vessel constriction then this may decrease scalp blood flow. Therefore, to identify impedance changes due to the Valsalva manoeuvre and not from breath holding, two control experiments were performed: 1) A breath holding experiment without strain for the same period of time as the Valsalva and 2) An experiment which consisted of normal breathing. Each experiment lasted 100 s and consisted of 500 consecutive impedance measurements: 40 s of baseline, 20 s of either Valsalva, breath holding without strain or normal breathing, and 40 s of recovery. Each experiment was repeated 5 times, data was excluded if it contained movement artefact (determined by sudden 0.5 % or greater changes in impedance during normal breathing activity), and the results averaged.

4.3 Results

4.3.1 Calibration in tanks

The estimated 0.5 % impedance increase change introduced into the tank phantom produced similar impedance changes for both local impedance measurements made through the specially designed scalp impedance electrode arrays, 0.45 ± 0.07 % (Mean ± SD) and the polar drive measurements of impedance made through the EEG electrodes, 0.46 ± 0.05 %. There was no significant difference in the impedance measured by the two methods. This demonstrated that the scalp impedance arrays could be used to measure known changes in impedance, with a similar accuracy to the much larger surface area EEG electrodes.

4.3.2 Calibration in humans during Valsalva manoeuvre

Scalp impedance changed reproducibly during the Valsalva manoeuvre. These impedance changes mirrored changes of blood pressure demonstrated by Dawson et al. (1999) (Dawson *et al.* 1999). No impedance changes were measured at the scalp during breath holding or during normal breathing.

The impedance changes during Valsalva had several components (Figure 4.5): 1) An impedance decrease after strain onset, 2) An impedance increase above baseline 3-5 s later, 3) An impedance decrease below baseline until the end of strain, 4) An immediate rise of impedance after the release of strain which is followed by a larger impedance decrease which then returns to baseline after 10 s. These changes are what would be expected if blood flow in the scalp increased in proportion to blood pressure.

In all the experiments, peak to peak impedance changes with an amplitude of 0.05 % were seen with a frequency of 70 cycles per minute, similar to the subjects' heart rate of 72 beats per minute at the start of the experiment.

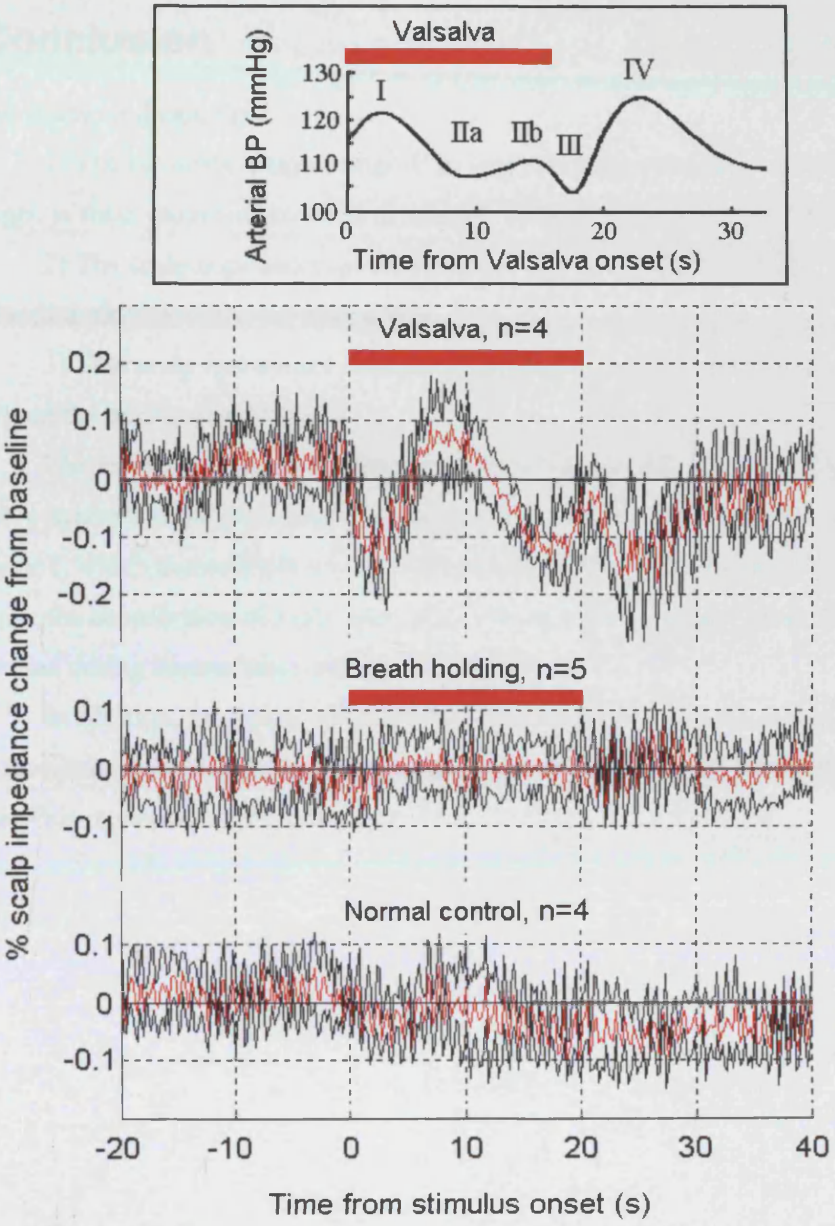

Figure 4.5 Scalp impedance during Valsalva manoeuvre

Upper figure: Timecourse of arterial blood pressure changes during a 15 second Valsalva manoeuvre carried out in 53 healthy adults (from Dawson et al 1999)..

Lower figure: Scalp impedance (Mean ± 2SE) recorded during a 20 second Valsalva manoeuvre, and control studies, performed in one adult subject: **1) Top graph:** Valsalva manoeuvre, **2) Middle graph:** Breath holding without Valsalva, and **3) Bottom graph:** Normal breathing.

A reproducible impedance change is only seen during the Valsalva manoeuvre, the impedance waveform is of a similar shape but in an opposite direction to the arterial blood pressure changes in the upper figure.

6.3 Conclusion

These studies indicate that:

1) The electrode arrays designed to measure scalp impedance measure similar impedance changes as those measured by EEG electrodes, despite the discrepancy of electrode size.

2) The scalp impedance electrode arrays can detect small changes in scalp blood volume produced during the Valsalva manoeuvre.

3) That scalp impedance changes occur due to pulsatile blood flow, with an amplitude of 0.05% of the baseline impedance.

The results from these calibration studies indicate that the scalp impedance electrodes can reliably measure small impedance changes in the scalp. From this, I conclude that the results in Chapter 2, which demonstrate no detectable scalp impedance changes during motor activity, exclude the contribution of scalp impedance changes to the trans-cephalic impedance changes measured during human brain activity.

In addition, this study illustrates that approximately 0.05% of noise measured during the EIT studies is physiological and is due to the pulsatile blood flow in the scalp during the cardiac cycle. This represents approximately one third of the noise measured in the adult EIT studies.

Appendix 5: References

Adey, W., R. Kado, et al. (1962). "Impedance Measurements in brain tissue of animals using microvolt signals." Experimental Neurology **5**: 47-66.

Agnew, W. F., T. G. H. Yuen, et al. (1975). "Electrical Stimulation of the Brain IV. Ultrastructural studies." Surgical Neurology **4**: 438-448.

Aladjolova, N. A. (1964). Slow electrical processes in the brain. Progress in Brain Research. **7:** 155-237`.

Altman, D., J. Perlaman, et al. (1993). "Cerebral oxygen metabolism in newborns." Pediatrics **92**: 99-104.

Amess, P., J. Penrice, et al. (1997). "Mild hyporthermia after severe transient hypoxia-ischaemia reduces the delayed rise in cerebral lactate in the newborn piglet." Pediatric Research **41**(6): 803-808.

Anderson, A., R. Marois, et al. (2001). "Neonatal auditory activation detected by functional magnetic resonance imaging." Magnetic Resonance Imaging **19**: 1-5.

Andrew, R. and B. MacVicar (1994). "Imaging Cell Volume Changes and Neuronal Excitation in the Hippocampal Slice." Neuroscience **62**(2): 371-383.

Arndt, S., T. Cizadlo, et al. (1996). "Normalising counts and cerebral blood flow intensity in functional imaging studies of the human brain." Neuroimage **3**: 175-184.

Arnold, M., G. Schroth, et al. (2002). "Intra-arterial thrombolysis in 100 patients with acute stroke due to middle cerebral artery occlusion." Stroke **33**: 1828-1833.

Ary, J., S. Klein, et al. (1981). "Location of Sources of Evoked Scalp Potentials: Corrections for Skull and Scalp Thicknesses." Biomedical Engineering **28**(6): 447-452.

Avis, N. and D. Barber (1994). "Image reconstruction using non-adjacent drive configurations." Physiological Measurement **15**(Supplement 2a): A153-160.

Avis, N. J., D. Barber, et al. (1992). "Back-projection distortions in applied potential tomography images due to non-uniform reference conductivity distributions." Clinical Physics and Physiological Measurement **13**(Suppl A): 113-117.

Azzopardi, D., N. Robertson, et al. (2000). "Pilot study of treatment with whole body hypothermia for neonatal encephalopathy." Pediatrics **106**(4): 684-694.

Babb, T. L., H. V. Soper, et al. (1977). "Electrophysiological studies of long-term electrical stimulation of the cerebellum in monkeys." Journal of Neurosurgery **47**: 353-365.

Baenziger, O., A. Mueller, et al. (1999). "Cerebral blood flow and neurological outcome in the preterm infant." European Journal of Paediatrics **158**: 138-143.

Bagshaw, A. P., A. D. Liston, et al. (2003). "Electrical impedance tomography of human brain function using reconstruction algorithms based on the finite element method." Neuroimage **20**(2): 752-64.

Balchin, S. (1997). Electrical Impedance Tomography: Application of a new imaging system. Clinical Neurophysiology. London, University College London.

Barber, D. and B. Brown (1984). "Applied Potential Tomography." Journal of Physics E: Scientific Instrumentation **17**: 723-731.

Barber, D. and B. Brown (1988). "Errors in reconstruction of resistivity images using a linear reconstruction technique." Clinical Physics and Physiological Measurement **9**(A): 101-104.

Bartocci, M., J. winberg, et al. (2001). "Cerebral hemodynamic response to unpleasant odors in the preterm newborn measured by near-infrared spectroscopy." Pediatric Research **50**(3): 324-330.

Bartocci, M., J. Winberg, et al. (2000). "Activation of olfactory cortex in newborn infants after odor stimulation: a functional near-infrared spectroscopy study." Pediatric Research **48**(1): 18-23.

Baskin, D. S., W. R. Mehler, et al. (1986). "Autopsy analysis of the safety, efficacy and cartography of electrical stimulation of the central gray in humans." Brain Research **371**: 231-236.

Battin, M., J. Dezoete, et al. (2001). "Neurodevelopmental outcome of infants treated with head cooling and mild hypothermia after perinatal aspyxia." Pediatrics **107**(3): 480-484.

Bayford, R., A. Gibson, et al. (2001). "Solving the forward problem in electrical impedance tomography for the human head using IDEAS (integrated design engineering analysis software) a finite element modelling tool." Physiological Measurement **22**(1): 55-64.

Bayford, R. H., K. G. Boone, et al. (1996). "Improvement of the positional accuracy of EIT images of the head using a Lagrange multiplier reconstruction algorithm with diametric excitation." Physiological Measurement **17**: A49-A57.

Belliveau, o. W., D. N. Kennedy, et al. (1991). "Functional Mapping of the Human Visual Cortex by Magnetic Resonance Imaging." Science **254**: 716-719.

Benabid, A., L. Balme, et al. (1978). "Electrical impedance brain scanner: principles and preliminary results of simulation." Journal of Life Sciences **8**: 59-68.

Benaron, D., S. Hintz, et al. (2000). "Noninvasive functional imaging of human brain using light." Journal of Cerebral Blood Flow and Metabolism **20**: 469-477.

Bertero, M. and P. Boccacci (1998). Introduction to inverse problems in imaging. London, Institute of Physics Publishing.

Binnie, C., A. Rowan, et al. (1982). A manual of electroencephalographic technology. Cambridge, Cambridge University Press.

Birzis, L. and E. Carregal (1965). "Electrical impedance and vasomotor changes accompanying synaptic transmission in sympathetic ganglia." Experimental Neurology **15**: 1-17.

Birzis, L. and S. Tachibana (1962). "Measurement of local cerebral blood flow by impedance change." Life Sciences **11**: 587-598.

Birzis, L. and S. Tachibana (1964). "Local cerebral impedance and blood flow during sleep and arousal." Experimental Neurology **9**: 269-285.

Boecker, H., A. Kleinschmidt, et al. (1994). "Functional cooperativity of human cortical motor areas during self-paced simple finger movements. A high resolution MRI study." Brain **117**: 1231-1239.

Bookheimer, S. Y. (1996). "Functional MRI Applications in Clinical Epilepsy." Neuroimage **4**: S139-S146.

Boone, K. and D. Holder (1996). "Effect of skin inpedance on image quality and variability in electrical impedance tomography: a model study." Medical and Biological Engineering and Computing **36**: 351-354.

Boone, K., A. M. Lewis, et al. (1994). "Imaging of cortical spreading depression by EIT: impplications for localization of epileptic foci." Physiological Measurement **15**: A189-A198.

Borch, K., O. Pryds, et al. (1998). "Regional cerebral blood flow during seizures in neonates." Journal of Pediatrics **132**: 431-435.

Born, A., E. Rostrup, et al. (2002). "Visual cortex reactivity in sedated children examined with perfusion MRI (FAIR)." Magnetic Resonance Imaging **20**: 199-205.

Born, P., H. Leth, et al. (1998). "Visual activationin infants and young children studied by functional magnetic resonance imaging." Pediatric Research **44**(4): 578-583.

Braun, A. R., T. J. Balkin, et al. (1997). "Regional cerebral blood flow throughout the sleep wake cycle: An $H_2{}^{15}O$ PET study." Brain **120**: 1173-1197.

Breckon, W. (1990). Image Reconstruction in Electrical Impedance Tomography. School of Computing and Mathematical Sciences, Oxford Polytechnic: 143.

Brown, B., D. Barber, et al. (1985). "Applied potential tomography: possible clinical applications." Clinical Physics and Physiological Measurement **6**: 109-121.

Brown, B. and A. Seagar (1987). "The Sheffield data collection system." Clinical Physics and Physiological Measurements **8**(A): 91-97.
Brown, B. H., R. A. Primhak, et al. (2002). "Neonatal lungs--can absolute lung resistivity be determined non-invasively?" Med Biol Eng Comput **40**(4): 388-94.
Brown, W. J., T. L. Babb, et al. (1977). "Tissue reactions to long-term electrical stimulation of the cerebellum in monkeys." J Neurosurgery **47**: 366-379.
Bydder, G., M. Rutherford, et al. (2001). "Diffusion-weighted imaging in neonates." Child's Nervous System **17**: 190-194.
Bye, A. and D. Flanagan (1995). "Saptial and Temporal Characteristics of Neonatal Seizures." Epilepsia **36**(10): 1009-1016.
Cannestra, A., N. Pouratian, et al. (2001). "Temporal spatial differences observed by functional MRI and human intraoperative optical imaging." Cerebral Cortex **11**: 773-782.
Catalan, M. J., M. Honda, et al. (1998). "The functional neuroanatomy of simple and complex sequential finger movements: a PET study." Brain **121**: 253-264.
Chugani, H. (1998). "A critical period of brain development: studies of cerebral glucose utilization with PET." Preventive Medicine **27**: 184-188.
Chugani, H., M. Phelps, et al. (1987). "Positron Emission Tomography study of human brain functional development." Annals of Neurology **22**: 487-497.
Coghill, R. C., C. N. Sang, et al. (1998). "Global cerebral blood flow decreases during pain." Journal of Cerebral Blood Flow and Metabolism **18**: 141-147.
Cohen, L. B., R. D. Keynes, et al. (1972). "Changes in axon light scattering that accompany the action potential: current-dependent components." Journal of Neurophysiology **224**: 727-752.
Colditz, P., G. Greisen, et al. (1988). "Comparison of Electrical Impedance and 133Xenon Clearance for the Assessment of Cerebral Blood Flow in the Newborn Infant." Pediatric Research **24**(4): 461-464.
Colditz, P., D. Murphy, et al. (1989). "Effect of infusion rate of indomethacin on cerebrovascular responses in preterm neonates." Archives of Diseases in Childhood **64**(fetal): 8-12.
Costeloe, K., D. P. L. Smyth, et al. (1984). "A Comparison between Electrical Impedance and Strain Guage Plethysmography for the study of Cerebral Blood Flow in the Newborn." Pediatric Research **18**(3): 290-295.
Csibra, G., G. Davis, et al. (2000). "Gamma oscillations and object processing in the infant brain." Science **290**: 1582-1585.
Dalziel, C. F. (1972). "Electric Shock Hazard." IEEE Spectrum: 41-50.
Dauth, G. W., R. Defendini, et al. (1977). "Long-term surface stimulation of the cerebellum in the monkey I. Light microscopic, electrophsyiologic and clinical observations." Surgical Neurology **7**: 377-384.
Dawson, S., R. Panerai, et al. (1999). "Critical closing pressure explains cerebral hemodynamics during the Valsalva maneuver." Journal of Applied Physiology 86(2): 675-680.
Dehaene-Lambertz, G., S. Dehaene, et al. (2002). "Functional neuroimaging of speech perception in infants." Science **298**(5600): 2013-5.
Derdeyn, C., T. Videen, et al. (2002). "Variability of cerebral blood volume and oxygen extraction: stages of cerebral haemodynamic impairment revisited." Brain **125**(3): 595-607.
Desmedt, J. and J. Mai (1970). "Somatosensory Evoked Potentials of the Normal Human Neonate in REM Sleep, In Slow Wave Sleep and in Waking." EEG and Clinical Neurophysiology **29**: 113-126.
DeYoe, E. A., P. Bandettini, et al. (1994). "Functional magnetic resonance imaging of the human brain." Journal of Neuroscience Methods **54**: 171-187.
Dietzel, I., U. Heinemann, et al. (1982). "Stimulus-induced changes in extracellular Na+ and Cl- concentration in relation to changes in the size of the extracellular space." Experimental Brain Research **46**: 73-84.

Dlugosz, L., J. Vena, et al. (1992). "Congenital defects and electric bed heating in New York State: a register-based case control study." American Journal of Epidemiology **135**(9): 1000-11.
Erberich, S. G., P. Friedlich, et al. (2003). "Functional MRI in neonates using neonatal head coil and MR compatible incubator." Neuroimage **20**(2): 683-92.
Eyuboglu, B., B. Brown, et al. (1987). "Localisation of cardiac related impedance changes in the thorax." Clinical Physics and Physiological Measurement **8**(A): 167-173.
Firbank, M., E. Okada, et al. (1998). "A Theoretical Study of the Signal Contribution of regions of the Adult Head to Near-Infrared Spectroscopy Studies of Visual Evoked Responses." Neuroimage **8**: 69-78.
Fox, P. T., M. A. Mintun, et al. (1986). "Mapping Visual Cortex with Positron Emission Tomography." Nature **323**: 806-809.
Frackowiak, R., K. Friston, et al. (1997). Human Brain Function. San Diego, Academic Press.
Friston, K. J., C. D. Frith, et al. (1990). "The relationship between global and local changes in PET scans." Journal of Cerebral Blood Flow and Metabolism **10**: 458-466.
Gabor, A. J., A. G. Brooks, et al. (1984). "Intracranial Pressure During Epileptic Seizure." Electroencephalography and clinical neurophysiology **57**: 497-506.
Gabriel, S., R. Lau, et al. (1996). "The dielectric properties of biological tissues: II. Measurements in the frequency range 10 Hz to 20 GHz." Physics in Medicine and Biology **41**: 2251-2269.
Geddes, L. A. and L. E. Baker (1967). "The specific resistance of biological material : A compendium of data for the biomedical engineer and physiologist." Med & biol. Engineering **5**: 271-293.
Gersing, E. (1991). "Messung der elektischen Impedanz von Organen- Apparative Ausrustung fur Forschung und klinische Anwendung." Biomed. Technik **36**: 6-11.
Geselowitz, D. (1971). "Application of electrocardiographic lead theory to impedance plethysmography." IEEE Transactions in Biomedical Engineering **18**(1): 38-41.
Gibson, A. (2000). Electrical Impedance Tomography of Human Brain Function. Department of Physiology. London, University College London**:** 293.
Gibson, A., R. Bayford, et al. (1997). The effect of skull impedance on electrical impedance tomography of the neonatal head. World Congress on Medical Physics and Biomedical Engineering, Nice, France, Med. & Biol. Eng. & Comp.
Gibson, A., R. Bayford, et al. (2000). "Two-dimensional finite element modelling of the neonatal head." Physiogical Measurement **21**: 45-52.
Gibson, A., R. H. Bayford, et al. (1999). "Development of a reconstruction algorithm for imaging impedance changes in the human head." Annals of New York Academy of Sciences **873**: 482-492.
Gibson, A., A. T. Tidswell, et al. (1999). A 3D reconstruction algorithm for imaging impedance changes in the human head. Biomedical Applications of EIT, London, UK.
Gjedde, A. and S. Marrett (2001). "Glycolysis in neurons, not astrocytes, delays oxidative metabolism of human visual cortex during sustained checkerboard stimulation in vivo." Journal of Cerebral Blood Flow and Metabolism **21**: 1384-1392.
Golub, G. and C. V. Loan (1996). Matrix Computations, John Hopkins University Press.
Gordon, B., R. P. Lesser, et al. (1990). "Parameters for direct electrical stimulation in the human: histopathologic confirmation." Electroencephalography and clinical Neurophysiology **75**: 371-377.
Griffiths, H. and A. Ahmed (1987). "A dual-frequency applied tomography technique: computer simulations." Clinical Physics and Physiological Measurement **8**(A): 103-107.
Grinvald, A., R. D. Frostig, et al. (1991). "High resolution optical imaging of functional brain architecture in the awake monkey." Proceedings of the National Academy of Sciences, USA **88**: 11559-11563.
Grinvald, A., E. Lieke, et al. (1986). "Fuctional architecture of cortex revealed by optical imaging of intrinsic signals." Nature **324**: 361-364.

Gunn, A., T. Gunn, et al. (1997). "Dramatic neuronal rescue with prolonged selective head cooling after ischemia in fetal lambs." Journal of Clinical Investigations **99**(2): 248-256.
Haglund, M., G. Ojeman, et al. (1992). "Optical imaging of epileptiform and functional activity in human cerebral cortex." Nature **358**: 668-671.
Harding, G., J. Grose, et al. (1989). "The pattern reversal VEP in short-gestation infants." EEG and Clinical Neurophysiology **74**: 76-80.
Harel, N., S.-P. Lee, et al. (2002). "Origin of negative blood oxygenation level-dependdent fMRI signals." Journal of Cerebral Blood Flow and Metabolism **22**: 908-917.
Harris, N., A. Suggett, et al. (1987). "Applications of applied potential tomography (APT) in respiratory medicine." Clinical Physics and Physiological Measurement **8**(A): 155-165.
Hasegawa, I., S. Kuriki, et al. (1983). "Dependence of electrical conductivity on fixed charge density in articular cartilage." Clincial Orthopaedics **177**: 283-288.
Hebden, J. C., A. Gibson, et al. (2002). "Three-dimensional optical tomography of the premature infant brain." Phys Med Biol **47**(23): 4155-66.
Hintz, S., D. Benaron, et al. (2001). "Bedside functional imaging of the premature infant brain during passive motor activation." Journal of Perinatal Medicineq **29**: 335-343.
Hodgkin, A. L. (1967). The Conduction of the Nervous Impulse. Liverpool, Liverpool University Press.
Hoge, R., J. Atkinson, et al. (1999). "Linear coupling between cerebral blood flow and oxygen consumption in activated human cortex." Proceedings of the National Academy of Science USA **96**: 9403-9408.
Hoge, R. and G. Pike (2001). "Oxidative metabolism and the detection of neuronal activation via imaging." Journal of Chemical Neuroamatomy **22**: 43-52.
Hoge, R. D., J. Atikinson, et al. (1999). "Stimulus dependent BOLD and perfusion dynamics in human V1." Neuroimage **9**: 573-585.
Holder, D., K. Boone, et al. (1994). "Specification for an electrical impedance tomogram for imaging epilepsy in ambulatory human subjects." Innivation et Technologie en Biologie et Medecine **15**(S1): 24-32.
Holder, D. and A. Gardner-Medwin (1988). "Some possible neurological applications of applied potential tomography." Clinical Physics and Physiological Measurement **9**(A): 111-119.
Holder, D. S. (1992). "Detection of cerebral ischaemia in the anaesthetised rat by impedance measurement with scalp electrodes: implications for non-invasive imaging of stroke by electrical impedance tomography." Clinical Physics and Physiological Measurements **13**(1): 63-75.
Holder, D. S., A. Rao, et al. (1996). "Imaging of physiologically evoked responses by electrical impedance tomography with cortical electrodes in the anaesthetised rabbit." Physiological Measurement **17**: A179-A186.
Holloway, V. (2000). Reorganisation of sensorimotor functin in children with brain disease`. Radiology and Physics Unit, Intitute of Child Health. London, University of London: 302.
Holthoff, K. and O. White (1996). "Intrinsic optical signals in rat neocortical slices measured with near-infrared dark-field microscopy reveal changes in extracellular space." Journal of Neuroscience **16**(8): 2740-2748.
Hossmann, K.-A. (1971). "Cortical Steady Potential , impedance and excitability changes during and after total ischemia of cat brain." Experimental Neurology **32**: 163-175.
Hrbek, A., M. Hrbkova, et al. (1968). "Somatosensory evoked responses in newborn infants." EEG and Clinical Neurophysiology **25**: 443-448.
Hrbek, A., P. Karlberg, et al. (1972). "Development of Visual And Somatosensory Evoked Responses in Pre-term Newborn Infants." EEG and Clinical Neurophysiology **34**: 225-232.
Hrbek, A. and P. Mares (1963). "Cortical evoked responses to visual stimulation in full-term and premature new-borns." EEG and Clinical Neurophysiology **16**: 575-581.

Ibanez, V., M. P. Deiber, et al. (1995). "Effects of stimulus rate on regional cerebral blood flow after median nerve stimulation." Brain **118**: 1339-1351.
Iramina, K., H. Kamei, et al. (1999). "Effects of stimulus intensity on fMRI and MEG in somatosensory cortex using electrical stimulation." IEEE Transactions on Magnetics **35**(5): 4106-4108.
Isobe, K., T. Kusaka, et al. (2001). "Functional imaging of the brain in sedated newborn infants using near infared topography during passive knee movement." Neuroscience Letters **299**: 221-224.
Johnson, M., M. d. Haan, et al. (2001). "Recording and analyzing high-density event-related potentials with infants. Using the Geodesic sensor net." Developmental Neuropsychology **19**(3): 295-323.
Joy, M., V. Lebedeev, et al. (1999). "Imaging of current density and current pathways in rabbit brain during transcranial electrostimulation." IEEE transactions on biomedical engineering **46**(9): 1139-1148.
Karni, A., G. Meyer, et al. (1995). "Functional MRI evidence for adult motor cortex plasticity during motor skill learning." Nature **377**: 155-158.
Kato, T., A. Kamei, et al. (1993). "Human visual cortical function during photic stimulation monitoring by means of near infrared spectroscopy." Journal of Cerebrall Blood Flow and Metabolism **13**: 516-520.
Kerner, T., A. Hartov, et al. (2001). "An improved data acquisition method for electrical impedance tomography." Physiological Measurement **22**: 31-38.
Kerner, T., A. Hartov, et al. (2002). "Imaging the breast with EIS: an initial study of exam consistency." Physiological Measurement **23**: 221-236.
Kim, S., J. Ashe, et al. (1993). "Functional imaging of human motor cortex at high magnetic field." Journal of Neurophysiology **69**(1).
Kinahan, P. and D. Noll (1999). "A direct comparison betweeen whole-brain PET and BOLD fMRI measurements of single-subject activation response." Neuroimage **9**: 430-438.
Kinnala, A., H. Suhonen-Polvi, et al. (1996). "Cerebral metabolic rate for glucose during the first six months of life: an FDG positron emission tomography study." Archives of Diseases in Childhood **74**: F153-F157.
Kosterich, J., K. Foster, et al. (1984). "Dielectric properties of fluid saturated bone: the effect of variation in conductivity of immersion fluid." IEEE Transactions on Biomedical Engineering **31**(4): 369-373.
Kosterich, J. D., K. R. Foster, et al. (1983). "Dielectric permittivity and electrical conductivity of fluid saturated bone." IEEE Transactions on Biomedical Engineering **30**(2): 81-86.
Kwong, K. K., J. W. Belliveau, et al. (1992). "Dynamic magnetic resonance imaging of the human brain activity during primary sensory stimulation." Proceedings of the National Academy of Science USA **89**: 5675-5679.
Lacy-Hulbert, A., J. C. Metcalfe, et al. (1998). "Biological responses to electromagnetic fields." FASEB **12**: 395-420.
Lattikka, J., T. Kuurne, et al. (2001). "Conductivity of living intracranial tissues." Physics Medicine and Biology **46**: 1611-1616.
Law, S. K. (1993). "Thickness and Resistivity variations over the upper surface of the human skull." Brain Topography **6**(2): 99-109.
Lemieux, L., K. Krakow, et al. (2001). "Comparison of spike-triggered functional MRI BOLD activation and EEG dipole model localization." Neuroimage **14**(5): 1097-104.
Lemieux, L., A. Salek-Haddadi, et al. (2001). "Event-related fMRI with simultaneous and continous EEG: description of the method and initial case report." Neuroimage **14**: 7780-787.
Li, C., A. Bak, et al. (1968). "Specific resistivity of the cerebral cortex and white matter." Experimental Neurology **20**: 544-557.

Li, F., M. Silva, et al. (2000). "SEcondary decline in apparent diffusion coefficient and neurological outcome after a short period of focal brain ischemia in rats." Annals of Neurology **48**: 236-244.
Linet, M. S., E. E. Hatch, et al. (1997). "Residential exposure to magnetic fields and acute lymphoblastic leukemia in children." New England Journal of Medicine **337**(1): 1-7.
Lipton, P. (1972). "Effects of membrane depolarization on light scattering by cerebral cortex slices." Journal of Physiology **231**: 365-383.
Liston, A., R. Bayford, et al. (2002). "A multi-shell algorithm to reconstruct EIT images of brain function." Physiological Measurement: in press.
Logothetis, N., H. Guggenberger, et al. (1999). "Functional imaging of the monkey brain." Nature Neuroscience **2**(6): 555-562.
Logothetis, N., J. Pauls, et al. (2001). "Neurophysiological investigation of the basis of the fMRI signal." Nature **412**: 150-157.
Lux, H., U. Heinemann, et al. (1986). Ionic changes and alterations in the size of the extracellular space during epileptic activity. Advances in Neurology. A. Delgado-Escueta, A. Ward, D. Woodbury and R. Porter. New York, Raven Press. **44:** 619.
MacVicar, B. A., D. Feighan, et al. (2002). "Intrinsic optical signals in the rat optic nerve: role for K(+) uptake via NKCC1 and swelling of astrocytes." Glia **37**(2): 114-23.
Malonek, D., U. Dirnagl, et al. (1997). "Vascular imprints of neuronal activity: Relationships between the dynamics of cortical blood flow, oxygenation and volume changes following sensory stimulation." Proceedings of the National Acadamy of Science USA **94**: 14826-31.
Mangall, Y., A. Baxter, et al. (1987). "Applied Potential Tomography: a new non-invasive technique for assessing gastric function." Clinical Physics and Physiological Measurement **8**(A): 119-129.
Maquet, P., C. Degueldre, et al. (1997). "Functional neuroanatomy of human slow wave sleep." The Journal of Neuroscience **17**(8): 2807-2812.
Martin, E., P. Joeri, et al. (1999). "Visual processing in infants and children studied using functional MRI." Pediatric Research **46**(2): 135-140.
Martin, E., T. Thiel, et al. (2000). "Effect of pentobarbital on visual processing in man." Human Brain Mapping **10**: 132-139.
Mazziotta, J. C. and M. Phelps (1984). "Human sensory stimulation and deprivation: Positron Emission Tomographic results and strategies." Annal Neurology (supplement) **15**: S50-S60.
McArdle, F. J., B. H. Brown, et al. (1988). "The effect of the skull of low-birthweight neonates on apllied potential tomography imaging of centralised resistivity changes." Clinical Physical and Physiological Measurement **9**(Supplement A): 55-60.
McCann, J., F. Dietrich, et al. (1998). "The genotoxic potential of electric and magnetic fields: an update." Mutation Research **411**: 45-86.
McCredie, M., P. Maisonneuve, et al. (1994). "Perinatal and early postnatal risk factors for malignant brain tumours in New South Wales children." Int Journal Cancer **56**(1): 11-15.
McCreery, D. B. and W. F. Agnew (1990). Mechanisms of Stimulation-Induced Neural Damage and Their Relation to Guidelines for Safe Stimulation. Neural Prostheses: Fundamental Sudies. D. B. McCreery and W. F. Agnew. New Jersey, Prentice Hall: 298-317.
Meek, J., M. Firbank, et al. (1998). "Regional Haemodynamic Responses to visual stimulation in awake infants." Pediatric Research **43**(6): 840-843.
Meek, J. H., C. E. Elwell, et al. (1995). "Regional changes in cerebral haemodynamics as a result of a visual stimulus measured by near infrared spectroscopy." Proceedings of the Royal Society London Biology Science **261**: 351-356.
Mentis, M., G. Alexander, et al. (1998). "Increasing required neural response to expose abnormal brain function in mild versus moderate or severe Alzheimer's disease: a PET study using parametric visual stimulation." American Journal of Psychiatry **155**: 785-794.

Mentis, M. J., G. E. Alexander, et al. (1997). "Frequency variation of a pattern-flash visual stimulus during PET differentially activates brain from striate through frontal cortex." Neuroimage **5**: 116-128.
Mentis, M. J., B. Horwitz, et al. (1996). "Visual cortical dysfunrtion in Alzheimer's disease evaluated with a temporally graded 'stress test during PET." American Journal of Psychiatry **153**(1): 32-40.
Metherall, P., D. C. Barber, et al. (1996). "Three dimensional electrical impedance tomography." Nature **380**: 509-512.
Miller, S., J. Weiss, et al. (2002). "Seizure-associated brain injury in term newborns with perinatal asphyxia." Neurology **58**: 542-548.
Minns, R. A. and J. K. Brown (1978). "Intracranial Pressure Changes Associated with Childhood Seizures." Developmental Medicine and Child Neurology **20**(561-569): 561-569.
Miyasaka, N., T. Nagaoka, et al. (2000). "Histopathologic correlates of temporal diffusion changes in a rat model of cerebral hypoxia/ischemia." American Journal of Neuroradiology **21**: 60-66.
Mora, B. N., G. J. Carman, et al. (1989). "In vivo localisation of the human visual cortex using positron emission tomography and magnetic resonance imaging." TINS (?trends in neuroscience) **12**(8): 282-284.
Morita, T., T. Kochiyama, et al. (2000). "Difference in the metabolic response to photic stimulation of the lateral geniculate nucleus and the primary visual cortex of infants: an fMRI study." Neuroscience Research **38**: 63-70.
Muller, M. and G. Somjen (1999). "Intrinsic optical signals in rat hippocampal slices during hypoxia-induced spreading depression -like depolarization." Journal of Neurophysiology **82**: 1818-1831.
Murphy, D., P. Burton, et al. (1987). "Impedance imaging in the newborn." Clinical Physics and Physiological Measurement **8**(Suppl A): 131-140.
Niblack, W. (1986). An Introduction to Digital image Processing. London, Prentice Hall International.
Nirkko, A., C. Ozodba, et al. (2001). "Different ipsilateral representations for distal and proximal movements in the sensorimotor cortex: activation and deactivation patterns." Neuroimage **13**(5): 825-835.
Ogawa, S., R. S. Menon, et al. (1993). "Functional brain mapping by blood oxygenation level-dependent contrast magnetic resonance imaging A comparison of signal characteristics with a biophysical model." Biophysical Journal **64**: 803-812.
Oostende, S. V., P. V. Hecke, et al. (1997). "fMRI Studies of the Supplementary Motor Area and the Premotor Cortex." Neuroimage **6**: 181-190.
Oostendorp, T., J. Delbeke, et al. (2000). "The conductivity of the human skull: results of in vivo and in vitro measurements." IEEE Transations on Biomedical Engineering **47**(11): 1487-1492.
Palmer, J., A. de-Crespigny, et al. (1999). "High Resolution mapping of discrete representational areas in rat somatosensory sortex using blood volume dependent functional MRI." Neuroimage **9**: 383-392.
Pena, M., A. Maki, et al. (2003). "Sounds and silence: an optical topography study of language recognition at birth." Proc Natl Acad Sci U S A **100**(20): 11702-5.
Penrice, J., E. CAdy, et al. (1996). "Proton magnetic resonance spectroscopy of the brain in normal preterm and term infants, and early changes after perinatal hypoxic-ischaemia." Pediatric Research **40**: 6-14.
Perlman, J., P. Herscovitch, et al. (1985). "Positron emission tomography in the newborn: Effect of seizure on regional cerebral blood flow in an asphyxiated infant." Neurology **35**: 244-247.
Pike, A., N. Marlow, et al. (1997). "Posterior tibial somatosensory evoked potentials in very preterm infants." Early Human Development **47**: 71-84.

Preston-Martin, S., J. Gurney, et al. (1996). "Brain tumour risk in children in relation to use of electric blankets and water bed heaters. Results from the United States West Coast Childhood Brain Tumour Study." American Journal of Epidemiology **143**(11): 1116-22.
Pudenz, R. H., L. A. Bullara, et al. (1975). "Electrical Stimulation of the Brain II. Effects on the blood-brain barrier." Surgical Neurology **4**: 265-270.
Pudenz, R. H., L. A. Bullara, et al. (1975). "Electrical Stimulation of the Brain III. The neural damage model." Surgical Neurology **4**: 389-400.
Ramsay, S. C., K. Murphy, et al. (1993). "Changes in global cerebral blood flow in humans: effect in regional cerebral blood flow during a neural activation task." Journal of Physiology **471**: 521-534.
Ranck, J. (1963). "Analysis of specific impedance of rabbit cortex." Experimental Neurology **7**: 153-174.
Ranck, J. (1966). "Electrical impedance in the subicular area of rats during paradoxical sleep." Experimental Neurology **16**: 416-437.
Ranck, J. B. (1963). "Specific impedance of rabbit cerebral cortex." Experimental Neurology **7**: 144-152.
Rao, A. (2000). Electrical Impedance Tomography of Brain Activity: Studies into its Accuracy and Physiological Mechanisms. Department of Physiology. London, University College London: 228.
Rao, A., A. Gibson, et al. (1997). "EIT images of electrically induced epileptic activity in anaesthetised rabbits." Med & Biol. Eng & Comp. **35**(1): 3274.
Rector, D., G. Poe, et al. (1997). "Light Scattering changes Follow Evoked Potentials from Hippocampal Schaeffer Collateral Stimulation." Journal of Neurophysiology **78**: 1707-1713.
Robertson, N., R. Lewis, et al. (2001). "Early increases in brain myo-inositol measured by proton magnetic resonance spectroscopy in term infants with neonatal encephalopathy." Pediatric Research **50**(6): 692-700.
Rush, S. and D. Driscoll (1968). "Current Distribution in Brain From Surface Electrodes." Anaesthesia and Analgesia **47**: 717-727.
Sadato, N., G. Campbell, et al. (1996). "Complexity affects regional cerebral blood flow during sequential finger movements." Journal of Neuroscience **16**(8): 2693-2700.
Sakatani, K., S. Chen, et al. (1999). "Cerebral blood oxygenation changes induced by auditory stimulation in newborn infants measured by near infrared spectroscopy." Early Human Development **55**: 229-236.
Salek-Haddadi, A., M. Merschhemke, et al. (2002). "Simultaneous EEG-Correlated Ictal fMRI." Neuroimage **16**(1): 32-40.
Sato, C., M. Nemoto, et al. (2002). "Reassessment of activity-related optical signals in somatosensory cortex by an algorithm with wavelength-dependent path length." Jpn J Physiol **52**(3): 301-12.
Sato, K., T. Narai, et al. (2002). "Intraoperative intrinsic optical imaging of neuronal activity from subdivisions of the human primary somatosensory cortex." Cerebral Cortex **12**: 269-280.
Schneider, W., D. C. Noll, et al. (1993). "Functional topographic mapping of the cortical ribbon in human vision with conventional MRI scanners." Nature **365**: 150-153.
Sheth, R. (1999). "Electroencephalogram Confirmatory Rate in Neonatal Seizures." Pediatric Neurology **20**: 27-30.
Siddiqui, S., D. Brown, et al. (1980). "Detection of neonatal intraventricular haemorrhage using transcephalic impedance." Develop. Med. Child Neurol **22**: 440-447.
Singh, K., A. Smith, et al. (1999). "Spatiotemporal Frequency and Direction Sensitvities of Human Visual Areas Measured Using fMRI." Neuroimage **12**: 550-564.
Smallwood, R. H., A. R. Hampshire, et al. (1999). "A comparison of neonatal and adult lung impedances derived from EIT images." Physiol Meas **20**(4): 401-13.

Sokol, S. (1978). "Measurement of Infant Visual Acuity from Pattern Reversal Evoked Potentials." Vision Research **18**(1): 33-39.
Soul, J., R. Robertson, et al. (2001). "Time course of changes in diffusion weighted imaging in a case of neonatal encepholopathy with defined onset and duration of hypoxic-ischemic insult." Pediatrics **108**(5): 1211-1214.
Tan, W., C. Williamd, et al. (1993). "Pretreatment with monoganglioside GM1 protects the brain of fetal sheep against hypoxic-ischemic injury without causing systemic compromise." Pediatric Research **34**: 18-22.
Tan, W., C. Williams, et al. (1996). "Accumulation of cytotoxins during the development of seizures and edema after hypoxic-ischemic injury in late gestation fetal sheep." Pediatric Research **39**(5): 791-797.
Tarassenko, L. (1985). Electrical impedance techniques for the study of the cerebral circulation and cranial imaging in the newborn. Oxford, University of Oxford: 304.
Tarassenko, L., M. Pidcock, et al. (1985). "The development of impedance imaging techniques for use in the newborn at risk of intra-ventricular haemorrhage." IEEE International Conference on Electric and Magnetic Fields in Medicine and Biology: 83-87.
Thorenson, M., J. Penrice, et al. (1995). "Mild hypothermia after severe transient hypoxia-ischaemia ameliorates delayed cerebral energy failure in the newborn piglet." Pediatric Research **37**(5): 667670.
Thoresen, M., M. Simmonds, et al. (2001). "Effective selective head cooling during posthypoxic hypothermia in newborn piglets." Pediatric Research **49**(4): 594-599.
Thronton, J., R. Ordidge, et al. (1997). "Anisotropic water diffusion in white and gray matter of the neonatal piglet brain before and after transient hypoxia-ischamia." Magnetic Resonance Imaging **15**(4): 433-440.
Tidswell, A., A. Bagshaw, et al. (2003). "A comparison of headnet electrode arrays for electrical impedance tomography of the human head." Physiological Measurement **24**: S1-18.
Tidswell, A., A. Gibson, et al. (2001). "Three Dimensional Impedance Tomography of Human Brain Activity." Neuroimage **13**(2): 283-294.
Tidswell, A., A. Gibson, et al. (2001). "Validation of a 3-D reconstruction algorithm for EIT of human brain function in a realistic head shaped tank." Physiological Measurement **22**(1): 177-185.
Tidswell, A., A. Gibson, et al. (2001). 3D Electrical Impedance Tomography of Neonatal Brain Activity. 3rd EPSRC Engineering Network Meeting: Biomedical Applications of EIT, University College London.
Tidswell, A., J. Wyatt, et al. (2002). Electrical Impedance Tomography of Neonatal Brain Function. Medical Research Society Meeting 2002, London.
Tidswell, A. T., A. Gibson, et al. (2001). "Electrical Impedance Tomography of human brain activity with a two-dimensional ring of scalp electrodes." Physiological Measurement **22**(1): 167-175.
Tidswell, T., J. Wyatt, et al. (2001). "Functional Imaging of Neonatal Evoked Responses with Electrical Impedance Tomography." Neuroimage **13**(6): S1268.
Tootell, R. B. H., J. B. Reppas, et al. (1995). "Functional Analysis of Human MT and Related Visual Cortical Areas Using Magnetic Resonance Imaging." Journal of Neuroscience **15**(4): 3215-3230.
Tucker, D. (1993). "Spatial sampling of head electrical fields: the geodesic sensor net." Electroencephalography and Clinical Neurophysiology **87**: 154-163.
Tzourio-Mazoyer, N., S. D. Schonen, et al. (2002). "Neural correlates of woman face processing by 2-month-old infants." Neuroimage **15**: 454-461.
Van-Harreveld, A. and S. Ochs (1956). "Cerebral Impedance Changes after circulatory arrest." American Journal of Physiology **187**: 180-192.

Van-Harreveld, A. and J. Schade (1962). "Changes in the electrical conductivity of cerebral cortex during seizure activity." Experimental neurology **5**: 383-400.
Villringer, A., J. Planck, et al. (1993). "Near infrared spectroscopy (NIRS): a new tool to study hemodynamic changes during activation of brain function in human adults." Neuroscience letters **154**: 101-104.
Vollmer-Haase, J., H. W. Folkerts, et al. (1998). "Cerebral haemodynamics during electrically induced seizures." Neuroreport **9**: 407-410.
Volpe, J. (1995). Neurology of the Newborn. Philadelphia, W. B. Saunders Company.
Weiller, C., M. Juptner, et al. (1996). "Brain representation of active and passive movements." Neuroimage **4**: 105-110.
Williams, C., A. Gunn, et al. (1991). "Time course of intracellular edema and epileptiform activity following prenatal cerebral ischemia in sheep." Stroke **22**: 516-521.
Yablonskiy, D., J. Ackerman, et al. (2000). "Coupling between changes in human brain temperature and oxidative mnetabolism during prolonged visual stimulation." Proceedings of the New York Academy of Sciences **97**(13): 7603-7608.
Yamada, H., N. Sadato, et al. (1997). "A rapid brain metabolic change in infants detected by fMRI." Brain Imaging **8**(17): 3775-3778.
Yamada, H., N. sadato, et al. (2000). "A milestone for normal development of the infantile brain detected by functional MRI." Neurology **55**: 218-223.
Yamamoto, T. and Y. Yamamoto (1976). "Electrical properties of the epidermal stratum corneum." Medical and Biological Engineering: 151-158.
Ye, F. Q., A. M. Smith, et al. (1997). "Quantitation of regional cerebral blood flow increases during motor activation: a steady state arterial spin tagging study." Neuroimage **6**: 104-112.
Yerworth, R., R. Bayford, et al. (2002). "Design and performance of the UCLH Mark 1b 64 channel electrical impedance tomography (EIT) system, optimized for imaging brain function." Physiological Measurement **23**: 149-158.
Zaramella, P., F. Freato, et al. (2001). "Brain audirtory activation measured by near-infra red spectroscopy (NIRS) in infants." Pediatric Research **49**(2): 213-219.
Zeki, S. (1990). "A century of cerebral achromatopsia." Brain **113**: 1721-1777.
Zeki, S., J. D. G. Watson, et al. (1993). "Going beyond the information given: the relation of illusory visual motion to brain activity." Proceedings of the Royal Society of London, Biological Science **252**: 215-222.
Zeki, S., J. D. G. Watson, et al. (1991). "Direct demonstration of functional specialization in human visual cortex." The Journal of Neuroscience **11(3)**: 641-649.